Development of scalable functionalized membranes for bioprocessing applications

Dissertation

zur Erlangung des akademischen Grades Doktor der Naturwissenschaften

Doctor rerum naturalium

(Dr. rer. nat.)

Vorgelegt von

Tanmay Netke

Fakultät für Chemie

der

Universität Duisburg-Essen,

Essen, 03-Nov-2022

Supervisor: Prof. Dr. Mathias Ulbricht

DuEPublico
Duisburg-Essen Publications online

UNIVERSITÄT DUISBURG ESSEN
Offen im Denken

ub | universitäts bibliothek

This dissertation is made available via DuEPublico, the institutional repository of the University of Duisburg-Essen and is also available as printed version.

DOI: 10.17185/duepublico/78161
URN: urn:nbn:de:hbz:465-20241015-101633-8

All rights reserved.

Approved by the examining committee consisting of:

Chair: Prof. Dr. Stefan Rumann

Advisor: Prof. Dr. Mathias Ulbricht

Reviewer: Prof. Dr. Stephan Panglisch

Date of oral examination: 03.11.2022

DECLARATION

The work presented here was performed from May 2018 till May 2021 at GVS Filter Technology, Bologna, Italy and at the Lehrstuhl füe Technische Chemie II of the University of Duisburg-Essen and supervised by Prof. Dr. Mathias Ulbricht.

This version of the thesis is created for the purpose of examination only and shall be kept confidential; the publication of the thesis will be postponed in order to ensure that intellectual property can be secured.

I declare that this dissertation represents my own work, except where due acknowledgement is made.

…….

ABSTRACT

In the recent years pharmaceutical and biomedical fields have emerged to become a huge market for the membrane technology. Hydrophilized polyether sulfone (PES) and polyvinylidene fluoride (PVDF) membranes are currently most abundantly used for the bio-pharmaceutical applications. Various surface functionalization techniques have been remarkably evolved over the past decades towards developing membranes for such applications. Functional membranes such as ion-exchange membranes or membrane absorbers are widely used to increase the separation efficiencies; stimuli responsive membranes, e.g., to pH or temperature, are explored. Despite these developments, many functionalization techniques are limited to lab-scale implementation. Moreover, there is still limited separation performance due to poor selectivity as a result of different types of fouling.

This project therefore focuses on industrial production of functionalized microfiltration (MF) PVDF membranes for bio-pharmaceutical applications. The functionalization is carried out via scalable two-step graft coating polymerization involving redox initiation of radical reactions with ethylene glycol dimethacrylate (EGDMA) as the cross-linker. Either vinyl monomers or hydrophilic polymers were added in order to introduce specific functionality in the coating. EGDMA dominated the polymerization due to higher reactivity, higher local concentration at the interface and efficient homopolymerization. Vinyl monomers drove the thermodynamics and kinetics towards more efficient functionalization compared to the long chain polymers.

Acrylic acid and 2-hydroxyethyl methacrylate (HEMA) as functional monomers presented a promising platform to obtain superior anti-fouling surface properties. The EGDMA-monomer ratio played an integral role in influencing the final membrane properties. EGDMA governed the structural changes while monomer defined the surface properties obtained upon modification. Polyacrylic acid formed pH-responsive dangling chains which could repel particles from entering the membrane pores through electrostatic repulsions. Poly(HEMA) formed a hydration layer on the surface reducing the particle adhesion onto the membrane surface.

Acrylic acid and HEMA functionalized flat sheet membranes were industrially produced in a roll-to-roll process. The membrane demonstrated compatibility towards wide range

of chemicals, high thermal and mechanical stability, and retained their properties after sterilization. Furthermore, in addition to the very low protein binding ability (< 2 μg/cm^2), the membranes showed higher particle retention than the competitor membrane with smaller pore sizes due to the reduced membrane-particle adhesion.

Furthermore, a relationship between the membrane pore size and polymerization efficiency was established to extend the functionalization to base membranes with varying pore sizes. The results revealed a gradient of polymerization in the cross-section of the membrane which reduced with increasing pore size.

Commercial MF membranes have been successfully functionalized via developed methodology at an industrial scale to obtain desired surface properties to minimize fouling and enhance the separation performance. The preliminary performance and characterization results for the developed prototypes show considerable potential to implement developed membranes for bioprocessing applications.

ACKNOWLEDGEMENT

Throughout my journey of doctoral studies, I have been fortunate to receive a great deal of support from a number of people.

First and foremost, I would like to thank Prof. Dr. Mathias Ulbricht for offering me an opportunity to be part of his working group for my Ph.D. I am deeply grateful for the invaluable advice, constant support, continued guidance, patience, and for the much-needed encouragement at difficult times. I always cherished the fruitful discussions with him and learnt how to steer my research in the right direction. I greatly appreciate his willingness to spend time with his students generously. It was an honor to pursue my Ph.D. in his group.

I would also like to express my gratitude to Dr. Marta Bonora for her sincere advice, constructive feedback, continual support to navigate throughout my stay at GVS Filter Technology, Bologna, Italy. I would also like to thank Dr. Luca Querze and Dr. Nino Gaeta for believing in me.

The work performed was part of "TRAIN-EV" project funded by the European Union's Horizon 2020 research and innovation programme under the Marie Sklodowska-Curie grant agreement No 722148. Thank you for making this possible.

I would like to thank Prof. Dr. -Ing. Stefan Panglisch for accepting the offer to be the reviewer for my dissertation. Also, I am grateful to Prof. Dr. Stefan Rumann for taking time to chair the examination committee.

I wish to offer my sincere gratitude to all the members in the TRAIN-EV consortium for their insightful comments and suggestions throughout the project.

I am deeply grateful to Dipl.-Ing Tobias Kallweit, M.Eng. Pascale Wüncher, Claudia Schenk, Mrs. Roswitha Nordman, and Dr. Christina Kamp-Meltzer. I highly appreciate the great support, precious efforts with logistics, organization and conducting several valuable experiments for the project. It helped me a lot during my visits to UDE from Bologna.

Moreover, I would like to thank my friends and former colleagues at TC-II for creating a friendly and motivating work environment. In particular I would like to thank Philip Jahn,

Sebastian Buchholz, Vanessa Schnecke, Derek Koch, Qirong Ke, Patrick May, and Marcel Matthias for their sincere efforts to help me during my time at UDE. Special thanks to Ibrahim Elsherbiny for his endless support and advice. I would also like to thank Prof. Dr. Epple's group for allowing the use of their lab instruments.

Furthermore, I am very thankful to my friends and former colleagues at GVS Filter Technology for making me feel at home. Specifically, I would like to thank Filippo Grolli, Alice Carati and Brunella Merante for memorable and enjoyable time together in GVS.

In parallel, I would like express my gratitude towards all my friends all around; especially Valentina Grganovic, Giovanni Fabbretti, Tasneem Ghazaly, Camilla Bertoluzza, Marco Fava, Mark Wischmeyer, Giovanna Danna, and Rahul Patil for being a source of strength during the tough times.

Finally, I owe the deepest gratitude to my parents and my brother for their unconditional love and immense support without which I could not have done this. I owe a big part of my success to them.

I thank everyone who was involved in any capacity to help me in my journey. I wish you all the best.

TABLE OF CONTENTS

1 INTRODUCTION

1.1 Problem definition

Impressive breakthroughs in molecular biology and biotechnology have been successfully exploited in the industry over the past decades. This has motivated equally innovative developments in biochemical engineering including purification and separation technologies, that have created opportunities for membranes and membrane processes[1]. In the past, membrane systems mainly developed for water treatment were adopted for bioprocessing applications for e.g., bacteria and virus removal from biofluid streams[2]. Today the worldwide market size of membranes in pharmaceutical industry alone has reached over USD 5.2 billion and is projected to grow at the yearly rate of 12 % until 2027[3]. Ability to operate at room temperature without phase change, low energy consumption and easy scalability make membranes an attractive candidate for bioseparations. The use of membranes in purification and separation of biological products is growing rapidly, thus becoming increasingly important in both academia and industry. The recent work by Zydney[4] discusses the recent developments in membrane industry and provides an overview about the future challenges and unique opportunities for membranes technologies in biopharmaceuticals.

The most widely used membrane processes in biotechnology utilize porous membranes with varying pore size; microfiltration (MF) 0.1 – 10 µm and ultrafiltration (UF): 0.02 – 0.1 µm. Porous membranes have been successfully implemented in various stages of bioseparation operations such as purification, concentration, and fractionation. They are extensively used for removal for bacteria, insoluble colloidal particles, viruses, and cell debris from the process fluids prior to a more sophisticated operation such protein recovery or extracellular vesicle isolation using chromatography.

Typical porous membranes utilized in bioprocessing application are composite membranes with dual functionality having bulk properties different from the desired surface properties. Composite membranes are preferred over membranes produced with addition of hydrophilic additives because the hydrophilic additive can be washed out eventually on continuous contact with the aqueous phase resulting in loss of hydrophilic properties. Conventional methodology currently used to achieve these membranes is by

coating a surfactant or a water-soluble polymer such as PVP on the surface with desired properties. However, this approach is undesirable since the coating is not permanent and upon exposure to any process fluid could result in removal of the coating. Membranes treated with physical coatings for example using dip-coating methodology are unable to rewet once dried after wetting with water, incapable of steam sterilizing, and show high extractable levels. These properties are undesirable in bioprocessing applications which involves sterilization and subsequent permeate analysis.

Graft polymerization has been proposed and demonstrated in several patents[5,6] as an alternative to modify surface properties by chemical bonding. However, using currently available techniques it is difficult to modify the entire surface of the porous membrane including the pore walls without affecting the membrane porosity due to the pore blockage. Moreover, selection of the appropriate polymer or oligomer for modification is crucial for the final membrane to be compatible with broad range of materials and substances. Formation of non-white colored membrane exhibiting colored extractables upon graft polymerization using primary amine has been reported[7]. Hence, the membrane should not be colored upon surface modification, should exhibit very low levels of extractables, and should demonstrate very low protein adsorption[8]. Addition to the intrinsic membrane properties, membrane fouling is a major challenge during a membrane process that adversely affects the flux and selectivity. Fouling results from several mechanisms: pore blockage upon accumulation of retained substances on the membrane surface and within the pores, pore constriction upon non-specific adsorption, and protein binding on the membrane surface. Fouling increases the operation costs, and reducing the membrane life. Therefore, it would be highly desirable to provide a composite membrane consisting of both: preferable bulk properties such as mechanical, thermal and chemically stability and desired anti-fouling surface properties as a result of polymer functionalization.

Numerous anti-fouling strategies have been reported in the last decade after understanding the underlying fouling mechanisms. It is well known that hydrophilic surfaces generated by functionalization demonstrate promising anti-fouling behavior. The characteristics of the hydrophilic layer such as extent of hydration, graft density, cross-linking density, and surface charge govern the interactions with foulants. Furthermore, stimuli responsive surfaces can also be obtained to additionally enhance the filtration efficiency. Multiple studies have demonstrated several functionalization

approaches to improve anti-fouling behavior. However, their application at the industrial scale: requires sophisticated post-treatment lines, additional energy sources (UV, plasma, etc.) therefore additional cost, is limited to certain polymers, or is limited by the process design.

In biotechnology, the contents of the process fluid vary depending on the process and operation; however, current filter products such as Millipore Amicon Ultra, Sartorius Vivaspin, and syringe filters in the market utilize generic hydrophilic membranes largely based on PES or PVDF. These membranes are typically used for ultrafiltration / microfiltration processes and possess negative surface charge to minimize the adhesion of negatively charged biological foulants. These membranes are universally used for various biological processes which causes problems such as non-specific adhesion, clogging of soft-particles, low yield and low recovery of bio-products. The economic limitations and upscaling constraints in addition to unpredictable market demands prevents manufacturers from producing a range of hydrophilic membranes with multifunctionalities to serve various purposes.

This work aims to develop a versatile, cost-effective, robust post-treatment methodology to functionalize base membranes with functional polymers of choice. The goal of this project is to bridge the gap by developing different industrial prototypes with a reactive coating on the surface and inside the pores to minimize fouling and maximize recovery.

1.2 Aim of the work

To obtain hydrophilic membranes with anti-fouling properties, functional polymers capable of hydrogen bonding with water molecules should be introduced onto the membrane. Polyvinylidene fluoride (PVDF) can be considered as the base membrane material since it is a widely used substrate for surface modification via graft polymerization strategy. Besides, industrial scale PVDF base membrane with required characteristics within microfiltration (MF) range can be easily obtained since it is manufactured in GVS. Therefore, 0.45 µm PVDF membrane was chosen as an ideal starting material for modification and grafting hydrophilic cross-linkable functional polymer chains is considered to be an ideal strategy for achieving anti-fouling surface properties.

Within this framework, the first aim of this project is to develop a “Lego-like” scalable membrane functionalization methodology to graft functional polymer onto the PVDF surface and inside the pore walls. The two features that result in “Lego-like” character are: 1) adjustable structural properties of the grafter polymer chains based on cross-linker/polymer concentration ratio; and 2) surface properties of choice based on the selected functional polymer. Redox initiated graft coating polymerization is thought to be fit for this approach: pre-forming an active coating of cross-linker and initiator via absorption, and later surface-initiated polymerization upon introduction of the activator and polymer to form reactive hydrogel coating consisting of functional polymer chains. Therefore, versatile methodology should be transferable to other substrates, cross-linkers and polymers containing vinyl group or abstractable hydrogen atoms. The work would focus on screening different cross-linker and polymer types along with various reaction parameters to identify suitable scalable formulation for fouling resistant membranes.

The second aim of this project is to develop two industrial prototypes with varying surface properties: 1) grafting polyHEMA chains on the surface and within the pore walls to create a hydration layer to minimize the interactions between surface and the foulants; and 2) grafting polyacrylic acid chains to obtain pH responsive surface, which at high pH deprotonates carboxylic group that can repel negatively charged foulants through electrostatic repulsions. The aim can be achieved by developing and evaluating several lab-scale prototypes with different reaction parameters for their properties and performance: particle retention and protein binding. Based on the evaluation, two formulations for the industrial upscaling could be chosen.

In order to be qualified as the new hydrophilic products, the prototypes should fulfil the required criteria for thermal and mechanical stability, chemical inertness, and coating integrity.

Furthermore, before introducing a new membrane, product specifications should be established. Thus, as a third aim, the prototypes are to be analyzed for their pore size and surface properties according to the industrial norms. Moreover, the particle retention and protein binding performance of the industrial prototypes is compared with a competitor’s PVDF based hydrophilic membrane widely used for bioseparations.

Considering the wide market opportunity for microfiltration membranes (not limited to one pore size) in biotechnology, the final fourth aim of his work is to establish a relationship between pore size of the base membrane and the efficiency of the functionalization. This relationship should help fine-tune the modification parameters based on the base membrane characteristics to obtain functionalized membranes for a wide range of pore sizes.

1.3 Scope of the work

In order to achieve the above-mentioned aims, the following tasks for each aim should be achieved:

I. Proof of the concept for the "Lego-like" two-step graft coating polymerization
   a. Modification of flat sheet PVDF membrane with with a monomer (acrylic acid) and a polymer (PVP)
   b. Characterization of the modified membranes to confirm the change of membrane structure and surface chemistry
   c. Modification with varying polymer concentrations at fixed cross-linker (EGDMA) concentration to understand the influence of polymers on the final membrane properties
   d. Modification with different cross-linkers: EGDMA and TrGDMA at varying concentrations but fixed polymer concentration to understand the influence of cross-linker on the final membrane properties

II. Development of two industrial prototypes
   a. Modifications with EGDMA as the cross-linker for developing pH responsive polyacrylic acid and hydrophilic polyHEMA prototypes at different polymer and cross-linker formulations
   b. Characterization of the final modified membranes to establish a relationship between formulation and structural and surface chemistry changes
   c. Investigation of the particle blocking mechanism
   d. Evaluation of the protein binding kinetics
   e. Identification of the best formulation for both the prototypes based on the surface properties, particle retention, and protein adsorption

III. Characterization and performance evaluation of the prototypes
    a. Comparison of the characteristics of the prototypes with the competitor membrane
    b. Comparison of the particle recovery and protein binding abilities with the competitor membrane

IV. Understanding the effect of pore size on functionalization
    a. Characterization of the base membrane properties with different pore sizes
    b. Investigation of the grafting efficiency inside the pore structure as a function of pore size

2 THEORETICAL BACKGROUND

2.1 Membrane processes in biotechnology

A membrane is a barrier between two phases which allows size-based separation of the components resulting in mass transport; typically driven by the difference in concentration, pressure, temperature or electric potential. Inspired from the biological membranes, synthetic polymeric membranes are mainly used in wide range of membrane applications such as water treatment, biotechnology, and food technology.

The use of membrane processes in biotechnology is rapidly growing due to the broad application spectra in both upstream and downstream bioprocessing at low operation costs. Membranes play an integral part in important bioprocesses such as fractionation, clarification, purification and recovery of the bioproducts[9]. Membrane processes have overcome several bioprocessing limitations such as use of extensive downstream processing for generation of complex mixtures, the production of low concentration solution using cell cultures, and contamination of cell cultures with unwanted biological species[10]. Figure 2.1 shows the use of membrane technology in a typical downstream process of biomolecules.

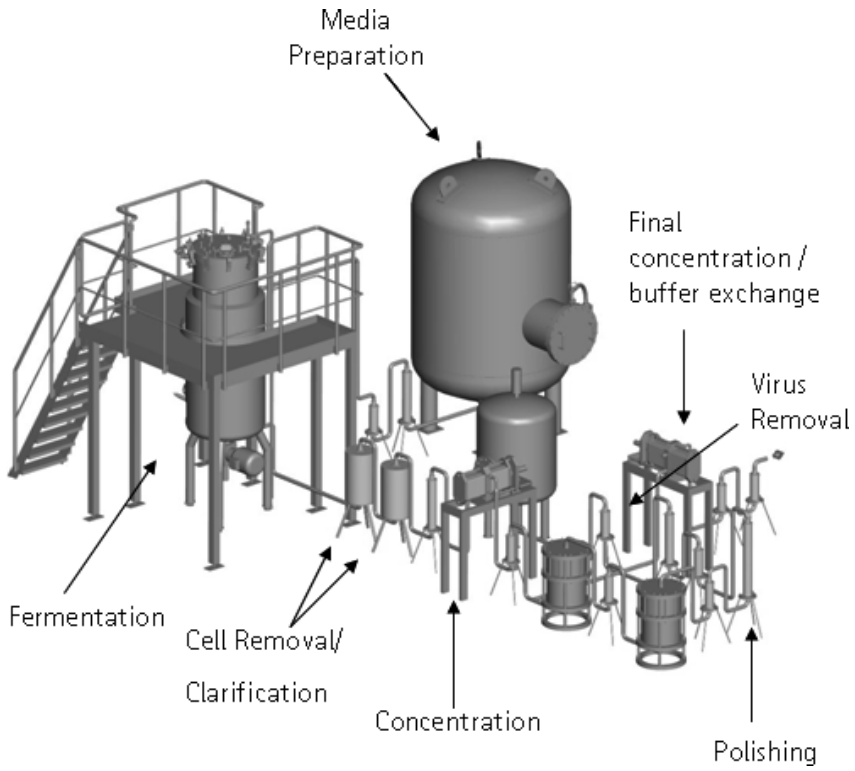

Figure 2.1. Use of membrane technology in the downstream of biomolecules[11]

Established membrane processes in biotechnology are mainly based on the molecular size but to some extent on shape and charge, to separate components in a solution or colloidal dispersion. Membranes are also being utilized more than a selective barrier by exploiting their large internal adsorptive surface areas. These properties make them excellent tools for entrapping enzymes, ion exchange, and affinity-based separations.

Due to the sensitivity of the biological substances to the external factors such as temperature and electrical potential, majority of the membrane separations are pressure driven which also consumes less energy. The pressure driven membrane processes can be categorized into four major groups based on the membrane pore size: microfiltration (MF), ultrafiltration (UF), nanofiltration (NF), and reverse osmosis (RO). Figure 2.2 shows the schematics of the membrane processes and separable solutes.

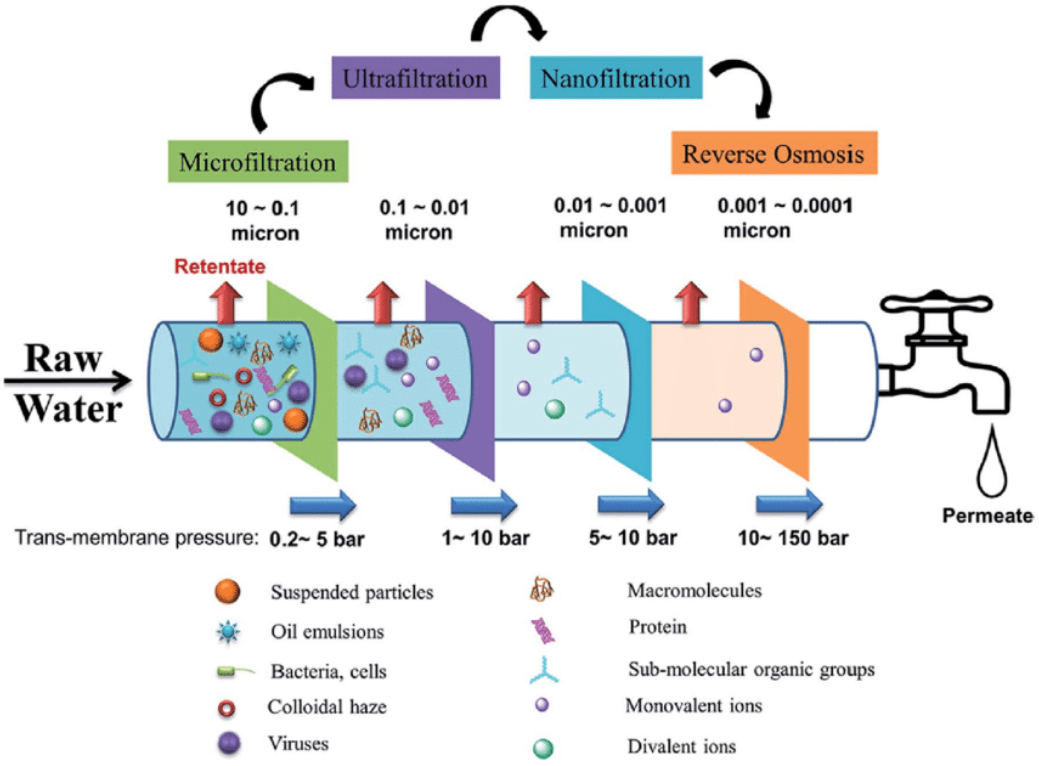

Figure 2.2. Membrane processes and separable solutes[12]

MF membranes are utilized in sterile filtration, particle (cell) removal, cell harvesting, and ultrapure water preparation for filtering large molecules such as bacteria and colloids. UF membranes are typically used for concentrating DNA, proteins, or polysaccharides, for antibiotics and virus clarification, and for buffer exchange. NF membranes retain solutes with molar mass ranging between 1 kDa and 3 kDa such as sugars[13], polypeptides, antibiotics[14] and multivalent ions[15] at pressure between 10 to 30 bar. Size-based

molecular sieving and Donnan exclusions arising from repulsion of charged species and membrane are two mechanisms involved in NF process. RO membranes retain solutes below 1 kDa molar masses and are used to concentrate low molecular weight substances such as salts, amino acids and sugar solutions[16,17]. RO processes require pressure in excess of the osmotic pressure of the feed, to force the solvent through the membrane via solution-diffusion mechanism where transport is governed by the solubility and diffusivity of the penetrant in the membrane.

The differentiation of the membrane unit operations should be done based on the area of application as not all the classified membranes are employed in all process steps. Microfiltration membranes are integrated into downstream bioprocessing along with ultrafiltration membranes for the initial harvest to obtain high concentration of cells and removal of debris to protect the subsequent purification steps. The application of reverse osmosis and nanofiltration membrane processes is not that common due to lack of separation problems concerning less than 0.01 µm molecular size at very high operational pressure, high volume, and low target molecule amount in the feed[11]. Hence, from an economic standpoint integration of those membrane processes is not feasible[18] and therefore not included in the further discussions.

In the field of biotechnology including biopharmaceutical, typically sequence of separations steps are integrated in a process. These separation steps mainly consist of micro- and ultra-filtration, operated in static (dead-end) or dynamic (cross-flow) mode illustrated in Figure 2.3.

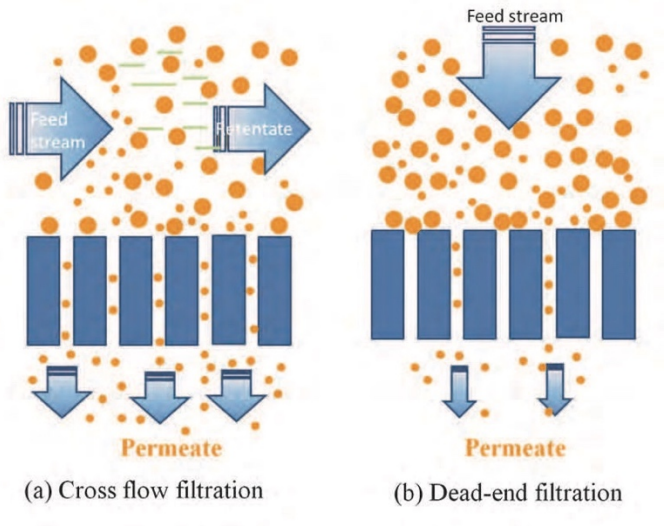

Figure 2.3. Different mode of operations for filtration processes: Dead-end vs Cross-flow[19]

Dead-end filtration is characterized by the feed flowing perpendicular to the membrane surface. The particles bigger than the membrane pores are rejected in the membrane structure or at the surface; permeate is typically product stream. While operational simplicity is an advantage, rapid deposition of solutes and particles directly into the membrane leading to fouling is a major disadvantage of dead-end filtration. The selectivity and flux can be enhanced to increase the lifetime by utilizing composite membranes with graded pore-sizes, and implementing additional separation mechanism through electrostatic and hydrophilic surface modifications. Dead-end filtration in biotechnology has been successfully implemented for clarification of antibody solutions[20,21], for decontamination of protein solutions prior to chromatography[22], for removal of DNA from cell cultures[23], and for standard sterile filtration step to lower the bioburden.

Cross-flow or tangential flow filtration is characterized by the feed flowing parallel to the membrane surface and retentate typically is product stream. The formation of filtration cake is minimized and an equilibrium is reached between increase and decrease of filtration cake. Cross-flow filtration is mainly used for high volume feed stocks with a relatively high amount of membrane blocking substances.

2.2 Membranes for biotechnology

MF and UF membrane processes use porous membranes, while NF and RO processes use non-porous or dense membranes. Majority of the membranes used in biotechnology are porous membranes with various functional properties depending on the application. This section emphasizes on the properties of porous membranes, transport through the porous membranes, and discusses the applications of porous membranes in biotechnology by demonstrating several examples.

2.2.1 Porous membranes

Porous membrane concerned with biotechnology are further classified based on the morphology and is depicted in Figure 2.4.

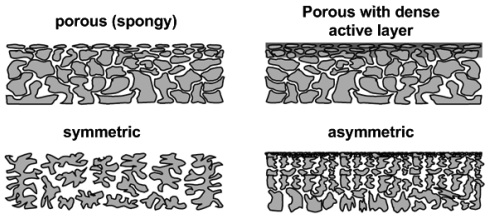

Figure 2.4. Classification of membranes based on the morphology[24]

Porous membranes are manufactured from a variety of materials such as polymers (e.g., PES, PTFE, PVDF), ceramics (e.g., aluminum, zirconium oxide), glasses (e.g., borosilicate glass fiber), and metals (e.g., silver and stainless steel). However, majority of the membranes utilized in bioseparations are produced via synthetic polymers. Regenerated cellulose, hydrophilic polyether sulfone and hydrophilic PVDF are most commonly used membrane materials[25] due to their low protein binding ability property. The choice of membrane is driven by the material requirements which define structural properties and macroscopic characteristics like thermal, chemical, and mechanical stability along with microscopic characteristics like the specific component permeability. Based on the technique used for membrane preparation, the underlying pore morphology varies significantly. Porous membranes usually have an isotropic network of polymer fibers due to a highly interconnected pore structure with a broad pore size distribution. The pore size rating typically refers to the size of particles or molecular weight that have more than 90 % retention. The retention is defined as follows:

$$R = \left(1 - \frac{C_{permeate}}{C_{feed}}\right) \times 100\ \%$$

For a porous membrane to be used for a bioprocess application following requirements should be taken into account[11]:

- Uniform flow distribution,
- Mechanical, thermal, and chemical stability,
- High throughput volume,
- Low protein binding, and
- Economic production,

Generally, for bioprocessing applications membranes are integrated into modules to enhance the mass transport. An ideal module should satisfy the following requirements:

- High packing density,

- Good cleanable and sterilizable,
- Low pressure loss,
- Low polarization affects, and
- Testability.

2.2.2 Transport through porous membranes

This section introduces an overview on mass transfer mechanism in porous membranes which impacts the permeate flux and selectivity. Mass transfer through porous membranes is a complicated phenomenon and cannot be explained accurately by any unified theory due to the varying chemical nature of membrane materials: hydrophilic, hydrophobic or charged; that affects membrane-solvent interactions further influencing mass transport. The structural parameters of the porous membranes are closely linked to the transport and separation mechanism. Figure 2.5 depicts the fundamental structural properties of porous membranes.

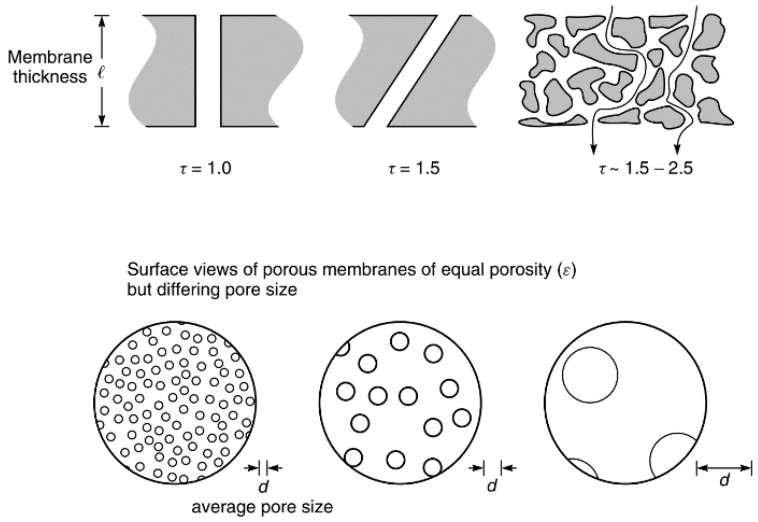

Figure 2.5. Representation of structural properties of porous membranes: tortuosity (top), porosity and pore size (bottom[26])

Tortuosity is the ratio of pore length to selective layer thickness and lies between 1.5 to 2.5; at lower tortuosity molecules permeate quicker due to the shorter channel length. Porosity is the measure of membrane void volume compared to the total bulk volume and ranges between 30 % to 80 %. Although higher porosity increases permeate flux but also decreases the mechanical stability[26].

Pressure-driven convective flow transport through porous membranes is commonly described by two approaches based on the pore flow model in capillary tubes that assumes membrane pores to be ideal: evenly sized and distributed cylindrical pores.

The first approach makes use of the differential momentum balance equation and Newton's law of viscosity to describe the laminar fluid flow through the cylindrical capillaries[27,28]. Upon integration, the popular Hagen-Poiseuille equation to calculate the permeate flux for the convective velocity through the porous membrane is shown below:

$$J = \frac{\varepsilon . d^2_{pore}}{32 . \mu . \tau} . \frac{\Delta p}{l_{pore}}$$

Where, τ is the tortuosity of the capillaries and d_{pore} is the diameter of the capillaries.

Furthermore, Darcy's law is the basic equation that can be employed for the porous medium to describe the rate of fluid flow through cylindrical pores and therefore enabling the calculation of the membrane area for a targeted separation at given conditions. The equation describing Darcy's law is shown below:

$$Q = \frac{-k\,A}{\mu} . \frac{(P_b - P_a)}{L}$$

Where, Q [m^3/s] is the volume flow rate, k [m^2] is the empirical constant for permeability of the medium, A [m^2] is the cross-sectional area to flow, $(P_b - P_a)$ is the pressure drop, μ [kg/(m.s) or Pa.s], is the viscosity and L [m] is the membrane thickness.

However, mass transfer calculations for membranes used is much more complicated due to irregular shapes and connectivity[29].

In the second approach, the Kozeny-Carman equation can be applied when membranes resemble an arrangement of near-spherical particles[30]:

$$J = \frac{\varepsilon^3}{K . \mu . S^2 (1 - \varepsilon)^2} . \frac{\Delta p}{l_{pore}}$$

Where, J is the permeate flux, Δp is the pressure drop, ε is surface porosity, K is a constant, μ is the dynamic viscosity of the permeate, S is the specific area per unit volume, and l_{pore} is the thickness of the porous layer.

The dominant mechanism governing the separation of porous membranes is sieving effect: rejection of molecules or particles larger than the membrane pores at the membrane surface (see Figure 2.6).

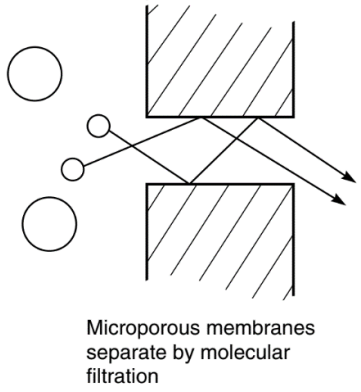

Figure 2.6. Size exclusion mechanism in a porous membrane[26]

Feed components are captured or adsorbed during the membrane-solvent interaction through different separation phenomena. This occurs during the dead-end filtration when components are small enough to enter the membrane. But they are stopped from permeating because of one or more of the four scenarios shown in Figure 2.7. Therefore, in addition to the sieving effects particles could be captured inside the pores by either electrostatic adsorption, Brownian diffusion, or inertial impaction.

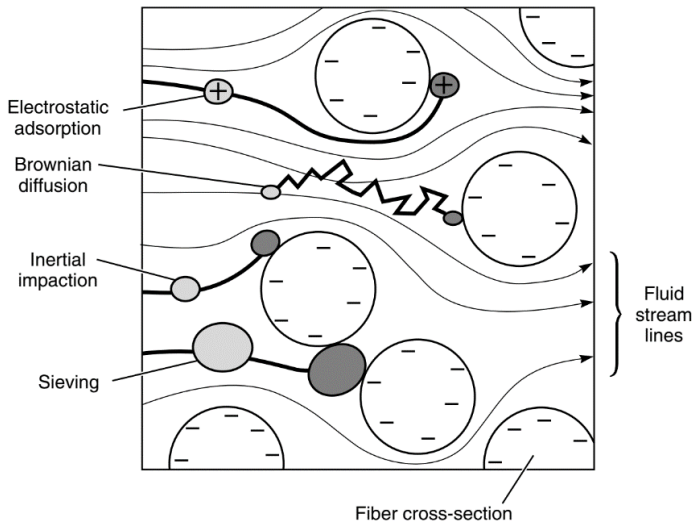

Figure 2.7. Capture mechanism inside the porous membrane[26]

2.3 Porous membrane applications in biotechnology

Membrane processes were explored for bioseparations even before the emergence of the advanced membrane industry. J. D. Ferry[31] in 1936 reported the employment of membrane technology for various applications such as enzyme concentration, sterile filtration, protein free cell culture preparation, and analysis of bacteriophages and viruses. However, these systems were limited to analytical-scale operations due to the shortcomings of the available membranes. Variety of new membrane materials resistant to fouling, and better chemical stability are being developed to overcome the shortcomings. Currently porous membranes are widely used throughout the production, formulation, and purification of biotechnology products. This section discusses in brief the various representative applications of the microfiltration membranes.

MF membranes are extensively used in dead-end configuration for sterile filtration for bacteria removal before formulation of many products, and for cell debris removal suspended in the fermentation broth during the initial clarification. Typically, 0.2 µm pore size membranes are used for sterile filtrations which are validated by absolute removal of Brevundimonas diminuta[32]. Furthermore, to prevent the passage of smaller microorganisms some users use 0.1 µm pore size membranes to assure the enhanced sterility[33].

Additionally, MF depth filters have been specifically developed for the removal of submicron colloidal and insoluble particles from the process streams to reduce the bioburden prior to a terminal sterilization step[32]. Many processes now also employ a pre-filter with larger pore size before a normal flow filter to improve the product yield and throughput.

Mammalian cell lines are often utilized in the production of proteins with therapeutic, or diagnostic applications. But the cell lines could be contaminated with viruses or other unwanted particulates introduced by addition of supplements during the fermentation process, or through manual handling or manipulation during processing[34]. Another important application of MF is to separate viruses from the valuable proteins[35,36].

Moreover, MF is also exploited in antibiotic production such as penicillin G, where it is used for the removal of biomass before recovering them from their fermentation broths subsequently via solvent extraction and subsequent crystallization[37–39]. Filtration in

combination with diafiltration is also used to obtain very high yields for the initial recovery of antibiotics.

Better understanding about the effects of solution environment, membrane properties and process hydrodynamics have also let to notable improvements in filtration performances (UF and MF). For instance, numerous recent studies reported controlled rate of protein transport through membranes by manipulating solution pH and/or the ionic strength[40–42]. The studies reported higher efficiency of the process when operated at the IEP of the transmitted protein and away from the retained protein. The separation is enhanced at low ionic strength which increases the thickness of the double layer of the charged solute, leading to higher retention, readily permeating the uncharged solute through the membrane. These electrostatic interactions can further be exploited in several other bioseparations processes to increase the efficiency. Charlton et el. demonstrated removal of particles smaller than the pore size such as viruses and DNA by electrostatic interactions[23].

The manufactured membranes are further installed into an application-specific arrangement called membrane modules for a more practical and manageable use in technical processes. Module configurations in addition to the membrane remarkably improve the membrane device performance[25] by enhancing the mass transfer. Commercially available configurations include hollow fiber, spiral wound, plate and frame, tubular and vortex flow devices. Some examples of modules configurations are shown in Figure 2.8.

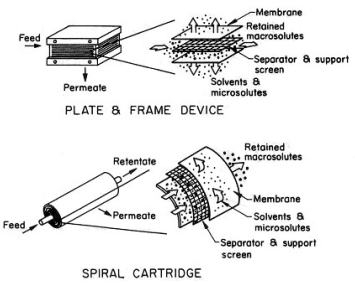

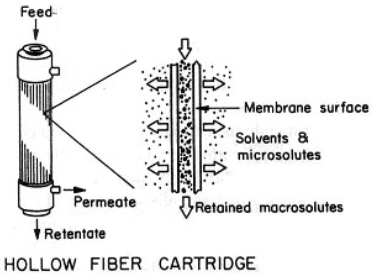

Figure 2.8. Certain examples of the module configurations[43]

MF competes with centrifugation and expanded-bed chromatography for the initial clarification of therapeutic products from cell cultures (mammalian, yeast, and bacteria) but has several advantages over centrifugation: lower operational cost, less time-consuming, requires no additional clarification prior to purification and most importantly is scalable and hence can operate with high volumes[2].

2.4 Membranes for extracellular vesicle separation

This section provides insights into the role of membranes in the emerging field of extracellular vesicles (EVs). EVs are membrane covered heterogenous group of nanoparticles detected in the bodily fluids such as urine, blood, synovial fluid and breast milk[44], secreted by cells of all tissues and organs in both healthy and pathological origins. There are two major categories of EVs (see Figure 2.9): exosomes (30 – 100 nm) as a result of fusion of intracellular multivesicular bodies with the plasma membrane[45] and microvesicles (100 – 1000 nm) which result from the outward budding of the plasma membrane[46].

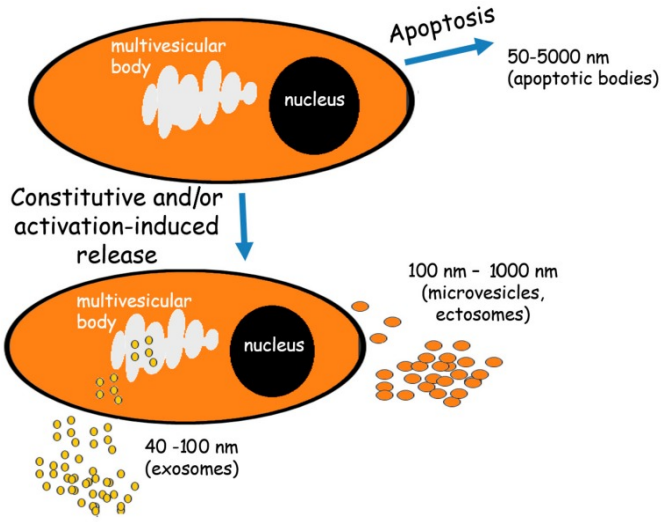

Figure 2.9. Origin of different types of extracellular vesicles from the cells[47]

EVs are composed of vital biologically active molecules: proteins, lipids, DNA and RNA carrying the information about the functional state of the parental cells. EVs have been reported to be a major player in intracellular communication and transport of molecules with potential diagnostic significance[48]. Due to these properties, EVs have gained a lot of interest in recent years for its potential as biomarkers[49], drug delivery vehicles[50] and therapeutic agents[51] majorly in cancer treatment, and cardiovascular diseases.

However, isolation of EVs is a challenging task and requires standardized and reliable methods. The traditional methods to enrich EVs from biofluids involve centrifugation and ultracentrifugation. These however, require dedicated expensive equipment, long run times, and result in low yields due to aggregation of proteins, and non-EV related contaminations[52]. Studies have also proposed various chemical agents to facilitate EV isolation by altering the solubility or dispersity of EVs in the biological fluids. However, uncertainty of reagents to distinguish between exosomes, microvesicles and protein aggregates remains a concern[46]. Recent microfluidic and immunoaffinity based techniques are promising for some applications but the limited sample throughout volume and lack of validation methods are major disadvantages[53]. Nevertheless, scalable and reproducible concentration of EVs from complex biological fluids prior to isolation remains a major challenge. Filtration is fast, robust, easy to use and cost effective making it a promising technique for concentration and purification.

Filtration can be utilized to separate EVs from the larger contaminants such as cell debris before isolating them with sophisticated techniques like chromatography. Several

isolation protocols have been proposed in the literature which implement filtration. Lamparski et al.[52] proposed tangential flow filtration and ultracentrifugation to harvest exosomes from cell culture supernatants which has been implemented in clinical trials[54,55]. This method utilizes ultracentrifugation that is incompatible with high throughput volumes and subsequently with development of clinically operable EV diagnostics or therapies. Heinemann et al. demonstrated simplified, robust, and clinically applicable method for exosome isolation from biofluid using sequential filtration steps of dead-end filtration, tangential flow filtration, and low-pressure dead-end track-etched membrane filtration (see Figure 2.10). This approach yields high purity exosomes with defined size distribution, free of proteins, larger EVs, and cell debris as confirmed by nanotracking analysis, electron microscopy, and mass spectroscopy.

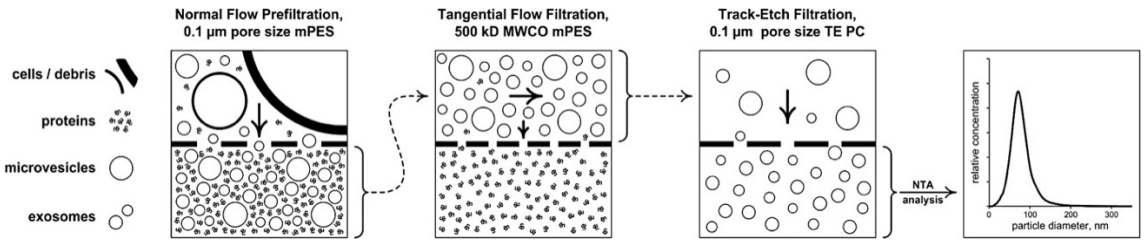

Figure 2.10. Sequential filtration steps for isolation of exosomes from cell supernatant

The membrane filtration is used sporadically for EV filtration due to the challenges posed by the EVs: low concentration, soft morphology making them prone to deterioration, and variable properties depending on the origin. The widely used membranes for EV isolation protocols are ultrafiltration and microfiltration membranes based on PES and PVDF. However, the current membranes suffer from fouling, non-specific binding, high extractables and loss of coating resulting in low yields[56]. The membranes have different binding capacities depending on the EVs and the type of membrane, therefore choice of filter severely impacts EV recovery.

In the last decade, the field of extracellular vesicles has made promising developments particularly in therapeutics and diagnostics including early detection of cancer as suggested by the growing publications[57]. However much remains unexploited for membrane filtration application in EV isolation. Hence, EV field has attracted a lot of attention from the membrane industry due to the untapped market and a lot of work is being carried out in developing membranes specifically for EV isolation.

2.5 Challenges for membrane processes in biotechnology

Application of filtration technology in bioseparation utilizes membrane filters which are ideally mechanically and thermally stable, and chemically inert in addition to having desirable surface properties which include wettability, low protein binding, biocompatibility, and controlled surface chemical reactivity. Most of the membranes employed in biotechnology applications are obtained by surface modification of a base membrane. The poor selectivity leading to low yields and inefficient membrane filtration could be more often traced back to poor membranes and filtration related adverse effects such as concentration polarization and fouling. This section discusses the phenomena of concentration polarization and fouling in detail.

2.5.1 Polarization and fouling phenomenon

In pressure driven membrane processes, especially microfiltration and ultrafiltration severe flux decline can be caused due to several factors such as concentration polarization, adsorption, gel layer formation, and pore plugging. These factors bring about additional resistance on the retentate side to the transport across the membrane. The convective flux in a pressure driven membrane process is given below.

$$J = \frac{\Delta P}{\eta R_{tot}}$$

Where, ΔP is the pressure difference, η is the viscosity of the feed solution and R_{tot} is the total resistance. Total resistance is the sum of various resistances toward the mass transport across the membrane during pressure driven filtration as shown below:

R_{tot} = R_m (membrane resistance) + R_{cp} (concentration polarization resistance) + R_g (gel layer resistance) + R_p (pore-blocking resistance) + R_a (adsorption resistance)

Resistance caused by the accumulated retained molecules near the membrane surface on the feed side due to formation of a concentrated layer is called concentration polarization. When the concentration of the accumulated solute molecules becomes very high it forms a layer exerting gel layer resistance. Furthermore, pore blocking and adsorption resistance arise upon membrane fouling caused by the solute particles blocking inside the membrane pores. Flux-decline due to concentration polarization and fouling including protein

binding/adsorption (although distinguishable but not completely independent of each other) are discussed in a greater detail in the following sub-sections.

2.5.1.1 Concentration polarization

During the membrane filtration process, when the driving force (pressure) acts on the feed solution solvent flows to the permeate side where as solutes are retained on the feed side. The concentration of the retained solutes gradually increases as they accumulate near the membrane surface. Consequently, the increased concentration generates diffusive flow back into the feed bulk but a steady-state is established after a certain period of time as the convective transport towards and diffusion away from the membrane balance in a continuous filtration process[43]. A concentration profile is generated (see Figure 2.11) in the boundary layer (thickness δ) as a result of mass balance.

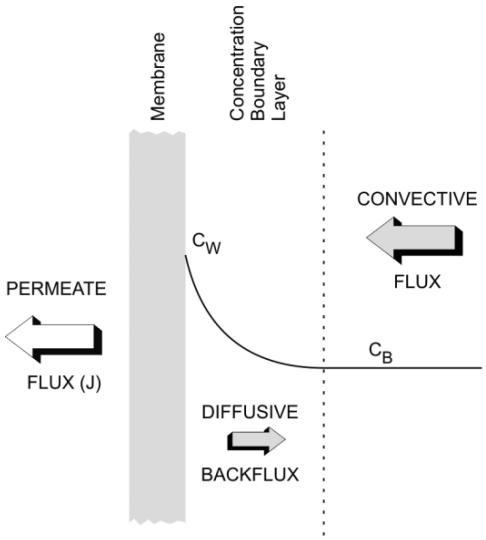

Figure 2.11 Concentration polarization under steady state conditions in a pressure driven membrane filtration process[58]

The film theory model describes mass balance and concentration polarization mathematically[26,59]:

$$J_{C_p} = J_{C_B} - D_i \frac{dc}{dx}$$

Where J is the permeate flux, D_i is the diffusion coefficient of solute i, c_p is permeate concentration, c_B is feed concentration, and $\frac{dc}{dx}$ is change in concentration with distance from the membrane surface.

The above equation can be integrated over the boundary layer thickness resulting in:

$$\frac{c_W - c_p}{c_B - c_p} = e^{\frac{J\delta}{D}}$$

Where c_W is the concentration at the membrane surface.

For complete retention of the solute i, $c_p = 0$ and thus the above equation becomes:

$$\frac{c_W}{c_B} = e^{\frac{J\delta}{D}}$$

This concentration polarization reaction illustrates the effect of polarization on flux and mass transfer coefficient ($k = \frac{D}{\delta}$).

The consequences of concentration polarization on the flux and selectivity of the filtration process can be summarized as follows:

- Lower selectivity: The calculated retention can be lower than the actual retention due to the increased solute concentration at the surface. For e.g., in case of low molecular weight solutes.
- Higher selectivity: For the mixture of solutes, higher molecular weight solutes retained at the surface form a layer increasing the retention of low molecular weight solutes.
- Lower flux: The high concentration of the solute in the boundary layer can increases the flux resistance, therefore decreases the permeability.

Hence, often concentration polarization is a precursor for membrane fouling[59].

2.5.1.2 Membrane fouling

The phenomenon of irreversible deposition of undesirable particulate matter (colloids, particles, emulsions, macromolecules, salts, etc.) from the process fluid onto the membrane surface and/or pores is defined as membrane fouling. Fouling not only affects the membrane selectivity but also causes flux decline increasing the process time, decreasing the membrane life and hence increasing the operating cost. Membrane fouling remains a bottleneck challenge for membrane technology in bioprocessing applications[60,61].

Microfiltration and ultrafiltration processes are mainly prone to fouling because of the susceptibility of the porous membranes to fouling. These membranes are used to remove bacteria, cell debris, insoluble aggregates, and particles from feedstock solutions, to protect downstream units from contaminations. Fouling characteristics of the feed solution determine the capacity of the filter. Therefore, for pressure driven processes the extent of fouling depends on type of separation and type of membrane used. Generally, four types of foulants can be distinguished: Colloidal: silica, polystyrene, clay, etc., Organic: macromolecules, biological substances, etc., Inorganic: metal hydroxides, calcium salts, etc., and Biofouling: bacterial cell film at the membrane surface. However, colloidal and organic fouling are the most relevant in bioprocessing applications hence are extensively discussed in this thesis.

The flux decline due to fouling can be calculated mathematically based on the filtration model. The deposition of particles at the membrane surface is said to form a "cake layer" which resists (R_c) the mass transport during filtration in addition to the membrane resistance (R_m). The cake filtration model is usually used to determine the fouling index. The flux (J_v) during the filtration at a given driving force (ΔP) is given by[43]:

$$J_v = \frac{\Delta P}{\eta\,(R_m + R_c)}$$

Where $R_c = l_c\ (\text{cake thickness}).\, r_c(\text{specific cake resistance})$ and r_c is assumed to be constant over the cake layer.

The specific cake resistance can be expressed by the Kozeny-Zarman relationship:

$$r_c = 180\,\frac{(1-\varepsilon)^2}{[(d_s)^2\varepsilon^3]}$$

Where, d_s is the solute diameter and ε is the porosity of the cake layer. The cake layer thickness (l_c) is given by:

$$l_c = \frac{m_s}{[\rho_s(1-\varepsilon)A]}$$

Where, m_s is the mass of the cake, $\rho_s$is the solute density, and A is the membrane surface area. The mass of the cake is complex to determine but the effective thickness is usually several micrometers which includes many monolayers of macromolecules[62]. Moreover,

the cake layer thickness depends on the solute type (soft or hard particles) and more importantly on the operating conditions and time. As the layer grows with accumulating solutes the flux declines.

The cake layer resistance in case of complete solute rejection (R = 100 %) can be obtained from mass balance:

$$R_c = \frac{r_c\, c_b V}{c_c\, A}$$

Therefore, now the flux can be written as:

$$J = \frac{1}{A}\frac{dV}{dt} = \frac{\Delta P}{\eta\,[R_m + \frac{r_c\, c_b V}{c_c\, A}]}$$

Generally, membrane resistance is neglected and the above equation is integrated from t = 0 to t = t:

$$t = \frac{\eta\, c_b\, r_c}{2\, \Delta P\, c_c}\left(\frac{V}{A}\right)^2$$

The above equation shows a typical relationship for unstirred dead-end filtration with $V \approx t^{0.5}$. The flux behavior can be represented as:

$$J = \left(\frac{\Delta P\, C_c}{\eta\, c_b r_c}\right)^{0.5} t^{-0.5}$$

The equation suggests that the flux decline is determined by the cake layer formation: several theories have been developed to explain the fouling mechanism for cake formation but since it is a very complex phenomenon involving contributions from multiple processes, a single equation cannot be applied. However, a simplified empirical equation below is often used because it has contributions through the variable exponential factor:

$$J = J_0 t^n \qquad n < 0$$

Where, J is the actual flux, J_0 is initial flux, and n is the function of the cross-flow velocity.

Membrane fouling is a complex phenomenon with multiple dependent physical and chemical parameters such as concentration, temperature, pH, ionic strength, and specific interactions: dipole-dipole, hydrogen bonding. The membrane fouling experienced by the membrane as a result of membrane-particle interaction was first studied by Hermia[63]. Hermia related flowrate (Q) and time (t) to identify and distinguish four models of fouling patterns as shown in Figure 2.12.

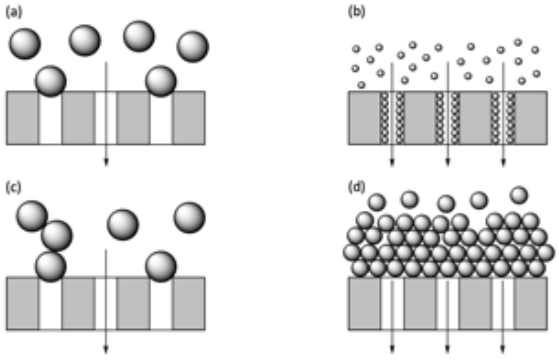

Figure 2.12. Fouling patterns during particle filtration: (a) complete blocking, (b) standard blocking, (c) intermediate blocking, and (d) cake layer formation[64]

Flux decline is typically analyzed based on one of the classical fouling models caused by pore blockage, by accumulation of particles on the upper surface of the membrane, or due to adsorption within the pore structure. Table 2.1 summarizes the governing equations for each model expressed in terms of the filtration time (t) and cumulative volume (V) for the flowrate (Q) at constant pressure operation and the transmembrane pressure (P) at constant flow operation.

Table 2.1. Governing equations for the classical fouling models at constant pressure and constant flow rate operation[2]

Constant pressure	Flow rate	Linearized form
Pore blockage	$\frac{Q}{Q_0} = \exp(-\beta t)$	$\ln(Q) = at + b$
Intermediate blockage	$\frac{Q}{Q_0} = (1+\beta t)^{-1}$	$\frac{1}{Q} = at + b$
Pore constriction	$\frac{Q}{Q_0} = (1+\beta t)^{-2}$	$\frac{t}{V} = at + b$
Cake filtration	$\frac{Q}{Q_0} = (1+\beta t)^{-\frac{1}{2}}$	$\frac{t}{V} = aV + b$

Constant flux	Pressure	Linearized form
Pore blockage	$\frac{P}{P_0} = (1 - \beta t)^{-\frac{1}{2}}$	$\frac{1}{P^2} = a - bV$
Intermediate blockage	$\frac{P}{P_0} = (1 - \beta t)^{-1}$	$\frac{1}{P} = a - bV$
Pore constriction	$\frac{P}{P_0} = (1 - \beta t)^{-2}$	$\frac{1}{P^{\frac{1}{2}}} = a - bV$
Cake filtration	$\frac{P}{P_0} = 1 + \beta t$	$P = a + bV$

For all equations it is assumed that the fouling rate is proportional to the aggregation of foulant at the membrane, without any back-transport or detachment mechanisms. The deposition of foulants on the external surface of the membrane leading to additional flow resistance is explained by cake filtration model. In the rest of the fouling models, the membrane pores are assumed to be parallel array of uniform cylindrical pores. Reduction of the pore size upon fouling within the membrane occurs in the pore constriction model. The standard and intermediate fouling models assume clogging of the pores by the foulant, where particle superposition takes place on the external membrane surface in the intermediate blockage model.

However, during the filtration the underlying fouling mechanism is a combination of fouling patterns. Therefore, simple fouling models are not enough to analyze the flux decline data. The transition in fouling behavior during the filtration has been reported by Ho and Zydney[65] with experimental evidence, where the initial flux decline is caused by pore constriction and/or pore blockage followed by cake layer formation. At the initial stages of filtration protein aggregates and cell debris deposited on the membrane surface are assumed to partially allow fluid flow after blocking the pores. As filtration progresses complete blocking takes place by cake layer formation over the regions that were already blocked by the initial deposition. The flowrate for the filtration run with transitioning fouling models was approximated by Ho and Zydney[65]:

$$\frac{Q}{Q_0} = \exp(-\beta t) + \frac{R_m}{R_m + R_p}[1 - \exp(-\beta t)]$$

Where $R_m = 1/L_p$ is the clean membrane resistance and R_p is the growing deposit resistance:

$$R_p = (R_m + R_{p0})\sqrt{1 + \alpha t} - R_m$$

Where R_{p0} is the initial deposit resistance and α is proportional to the specific resistance of the growing cake layer.

The combined fouling models for the pore blockage have been extended to include the effects of the complex pore morphology, including asymmetric structure[65] and pore interconnectivity[66] which allows partial fluid flow through the interconnected pores upon blockage reducing the flux decline.

Although membrane fouling remains a problem for bioprocessing applications[61], recent developments of composite membrane structures have enhanced particle removal with high overall throughput. Composite membranes consisting of multiple layers with different pore size and/or surface chemistry efficiently remove particles by surface sieving, depth filtration, and adsorption[2]. Recent reports of transport in composite membranes and fouling mechanisms[67] provide deeper insights which could potentially improve membrane performance.

2.5.1.3 Protein binding

Proteins are a valuable ingredient in the biological solution which have high tendency of adsorption onto the exposed membrane surface due to the high internal surface area. This phenomenon not only leads to the loss of valuable proteins but also results in reduction of the membrane permeation rate and influences the membrane retention by affecting the surface chemistry. Therefore, it is important to evaluate membranes for protein adsorption. Many have reported the protein adsorption mechanism in the literature[68–71]; however, protein adsorption is still not fully understood. Protein binding is a complex phenomenon that depends on multiple factors such as operating conditions[72,73], solution chemistry[74–80], surface physiochemical conditions[81,82], and pore morphology[67,83].

Protein binding to the membrane can be explained by understanding the thermodynamics between foulant, membrane surface, and solvent system. The thermodynamic principle states that, every system tries to minimize its Gibbs free energy. The protein binding

process for different surface types in terms of Gibbs free energy is exhibited in Figure 2.13.

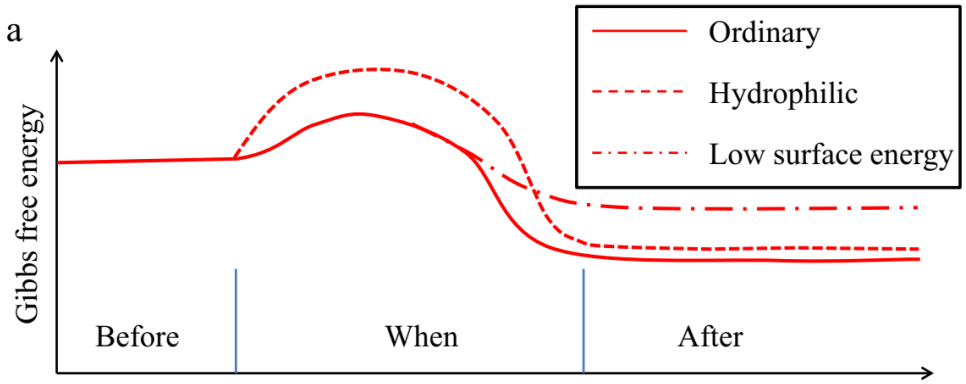

Figure 2.13. Gibbs free energy in stepwise adsorption of protein[84]

For instance, when water dissolved protein advances towards the membrane surface, its tertiary structure is disordered and it consequently loses its integrated water molecule which is accompanied by temporary increase in Gibbs free energy. However, when new attractive interactions such as electrostatic, hydrogen bonding or van-der-Waals forces are formed, the Gibbs free energy of the system decreases. Therefore, thermodynamics drives the protein adsorption which varies based on the physico-chemical surface properties. Hydrophobic surface show highest gain in Gibbs free energy upon adsorption, but hydrophilic surfaces manipulate the structure of the approaching proteins due to the presence of a hydrophilic barrier[85]. Figure 2.14 demonstrates conformational change in protein structure upon adsorption.

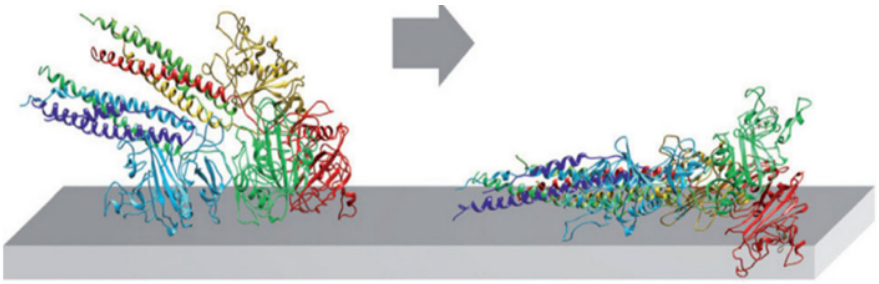

Figure 2.14. Conformational change of protein structure upon adsorption[86]

Generally, static adsorption method: simple submerging of the membrane in the protein solution, and dynamic adsorption method: membrane filtration, have been used to characterize protein adsorption properties in porous membranes. The different methods used estimate the contribution of adsorption to the overall filtration resistance are reported in the literature[87,88]. Although Nakamura and Matsumoto suggested different isotherms

for static and dynamic methods, the effect of flow through the pores on adsorption is not yet understood due to the difficulty in differentiating between the protein adsorption in the pores and on the surface.

Fundamentally, the adsorption of proteins onto the membrane surface including within the pores is determined by the electrostatic and hydrophobic interactions[10]. Typically, membranes with similar zeta potential to that of proteins lead to protein binding[74,77,78]. Since majority of the polymers used for the manufacturing of the membranes are hydrophobic, they are typically surface treated with hydrophilic macromolecules or ionic surfactants to reduce protein adsorption[89]. Therefore, two different approaches are usually adopted by the manufacturers to minimize protein binding. First, surface modification of commonly used membranes such as PES, PVDF, and PTFE. Second, fabrication of membranes from low protein binding materials.

2.6 Anti-fouling membrane development techniques

Majority of the polymers used for the membrane preparation are hydrophobic in nature making them susceptible to fouling. Moreover, polymers such as PVDF have very low surface energy (25 mN/m) resulting in poor wettability by water. It is well known that hydrophilic surfaces prevent the non-specific interactions with water subsequently preventing adsorption of foulants on the surface[90]. PVP is most commonly used polymer to obtain hydrophilic surfaces for commercial membranes. Because of its hydrophilicity and biocompatibility PVP is widely used to prevent fouling[91] by generating hydrophilic surfaces. Bi and coworkers[92] prepared hydrophilic PVDF membrane by crosslinking PVP to obtain hydrophilic surface with antifouling properties. Pieracci et al.[93] reported reduction in biofouling upon grafting PVP on PES membrane by photo initiation. Other than the hydrophilic feature the fouling resistant surfaces can be hydrogen bond donor[86,94], possess surface charge and can be responsive to the external stimuli such as pH and temperature depending on the functional polymer used for coating.

Polyacrylic acid modified membranes are known for their pH responsive behavior owing to the deprotonation of carboxyl chains depending on the pH. This behavior has been exploited to utilize the pH responsive materials for several purposes such as affinity membranes[95], drug delivery[96] and antifouling membranes[97]. The pore walls of the porous membranes grafted with polyacrylic acid can reversibly change the permeability and/or selectivity by alteration of the effective pore diameter as a result of conformation change

of the chains as a function of pH. The polyacrylic acid chains grafted on the outer surface of the membrane can influence the adsorption and fouling properties. Moreover, the pH-responsive binding or release to and from the chains can be further exploited depending on the application.

The fouling resistant strategy is mainly based on two mechanisms: the steric repulsion and formation of the hydration layer as shown in Figure 2.15. Adsorption of foulants on the hydrogel layer restrains the polymer chain mobility creating unfavorable entropy loss, therefore making adsorption entropically unfavorable[98]. Furthermore, through hydrogen bonding or ionic solvation a hydration layer is created on the surface that effectively prevents fouling[99]. Additional strategies to prevent fouling such as through electrostatic repulsion can also be implemented by introducing appropriate functional polymers on the surface.

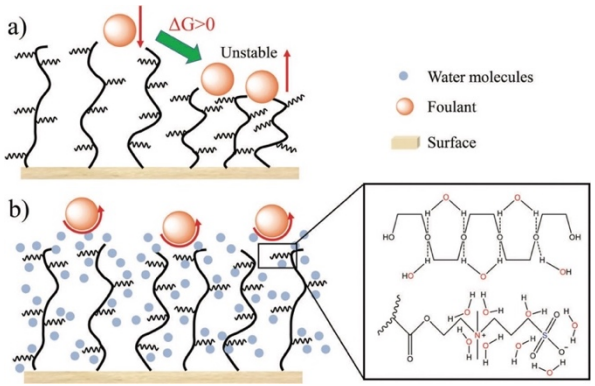

Figure 2.15. Two main mechanisms for fouling resistance strategy: (a) steric repulsion driven by entropic instability and (b) hydration layer formation on the membrane surface upon hydrogel grafting[90]

This section discusses the widely used techniques to not only overcome fouling but also to obtain thermally, mechanically, and chemically stable membranes with low extractables. Although morphological properties such as pore size distribution, porosity, tortuosity, and thickness have inarguable influence on fouling; the emphasis here is placed on the hydrophilic modification via various pathways. Versatile methods have been explored for modification of the membranes in the recent years. Advanced functional polymers for 'tailored' membrane synthesis and surface modification of the base membrane are two important techniques for obtaining fouling resistant hydrophilic membranes with diverse properties.

2.6.1 'Tailored' membrane formation

In order to achieve special surface properties in a one-step process using tailored macromolecules, two approaches can be utilized: membrane preparation from functional polymer, and addition of a functional polymer as a component during membrane formation. The first approach results in different bulk properties of the membranes. Functional graft copolymers of PVDF or fluorinated polyimides reported by Kang et al.[100–102] and the work of Xu et al[103]. about acrylonitrile-based copolymers containing phospholipid moieties could be representative examples of the membrane manufactured by the first approach. The second approach is particularly attractive to obtain matrix polymer blends for tailored pore structure and functional polymer blends for tailored surface properties. The blends with hydrophilic polymers such as PVP are mostly used to manufacture commercial hydrophilized polysulfone (PSf) or polyethersulfone (PES) membranes. However, the fraction of PVP can be washed out during the filtration process with aqueous medium. In biomedical applications such as dialysis these membranes may cause a critical problem due to release of PVP[71]. Customized functional macromolecules such as surface-active amphiphilic block or comb copolymers from e.g., PEG or a fluorinated polymer with efficient anchoring offer a promising alternative for membrane formation[104–107]. Such membranes were characterized by hydrophilic properties and low surface energy. The advantage of integration of macromolecular additives into the membrane manufacturing is that no additional step is required moreover high surface activity means no additional material cost. However, such membrane in reality is equivalent of developing a novel membrane: base membrane with functional surface[108,109] which could be a complex process for a scale-up.

2.6.2 Surface modification

Surface modification of the membrane intends to minimize undesired (secondary) interactions (adhesion or adsorption) which lead to fouling, or to introduce supplementary interactions (affinity, responsiveness or catalytic properties) for enhancing the selectivity or even establishing a novel separation function[110]. Surface coating and surface grafting are two main categories of surface modification. Figure 2.16 demonstrates PVDF membrane surface modification by surface coating and surface grafting. Formation of a reactive coating usually by hydrogel layer formation on the surface is another surface modification strategy which combines the aspects of coating and grafting.

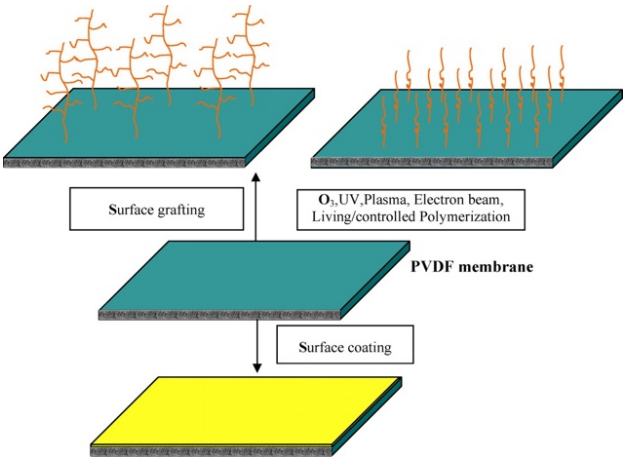

Figure 2.16. Representation of surface coating and surface grafting for PVDF base membrane[110]

Surface coating and surface grafting along with the formation of reactive hydrogel coatings are discussed in detail with demonstrating few examples from the literature in the following sub-sections.

2.6.2.1 Surface coating

In surface coating, a hydrophilic layer is simply coated on the hydrophobic surface to improve both the hydrophilicity and fouling resistance. The coated layer binds the base membrane through physical adsorption, cross-linking, or sulfonation. Several reagents have been reported for surface coating, for example PVDF membrane was modified by coating dilute polyvinyl alcohol (PVA) followed by solid-vapor interfacial cross-linking which resulted in increased water permeability[111]. Hydroxyl (-OH) and sulfonyl (-SO_3) groups are usually incorporated on the surface to obtain negative surface charge that retains particles smaller than the pore size due to electrostatic repulsions. But these groups could be oxidized in the air and intense sulfonation could affect the bulk and surface properties of the membrane decreasing the mechanical strength. In one study, PVP was introduced on the surface after alkaline modification to purify flavonoids from crude Gingko biloba extraction[112]. Boributh et al.[113] proposed a combined flow through and surface flow method to coat both membrane surface and pore walls with chitosan solution. In most cases glycerol is coated on the modified membrane to maintain the wettability during the transportation; which can be washed away before the operation.

However, the major problem with surface coating is the instability of the coated layer because of the weak bonding with the membrane which can be washed away during the

operation or cleaning process. Furthermore, often reduction in flux is observed due to unwanted accumulation of coated layer on the surface pores.

2.6.2.2 Surface grafting

In surface grafting, polymer chains are covalently bonded to the membrane surface offering chemical stability and avoiding delamination of the grafted chains unlike physical coating[114].

Surface functionalization by grafting can be achieved by grafting single or a mixture of two (or more) monomers with two different approaches[115]. 'Grafting-to' approach couples polymers to surfaces, while 'grafting-from' approach polymerizes monomers using initiation at the surface. Although, for 'grafting-to' method polymer to be coupled can be well controlled by synthesizes but the grafting densities achieved are limited. Whereas, for 'grafting-from' method surface anchored polymers are less controlled but grafting densities and chain lengths of choice can be obtained under favorable reaction conditions.

The chemical reactions to graft polymers on the membrane surface can be achieved by various pathways such as physical activation of chemical reactions using: high energy radiation (electron beam or gamma rays), plasma, and UV irradiation or chemical activation, for e.g., redox initiation. Moreover, recently "living"/controlled polymerization grafting such as atom transfer radical polymerization (ATRP) and reversible addition-fragmentation chain transfer polymerization (RAFT) have been widely utilized for better controlled, versatile, and ionic free radical polymerization[116–118].

'Grafting-to' reactions for introducing macromolecular functional layers on the membrane surfaces have been carried out by multiple ways in the literature. Direct coupling on cellulose derivatives[119], polyamides or polysulfones[120]; primary functionalization on the membrane with amino, carboxyl, or other reactive groups followed by coupling; adsorption and subsequent physically activated coupling via UV irradiation[121,122] or plasma[123]. Usually 'grafting-to' reactions are used to functionalize UF or MF membranes with hydrophilic macromolecules such as PEG or PVP, or with functional polymers like polypeptides or polysaccharides with an intention to reduce protein fouling and minimize non-specific binding.

'Grafting-from' reactions almost exclusively utilize radical polymerization reactions in aqueous or organic medium for surface grafting variety of functional monomers such as acrylates, acrylamides, or other functional vinyl monomers to obtain interesting surface properties. Figure 2.17 shows the schematics of some examples of 'grafting-from' reaction.

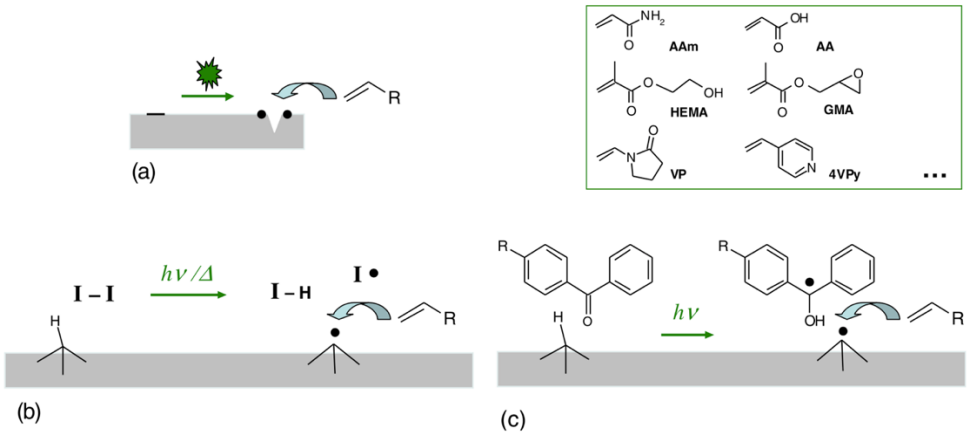

Figure 2.17. Grafting-from reaction to copolymerize functional monomers on membrane through different initiation processes: (a) physical excitation with plasma or radiation, (b) radical transfer in the solution generated by external energy such as heat or light, (c) photoinitiation to start the polymerization[110]

In addition to the physical activation (electron beam, UV irradiation, or plasma), graft polymerization by membrane polymer radicals has also been explored[114,124]. The polymer radicals in the presence of monomers can be used to create starter radicals[125–127]. UV-sensitive membrane polymers like PES can be directly functionalized via UV excitation in the presence of monomer, where starter radicals are generated via dissociation of the main chain[128–130]. Membrane material sensitivity and excitation conditions are the main limitations for physical activation techniques which under unfavorable conditions cause undesired changes of membrane morphology and/or uneven modification. Generation of radicals by chemical methods for functionalization without any external means could be implemented for membranes in modules. For example, generation of starter radicals via decomposition of peroxides in a solution containing membrane material[131,132]. Initially coupled monomer during functionalization can be used to attach growing polymer during polymerization in the solution which could yield branched and cross-linked chains[133].

2.6.2.3 Reactive coating

Formation of an anti-fouling reactive coating typically involves hydrogel layer formation on the surface. A class of three-dimensional cross-linked hydrophilic polymer networks insoluble in water are known as hydrogels. In aqueous medium, hydrogel mass consists

of up to 99% of water due to their tendency of swelling. Hydrogels are highly permeable and demonstrate less friction with surrounding matter as a result of combination of characteristics such as high-water uptake, elastomeric rubber-like properties, soft morphology, and highly porous networks. These features make hydrogel a promising biocompatible material used in variety of products such as contact lenses, diapers, and biomedical applications with proven anti-fouling properties. The low elastic modulus and high-water uptake are the crucial contributors in reducing the drag force and surface energies which subsequently reduces fouling.

The influence of hydrogel layer on the porous membrane performance depends on the nature of the base membrane (pore size and structure) and hydrogel characteristics (cross-linking degree, thickness, functional groups). However, for MF/UF hydrogel modified membranes the resistance due to hydrogel layer is relatively higher than intrinsic membrane resistance; which results in increased selectivity but decreased permeability.

It is possible to obtain hydrogel layer coating on the membrane surface either via in-situ polymer synthesis or via coating using the following mechanisms[110]:

1. Adsorption or adhesion of the functional hydrogel layer on the base membrane,
2. Interpenetrating network by mixing the functional polymer and the base membrane polymer in an interphase, and
3. Interpenetration between the functional polymer and the membrane pore structure.

The thickness of the hydrogel layer could be significantly higher than the functional layer obtained by surface modifications through interfacial reactions.

Plasma polymerization, chemical vapor deposition, or sputtering of metals or non-metals is often applied for membrane modifications. These methods result in a coating restricted to the outer surface of the membrane resulting in a composite membrane[134,135]. Further methods from solutions, such as coating with polymers[136], polycondensation[137], reactive coatings[138,139], and electrolytic deposition could be adapted to modify the entire surface of the membrane including the pores.

A reactive coating strategy was patented by Millipore corp. in 1986 for in-situ cross-linking copolymerization of acrylate monomers to hydrophilize microporous

hydrophobic membranes (e.g., PVDF, PP) at the industrial scale[8]. Permanent hydrophilization by formation of a thin polymer layer takes place through interpenetration of added polymer network and base membrane pore structure with a possibility of coupling via radical reactions at the surface.

A relatively new method based on supramolecular assembly is layer-by-layer adsorption of polyelectrolytes. This method is characterized by vertical organization and stabilization of the layers in addition to the possibility to manipulate both outer and internal layer structures on variety of base materials[140].

2.7 Surface initiated redox polymerization

Free radicals are required to initiate the chain growth in radical polymerization. Free radicals are generated as a product of the initiation reaction from the initiating system mainly by two pathways: homolytic decomposition of the covalent bonds by energy absorption and electron transfer to ions or atoms containing unpaired electrons followed by bond dissociation in the acceptor molecule (redox initiation)[141]. Redox initiation has several advantages over homolytic decomposition such as short induction period, relatively low activation energy, favorable mild reaction conditions, less probability of side reactions at mild conditions, and high yield in short time[142]. For these reasons redox initiation is favorable to implement at the industrial level with low operational costs. This section discusses the reaction mechanism involved in redox initiated polymerization and elaborates on the industrial aspect for the development of functionalized membranes at large scale.

2.7.1 Reaction Mechanism

The initiating system for redox initiation involves an oxidant (initiator) and a reducing agent (activator). Typically used oxidants consist of peroxides, persulphates, and permanganate. While typically used reducing agents are salts of metals like Fe^{2+}, Cu^{2+}, Cr^{2+}, Co^{2+}, etc., oxyacids of sulphur and hydroxy acids. For fundamental studies for initiating radical polymerization in the aqueous medium the redox initiating system of peroxide and iron salts also known as Fenton's reagent has received special attention and has been widely adopted in many studies. In this section, one established variant of Fenton's reagent initiated radical polymerization to obtain reactive coating on the membrane surface has been explored and explained in more detail. The process involves

pre-forming a coating layer on the substrate with a cross-linking agent and hydrogen peroxide (initiator) prior to the introduction of iron chloride (activator) and monomers to initiate the chain-growth at the surface.

Iron chloride dissociates into ferrous ions in aqueous solution and a spontaneous redox reaction between H_2O_2 and Fe^{2+} generates hydroxyl radicals as a result of redox potential difference. The reaction mechanism involves an electron transfer from ferrous ion to the peroxide dissociating the oxygen bond and generating hydroxyl radical[143] (see Figure 2.18). The difference in potentials of Fe^{2+} (E^0 (Fe^{3+}/ Fe^{2+}) = + 0.77 V vs SHE) and H_2O_2 (E^0 (H_2O_2/$HO^{\bullet}$) = + 0.80 V vs SHE) is the thermodynamic driving force for the electron transfer [144].

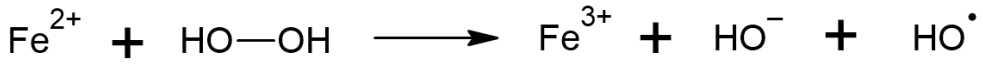

Figure 2.18. Fenton reaction: dissociation of hydrogen peroxide by ferrous ion

Initiating system of H_2O_2 and Fe^{2+}, first reported by H. J. H. Fenton in 1894 [145] is widely used for polymerization of several vinyl monomers in an aqueous medium[146–148] in the presence of sufficient monomers. Peroxides are a well-known source of radicals in the presence of metal ions [149].

The generated hydroxyl radicals very reactive and short-lived [150], thus rapidly react with the surrounding organic substrates. Highly reactive $HO^{\bullet}$ also reacts with non-specific organic/inorganic substrates present in the reaction mixture resulting in various competitive processes (see Figure 2.19) inhibiting polymerization [151–154]. Hebeish et al.[155] argued that equation (ii) in Figure 2.19 occurs to a great extent when H_2O_2 is present in large excess compared to Fe^{2+}. Moreover, Fe^{3+} ions generated through the reactions can react with hydroxide anions ($HO^{—}$) forming insoluble ferric hydroxide which further reduces polymerization efficiency by consuming ferrous ions[144].

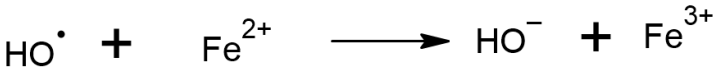

(i)

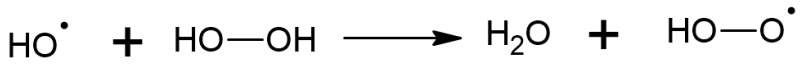

(ii)

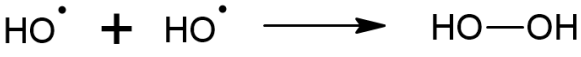

(iii)

Figure 2.19. Side reactions occurring during the polymerization which reduce the polymerization efficiency

Ascorbic acid is a good electron donor[156] that acts as a regenerating agent by reducing the inactive ferric ions back into the active ferrous ions as shown in Figure 2.20. This helps in maintaining the number of ferrous ions available for decomposing hydrogen peroxide to create hydroxide radicals. Therefore, ascorbic acid often is used as an additive in the reaction mixture to increase the efficiency of polymerization.

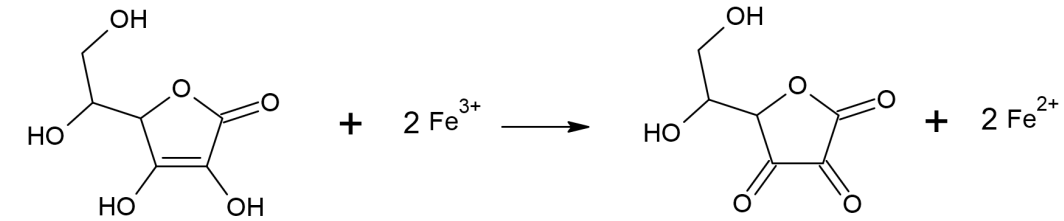

Figure 2.20. Regeneration of ferrous ions by ascorbic acid

In case of a porous membrane as a substrate, pre-formed coating prior to polymerization takes place by physical absorption of hydrogen peroxide and the cross-linking agent in a wetting solvent. Upon introducing the 'wet' membrane in the monomer solution containing iron chloride, hydrogen peroxide present in the membrane matrix diffuses out in the bulk while ferrous ions diffuse from the bulk into the membrane matrix. The Fenton reaction is initiated at the membrane interface where H_2O_2 and Fe^{2+} meet during diffusion[157]. The highly reactive hydroxide radicals are formed at the interface. The short-lived $HO^{\bullet}$ rapidly react with surrounding organic substrates: cross-linker and monomers near the interface generating starter organic radicals ($R^{\bullet}$) which react with surrounding organic molecules to initiate the chain-growth[158] on the membrane surface. The growing chain propagates from the interface through cross-linking monomers and forming a layer of polymer chains on the surface and within the pore wells. The growing chain terminates by disproportionation or combination of radicals.

The redox initiated radical polymerization presents a relatively simple post-treatment approach for membrane functionalization. Although, functionalization takes place in two steps, no external source of energy is required and reaction occurs under favorable conditions. More importantly, wide range of substrates, cross-linkers and monomers capable of participating in polymerization either via hydrogen abstraction or addition can be utilized for functionalization.

2.7.2 Industrial aspect: new product development

Several approaches have been adopted by the industries for developing functionalized flat sheet membranes to be utilized in various pharmaceutical products. The functionalization is typically carried out as a post treatment of the base material. Radical polymerization is widely used to obtain reliable functionalized membranes via numerous pathways such as UV, redox initiation, and heat. From an industrial aspect, the emphasis is given on cost reduction for producing such membranes. Batch and continuous processes are two types of industrial processes used for post treatment. Batch process involves batch wise modification of the base material in the designated industrial line or a module. Whereas, continuous process involves roll to roll modifications of the base membranes as they are produced; either as a continuation of the same industrial line or in a different industrial line. The continuous roll to roll process is preferred because it is faster and robust, and can modify large quantities of membranes in a short time.

3 MATERIALS AND METHODOLOGY

3.1 Chemicals and membrane materials

Table 3.1. List of chemicals used in this work

Chemicals	Abbreviation	Manufacturer
2-Hydroxy ethyl methacrylate	HEMA	Evonik
Acetic acid >99.8%	CH_3COOH	Honeywell Fluka
Acetone	$(CH_3)_2CO$	Carlo Erba
Acrylic acid	AA	Acros Organic
AdvanStain Ponceau S dye	Ponceau S	Advansta
Ammonium hydroxide	NH_4OH	Sigma Aldrich
Bovine serum albumin	BSA	Sigma Aldrich
Butanol	C_2H_8OH	Merck
Butyl acetate 99.7 %	$C_6H_{12}O_2$	Sigma Aldrich
Copper (II) sulfate pentahydrate	$CuSO_4.5H_2O$	PanReac AppliChem
Cyclohexane	C_6H_{12}	Sigma Aldrich
Dimethyl acetamide	DMAC	Brenntag
Dimethyl formamide	DMF	Sigma Aldrich
Dimethyl sulfoxide	DMSO	Sigma Aldrich
Ethanol absolute	C_2H_5OH	PanReac Applichem
Ethyl acetate	$C_4H_8O_2$	VWR chemicals
Ethylene glycol dimethacrylate	EGDMA	Evonik
Gasoline	Gas	Brenntag
Glycerol	$C_3H_8O_3$	Carlo Erba
Hexane	C_6H_{14}	Carlo Erba
Hydrochloric acid	HCl	Riedel-de-Haen
Hydrochloric acid min. 37 %	HCl	Riedel-de Haen

Hydrogen peroxide 40 %	H_2O_2	Carlo Erba
Iron chloride tetrahydrate	$FeCl_2.4H_2O$	Carlo Erba
Isopropanol	IPA	Brenntag
L (+) Ascorbic acid	Vit C	Acros Organic
Latex beads, polystyrene -COOH 0.22um	PS	Polyscience Inc.
Methanol	CH_3OH	Sigma Aldrich
Poly(acrylic) acid	PAA	Sigma Aldrich
Polyethylene glycol	PEG 400	Fluka
Polyvinyl pyrrolidone 10 kDa	PVP	Sigma Aldrich
Potassium Chloride	KCl	Sigma Aldrich
Potassium hydroxide	KOH	Sigma Aldrich
Potassium iodide	KI	Carlo Erba
Potassium permanganate	$KMnO_4$	Carlo Erba
Sodium dodecyl sulfate 85 %	SDS	Acros Organic
Sodium hydroxide	NaOH	Riedel-de-Haen
Sulfuric acid 96 %	H_2SO_4	Carlo Erba
Tetrahydrofuran	C_4H_8O	Riedel-de-Haen
Toluene	$C_6H_5CH_3$	AnalaR
Tri- Ethylene glycol dimethacrylate	TrGDMA	Evonik
Triethylamine	$C_6H_{15}N$	Riedel-de-Haen

In this work, in-house PVDF flat sheet membranes with a polyester support produced by GVS via non-solvent induced phase separation pathway[159] were used as the base material for all the post treatments. The base membranes used in this work had varying nominal pore sizes - 0.1 μm, 0.2 μm, 0.45 μm, 0.8 μm and 1.2 μm - within the microfiltration range. However, 0.45 μm nominal pore size was chosen for the detailed study and consequent prototype development. The base membrane properties will be discussed in detail in section 5.1 and 5.6.

The hydrophilic membranes widely used for bio-separation applications: 0.22 µm Durapore, Millipore and 0.22 µm PES, Millipore were considered for the comparison study. Durapore membrane is produced by a polymerization post treatment of an unsupported PVDF membrane[160] making it highly relevant for comparison. According to the survey conducted among the project partners working with isolation of extracellular vesicles in this consortium and based on the literature[25,161], PES membranes are used in multiple filter devices such as centrifugal filters and syringe filters for concentration or purification of bio-fluids.

Durapore, Millipore, PES, Millipore and prototypes developed in this work demonstrate different physico-chemical surface properties due to their varying morphology, structure and chemistry, which will affect the membrane performance. The differences in the membrane properties and performance will be discussed in more details in the section 5.6.

3.2 Membrane functionalization

The post treatment methodology was designed to have a robust, versatile, fast, and scalable functionalization pathway. The membrane functionalization was performed with a "two-step graft coating polymerization" methodology which combines the characteristics of dip-coating and graft polymerization to obtain membranes modified throughout the porous structure without narrowing or blocking of the pores within few minutes. Figure 3.1 shows each step involved in the membrane functionalization methodology.

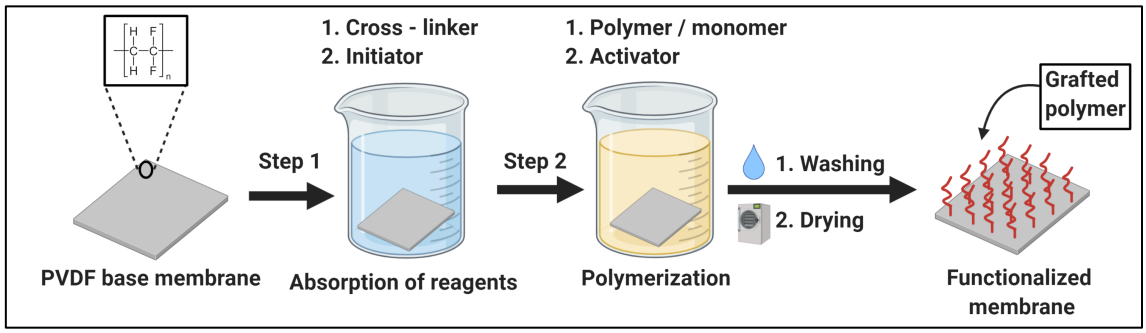

Figure 3.1. Two-step graft coating polymerization methodology used for membrane functionalization

In the first step, a 44 mm diameter PVDF base membrane disk is immersed in 35 mL "solution 1" containing the cross-linker and an initiator: hydrogen peroxide (6 wt.%) dispersed in isopropyl alcohol (IPA) for 2 min 30 sec allowing absorption of the reagents.

In the second step, the same membrane disk was immersed in 35 mL "solution 2" containing a polymer, an activator: iron chloride ($FeCl_2.4H_2O$) (0.28 wt.%) and ascorbic acid (Vit C) (1 wt. %) dispersed in RO water for another 2 min 30 sec allowing enough time for the polymerization to take place. After the polymerization the modified membrane is placed in a 50 mL 0.1 wt.% surfactant (SDS/ALS) solution for 5 min to remove unreacted chemicals from the membrane. And as a final washing step the membrane disk is then placed in 50 ml RO water overnight to washout the surfactant solution before drying in the oven at 80ºC for 30 min. The beakers containing solutions were placed inside a shaker at 100 rpm at the room temperature. For each formulation six disks were modified at a time using six different beakers for each solution. The concentration of cross-linker and polymer and consequently the solvents were varied based on the experiment, whereas the concentration of other reagents (mentioned above) was fixed based on the previous study[162] and preliminary experiments. In this work, two different cross-linkers and three different polymers – one long chain polymer and two monomers - were studied as shown in the Figure 3.2. The effect of type of cross-linker, monomer, polymer and their concentration is discussed in details in the sections 5.3, 5.4 and 5.5.

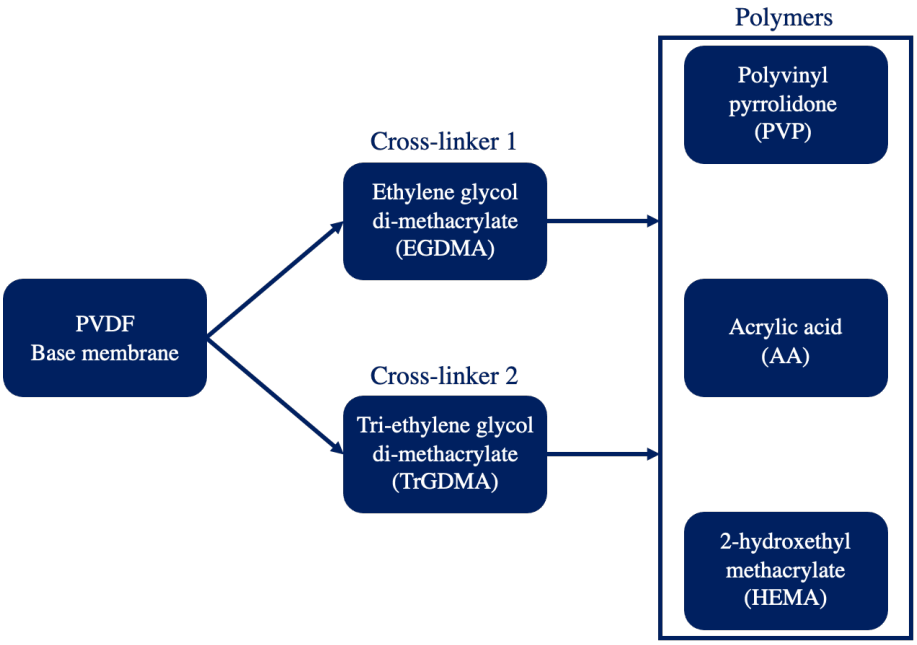

Figure 3.2. Membrane functionalization approach used in this work: each cross-linker was paired with each available polymer where the concentrations of both cross-linker and polymer were varied to find the right formulation

The modifications were performed on supported PVDF base membrane with nominal pore size of 0.45 µm unless stated otherwise. The formulations used for the study of each are mentioned in the tables below:

1. PVP: For each chosen PVP concentration 3 modifications were performed by selecting different EGDMA concentrations. In total 9 modifications were performed for PVP – EGDMA.

Table 3.2. EGDMA-PVP formulation for membrane modification

EGDMA (wt. %)	PVP (wt. %)		
5	5	10	20
10	5	10	20
15	5	10	20

2. AA: For acrylic acid additional two sets of formulations with lower EGDMA concentration were introduced and in total 15 modifications were performed.

Table 3.3. EGDMA-acrylic acid formulation for membrane modification

EGDMA (wt. %)	Acrylic acid (wt. %)		
1.25	5	10	20
2.50	5	10	20
5.00	5	10	20
10.00	5	10	20
15.00	5	10	20

The same formulation was replicated with the different cross-linker – TrGDMA.

4. HEMA: For HEMA additional two sets of formulations with lower EGDMA concentration were introduced and in total 15 modifications were performed.

Table 3.4. EGDMA-HEMA formulation for membrane modification

EGDMA (wt. %)	HEMA (wt. %)		
1.25	5	10	20
2.50	5	10	20
5.00	5	10	20
10.00	5	10	20
15.00	5	10	20

The same formulation was replicated with the different cross-linker – TrGDMA.

In addition to the above-mentioned formulations, modification study without polymer was also performed to understand the effect of cross-liker alone.

The goal of performing these set of lab modifications was to identify the best formulation with suitable cross-linker & polymer pair in terms of its desired properties and performance.

3.3 Industrial upscaling

The industrial upscaling was performed for the HEMA modification with the formulation shown in the Table 3.5. The formulation was chosen after analyzing multiple the properties and performance of the multiple modifications carried out in the lab.

Table 3.5. Industrial trial formulation for the modification of HEMA

Solution 1 [wt. %]			Solution 2 [wt. %]			
H_2O_2	EGDMA	IPA	HEMA	$FeCl_2.4H_2O$	Vit C	RO water
6	1.5	92.5	6.5	0.28	1	92.22

The industrial upscaling was also performed for the acrylic acid modification with the formulation shown in the Table 3.6. The formulation was chosen after analyzing multiple the properties and performance of the multiple modifications carried out in the lab. However, the work in this thesis includes the further investigations only with HEMA industrial trial due to the time constrain.

Table 3.6. Industrial trial formulation for the modification of acrylic acid

Solution 1 [wt. %]			Solution 2 [wt. %]			
H_2O_2	EGDMA	IPA	AA	$FeCl_2.4H_2O$	Vit C	RO water
6	2.5	91.5	10	0.28	1	88.72

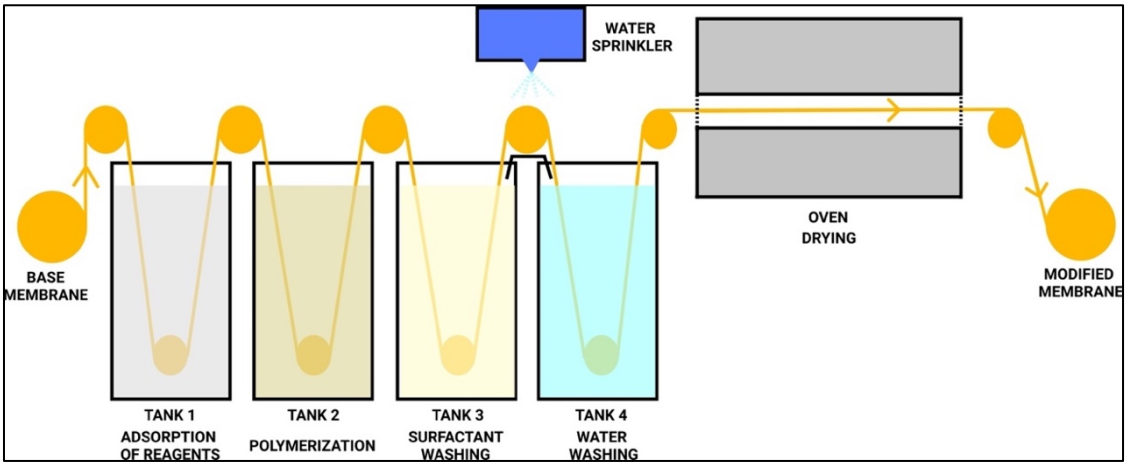

Figure 3.3. Schematics of the industrial post treatment line at GVS Filter Technology

The industrial line used for the post treatment with HEMA consists of 4 tanks of 60 L capacity through which the base PVDF membrane of 60 cm width is passed through with the help of a rollers at the speed of 0.7 m/min. Tank 1 contains solution 1, tank 2 contains solution 2, tank 3 contains 0.1 % ALS and tank 4 contains RO water after which membranes is dried at 85ºC in the oven before collection. Additionally, sprinklers are installed to further make sure removal of excess of surfactant and avoid contamination of tank 4. The trials were performed with 50 mts. of the membrane after which the efficiency of the modification was reduced. During the post treatment with membrane rolls more than 50 mts. solutions in the tank 2, 3 and 4 are renewed in a timely manner. The schematics of the industrial line for post treatment is shown in the Figure 3.3.

3.4 Polymer characterization

Visual inspection was used to characterize the polymerization taking place in the second step of the methodology. The bulk polymerization solution obtained upon addition of solution 1 to solution 2 was investigated without the introduction of the membrane. The first study was carried out for four different types of polymers with EGDMA and followed by the second study with TrGDMA. The following three polymers were used in this study:

a. Polyvinyl pyrrolidone (PVP)
b. Acrylic acid monomer (AA)
c. 2-hydrox ethyl methacrylate (HEMA)

For each chosen concentration of polymer four different concentrations of cross-linkers were investigated. The concentrations of polymer and cross-linker used are shown in the Table 3.7. The concentration of hydrogen peroxide (6 wt.%) in solution 1 and iron chloride ($FeCl_2.4H_2O$) (0.28 wt.%) and ascorbic acid (Vit C) (1 wt. %) in solution 2 was always kept constant whereas solvent concentration (IPA & RO water) was varied according to the cross-linker and polymer.

Table 3.7. Polymer and cross-linker concentrations used for the visual inspection tests

Polymer [wt. %]	Cross-linker [wt. %]			
5	1.25	2.5	5	10
10	1.25	2.5	5	10
15	1.25	2.5	5	10

Once the solutions were prepared according to the formulation mentioned above, 10 ml of solution 1 was added to the 10 ml of solution 2 in a 100 mL beaker and a picture was taken after allowing two solutions to react for 15 min.

3.5 Membrane characterization

3.5.1 Hydrogel grafted

The amount of hydrogel grafted was quantified by weighing the samples in both dried and hydrated form. The samples were dried inside a climatic chamber (DY110 C, Angelantoni test technologies, Italy) at 80ºC without moisture until the constant weight was obtained. This measurement determines the surface density of the coating throughout the porous structure. The hydrogel grafted was calculated according to the formula:

$$HG\left[\frac{mg}{cm^2}\right] = (W_d - W_0)/S \quad (1)$$

Where W_d [mg] is the weight of the dry modified sample, W_0 [mg] is the initial weight of the unmodified sample and S [cm^2] is the area of the sample.

3.5.2 Water uptake

The water uptake for samples was measured to understand the ability of modified membranes to hold water in the porous structure. The hydrated state weight of the samples was measured after immersing samples 24 h in RO water at room temperature and removing the excess water from the surface using absorbent paper. Then the samples were dried at a constant temperature of 80°C in the climatic chamber (DY110 C, Angelantoni test technologies, Italy) without moisture until a constant dried weight was reached. The amount of water uptake was measured using the formula:

$$\text{Water uptake } [\%] = \left(\left(W_{eq} - W_d \right) / \left(W_d \right) \right) \times 100\ \% \qquad (2)$$

Where W_{eq} [mg] is the weight of the sample with absorbed water at equilibrium and W_d [mg] is the weight of the dry modified sample.

3.5.3 Porometry

The efficiency and the effectiveness of the filtration is governed by the pore structure of the membrane. Porometry is a technique capable of measuring all the pore structure characteristics relevant to filtration such as pore size distribution, number of pores, largest pore size, etc. The measurement consists of impregnation of the porous samples with a wetting liquid and subsequent displacement of the wetting liquid with a non-reacting gas at increasing pressure. Wetting liquid with low surface tension is used which reduces the liquid-solid interfacial free energy allowing it to spontaneously fill the membrane pores. The pressure required to displace the wetting liquid from the pores is given by the Young-Laplace equation:

$$P = \frac{4\,\gamma\,\cos\theta}{D} \qquad (3)$$

Where P is the pressure required to displace the wetting liquid from the pore, γ is surface tension of the wetting liquid, θ is the contact angle liquid with the pore surface and D is the pore diameter. The gas flow rate through the wet sample at low pressure is zero as all the pores are blocked by the wetting liquid. With increasing pressure, the bigger pores followed by smaller become empty and the gas starts flowing through the pores. At sufficiently high pressure all the pores become empty and the flow through the wet sample becomes equal to the dry sample. Based on the pressure applied and the gas flow rates

during the software calculates the pore diameter, pore distribution, gas permeability and porosity[163]. The Figure 3.4 shows the flow through the wet sample and dry sample during the porometry measurement.

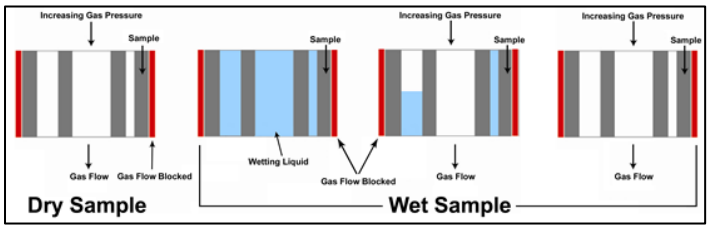

Figure 3.4. Flow of gas through dry sample and wet sample during the porometry measurement[163]

In this work the porometry measurements were performed using Porometer 3G (Quantachrome). First a flat sheet membrane disk of 25 mm diameter was cut and its weight and thickness were measured. Then the disk was immersed in the wetting liquid (Porofil) and the excess liquid was removed using a tissue; the weight of the wet disk was measured before placing the disk inside the porometer holder. All the required information was filled in the software such as the pressure range, dry weight, wet weight, thickness, and the measurement was started. The instrument first plots the wet curve followed by the dry curve once all the wetting liquid has been displaced by the pressurized air. Figure 3.5 shows a typical representation of the porometry plot after the measurement.

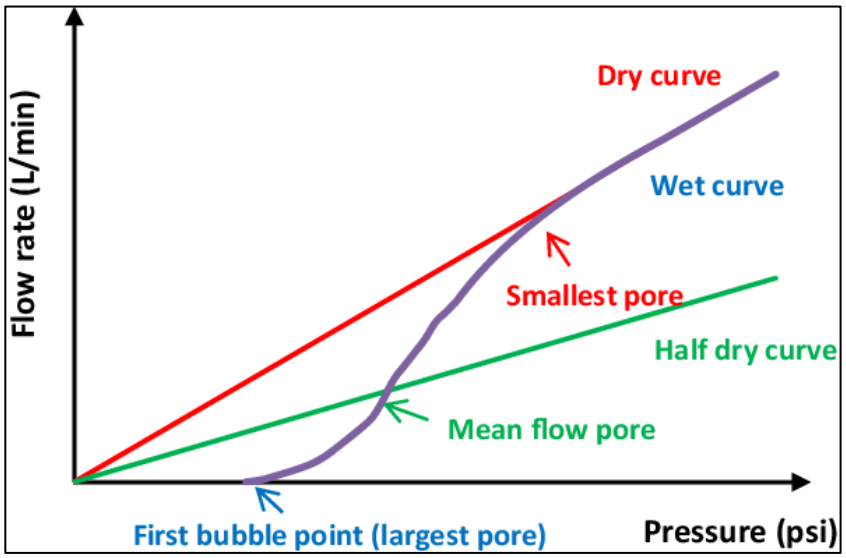

Figure 3.5. Representation of a wet curve and dry curve[164]

3.5.4 Water flow rate

To evaluate the permeance of the modified membranes water flow rate measurements were performed for all the membranes using RO water. The membrane disk of 25 mm in

diameter was placed in a syringe filter holder and connected to the outlet tube with a digital manometer to adjust the differential pressure. The water flow rate measurements were performed at a differential pressure of 0.5 bar. Before each measurement membranes were stored in water overnight and RO water was pushed through the membrane at 1 bar for 5 minutes to ensure no air bubbles are trapped and to wash out the contaminants. During the water flow rate measurement RO water (permeate) was collected at least 5 times every 1 min. Average of at least 3 disks from the same sample was reported. The following formula was used to calculate the water permeance:

$$\text{Permeance } [\frac{\text{ml}}{\text{bar.cm}^2\text{.min}}] = \frac{\Delta V}{\Delta P \,.\, A \,.\, T} \quad (4)$$

Where ΔV [mL] is the amount of volume of RO water collected in 1 minute, ΔP is the differential pressure across the membrane – 0.5 bar, A is the effective active area of the membrane – 4.15 cm^2 and T is the time of flow – 1 min.

3.5.5 Scanning electron microscopy (SEM)

Scanning electron microscope produces high resolution images of the surface morphology of the sample. A focused beam of electrons is bombarded on a conductive sample under vacuum at a certain kinetic energy. The interaction of electrons with the sample can be elastic: electrons are deflected and scattered resulting in back-scattered electrons (> 90° deflection) or inelastic: secondary electrons are emitted with a different energy from incident electrons. The secondary electrons and back-scattered electrons along with X-rays are collected by the specialized detectors to build-up the final image of the sample surface or other information on the computer display[165,166].

In this work, EM30 (COXEM) table-top SEM was used to obtain the images of the membrane surface and Quanta 400 FEG, FEI SEM was used to obtain cross-section images. The high-resolution images of the modified and unmodified membranes along with membranes post-particle filtration enabled evaluation of the modification and filtration process. The samples were sputtered with gold using SPT 20 (COXEM) ion coater to induce conductivity and avoid accumulation of electrons during the measurement. The samples for the cross-section imaging were prepared by rinsing and then freeze-drying in liquid nitrogen before carefully breaking them and placing in the ion coater.

3.5.6 Attenuated total reflection infrared spectroscopy (ATR-IR)

Atoms are continuously moving within the molecule without altering the center of mass and without any rotation. These movements of atoms are called molecular vibrations. FTIR probes the vibrations of the molecular bonds because infra-red frequencies overlap with the molecular vibration frequencies. The infrared radiation range typically used for FTIR is 4000 cm^{-1} to 400 cm^{-1}. When the incident IR light frequency overlaps with the molecular vibration frequency the energy is absorbed and the molecular vibration moves to the higher energy state. This results in a characteristic absorption bands that can be used to identify the presence of corresponding functional groups[167].

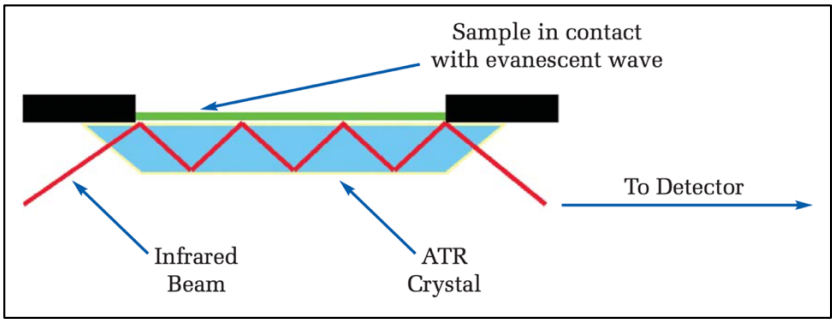

Figure 3.6. Working of attenuated total reflection Fourier transform infrared spectroscopy[168]

In this work attenuated total reflectance – Fourier transform infrared spectroscope (Bruker ALPHA II) was used to detect the functional groups on the chemically modified and unmodified membrane surfaces. An incident IR beam is directed on to a dense crystal with high refractive index at a certain angle. An evanescent wave is created upon multiple internal reflectance which interacts with the sample in contact with the crystal. The wave is absorbed by the sample surface (0.5 – 5 μm) and reflected back through the crystal on to the detector[169]. The schematics of the working of ATR-FTIR is shown in Figure 3.6. The samples were washed and dried before the measurement and every sample's top layer was scanned 32 times in the range of 4000 cm^{-1} to 400 cm^{-1} with the resolution of 1 cm^{-1}.

3.5.7 Zeta potential

Membrane surface charge is an important property contributing to fouling and adsorption. All polymeric membranes carry ionizable features at the surface as a result in an aqueous solution membrane surface carries a charge whose magnitude depends on type of group on the surface, environmental pH and ion concentration. Zeta potential indicates the actual surface charge of a solid surface in contact with liquid. At the solid-liquid interface, the development of a net charge affects the distribution of ions in the surroundings

forming an electrical double layer, this leads to the formation of streaming potential as shown in the Figure 3.7.

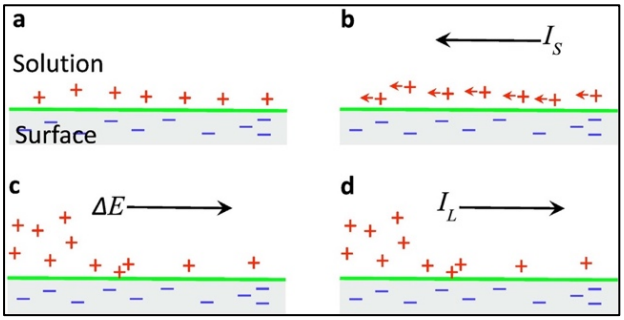

Figure 3.7. Processes which lead to the formation of the streaming potential: a) electrical double layer at a charged surface; b) electrolyte flow causes a streaming current, Is, to arise; c) accumulation of ions downstream; d) direction of the flow of the leak current[165]

The high concentration of counter-ions at the surface form an immobile Stern layer beyond which the ions are free to move forming the diffuse Gouey-Chapman layer. Actual membrane surface potential is complicated to measure due to the highly attractive Coulomb interactions at the surface, therefore zeta potential is measured at the shear plane as shown in the Figure 3.8[170].

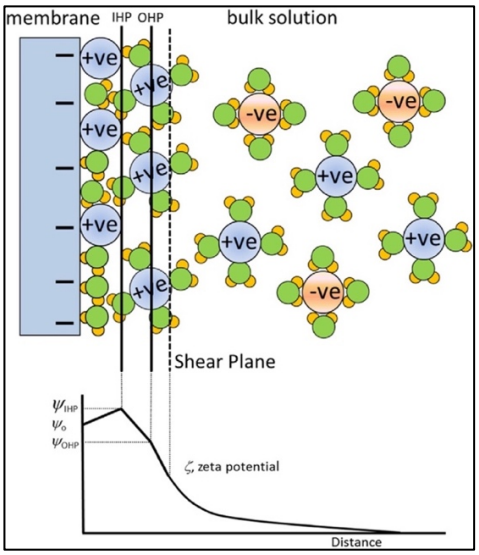

Figure 3.8. The shear plane separating the inner Helmholtz plane (IHP) and the outer Helmholtz plane (OHP) beyond which diffuse layer exists in the bulk solution. The zeta potential at the shear plane decreases with the distance[171]

When an electrolyte is pumped using an external pressure either tangentially (across a narrow channel of 2 membranes surfaces) or transversely (through the porous structure), the diffuse layer will move in the direction of the flow generating streaming current and consequently streaming potential. Conduction or leak current in the opposite direction is generated as counter-charges accumulate downstream. At equilibrium, leak current

counter-balances the streaming current and the measured potential difference across the membrane at this point is the streaming potential[172,173]. Helmholtz-Smoluchowski equation which relates zeta potential to the streaming potential and the applied pressure is given by[174,175]:

$$\zeta = \frac{\Delta U}{\Delta p} \cdot \frac{\eta}{\varepsilon\varepsilon_0} \cdot \frac{L}{A.R} \qquad (5)$$

Where ζ is the zeta potential, $\frac{\Delta U}{\Delta p}$ is the slope of streaming current versus pressure difference, η and $\varepsilon\varepsilon_0$ are the viscosity and dielectric coefficient of the electrolyte solution, L is the height of the streaming channel, A is the cross-section area of the streaming channel and R is electrical resistance of the channel.

All the zeta potential measurements for the modified and unmodified membranes were performed tangentially using SurPASS electrokinetic analyzer (Anton Paar). Flat sheet membrane samples were cut into 2.5 mm disks and immersed in 1mM KCl solution overnight before the measurement. The samples were fixed on the holders and the channel gap was adjusted to 100 ± 5 nm and the measurements were started at around pH 2 with 1 mM KCl as the electrolyte solution with 400 mbar as the differential pressure. After each measurement the pH was adjusted by automatically using 0.1 M KOH solution and zeta potential was determined until pH 11.

3.5.8 Contact angle measurement

The contact angle measurements were performed to investigate the hydrophilicity of the membrane surface. Contact angle represents degree of wetting when solid and liquid interact. Low contact angle (< 90°) corresponds to high wettability while high contact angle (> 90°) corresponds to low wettability[176]. The change in contact angle at the membrane surface with time was measured using OCA 15EC goniometer (Data physics) via sessile drop method and final measurements were recorded in terms of total wetting time.

Modified and unmodified membrane samples were fixed on a glass slide using a double tape and 5 µl of RO water was dosed onto the sample using a Hamilton syringe at room temperature. Measurements were performed at least 3 times at different spots for each

sample. The movement of the drop was recorded using the device camera and the contact angle was analyzed using the software with Ellipse fitting calculations.

3.5.9 Energy dispersive X-ray (EDX) spectroscopy

EDX spectroscopy is capable of detecting elements with atomic number higher than Boron with at least 0.1 % concentration using scanning electron microscope. It can be used to detect elemental composition, identification and evaluation on the surface and through the cross-section. When a beam of electrons in the SEM interacts with the sample, it excites an electron form the nucleus of the atom, ejecting it from the nucleus and creating a whole. A higher energy electron from the outer shell replaces the missing electron releasing the superfluous X-rays. The X-rays generated are unique to each element which can be measured and differentiated for its concentration in the sample[119].

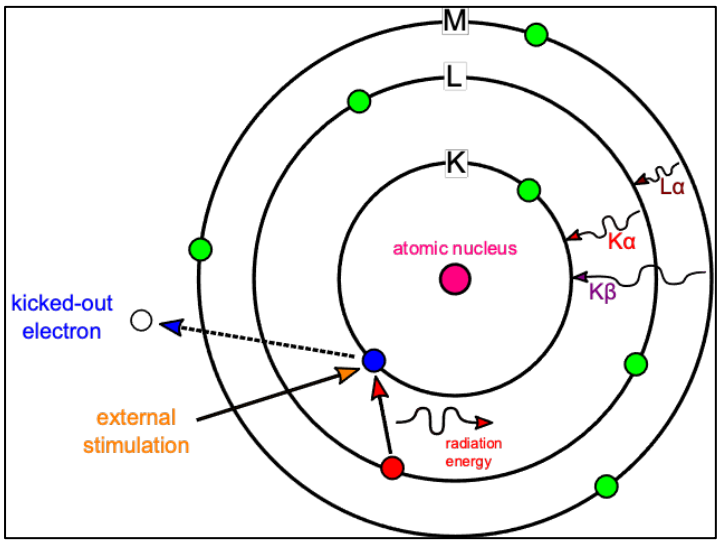

Figure 3.9. Principle of EDX measurement[177]

In this work Apreo S LoVac (Thermo Fischer) was used to identify and map the concentration of copper throughout the cross-section of the membranes with different pore sizes. EDX spectroscopy was used to investigate the variation of acrylic acid concentration through the cross-section of the modified membranes. Base membranes with pore size 0.1 µm, 0.2 µm, 0.45 µm, 0.8 µm and 1.2 µm were modified with acrylic acid using the methodology mention in section 3.2. The composition of modifying solution is shown in Table 3.8.

Table 3.8. Formulation of the solutions for the modification of membranes with different pore sizes

Solution 1 [wt. %]			Solution 2 [wt. %]			
EGDMA	H_2O_2	IPA	Acrylic acid	Vit. C	$FeCl_2.4H_2O$	RO water
2.5	6	91.5	10	1	0.28	88.72

Each modified membrane disk with 25 mm diameter was immersed in 25 ml of 0.4 mg/ml copper sulphate pentahydrate solution for 24 hrs. at pH 7. This allowed enough time for dissociation of carboxylic groups enabling copper to attach. After which each disk was placed in a syringe filter holder and washed by pushing 10 ml of RO water 3 times to remove unbound copper. Then the disks were allowed to dry at room temperature. Finally, the disks were immersed and rinsed in liquid nitrogen to break them for the measurement. PVDF base membrane of nominal pore size 0.45 µm and a HEMA modified membrane of 0.45 µm was used as a reference.

3.5.10 Flux at different pH and effect of drying

Membranes modified with acrylic acid exhibit pH responsive behavior. At low pH, carboxyl groups are protonated resulting in volume shrinkage of the polymer. At high pH, dissociation of carboxylic group results in carboxylate ions with high charge density causing the polymer chains to swell. The polymer configurational change as a consequence of pH manipulates the effective membrane pore size and hence the permeability. The configurational change is a function of the pKa of (poly)acrylic acid whose value is approximately 4.3 – 4.9[178].

For every modified membrane with acrylic acid the permeance was measured with RO water at pH 3, pH 7 and pH 11 according to the procedure mentioned in section 3.5.4. Three membrane disks were stored in pH 3 solution for 24 h and the permeance was measured with RO water at pH 3. The same disks were then stored for 24 h in pH 7 and pH 11 after which the permeance was measured with pH 7 and pH 11 respectively.

In another set of experiment, the membrane disks were dried at 80°C overnight after the measurement at each pH. The drying step was introduced to understand the effect of temperature on the swelling of acrylic acid chains.

3.5.11 Water Bubble point

The biggest pore opening in the membrane plays a vital role in defining the effectiveness of the filtration. Water bubble point is performed to determine the pressure at which air passes through the biggest pore opening in a wet membrane. The pressure is related to the pore size by Young-Laplace equation:

$$D = \frac{4\,\gamma\,\cos\theta}{P} \qquad (6)$$

Where D is the pore diameter, γ is the surface tension of water, θ is contact angle of water with the membrane surface and P is the applied pressure.

The water bubble point was tested on the in house GVS apparatus. The membrane sample was immersed in RO water overnight to make sure complete wetting of the pores. Then the wet membrane was placed in the sample holder above which water was filled. The pressurized air was pushed through the membrane by increasing pressure constantly. The pressure was recorded as the water bubble point at which the first air bubble was spotted.

3.6 Membrane performance characterization

Based on the characterization of the lab modifications performed as per the formulations mentioned in the section 3.2, nine lab modifications were chosen for the performance study and compared with the competitor (reference) membranes. The Table 3.9 shows the details about the selected lab modifications along with the competitor (reference) membranes.

Table 3.9. List of selected lab modifications and reference membranes for the performance study

Membrane code	Cross-linker [wt.%]	Polymer [%]	Manufacturer	Pore size [µm]
AA-1	EGDMA [2.5]	Acrylic acid [5]	GVS	0.45
AA-2	EGDMA [2.5]	Acrylic acid [10]	GVS	0.45
AA-3	EGDMA [1.25]	Acrylic acid [10]	GVS	0.45
HE-1	EGDMA [2.5]	HEMA [5]	GVS	0.45
HE-2	EGDMA [2.5]	HEMA [10]	GVS	0.45

HE-3	EGDMA [1.25]	HEMA [10]	GVS	0.45
HT-1	TrGDMA [2.5]	HEMA [5]	GVS	0.45
HT-2	TrGDMA [2.5]	HEMA [10]	GVS	0.45
HT-3	TrGDMA [1.25]	HEMA [10]	GVS	0.45
DM*	-	-	Millipore	0.22
PM**	-	-	Millipore	0.22

NOTE: the concentration of other reagents in the modification of PVDF base membrane was kept always the same. *DM is Durapore membrane based on PVDF, **PM is a PES membrane.

3.6.1 Filtration study

Multiple prototypes with different formulations for HEMA and acrylic acid were obtained after narrowing down the modifications based on their characteristics such as: amount of hydrogel grafted, water uptake and permeance. Table 3.9 above shows the list of membranes considered for the filtration study.

The filtration study was carried out by filtrating 0.26 mg/ml of commercially available fluorescent dyed -COOH labelled polystyrene particles of 200 nm provided by PolyScience Inc. The size and the surface charge of the particles was measured using DLS according to the procedure mentioned in section 3.6.2. The characteristics of the feed solution used for the filtration study in shown in Table 3.10.

Table 3.10. Polystyrene (PS) particle characteristics

Particle type	Size [nm]	Charge [mV]	Particle concentration [particles/ml]
Fluorescent PS (-COOH functionalizaed)	218 ± 3	- 45 ± 5	5.68*10e12

44 mm diameter of the sample was placed inside a 50 ml 1050 Amicon cell (Millipore). The Amicon cell was connected to a pressurized reservoir tank. The pressure was monitored using a digital manometer; the schematics of the filtration set-up is shown in Figure 3.10.

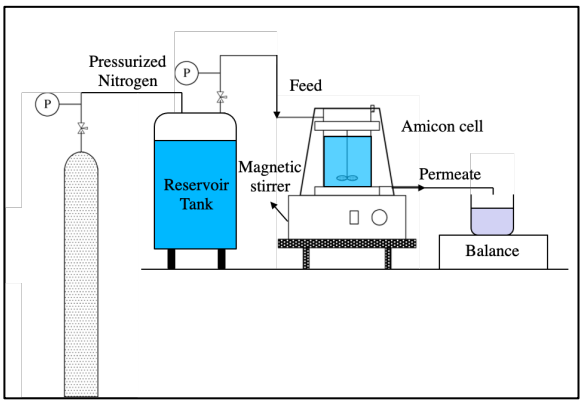

Figure 3.10. Schematics of the filtration set-up

Initially, membrane compaction was performed at 1 bar for 10 minutes with RO water. This step also washed out the contaminants in the system and membrane. Then the water permeance was measured by collecting and weighing the filtered RO water every two minutes at a constant pressure of 0.1 bar for 40 min. The water permeance was calculated using the formula mentioned below:

$$\text{Permeance} = \frac{v}{p \,.\, A \,.\, t} \qquad (7)$$

Where v is the volume of RO water collected every two minutes [mL] = weight of the collected water [g], p is the applied differential pressure [bar], A is the active membrane area [cm^2] and t is the time of collection [min.].

The schematics of the comprehensive filtration study is shown Figure 3.11.

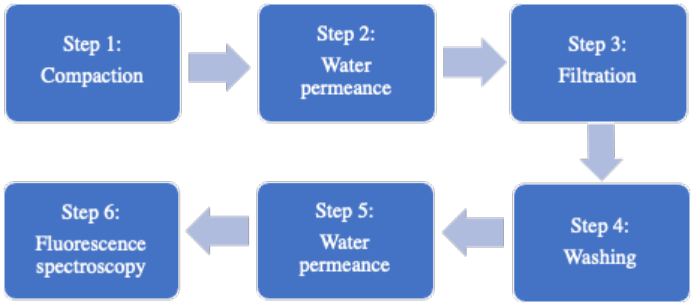

Figure 3.11. Stepwise comprehensive filtration experiments

Sequential filtration was performed in the third step by filtering 50 ml of feed solution at 0.1 bar differential pressure under the influence of stirring at 300 rpm. The permeates were collected every 3 mL in the pre-weighed glass vials and the time required for each collection was recorded. The permeance of the filtration for each permeate was calculated using the equation (7) above. The filtration was continued until 5 mL of retentate was left

in the amicon cell. To understand the pattern of blocking of the membrane during filtration, total filtration resistance, membrane resistance and cake layer resistance was calculated during the sequential filtration as it progressed. The following equations were used:

$$R_t \left[\frac{1}{m}\right] = \frac{P}{\eta_{particle} \cdot J_{particle}} \quad (8)$$

Where R_t is the total filtration resistance, P [Pa] is the differential pressure, $\eta_{particle}$ [Pa.s] is the kinematic viscosity of the polystyrene particles and $J_{particle}$ [m^3/m^2. s] is the particle filtration flux.

$$R_m \left[\frac{1}{m}\right] = \frac{P}{\eta_{water} \cdot J_{water}} \quad (9)$$

Where R_m is the membrane resistance, P [Pa] is the differential pressure, η_{water} [Pa.s] is the kinematic viscosity of water and J_{water} [m^3/m^2. s] is the water flux.

$$R_c \left[\frac{1}{m}\right] = R_t - R_m \quad (10)$$

Where R_c is the cake layer resistance, R_t is the total filtration resistance, R_m is the membrane resistance.

The retentate was collected in a separate glass vial and the amicon cell was washed with 10 ml of RO water at pH 7 by leaving the amicon cell on a shaker for 15 min before collecting the washed water. The cell was further rinsed with water two more times to eliminate any unbound particles present on the surface of the membrane.

The water permeance was measured again after filtration and washing step to determine the drop in permeance due to fouling of the particles during filtration. The drop in permeance (D) was calculated using the formula mentioned below:

$$D\ [\%] = \frac{\text{water permeance after filtration}}{\text{water permeance before filtration}} \times 100 \quad (11)$$

And finally, the collected permeates, retentate and feed were analyzed by fluorescence spectrophotometer for determining the particle concentration and consequently calculating the retention during the filtration.

$$\text{Retention } [\%] = \left(1 - \frac{C_p}{C_f}\right) \times 100 \quad (12)$$

Where C_p is the concentration of the collected permeate and C_f is the concentration of the feed used for the filtration.

The particles trapped in the membrane after filtration were also calculated to monitor progress of the particles through the system.

$$\text{Particles in the membrane } [\%] = f_c - p_t - r_c - w_c \quad (13)$$

Where, f_c is the starting feed particle concentration (100 %), p_t is the cumulative permeate particle concentration, r_c is the retentate particle concentration and w_c is the particle concentration in the washing solution.

3.6.2 Particle characterization

3.6.2.1 Dynamic light scattering

Dynamic light scattering (DLS) is a non - invasive optical method used primarily to measure the size of the particles of polymers, proteins, nanoparticles and colloids in the sub-micron region (0.3 nm to 10 μm)[179]. Particles suspended within a liquid are continuously moving in Brownian motion due to the bombardment of the surrounding solvent particles. DLS investigates this Brownian motion to calculate the size of the particles. The size of the particles is calculated based on the translational diffusion coefficient using the Stokes-Einstein equation[180]:

$$d\,(H) = \frac{k\,T}{3\,\pi\,\eta\,D} \quad (14)$$

Where, d(H) is the hydrodynamic diameter, D is the translational diffusion coefficient, k is Boltzmann's constant, T is absolute temperature and η is the viscosity.

The incident monochromatic laser light is scattered in all directions (Rayleigh scattering) when it passes through the dispersion due to the differences in the refractive index. The intensity of the scattered light is detected by the instrument to calculate the translational diffusion coefficient. The intensity of the scattered light fluctuates depending on the Brownian motion of the particles. The bigger particles move slowly – low fluctuations whereas smaller particles move fast – higher fluctuations. Furthermore, two beams from

the scattered light can interfere either constructively or destructively depending on their phases. The software uses the correlation function which analyses the fluctuations in the intensity with time to obtain the size information by using various algorithms. In addition to the size distribution the instrument also gives an indication about the polydispersity index (PDI):

If the PDI < 0.1 then the dispersion is monodispersed.

If the PDI > 0.1 then the dispersion is polydispersed.

Although in DLS the size distribution obtained is based on the intensity measurement the software has the capability to obtain the distribution based on volume and number using different mathematical approaches[181,182].

In this work, the polydispersity index and size distribution of the feed solution was measured using DLS. 0.26 mg/ml of fluorescent polystyrene particles labelled with -COOH (Polyscience Inc.) dispersed in RO water were analyzed using Zetasizer Nano ZS (Malvern Instruments). 750 µL of sample solution was placed in a disposable capillary cell (DTS1070) and a monochromatic laser light was generated by a He-Ne laser (4 mW, λ=633 nm) with a scattering angle of 173°. The refractive index of particles was assumed to be similar to polystyrene (1.59). Every sample was measured 30 times, ten seconds each, to obtain an average value for the hydrodynamic diameter.

3.6.2.2 Zeta potential

Zeta potential is a physical property exhibited by all the particles dispersed in a liquid. Knowledge of zeta potential helps predict the long-term stability of the dispersion. According to the DLVO theory, the stability of the dispersion is dependent upon its total potential energy (V_T) which is sum of solvent potential energy (V_S), attractive potential energy (V_A) and repulsive potential energy (V_R)[183,184]:

$$V_T = V_S + V_A + V_R \tag{15}$$

However, solvent potential energy contributions are negligible compared to the contributions from V_A and V_R which operate over much larger distances. The attractive potential is given by:

$$V_A = -\frac{A}{12\,\pi\,D^2} \tag{16}$$

Where, A is the Hamaker constant and D is the particle separation.

The repulsive potential is given by:

$$V_R = 2\,\pi\,\varepsilon\,a\,\zeta^2\exp(-\kappa D) \tag{17}$$

Where, where a is the particle radius, π is the solvent permeability, κ is a function of the ionic composition and ζ is the zeta potential.

The DLVO theory suggests that the sum of attractive and repulsive forces that exist between the particles as they move in the solvent due to the Brownian motion determines the stability of the dispersion. The stronger repulsive forces create an energy barrier between the particles preventing flocculation. But if the attractive forces overcome the barrier the particles will adhere and coagulate. The variation of free energy with particle separation according to the DLVO theory is shown in Figure 3.12.

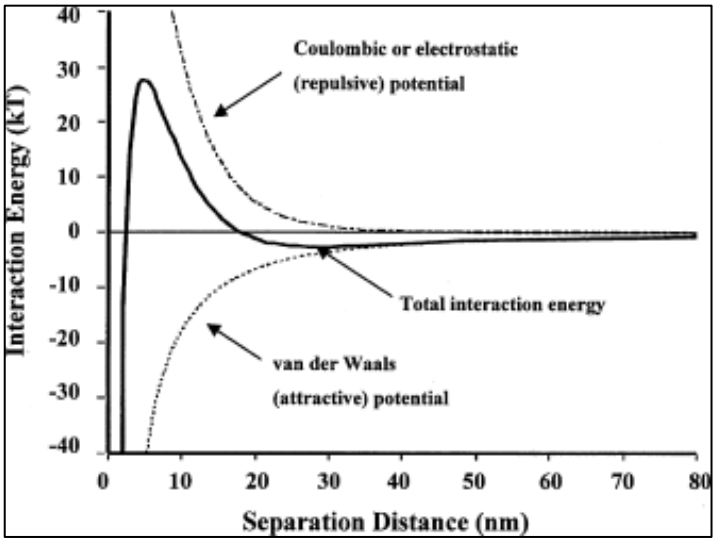

Figure 3.12. The variation of free energy with particle separation according to the DLVO theory[185]

Particles carry a charge when dispersed in aqueous media mostly due to ionization of surface groups or differential loss of ions from the crystal lattice or adsorption of charged species. As a result, a net charge is developed at the surface of every particle which affects the distribution of ions in the interfacial region. This attracts the counter ions from the solvent close to the surface around each particle forming an electrical double layer: inner stern layer where the ions are strongly bound and outer diffuse layer where the ions are

less firmly associated. A notional boundary exists within the diffuse layer in which ions and particles form a stable entity. When the particles move the ions within the boundary move it whereas those beyond the boundary stay with the bulk dispersant forming a slipping plane. The potential at this plane is the zeta potential[170] as shown in Figure 3.13.

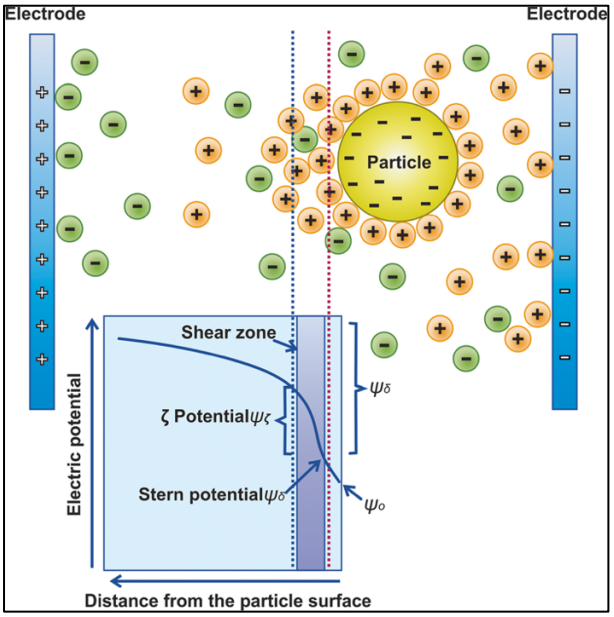

Figure 3.13. Electrical double layer at the surface of the particle and variation in zeta potential with the distance[186]

The magnitude of zeta potential indicates the stability of the dispersion. If all the particles have a large positive or negative magnitude, they will tend to repel each other and no aggregation will take place. However, if the zeta potential is > – 30 mV or < 30 mV then the particles will tend to agglomerate. The factors such as pH, conductivity of the aqueous solution and concentration of the formulation components play a role in defining the zeta potential[187,188]. When an electric field is applied to the aqueous media the charged particles are attracted towards the oppositely charged electrodes. The viscous forces oppose the movement of the particles, at equilibrium the particles move with a constant velocity. The velocity of a particle is referred to as its electrophoretic mobility in a unit electric field. The Henry equation relates zeta potential with the electrophoretic mobility[175,189]:

$$U_E = \frac{2\,\varepsilon\,Z\,f(\kappa a)}{3\,\eta} \qquad (18)$$

Where, U_E is electrophoretic mobility, Z is zeta potential, ε is dielectric constant, η is viscosity and f (κa) is Henry's function which measures the ratio of the particle radius to

electrical double layer thickness which according to the Smoluchowski approximation is 1.5.

In this work, the zetapotential of the feed solution was measured using Zetasizer Nano ZS (Malvern Instruments). 0.26 mg/ml of fluorescent polystyrene particles labelled with -COOH (Polyscience Inc.) dispersed in RO water. 750 µL of sample solution was placed in a disposable capillary cell (DTS1070) and an electric field of was applied across the cell. The refractive index of particles was assumed to be similar to polystyrene (1.59). Every sample was measured 30 times, ten seconds each, to obtain an average value for the hydrodynamic diameter.

3.6.2.3 Fluorescence spectroscopy

Fluorescence is a type of photoluminescence in which light energy raises an electron to the one of the various vibrational states in the excited electronic state. The excited electron loses its energy as a result of collisions with the surrounding molecules until it reaches the lowest vibrational state in the excited electronic state. Jablonski diagram in Figure 3.14 explains this phenomenon.

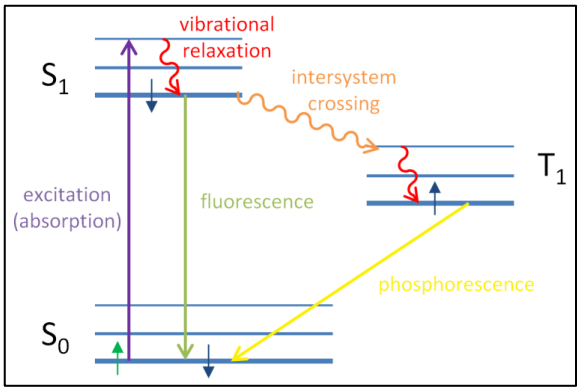

Figure 3.14. Jablonski diagram explaining the occurrence of fluorescence and phosphorescence[190]

Eventually, the molecule comes back to one of the various vibrational states of the ground electronic state by emitting a photon of lower energy and longer wavelength than the absorbed photon. Fluorescence spectroscopy analyzes the frequencies of the light emitted along with their relative intensities. In a typical fluorescence measurement, one can fix the excitation wavelength and measure the emission wavelength in the region of interest or fix the emission wavelength and measure the excitation wavelength in the region of interest[191,192].

In this work, fluorescence spectroscopy was used to analyze the particle concentration of fluorescent dyed polystyrene particles labelled with -COOH (Fluoresbrite® YG Carboxylate Microspheres 0.20µm, Polyscience Inc.) based on their emission intensities. These particles with 0.26 mg/ml of concentration were used as the feed for the filtration experiments and permeates were collected in a sequential manner. Carry Eclipse fluorescence spectrometer (Agilent Technologies, Santa Carla, USA) with a xenon flash lamp and a microtiter plate reader was used to perform these investigations. For this purpose, 350 µl of the sample to be measured was placed in each well of the 96 – well microtiter polypropylene plate (Greiner Bio-One International GmbH, Kremsmünster, Austria).

A calibration curve was obtained to relate the emission intensities with the known concentrations. The table below shows the concentrations along with the settings used for the calibration curve. Each measurement was an average of 3 runs and RO water was used as the baseline for all the measurements.

Table 3.11. The list of dilutions used for obtaining the calibration curve

Dilutions	Symbol	Concentration [mg/ml]	Particles/ml
1	B	26	5.91E+12
1:100	F_0	0.26	5.91E+10
1:250	F_1	0.104	2.37E+10
1:500	F_2	0.052	1.18E+10
1:1000	F_3	0.026	5.91E+09
1:2500	F_4	0.0104	2.37E+09
1:5000	F_5	0.0052	1.18E+09
1:7500	F_6	0.00347	7.89E+08
1:10000	F_7	0.0026	5.91E+08
1:25000	F_8	0.00104	2.37E+08
1:50000	F_9	0.00052	1.18E+08
1:75000	F_{10}	0.00035	7.89E+07
1:100000	F_{11}	0.00026	5.91E+07

Table 3.12. The instrument settings used for the fluorescence measurements

Samples	Excitation	Emission	PMP
$F_0 – F_5$	441 ± 10	486 ± 20	425
$F_6 – F_{11}$	441 ± 20	486 ± 20	505

Figure 3.15 shows the calibration curve obtained by using the polynomial fitting. Due to the non-linear behavior of the standard curve and after a comparison study with other potential fittings, polynomial fitting was chosen as the best fit.

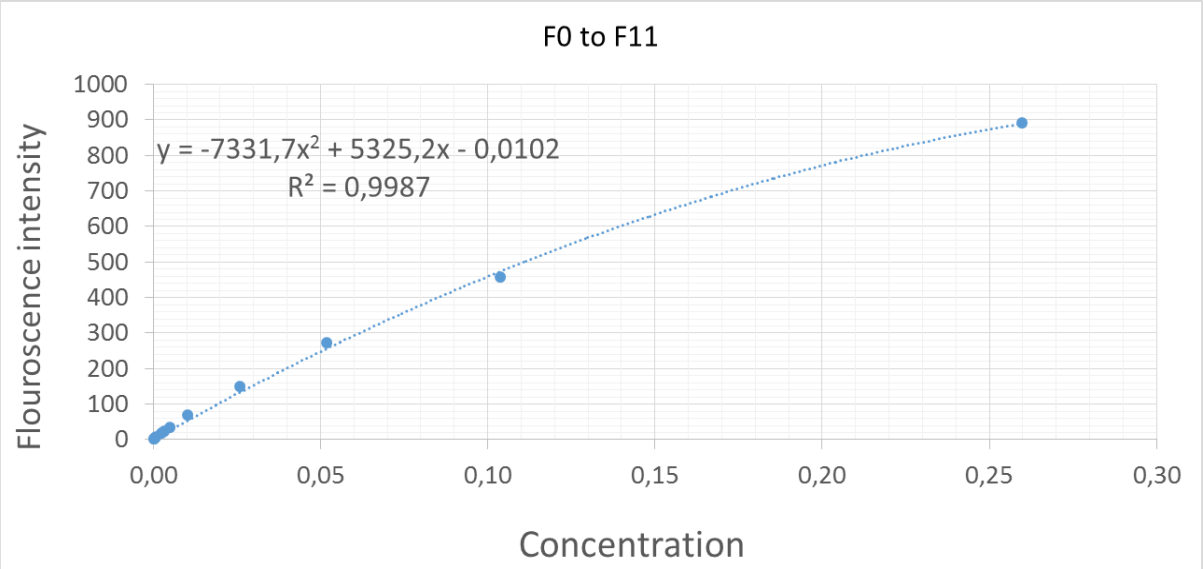

Figure 3.15. The non-linear calibration curve obtained for the dilutions. Polynomial fitting used to obtain the equation

3.6.3 Protein binding

The protein binding ability of the membranes was studied by using 1mg/mL of Bovine Serum Albumin (BSA) in 0.2 mol/L phosphate buffer solution at pH 7.2. The modified membranes along with the competitor membranes analyzed in this study are mentioned in table Table 3.9.

Base PVDF (unmodified) membrane was used as reference to understand the difference in protein binding before and after modification. The investigation for protein binding was done in two modes: static and dynamic. However, the protein binding study was performed only in the static mode on the modified membranes with different pore sizes.

3.6.3.1 Static protein binding

Static mode experiments were performed by exposing the outer surface of membranes to the BSA solution. This allowed protein to interact only with the active surface layer by diffusion. These results were useful to understand the protein – membrane surface adsorption and effect of the modification. 4.91 cm^2 (2.5 cm diameter) flat sheet membrane disk was placed in 5 ml of 1 mg/ml BSA solution (BSA challenge = 1020.41 µg / cm^2) for 1 hr. inside a shaker at 100 rpm at room temperature. Then the BSA solution was removed, the membrane surface was quickly rinsed 2 times with 5 ml RO water. The membranes were further analyzed for the amount of protein adsorbed.

3.6.3.2 Dynamic protein binding

Dynamic mode experiments were performed to expose the entire porous structure of the membrane to the protein solution. Protein solution was filtered through the membrane allowing it to maximize the interaction points. 4.4 cm in diameter flat sheet membrane disk was placed in a 50 ml Amicon cell (Amicon 1050, Millipore) without stirrer. First, the water permeance was measured followed by PBS permeance by filtering 50 ml volume at 0.1 bar pressure. 17 mg/ml of BSA solution was placed inside the Amicon cell in contact with 13.85 cm^2 active membrane area (BSA challenge = 1227.45 µg / cm^2) for 1 hr. inside a shaker at 100 rpm at room temperature. The BSA solution was filtered out through the membrane at 0.1 bar. After which 50 ml of PBS followed by 50 ml RO water were filtered through the membrane at 0.1 bar. All the measurements are average of at least 2 runs. The BSA permeance (P_{BSA}), water permeance (P_w), PBS permeance (P_P) before and after were calculated using the following equation:

$$P = \frac{V}{T \,.\, P \,.\, A} \tag{19}$$

Where, P [ml/min.cm^2.bar] is the permeance, V [ml] is the permeate volume collected, P [bar] is differential pressure and A [cm^2] is the active membrane area.

The drop in permeance was calculated for RO water and PBS to determine the reduction caused by the protein adsorption.

$$\text{Drop in permeance } [\%] = \left(1 - \frac{P}{P_0}\right) \times 100 \tag{20}$$

Where, P is the permeance after protein binding and P_0 is the permeance before protein binding.

The membranes were further analyzed for the amount of protein adsorbed.

3.6.3.3 Ponceau S protein quantification

The amount of BSA adsorbed by the membrane was further determined by Ponceau S staining quantification method. Ponceau S is a red colored sodium salt of a diazo dye. Ponceau S is a rapid and reversible stain mainly used for detecting proteins adsorbed by PVDF, nitrocellulose and cellulose acetate membranes. It is a negative stain which readily binds to positively charged amino groups of the protein as well as binds non-covalently to non-polar regions of the protein[193]. It has a low limit of detection and can detect up to 100 ng of BSA adsorbed onto nitrocellulose membrane[194].

The methodology described here was taken from previous work done by Matuschewski et al[195] and Millipore Corp[160]. The membrane after protein binding test was placed in 10 ml PBS solution for washing for 30 min. The PBS solution was thrown out and 2 ml of Ponceau S dye (AdvanStain Ponceau, AdvanstaInc.) was placed in contact with the membrane for 5 min. The dye was thrown out, to remove the unbound dye the membrane was washed 3 times with 5 ml of 5 % acetic acid for 5 min. each. After removing the unbound dye, the membrane was placed in 5 ml of 0.1 mol/L NaOH solution for 30 min. to remove the bound Ponceau S dye. All the experiments were carried out inside a shaker at 100 rpm at room temperature. The absorbance of the 0.1 mol/L NaOH solution after contact with the membrane was measured at 520 nm by having pristine 0.1 mol/L NaOH as the reference.

A calibration curve was obtained to establish a relationship between the amount of BSA adsorbed [µg] by the membrane and the Ponceau S dye absorbance observed using the UV-Vis spectrophotometer. The protein amounts were calculated by applying the known BSA amounts onto an unmodified PVDF membranes. Table 3.13 shows the BSA amounts used for the calibration curve and Figure 3.16 shows the obtained calibration curve.

Table 3.13. BSA samples used to immobilize of the PVDF base membrane for obtaining the calibration curve

Solution number	BSA Weight [ug]	Absorbance [a.u.]
1	0	0.00000
2	20	0.01595
3	60	0.05970
4	100	0.10445
5	150	0.15270
6	200	0.22370

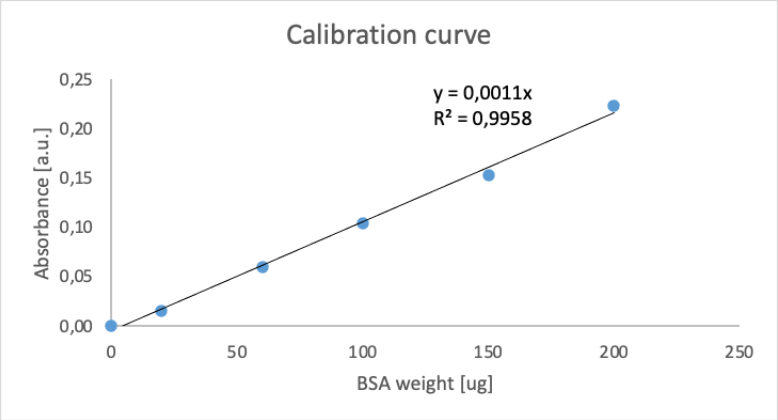

Figure 3.16. Calibration curve relating the BSA weigh with the corresponding Ponceau S absorbance

3.6.3.4 UV-Vis spectroscopy

The UV-Vis spectroscopy is a commonly used absorption or reflectance spectroscopy in analytical chemistry for quantitative or qualitative determination of analytes. The ultraviolet (UV) and visible (Vis) region are present in the electromagnetic spectrum at 10 – 400 nm and 400 – 750 nm respectively, in which atoms and molecules undergo electronic transitions from ground state to the excited states. The UV-Vis spectrophotometer measures the intensity of the light after passing through the sample (I) and compares it to the intensity of the incident light (I_0). According to the Beer-Lambert law, the absorbance is directly proportional to the concentration of the absorbing species in the solution and the path length[196].

$$A = \log_{10}\left(\frac{I_0}{I}\right) = \varepsilon c L \qquad (21)$$

Where, A is the absorbance [a.u.], I_0 is the intensity of the incident light at a given wavelength, I is the transmitted intensity, I_0/I is called transmittance, ε is the molar absorptivity constant, c is the concentration of the absorbing species and L is the path length.

In this work, UV1800 spectrophotometer (Shimadzu) was used to measure the absorbance at 520 nm of the NaOH solution in contact with the membrane after protein binding. 3.5 ml of sample was added to one of the quartz cuvettes and pristine 0.1 mol/L NaOH was added to another quartz cuvette as a reference. The average of 3 runs was taken as the final measurement.

3.7 Sterilization

Sterilization is a process that destroys all forms of microbial life such as bacteria, fungi, spores, etc. present on a surface of an object or in a fluid, for example in biological cell culture or food[197]. There are various physical and chemical methods to carry out sterilization such as heat, irradiation, high pressure, filtration and use of chemicals. The membranes and membrane devices used in pharmaceutical industries for bioprocessing applications are sterilized before their use. The typically used sterilization techniques for membranes are auto-clave, Eto sterilization and Gamma irradiation. A good membrane product should retain its properties after exposed to the harsh sterilization conditions. In this work we sterilized the industrially modified HEMA and Acrylic acid 10X10 cm^2 flat sheet membranes by autoclave for 20 min. at 121°C and gamma irradiation at 25 kGy. The membrane properties: water permeance, water bubble point, air flow and contact angle were determined before and after sterilization.

3.8 Chemical compatibility

Chemical compatibility tests were performed in the static mode for the industrially modified HEMA membrane. Two Flat sheet membrane disks of 44 mm diameter were kept in contact with 20 ml of chemical for 48 hrs. Then the samples were placed in water for 24 hrs. for washing before they were dried. The water bubble point, thickness and air flow of the membranes after contact with chemicals was determined. If the properties changed by more than 10 % of the pristine membrane the chemical was declared unsuitable for the membrane.

3.9 Thermal stability

To predict the shelf life of the membrane and membrane products an accelerated aging test is performed according to the ASTM standard (F1980 – 07) by exposing samples to high temperature with controlled humidity for a long period of time. In this work, we placed the membranes inside the climatic chamber at 90°C for 16 days which is equivalent to 5 yrs. of shelf life according to ASTM standard. The properties of membrane – water permeance, air flow, contact angle and water bubble point – were determined before and after the accelerated aging test to investigate the degradation due to thermal stress.

4 RESULTS AND DISCUSSION

4.1 Base membrane characteristics

Base membrane characteristics, such as thickness and morphology, affect the polymerization kinetics mechanism and subsequently the final membrane properties. This section establishes a criterion for selecting the base membrane for functionalization by analyzing the deviations in the characteristics to obtain the final membrane with consistent properties.

The base membrane used in this study was an industrially (in-house GVS) produced 0.45 µm flat sheet PVDF membrane cast on a polyester support via non-solvent induced phase separation (NIPS) method[198] in a batch process. Efficiency of the modification methodology – "two-step graft coating polymerization" – is governed by the base membrane's ability to absorb the solution one in the first step and to allow diffusion of a reagents in the second step. Thus, base membrane thickness and morphology (pore size and porosity) play an integral role in membrane functionalization. Base membrane with consistent characteristics results in stable properties of the modified membranes; reducing the irregularities caused by base membrane. The detailed study of polymerization mechanism is discussed in section 4.2 and the effect of base membrane characteristics on polymerization is demonstrated in section 4.7.

Three samples from different batches or "lots" (as called in the industry) of 0.45 µm PVDF production were characterized for their morphology and thickness to understand lot-to-lot fluctuations. Figure 4.1 compares the pore size distribution in (a) and corresponding airflow in (b). Considerable differences in the pore size and consequently in the airflow were observed. Therefore, the flow properties of the modified membranes could differ based on the chosen lot for modification.

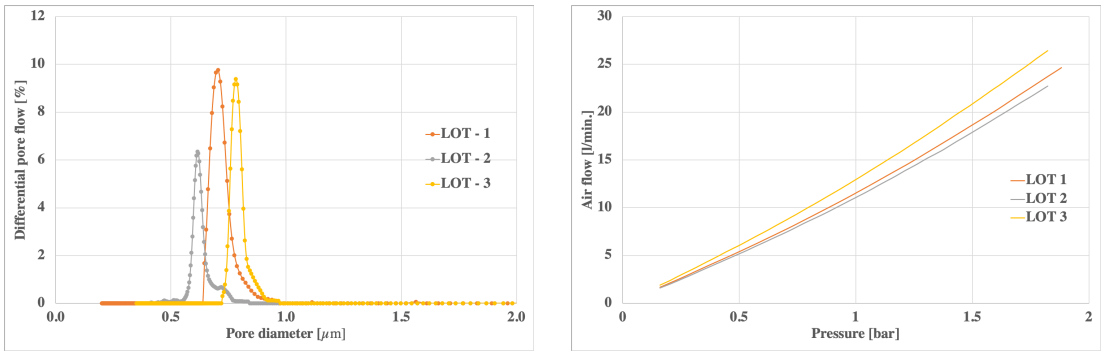

(a) (b)

Figure 4.1. Difference in the (a) pore size distribution and (b) air flow measurements of the different lots of 0.45 µm PVDF base membranes used for modification

The difference in (a) porosity and (b) thickness (see Figure 4.2) leads to distinctive kinetics and mechanisms of polymerization, thus affecting final membrane properties differently.

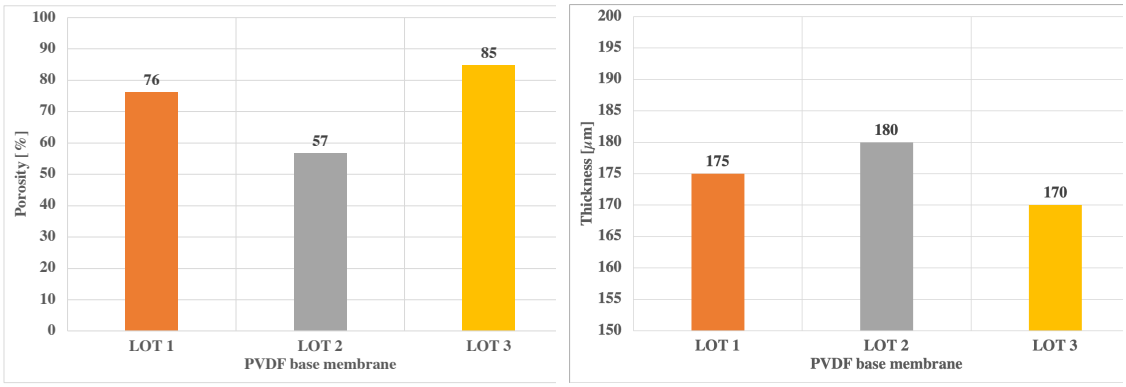

(a) (b)

Figure 4.2. Difference in the (a) porosity and (b) thickness for the different lots of 0.45 µm PVDF base membrane used for modification

The characteristics fluctuated from batch to batch due to inconsistencies during membrane casting in various factors such as PVDF concentration, coagulation bath composition and temperature, and moisture content during the industrial production of 250 m roll. The effect of these factors on the membrane characteristics are well established and widely studied in literature[159,199]. Furthermore, upscaling of the membrane casting also causes potential deviations due to contamination of the line, irregular speed of the line, and manual errors caused by operators.

Base membranes (nominal pore size 0.45 µm) were sorted for the pore size irregularities based on the air flow measurements as shown in Table 4.1. The membranes from the

same group were selected for one set of modification study to minimize the deviations in the final membrane properties due to the base membrane morphology deviations.

Table 4.1. Base membrane classification based on the air flow measurements

Base membrane group	Air flow [l/h] at 0.93 bar
I	700 – 800
II	800 – 900
III	900 – 1000
IV	1000 – 1100

4.2 Two-step graft coating polymerization

This section elaborates on the fundamental mechanisms involved in two-step graft coating polymerization which is a combination of dip-coating and graft polymerization. The process is divided into two steps in different solvent systems – organic and aqueous – to avoid homopolymerization in the water phase and increase process effectiveness. The first system consists of hydrogen peroxide and cross-linker dispersed in IPA. While the second system consists of iron chloride, monomer or polymer and ascorbic acid dissolved in water. Additionally, proof of successful PVDF membrane functionalization with a monomer (acrylic acid) and a polymer (10 kDa PVP) using EGDMA as a cross-linker is provided by presenting the characteristic properties of the modified membranes.

4.2.1 Reaction mechanism

In the first step, membrane was immersed in the first system allowing absorption of the reagents into the membrane matrix. The membrane should be immersed long enough to allow absorption throughout the porous structure. However, for smaller pore sizes longer immersion time might be necessary. Moreover, deeper penetration into the porous structure on prolonged immersion for smaller pores could possibly hinder the polymerization in the second step by making reagents inaccessible. This makes time the limiting factor in the first step. In the second step, the membrane from step-one was immersed in the second system. The diffusion of reagents takes place at the membrane-bulk interface initiating the reaction by forming free radicals followed by chain-growth polymerization leading to covalent bonds between PVDF and the modifying layer along

with formation of an interpenetrating cross-linked layer. The formation of radicals takes place by redox initiation in aqueous medium according to the equation shown in Figure 4.3.

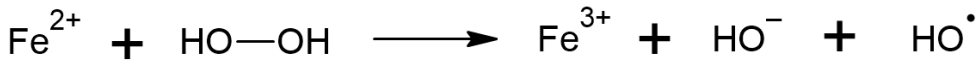

Figure 4.3. Formation of radicals via redox initiation

A reaction zone is created at the interface where the maximum number of reactions take place. The location of organic radicals is initially in the reaction zone but is subsequently delocalized upon rapid diffusion. As a result of rapid mass transport, the polymerization zone extends into the membrane matrix and bulk solution creating the following concentration profiles:

- Radicals decrease away from the interface,
- Reactions decrease away from the interface, and
- Unreacted reagents increase away from the interface

The diffusion of reagents, the formation of the reaction zone and the developed concentration profiles are shown in Figure 4.4.

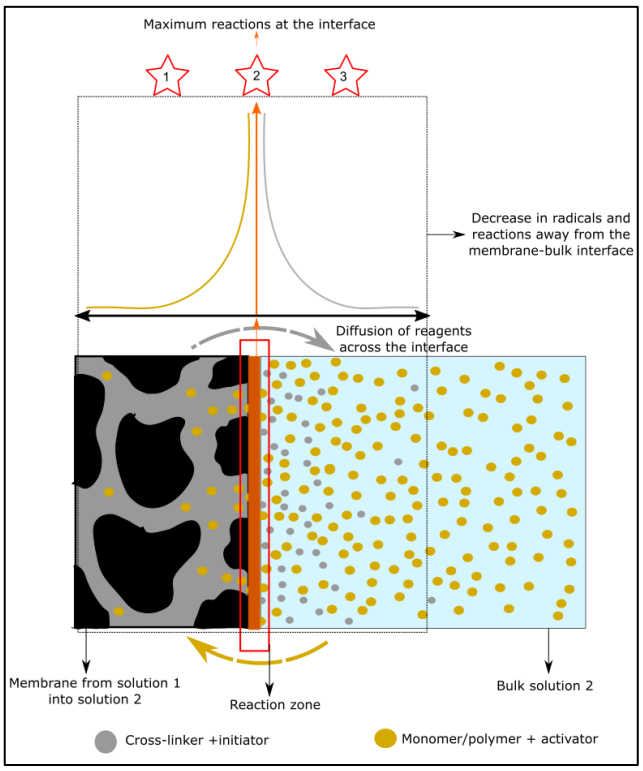

Figure 4.4. Diffusion of reagents, formation of the reaction zone at the membrane-bulk interface and developed concentration profile at the interface upon introduction of membrane from 'solution 1' to 'solution 2'. The stars represent: 1. Location inside the membrane, 2. Location at the interface, and 3. Location in the bulk

Part of generated hydroxide radicals readily react with IPA present in the membrane matrix to form more stable IPA radicals by radical transfer to solvent (see Figure 4.5). Kolthoff et al.[200] reported a similar phenomenon for the formation of hydroxyethyl radical from ethanol in the presence of oxygen. Although radical transfer to solvent leads to formation of a stable IPA radical, it commonly acts as a scavenger rather than initiating chain growth due to its stability. Therefore, OH radical majorly contributes in initiating chain growth polymerization.

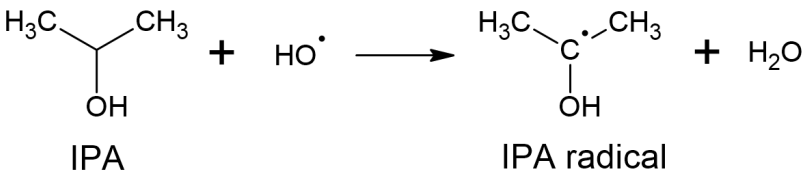

Figure 4.5. Formation of more stable IPA radical by solvent transfer

The start reactions and formation of organic macroradicals for each reagent in the system are shown below. Figure 4.6 and Figure 4.7 exhibit the formation of macroradicals for PVDF and PVP respectively, via hydrogen abstraction[201]. Due to the absence of double bond, abstraction of hydrogen by bond dissociation takes place to form a new radical. Similar study with abstraction of hydrogen atoms from cellulose in the presence of vinyl

monomers for grafting was carried out by Hebeish and Guthrie[155]. Furthermore, Brockway and Moser[202] reported failed graft polymerization onto starch with an azo alone initiator verifying the success of grafting primarily by Fenton's reagent.

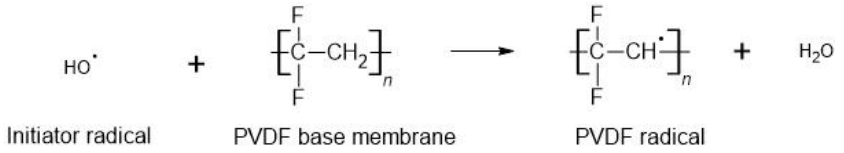

Figure 4.6. Formation of an active site on the PVDF base membrane by hydrogen abstraction[203]

In case of PVP there are several abstractable hydrogen atoms. The dissociation energy of the X-H bond to form the new radical dictates the rate of hydrogen abstraction. The thermodynamic calculations performed by Zhu and coworkers[204] show that C-H bonds at α-position to C=O group are lower in energy due to the stabilization of the radical. The most favorable PVP macroradical structure expected is highlighted in green and shown in Figure 4.7.

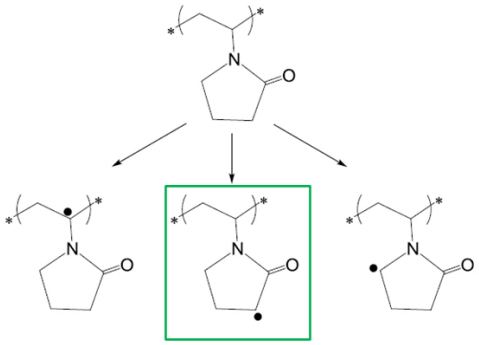

Figure 4.7. The most favorable PVP radical by hydrogen abstraction[205]

Figure 4.8 and Figure 4.9 represent the formation of radicals for EGDMA and acrylic acid respectively via addition mechanism. The starter radical adds to the π-bond by taking an electron and forms a new radical on the adjacent atom.

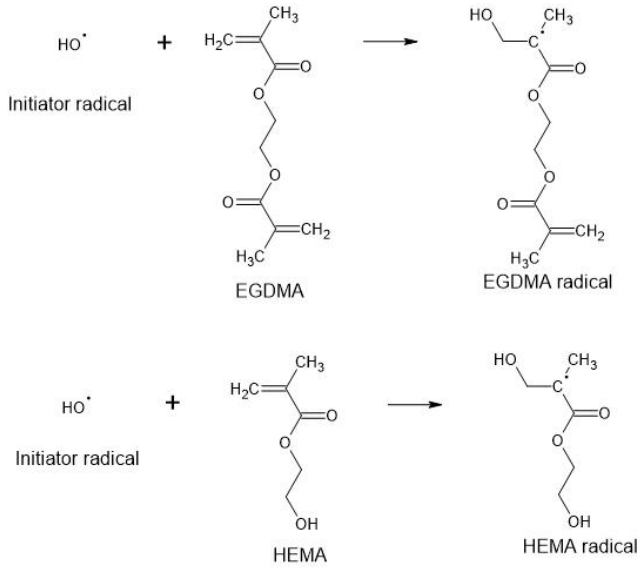

Figure 4.8. Formation of EGDMA radicals by addition mechanism which propagates the chain-growth polymerization

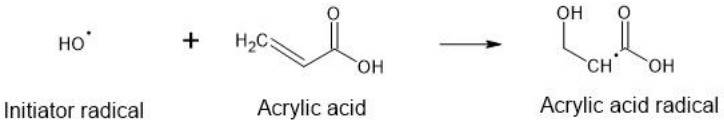

Figure 4.9. Formation of acrylic acid radicals by addition mechanism which propagates the chain-growth polymerization

EGDMA possess two π-bonds that participate in chain-growth, the unreacted double bond becomes a pendant on the growing chain; if another radical adds to this pendant double bond a cross-linkage is formed. Thus, it plays an integral role of bridging the polymer network by acting as a cross-linker. The polymerization takes place in an uncontrolled manner; therefore, the polymer network can grow in multiple pathways when macroradicals and growing chains react with other reagents in the bulk. The representative chain growth reaction for EGDMA via addition mechanism and the active pendant group is displayed in Figure 4.10. Polyacrylic acid chain growth occurs with the similar mechanism as EGDMA and therefore not shown.

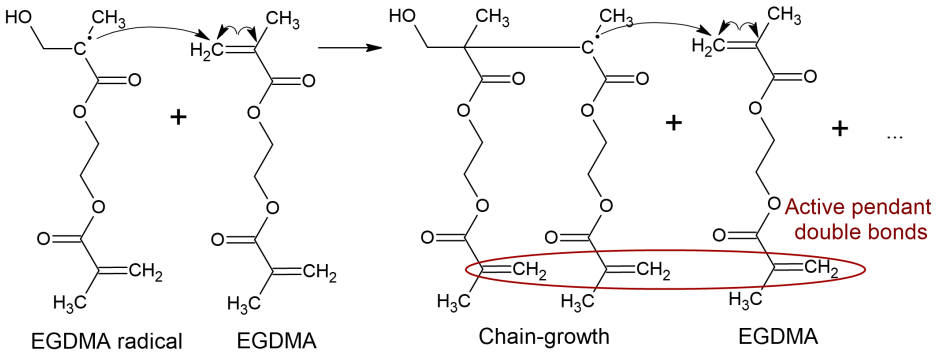

Figure 4.10. Chain-growth polymerization mechanism of EGDMA

Figure 4.11 shows the addition of PVDF macroradical to the pendant double bond in the growing EGDMA chain. A covalent bond is formed and the growing chain is grafted onto the PVDF membrane.

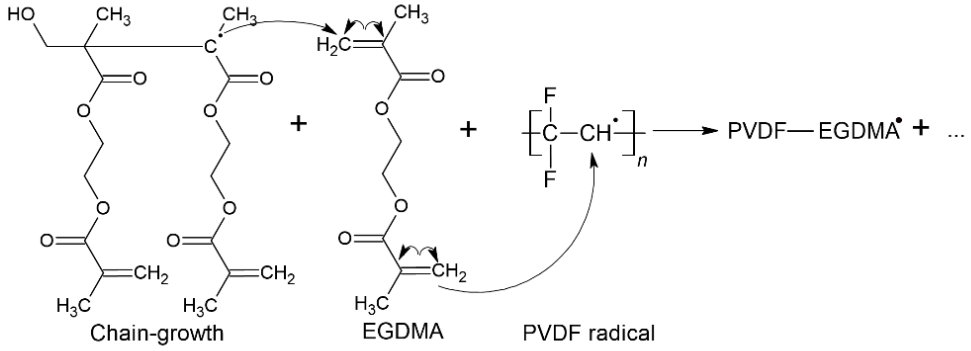

Figure 4.11. Cross-linking mechanism of the growing EGDMA chain: grafting of the polymerized chain

The PVP macroradicals react in the similar mechanism with EGDMA to participate in the network, and can also directly combine with PVDF radical terminating the reaction, but this is rare due to the bulky nature of long chain PVP.

The chain-growth starts rapidly at the interface once the radicals are formed: the viscosity of the reaction mixture at the interface increases over time which creates a barrier for diffusion[206]. Since diffusion is viscosity dependent, diffusion becomes more relevant for further propagation as the limiting factor for transfer of reagents. The efficiency of the chain-growth polymerization and the ability of polymers to incorporate themselves into the growing hydrogel network depends on the following factors:

1. The local concentration of the polymers in the reaction zone,
2. The reactivity of the polymers, and
3. Copolymerization efficiency of polymers

The factors affecting the efficiency of polymerization are discussed in greater details in sections 4.3 and 4.4. The rapid addition of monomer molecules to the growing polymer chain leads to the chain growth. The growing EGDMA chains react with PVP or polyacrylic acid chains to form the polymer network which is ultimately grafted on the PVDF membrane. An alternative polymerization also takes place simultaneously where an entangled network of cross-linked chains is entrapped on the surface. The polymerization reaction continues until all the active radicals are exhausted via combination or disproportion[207]. The ideal functionalized membrane surface with grafted hydrogel layer is shown in Figure 4.12.

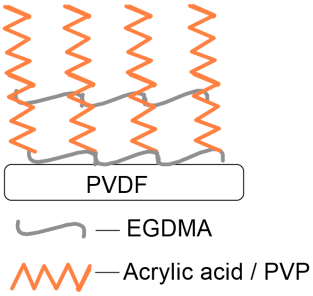

Figure 4.12. Ideal functionalized membrane surface with the grafted hydrogel structure

Several different types of substrates and water-soluble functional vinyl polymers can be utilized in two-step graft polymerization coating to obtain membranes with varying surface properties.

4.2.2 Membrane characterization

This sub-section attempts to summarize the major characteristics of the modified membranes with respect to the base PVDF membrane upon investigation of membrane surface properties with appropriate techniques. The representative formulation considered for the proof of the concept characterization experiments is shown in Table 4.2.

Table 4.2. Representative formulation used for the proof of the concept for PVP and PAA

Solution 1 [wt.%]			Solution 2 [wt.%]			
H_2O_2	EGDMA	IPA	PVP/PAA	$FeCl_2.4H_2O$	Vit C	RO water
6	5	89	5	0.28	1	93.72

Fourier transform infra-red (FTIR) spectroscopy was used to understand chemical modifications on the membrane surfaces. Zeta potential measurement provided an insight about the surface charge upon functionalization which affects the membrane performance. The hydrophilic nature of the membranes was evaluated using the contact angle measurements. Finally, the change in weight due to polymer grafting was also measured to confirm the presence of hydrogel coating.

IR spectroscopy

ATR-FTIR spectroscopy was used to perform qualitative characterization of the surface chemistry for modified membranes. IR spectroscopy was performed to prove the existence of the hydrogel layer on the membrane surface and failure in the absence of cross-linker. Figure 4.13 introduces all the IR charts displaying the characteristic peaks for polyacrylic acid and PVP in reference to the base PVDF membrane. The most evident difference was the presence of a strong C=O stretching peak at 1725 cm^{-1} for PVP and polyacrylic acid modified membrane[208,209]. This corresponds to the carbonyl groups present in EGDMA, PVP and carboxylic group of polyacrylic acid. The peak was stronger for PVP possibly due to a higher amount of EGDMA incorporation in the polymer network compared to polyacrylic acid (the mechanism discussed in detail later in section 4.3). This peak was significantly weaker for the PVP modification without EGDMA. This confirmed EGDMA's integral anchoring role in bridging polymer chains in the polymer network. This was further supported by absence of C-N vibrations at 1320 cm^{-1} corresponding to the PVP[210]. Butruk et al.[157] also reported slow polymerization (~ 1 h) in the absence of cross-linker for PVP grafting on polyurethane disk using Fenton reaction. When the membrane was covered with the hydrogel layer the intensity of the CH_2 stretching at 1402 cm^{-1} decreased for modified membraned compared to pristine PVDF[211]. Finally, a broad peak corresponding to the OH stretching was observed between 3100 cm^{-1} to 3500 cm^{-1} of the hydroxyl group in polyacrylic acid[212,213].

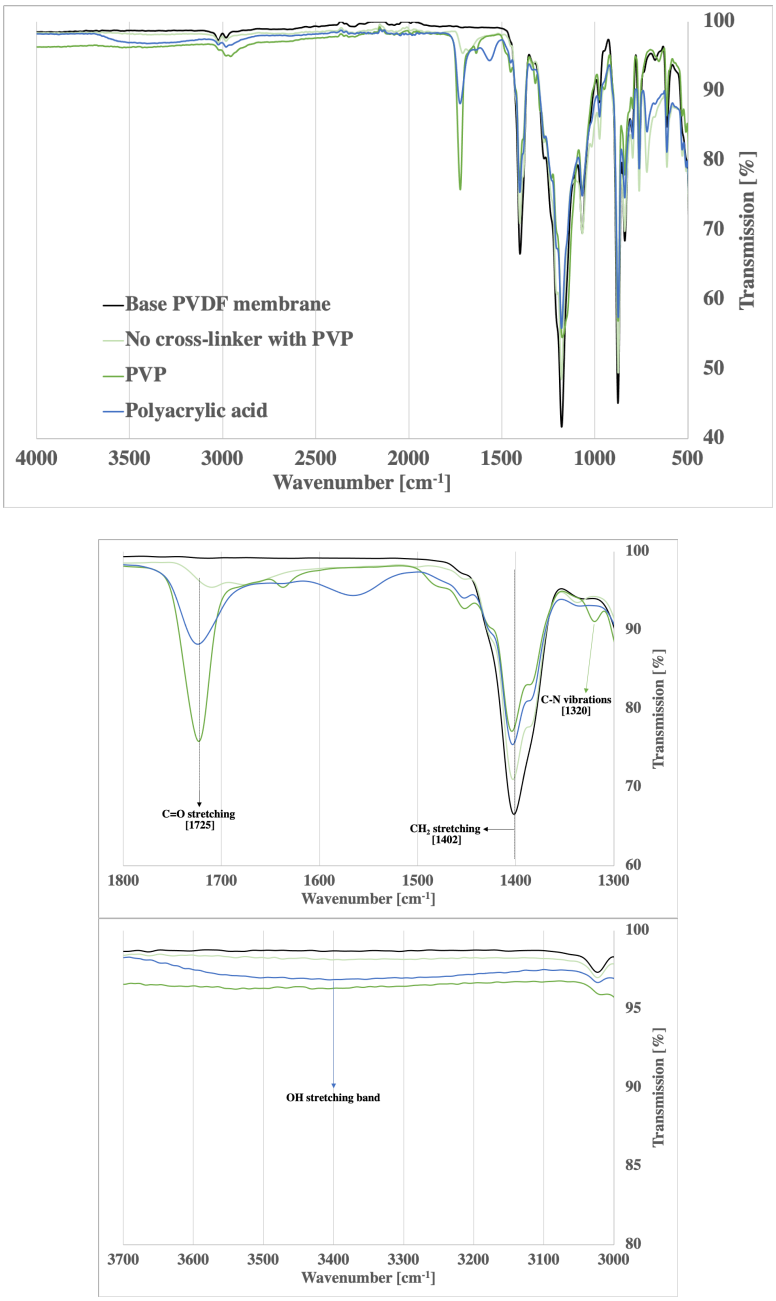

Figure 4.13 IR spectra and the enlargement of two IR ranges representing the characteristic peaks for polyacrylic acid and PVP modifications with and without EGDMA

Zeta potential

Zeta potential measurements of the representative modified membranes: polyacrylic acid and PVP, were compared with pristine PVDF base membrane and are presented in Figure 4.14. The base PVDF membrane showed overall negative charge with an IEP at a pH of approximately 4. It is established that hydrophobic surfaces due to preferable hydroxide or chloride (because of KCl used during the measurement) ions adsorption exhibit a negative zeta potential in aqueous solutions[214,215]. However, the surface charge depends on the pH. At high pH high concentration of HO^- renders surface charge negative and at

low pH high concentration of H_3O^+ renders surface charge positive. For PVP, the IEP shifted to ~ 3.5 with overall charge slightly more negative than base PVDF but with a similar trend. This shift could be attributed to the increase in hydrophilicity by PVP-EGDMA enhancing the negative surface charge due to the presence of polar carbonyl group[216]. Upon polymerization of polyacrylic acid onto the membrane surface multiple negatively charged pH responsive carboxyl groups are attached on the surface. As a result of high surface density of carboxyl groups, the polyacrylic acid modified membrane shows negative surface charge throughout the pH range without an IEP. Although the pKa value of polyacrylic acid is ~ 4.3, it is possible that several of the carboxyl groups are already dissociated even below pH 4 hence shifting the zeta potential in the negative range.

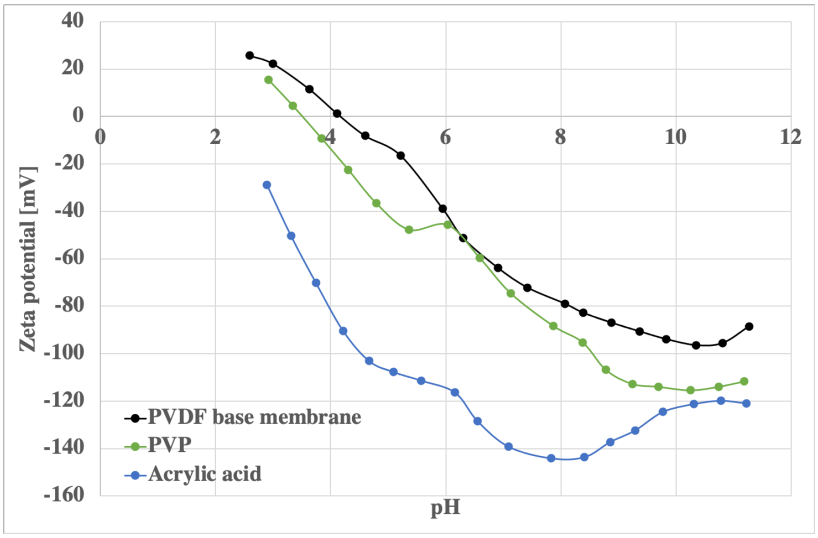

Figure 4.14. Zeta potential of the modified membranes and the PVDF base membrane as a function of pH

Contact angle

The very low surface energy of PVDF results in the poor wettability of the PVDF membrane with a constant water contact angle of 137°. PVP and polyacrylic acid covalently bond on the surface of PVDF membrane upon modification improving hydrophilicity, hence drastically reducing the contact angle (from 137° to ~45°) and wetting time (see Figure 4.15). The incorporation of hydrophilic -COOH group in polyacrylic acid and polar functional groups present in PVP impart the hydrophilicity to the membrane[217,218]. Hydrophilicity and porous top surface accelerates water droplet penetration due to capillary effects; these factors reduce the contact angle[219]. Unlike hydrophobic surfaces, hydrophilic surfaces due to high surface energy have high affinity towards water hence forming a hydration layer on the membrane surface as a result of

hydrogen bonding, thereby reducing the interactions of proteins and other particles from the feed with the membrane.

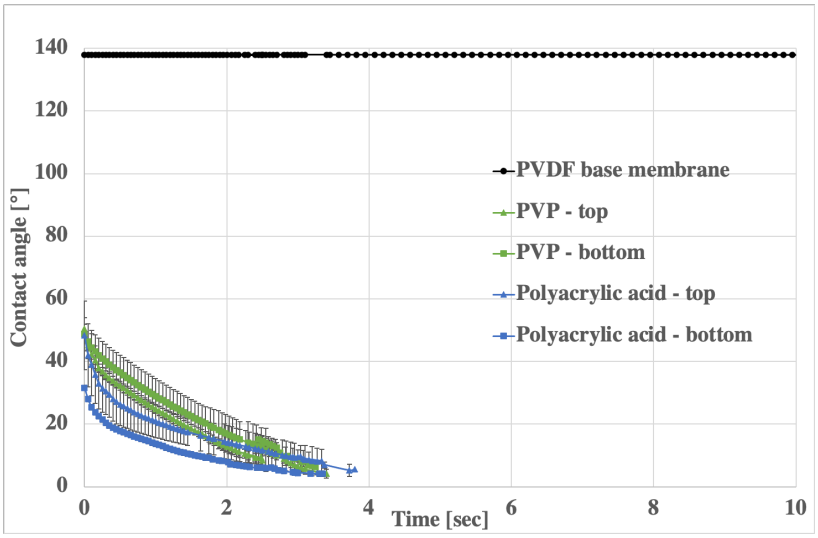

Figure 4.15 The change in contact angle with time of the top and bottom surface of polyacrylic acid and PVP modification

Hydrogel grafted

Along with the changes in the surface chemistry of the membrane, physical properties of the membrane also change upon modification such as weight of the membrane due to grafting of the hydrogel layer. Figure 4.16. illustrates the increase in weight percent due to the grafting of hydrogel layer. The higher value for polyacrylic acid than PVP is due to higher reactivity and diffusion coefficient of the monomers which allows higher number of acrylic acid molecules to be incorporated in the polymer network within same modification period. The difference between the reaction mechanism of PVP and polyacrylic acid is discussed in detail later in sections 5.3 and 5.4. Polymerization with only EGDMA (in the absence of any polymers) shows high amount of grafting indicating very efficient homopolymerization of EGDMA. Moreover, very low grafting in the absence of EGDMA emphasizes the anchoring role that a cross-linker plays in grafting polymer chains. In general, the results in Figure 4.16 proved successful grafting of the hydrogel layer in the presence of EGDMA.

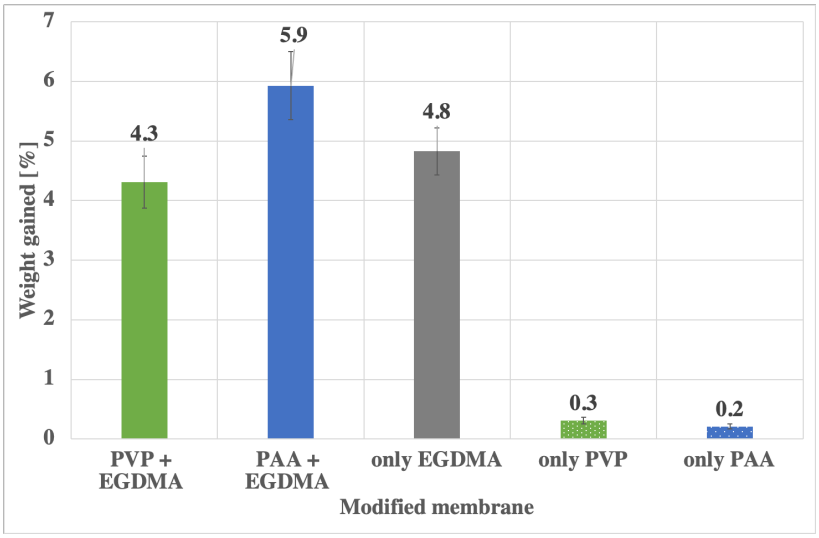

Figure 4.16. Weight gained after PVP and polyacrylic acid modifications with and without EGDMA as the cross-linker

The mechanism of functionalization by versatile two-step graft coating polymerization was discussed in detail and role of each participating reagent was explained. The successful modification of the membrane with PVP and polyacrylic acid confirmed the flexibility of the modification methodology.

4.3 Influence of polymer type on membrane functionalization

The influence of having a long chain polymer: PVP and a monomer: acrylic acid on polymerization and consequently on the final membrane properties was studied in detail in this section by understanding the reaction mechanism. This was a crucial step moving forward for selecting the appropriate compound for functionalization to obtain desired properties of the final membrane.

4.3.1 Functionalization with a polymer: 10 kDa PVP

Membranes were modified with different proportions of PVP concentration and keeping the fraction of other reagents constant (see Table 4.3). The flow properties (permeance), hydrogel layer characteristics, wettability, and morphology of the modified membranes were investigated.

Table 4.3. Modification formulation for 10 kDa PVP

Solution 1 [wt.%]			Solution 2 [wt.%]			
H_2O_2	EGDMA	IPA	PVP	$FeCl_2.4H_2O$	Vit C	RO water
6	5	89	5	0.28	1	93.72
6	5	89	10	0.28	1	88.72
6	5	89	20	0.28	1	78.72

The efficiency of polymerization depends on the successful incorporation of maximum number of PVP molecules in the hydrogel network. The reaction zone is formed after organic radicals are generated at the interface as discussed in section 4.2.1. The PVP concentration increases away from the reaction zone into the bulk whereas, hydroxyl and IPA radical concentration decreases away from the reaction zone. Figure 4.17 shows the concentration gradient for reagents in the polymerization reaction.

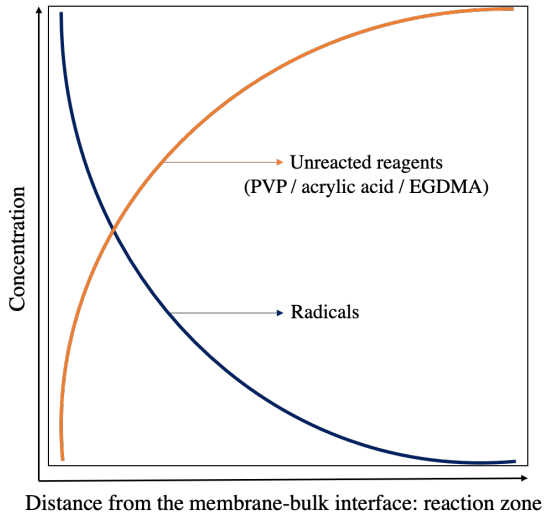

Figure 4.17. Concentration gradient of the radicals and reagents across the membrane-bulk interface

The participation of PVP and EGDMA in the chain growth depends on the local concentration in the reaction zone, reactivity and copolymerization efficiency. The movement of molecules in the reaction zone for propagation is a diffusion-controlled phenomenon. EGDMA molecules diffuse into the reaction zone at a faster rate than PVP due to the smaller size. Moreover, PVP molecules are dispersed in the bulk away from the interface unlike EGDMA molecules that are dispersed in the membrane matrix close to the interface; therefore, EGDMA mass transfer take is higher than for PVP. As a result, local concentration of EGDMA is more than PVP. The formation of macroradicals takes

place via hydrogen abstraction for PVP and via addition mechanism for EGDMA (see Figure 4.7 and Figure 4.8). The addition reaction is preferred energetically because the new bond formed is stronger than the broken π-bond thereby releasing energy; in contrast, energy is required for bond dissociation in hydrogen abstraction[220]. This makes EGDMA more reactive than PVP. As a result, polymerization rate of EGDMA molecules increases in the reaction zone forming a dominant growing polymer network at the interface further hindering the movement of PVP into the membrane matrix due to increased viscosity. This concept is known as glass-effect and was reviewed by Achilias in his work on modeling diffusion-controlled polymerization reactions[221].

Figure 4.18 depicts the schematics for the formation of PVP polymer network in three stages. Stage i – diffusion of reagents and formation of reaction zone, stage ii – faster polymerization of EGDMA at the interface hindering PVP movement across the interface, and stage iii – formation of the polymer network dominated by EGDMA.

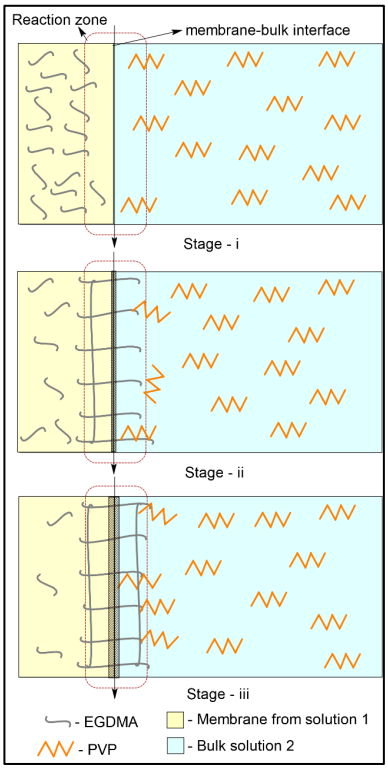

Figure 4.18. Visual interpretation of formation of the hydrogel network with PVP in three stages at the membrane-bulk interface (reaction zone)

With increasing PVP concentration the number of PVP molecules in the bulk increases, potentially increasing PVP molecules in the reaction zone. Initially, more PVP was available to react at 10 wt.% and 20 wt.% compared to 5 wt.%. However, due to the large size of PVP chains, the rate of diffusion from the bulk is slow. Moreover, the rate of

polymerization of EGDMA is reduced due to increase in consumption of initiator radicals by radical transfer to added PVP molecules. Nevertheless, PVP molecules due to large size do not penetrate the membrane matrix but participate in the polymer network on the outer surface of the membrane. The grafting of PVP in the surface hydrogel network increased with increasing concentration as seen from the weight gained in Figure 4.19. But the increase in weight was not proportional to the increase in PVP concentration. Besides, the weight gained in the absence of PVP was comparable (even higher than for 5 % PVP) to the values obtained in the presence of PVP. This further strengthened the hypothesis that EGDMA dominates the polymerization, thereby dominating the polymer network. The small increase with increasing PVP concentration can be attributed to the increased PVP participation in the surface polymer network. In addition to the chemical cross-linking, long PVP chains could also be involved in physical cross-linking or entanglement such as, trapping of PVP chains in EGDMA network.

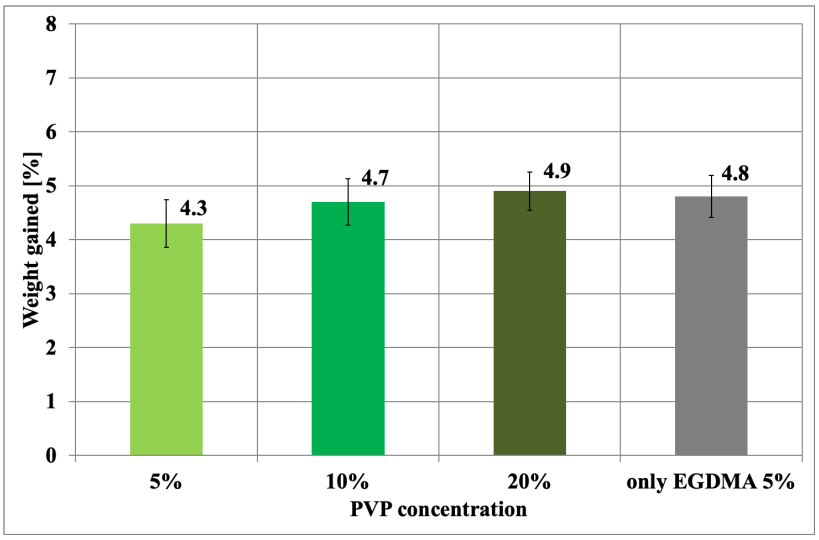

Figure 4.19. Comparison of weight gained after modification with different PVP concentrations and without PVP (only EGDMA)

The increased grafting efficiency of PVP in the surface hydrogel network at higher PVP ratio leads to enhanced ability of the hydrogel network to hold water at the surface as seen from the water uptake results in Figure 4.20. A loosely packed hydrogel structure on the surface consists of PVP chains possessing the ability to interact with water molecules due to the presence of the polar groups (N—C=O). In addition to pore filling the increased volume of the outer surface (without changing the structural geometry) upon surface PVP grafting creates more spaces for water to bind. Modified membrane without PVP (only

EGDMA) shows higher water uptake than 5 % PVP potentially due to the more open base membrane.

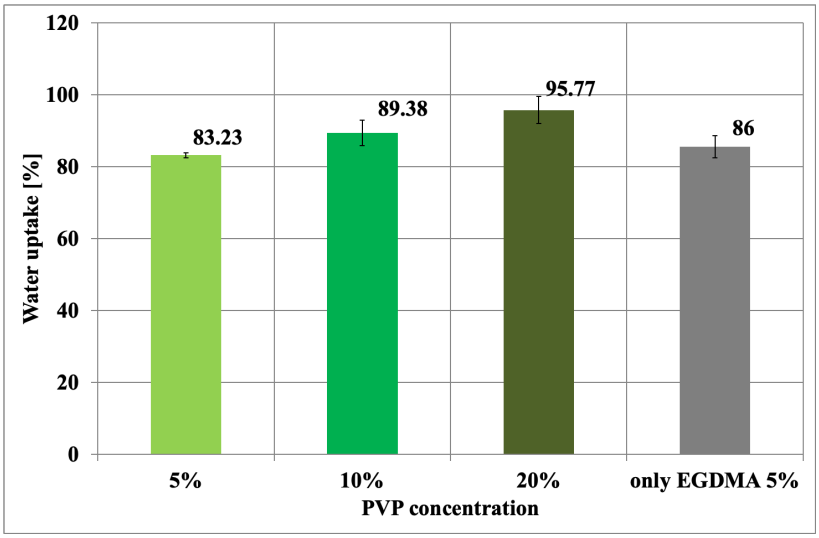

Figure 4.20. Comparison of water uptake after modification with different PVP concentrations and without PVP (only EGDMA)

Figure 4.21 schematically depicts the distribution of PVP and EGDMA molecules in the reaction zone and presents the predicted hydrogel network formed upon polymerization for different PVP concentrations. The PVP chains in polymer network increase with increasing concentration.

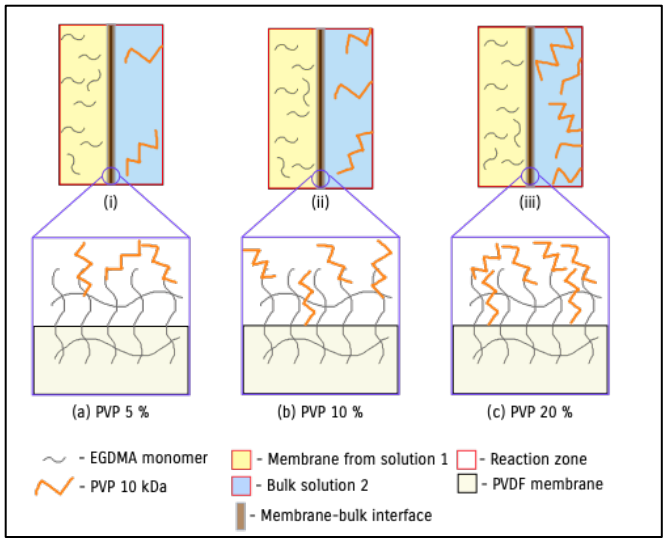

Figure 4.21. Visual interpretation of the formation of hydrogel network at the membrane-bulk interface for different PVP concentrations at 5 % EGDMA

Moreover, with increasing PVP concentration, the increased viscosity further reduces the diffusion rate. This means that once first set of PVP molecules react in the reaction zone to form polymer network, the polymerization rate of PVP molecules in the polymer

network drastically drops. As a result, EGDMA dominates the polymer network in the membrane matrix constricting the pores and subsequently reducing the water permeance as seen in Figure 4.22. The reason for the high drop in permeance between 5 wt.% and 10 wt.% could potentially be due to the difference in the characteristics of the base membranes used as explained in section 5.1. Additionally, it was seen that at high concentrations (10 wt.% and 20 wt.%) the effect of PVP on the final membrane properties was less significant suggesting saturation of PVP participation in the polymer network.

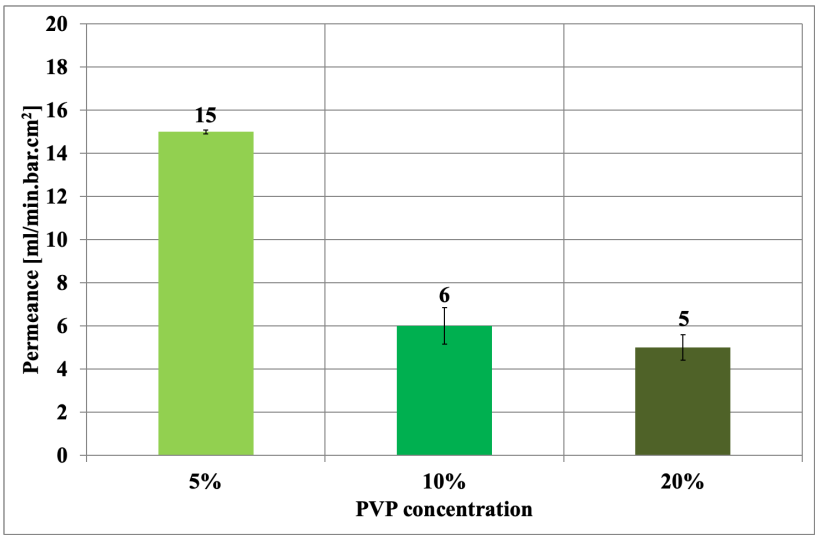

Figure 4.22. Comparison of water permeance after modification with different PVP concentrations

Contact angle

Wettability of the modified PVP membranes was evaluated using dynamic contact angle measurement (see Figure 4.23). 5 wt.% exhibited lowest surface wettability while 20 wt.% the highest, verifying the presence of more PVP on the surface with increasing concentration as argued above. Upon increasing PVP concentration, interaction of water with the surface increases allowing water to easily pass into the porous structure. However, at 5 wt.%, less PVP molecules were grafted on the surface less effectively increasing the wetting time.

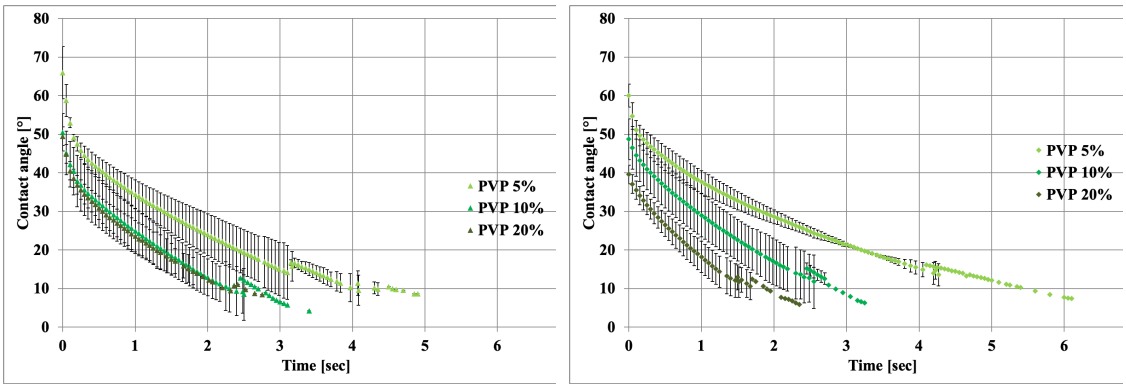

Figure 4.23. Change in contact angle with time for (a) top surface and (b) bottom surface after modifications with different PVP concentrations

SEM

Top and bottom surface morphologies of the modified membranes were examined by SEM at magnification of 5000. The number of open pores with increasing PVP concentration on the bottom surface appeared to be reduced due to coverage of PVP chains (see Figure 4.24) which also resulted in reduced water permeance. However, at 5 wt.% not many PVP molecules are present in the reaction zone, as a result EGDMA quickly reacts with majority of the radicals and extensive homopolymerization of EGDMA takes place. The micrographs also support the hypothesis of participation of PVP on the surface polymer network at high concentrations.

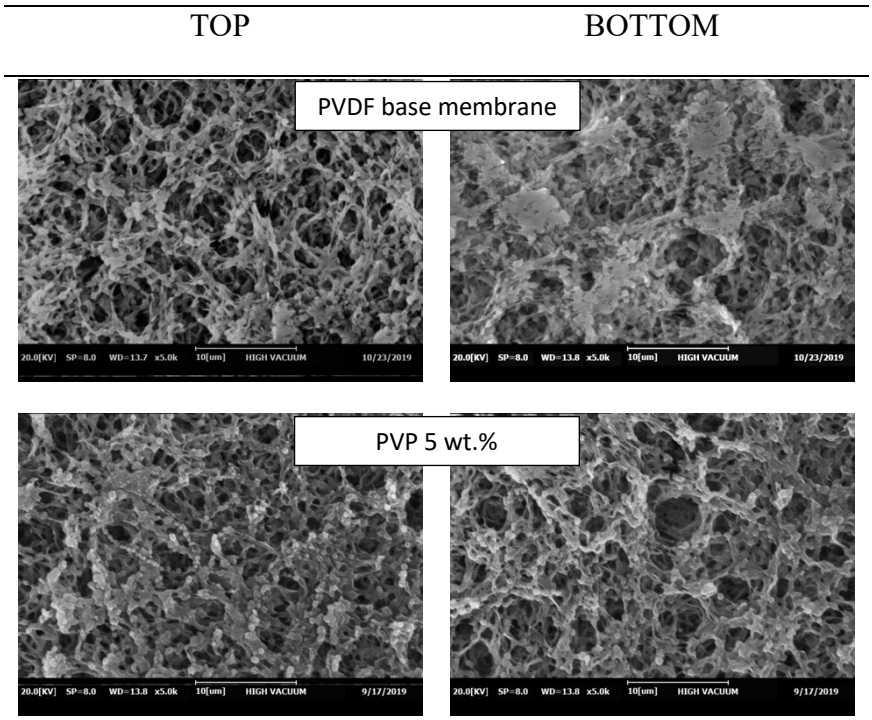

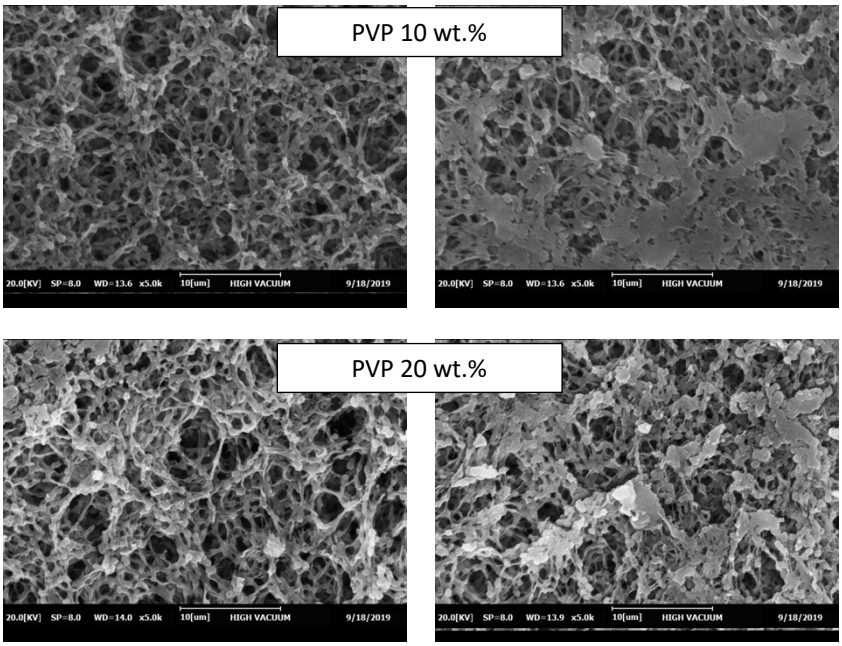

Figure 4.24 SEM micrographs of the top and bottom surface: after modification with different PVP concentration and the base membranes

4.3.2 Functionalization with a monomer: acrylic acid

A study similar to PVP modifications was carried out to analyze the influence of acrylic acid monomer on polymerization. 0.45 µm PVDF base membrane was modified with varying proportions of acrylic acid by keeping fractions of other reagents constant as shown in Table 4.4. The flow properties (permeance), hydrogel layer characteristics, hydrophilicity, and morphology of the modified membrane were investigated.

Table 4.4. Modification formulation for acrylic acid monomer functionalization

Solution 1 [wt.%]			Solution 2 [wt.%]			
H_2O_2	EGDMA	IPA	Acrylic acid	$FeCl_2.4H_2O$	Vit C	RO water
6	5	89	5	0.28	1	93.72
6	5	89	10	0.28	1	88.72
6	5	89	20	0.28	1	78.72

The polymerization mechanism for polyacrylic acid is different than PVP due to distinct size, structure and chemistry. At the same weight concentration higher moles of acrylic acid (72.06 g/mol) are present in the reaction mixture than PVP (10 kDa). The rate of diffusion of acrylic acid is higher than PVP due to its smaller size. Hence, local

concentration of acrylic acid in the reaction zone at the same concentration (wt.%) is higher than PVP. Moreover, thermodynamically initiator radicals prefer to react with acrylic acid because of the presence of a π-bond making acrylic acid more reactive than PVP.

Owning to these properties, acrylic acid competes with EGDMA for initiator radicals in the reaction zone. EGDMA is a methyl acrylate type monomer while acrylic acid is an acrylate linked to -COOH, therefore the reactivity of EGDMA is very different from acrylic acid. Due to the presence of two pi-bonds and vicinity to the interface the local concentration of EGDMA is higher than acrylic acid thereby, the rate of polymerization is also higher. From the thermodynamic perspective monomer interactions for EGDMA and acrylic acid differ resulting in change in distribution of monomers in the reaction mixture. Earlier work[222–224] in the literature claimed accelerated polymerization by "matrix effect" in which acrylic acid monomers aggregate prior to polymerization. This means in the presence of sufficient acrylic acid monomers their rate of polymerization in the reaction zone is higher than that of EGDMA. Hence, polyacrylic acid chain propagation and participation in the polymer network is much higher than PVP.

Figure 4.25 presents the schematics for the formation of polyacrylic acid polymer network in three stages. Stage i – diffusion of reagents and formation of the reaction zone, stage ii – faster polymerization of EGDMA and participation of polyacrylic acid in the growing polymer network, stage iii – increased polymerization rate of polyacrylic acid resulting in the grafting of long polyacrylic acid chains. In the initial stages of polymerization EGDMA dominates the network however, the growing chains of polyacrylic acid are added to the network in the later stages suppressing EGDMA homopolymerization.

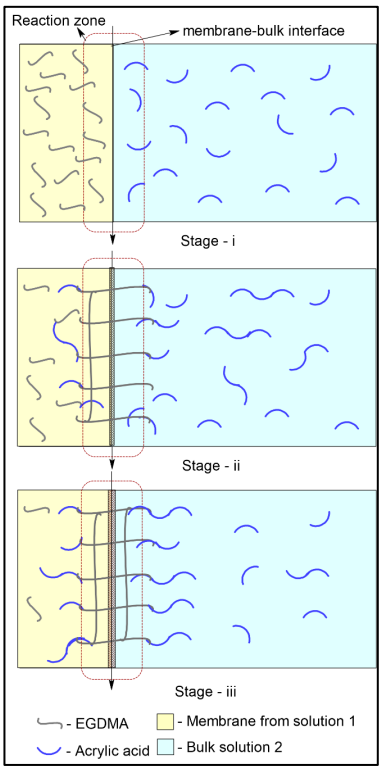

Figure 4.25. Visual interpretation of formation of the hydrogel network with acrylic acid in three stages at the membrane-bulk interface

Acrylic acid actively participates in the polymerization reaction and upon increasing the concentration the participation increases not only on the outer surface but also in the hydrogel network within the porous structure. The higher weight gain for polyacrylic acid modifications than PVP in Figure 4.26 confirmed active participation of acrylic acid in the polymerization. The weight gain was not proportional to the increase in acrylic acid concentration because EGDMA dominates at higher concentration of acrylic acid due to the gel-effect which hinders the diffusion of acrylic acid from the bulk towards the reaction zone.

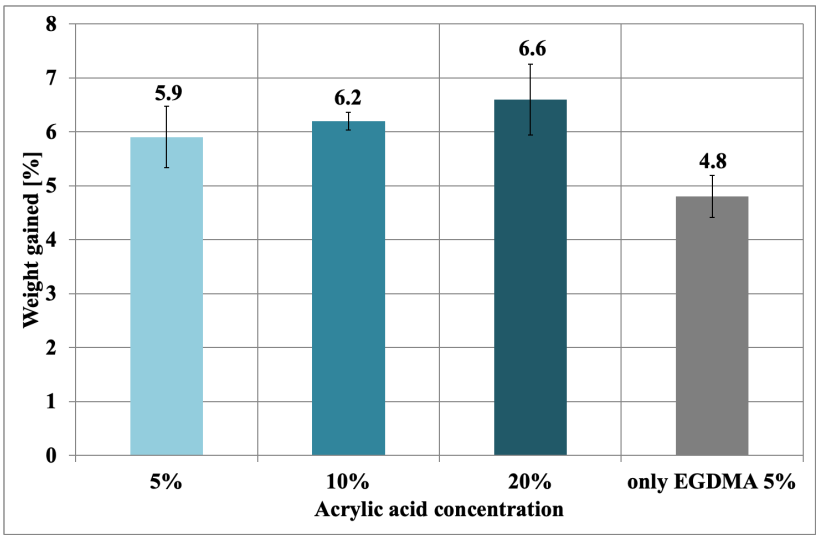

Figure 4.26. Comparison of weight gained after modification with different acrylic acid concentrations and without acrylic acid (only EGDMA)

The water uptake data in Figure 4.27 confirm the grafting of polyacrylic acid inside the porous structure. Polyacrylic acid unlike PVP due to its smaller size, higher reactivity and lower viscosity leads to better mass transfer hence, enters the porous structure. The grafting of polyacrylic acid chains inside the pores decreases the pore volume but increases the sites for water binding. The dual effect of pore filling and outer surface polymer network allows higher amount of water uptake than PVP. It is also evident that with increasing the acrylic acid content the water binding sights increase resulting in higher water uptake. The lower value for the modification without polyacrylic acid (only EGDMA 5 %) is due to the less hydrophilic nature of polyEGDMA in addition to the reduction of effective pore volume upon grafting.

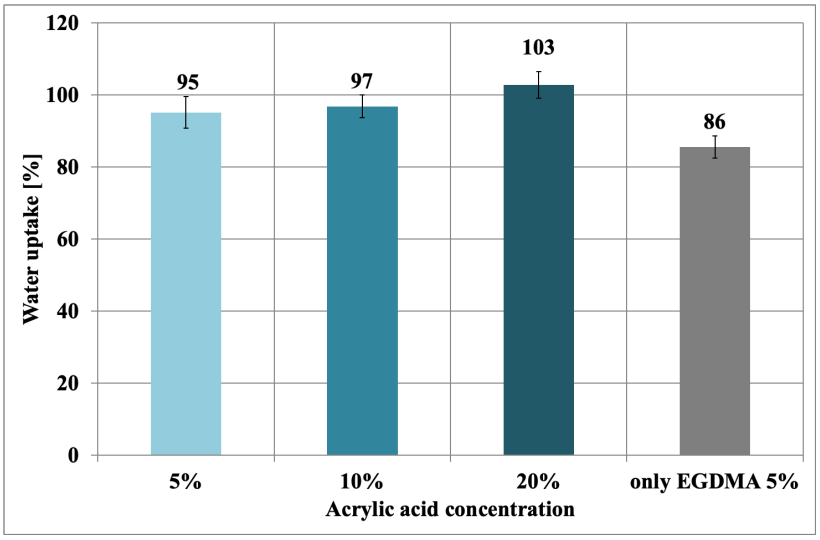

Figure 4.27. Comparison of water uptake after modification with different acrylic acid concentrations and without acrylic acid (only EGDMA)

Figure 4.28 schematically depicts the distribution of polyacrylic acid and EGDMA molecules in the reaction zone and presents the predicted hydrogel network formed upon polymerization for different acrylic acid concentrations. The polyacrylic acid chains in polymer network increase on the surface and within the porous structure with increasing concentration.

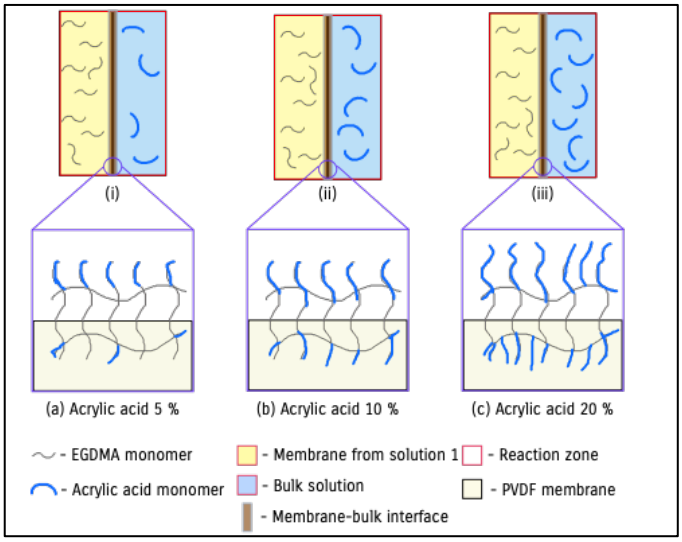

Figure 4.28. Visual interpretation of the formation of ideal hydrogel network at the membrane-bulk interface for different acrylic acid concentrations at 5 % EGDMA. In the realistic structure cross-links between poly(acrylic acid) chains also exist

The water permeance in Figure 4.29 drastically decreased with increasing acrylic acid concentration and the values are much lower than for PVP. The possible explanation is narrowing of the pores due to grafted polyacrylic acid chains inside the pores. The effect of narrowing of the pores was magnified at higher acrylic acid concentration because of swelling of the polyacrylic acid chains at pH 7. The presence of pH-responsive groups, such as carboxyl, pyridine and imidazole leads to conformational changes of macromolecular chains depending upon pH[225,226]. Polyacrylic acid in aqueous solution has a pKa of approximately 4.3-4.9, depending on the method used[227] for the measurement. This means at pH 7 carboxyl groups are deprotonated resulting in swelling, further narrowing the effective pore size. With increasing acrylic acid concentration, the swelling tendency of the hydrogel layer also increased as more chains are present in the hydrogel network.

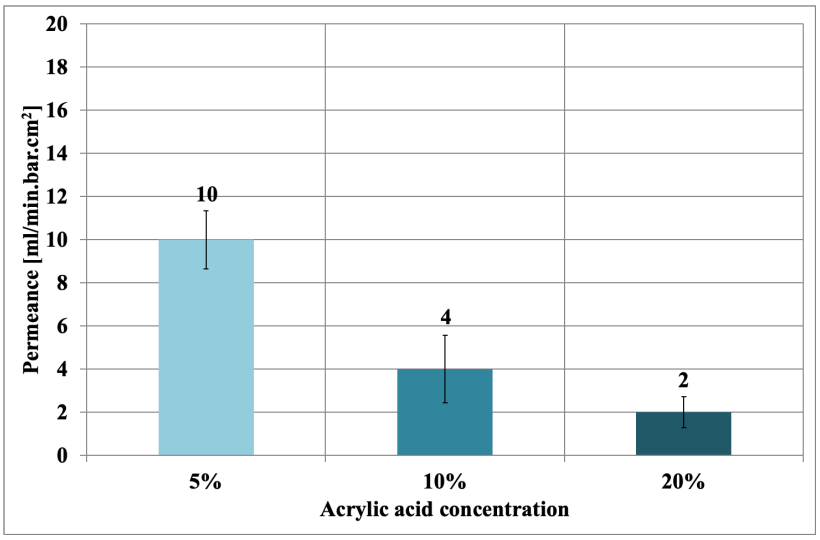

Figure 4.29 Comparison of water permeance after modification with different acrylic acid concentrations and without acrylic acid (only EGDMA)

Contact angle

Polyacrylic acid has a low hydration energy due to the presence of carboxyl groups which results in hydrophilic nature of the membrane. Polyacrylic acid chains have an intrinsic property of interacting with water molecules. The clear evidence is the similar wetting time observed for all concentrations in Figure 4.30, confirming the participation of acrylic acid in grafting even at low concentrations. The difference in the starting contact angle for the (a) top surface could be due to the base membrane or the spot of the measurement.

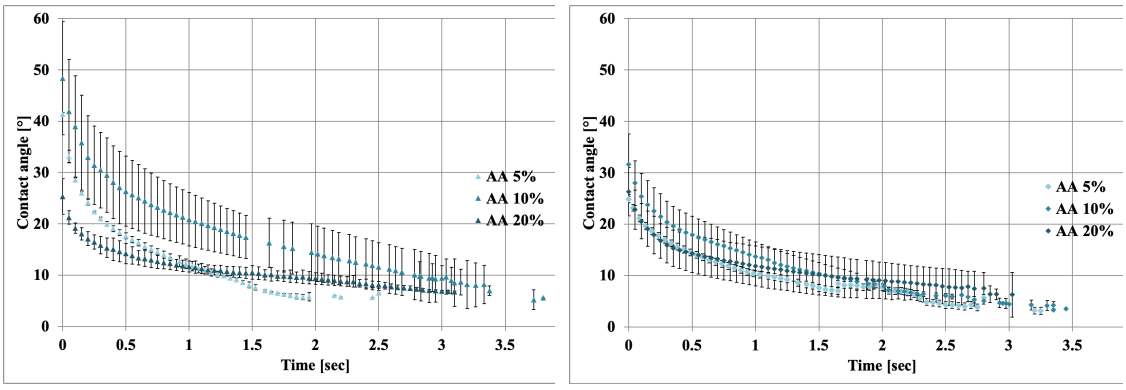

(a) (b)

Figure 4.30. Change in contact angle with time for (a) top surface and (b) bottom surface after modification with different polyacrylic acid concentration

SEM

SEM micrographs of the top and bottom surface in Figure 4.31 shows that at 5 wt.%, the grafted polymer was heterogeneously distributed within the porous structure and on the surface. At 10 wt.%, a thin layer of cross-linked polymer network was formed which

covered the base membrane and narrowed the pores. At 20 wt.%, a dense hydrogel layer covers the top of the membrane leading to cracks. Increased acrylic acid content increased the amount of grafted hydrogel forming a closely packed highly cross-linked poly(EGDMA-co-acrylic acid) polymer network constricted onto a small surface area resulting in cracks upon expansion.

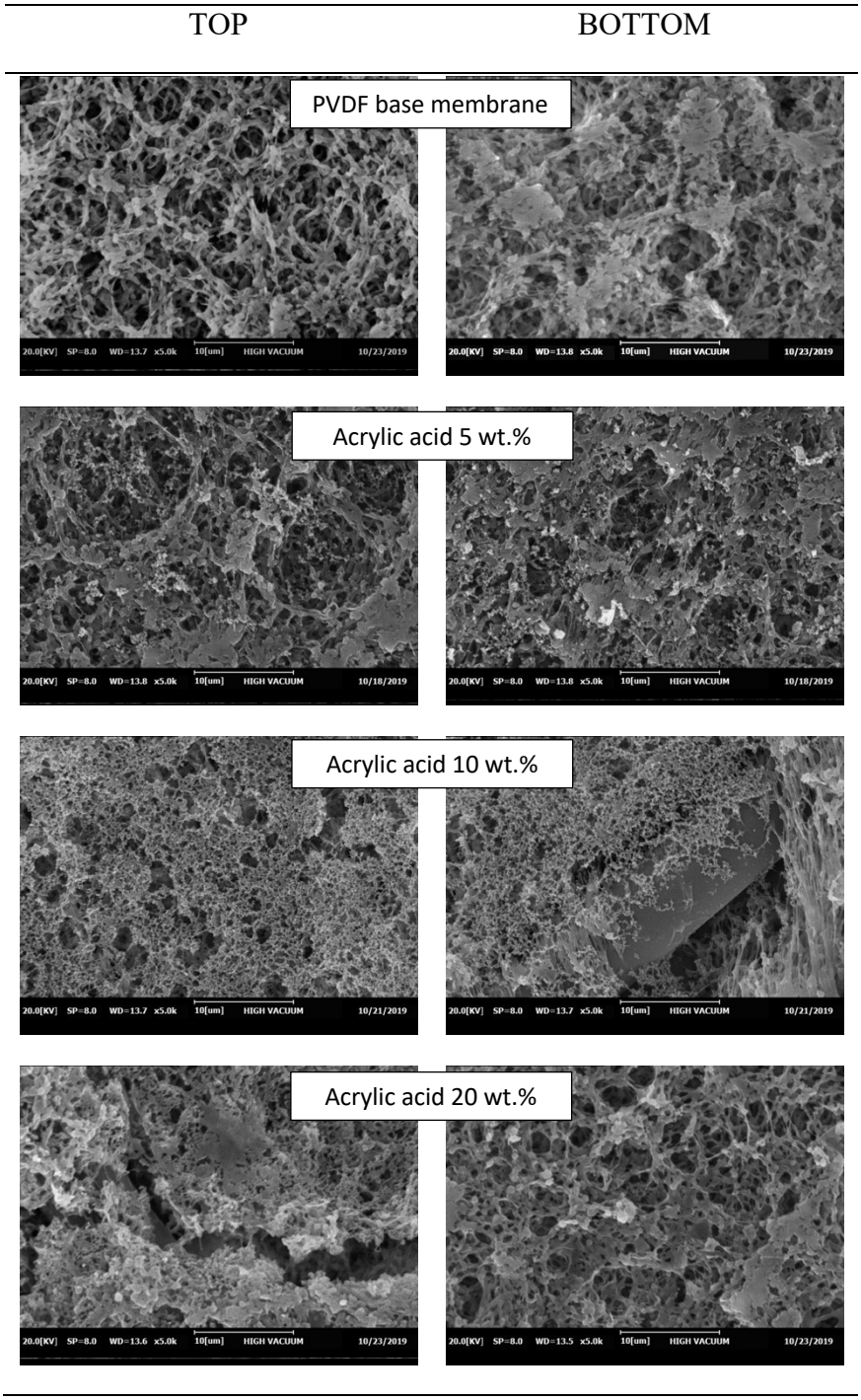

Figure 4.31. SEM micrographs of the top and bottom surface after modification with different polyacrylic acid concentration and the base membrane

The polymerization is dominated in both PVP and acrylic acid cases by EGDMA due to its higher reactivity, smaller size, better mass transport and efficient homopolymerization ability. The smaller size and lower viscosity drive better mass transfer, higher electron density drives higher reactivity, and thermodynamics drives smoother AA-EGDMA copolymerization. Therefore, vinyl monomers at higher concentration can be more efficiently utilized over long chain polymers for obtaining the desired surface properties throughout the surface including pores via two-step graft coating polymerization method.

4.4 Influence of cross-linker on membrane functionalization

This section investigates the behavior of cross-linker in the polymerization and discusses its impact on the final membrane properties. The proposed reaction mechanism in section 4.2 and 4.3 is further exploited to limit the dominance of cross-linker in the grafted hydrogel. An alternative less reactive cross-linker: TrGDMA was proposed. The work provided a good platform to select the appropriate fraction of the relevant cross-linker for the development of the prototype in the next work package.

4.4.1 Effect of cross-linker concentration: EGDMA

The role of EGDMA in polymerization at a constant acrylic acid and PVP concentration (5 wt.%) was analyzed by performing the modifications with varying EGDMA concentrations: 5 wt.%, 10 wt.% and 15 wt.%.

4.4.1.1 Functionalization with 10kDa PVP

Previous section debated that EGDMA dominates the polymerization especially in the presence of the long chain polymer as a result of higher local concentration, difunctional reactivity and mass transfer coefficient. Growing macroradicals of EGDMA with unsaturated groups react with each other in the reaction zone to form a three-dimensional, cross-linked polymer. The kinetics of polymerization is governed by difunctional EGDMA, as it integrates into the polymer population as soon as one of the two vinyl groups react[228]. PVP macroradicals formed in the reaction mixture combine with growing EGDMA radical on the membrane surface to terminate the chain-growth. The slow mobility and large size of PVP in addition to the increased viscosity at the interface experienced by EGDMA network creation prevents PVP from entering membrane pores. As a result, a polymer network of EGDMA with terminal PVP chains is formed on the

outer surface while a highly cross-linked EGDMA network dominates inside the porous structure.

At high EGDMA levels, the consumption of initiator radicals by EGDMA monomers increased, negatively affecting the generation of PVP radicals. This scenario accelerates homopolymerization of EGDMA resulting in rigid polymer network. Figure 4.32 illustrates linear increase in weight gain with increasing EGDMA concentration indicating diminishing role of PVP; bolstering the argumentation about increasing dominance of EGDMA in the presence of PVP.

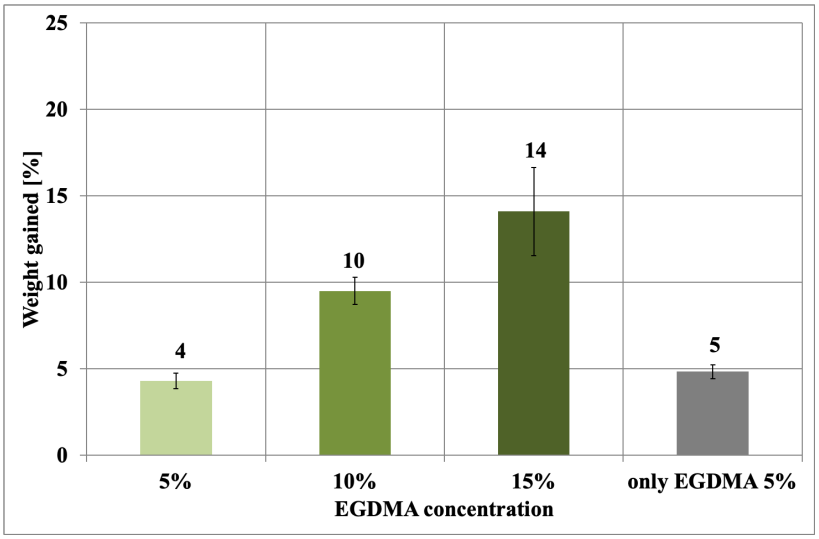

Figure 4.32. Comparison of weight gained after modification at different EGDMA concentrations with and without PVP (5 wt.% EGDMA)

EGDMA radicals diffuse inside the porous structure and continue to polymerize forming a rigid cross-linked network. Increasing the EGDMA content accelerated the conversion but yields a tight polymer network incapable of swelling with less hydrophilic nature. Consequently, narrowing the pores and reducing the pore volume due to grafting of tight polymer inside the pores. Hence, the water uptake decreased with increasing EGDMA concentration as shown in Figure 4.33 further confirming irrelevance of PVP inside the porous structure. The reduced pore size resulted also in water permeance drop observed in Figure 4.34. The drastic drop to 4 ml/min.bar.cm^2 at EGDMA 15 wt.% suggested blocking of the pores due to the formation of dense and highly cross-linked polymer network with very high EGDMA content.

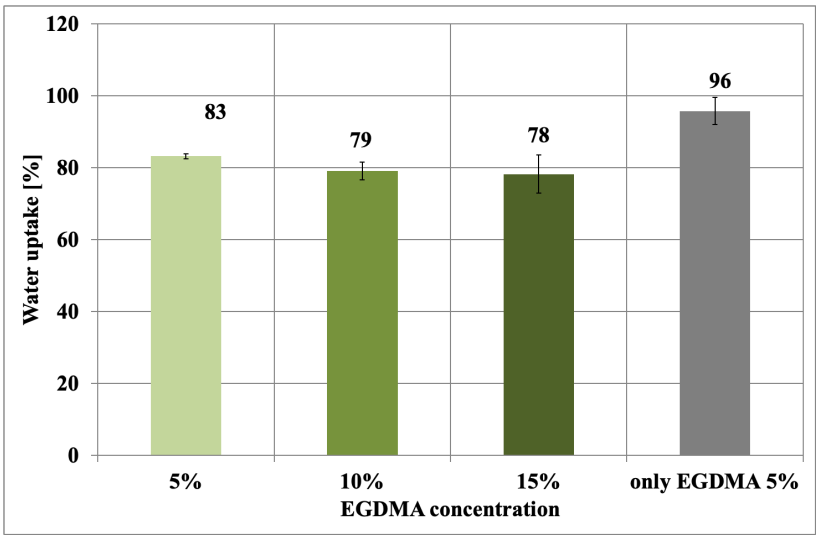

Figure 4.33. Comparison of water uptake after modification at different EGDMA concentrations with and without PVP (5 wt.% EGDMA)

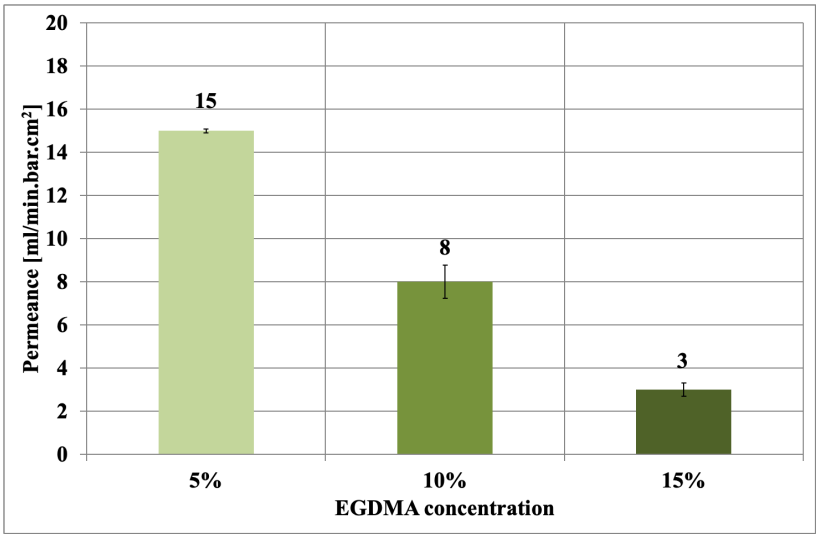

Figure 4.34. Comparison of water permeance after modification at different EGDMA concentrations with and without PVP (5 wt.% EGDMA)

Contact angle

As learnt above, increasing EGDMA concentration narrowed the pore size due to the formation of highly cross-linked dense polymer network within the porous structure. Moreover, with increasing content of EGDMA, participation of hydrophilic PVP decreased reducing the wettability of the membrane as demonstrated in Figure 4.35. Decreased water solubility of EGDMA due to increased dimethacrylate content at higher EGDMA concentration could also further inversely affect the surface hydrophilicity.

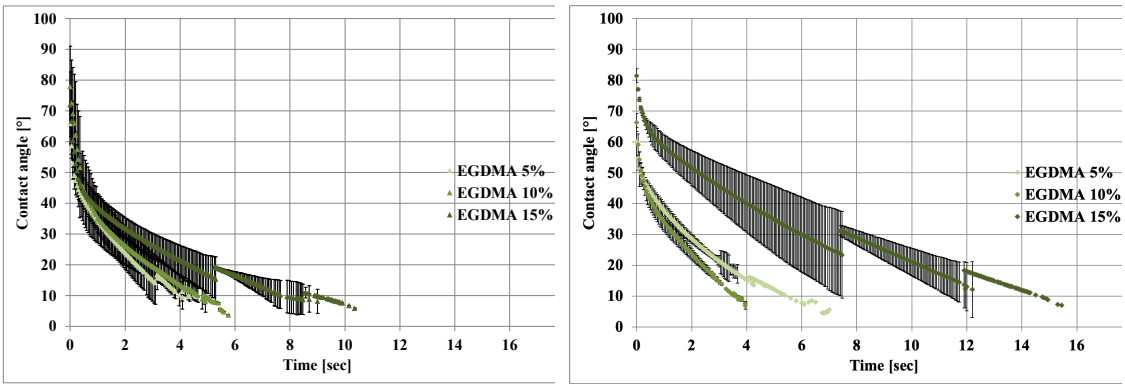

(a) (b)

Figure 4.35. Change in contact angle with time for (a) top surface and (b) bottom surface after modification at different EGDMA concentration

SEM

The membrane morphology of the modified membranes was scanned using the SEM and the micrographs obtained for the top and bottom surface are presented in Figure 4.36. The membranes were affirmed to form a dense layer covering pores upon increasing EGDMA concentration due to deposition of high amount of polymerized EGDMA. As predicted, at 15 wt.% a thick hydrogel layer was formed on the membrane surface making certain pores ineffective by complete blocking, further reducing the water permeance. Furthermore, the SEM analysis revealed formation of heterogenous polymer spheres at high EGDMA concentrations (above 5 wt.%). The increase in molecular weight upon polymerization of EGDMA creates highly branched chain polymer which shrinks into spheres to reduce the interfacial tension. These polymerized spheres are immiscible in the aqueous medium resulting in spontaneous phase segregation. Polymerization induced phase separation is a commonly observed phenomenon in a multicomponent mixture which occurs upon polymerization of one or more components[229–231]. The heterogenous polymer spheres originate from water insoluble polymerized EGDMA domains.

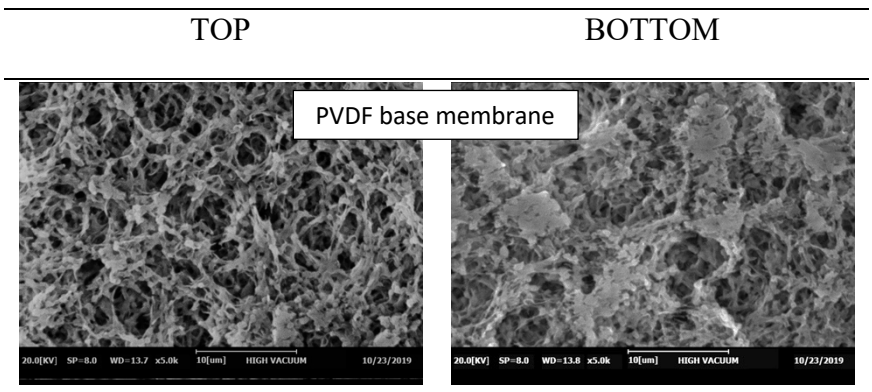

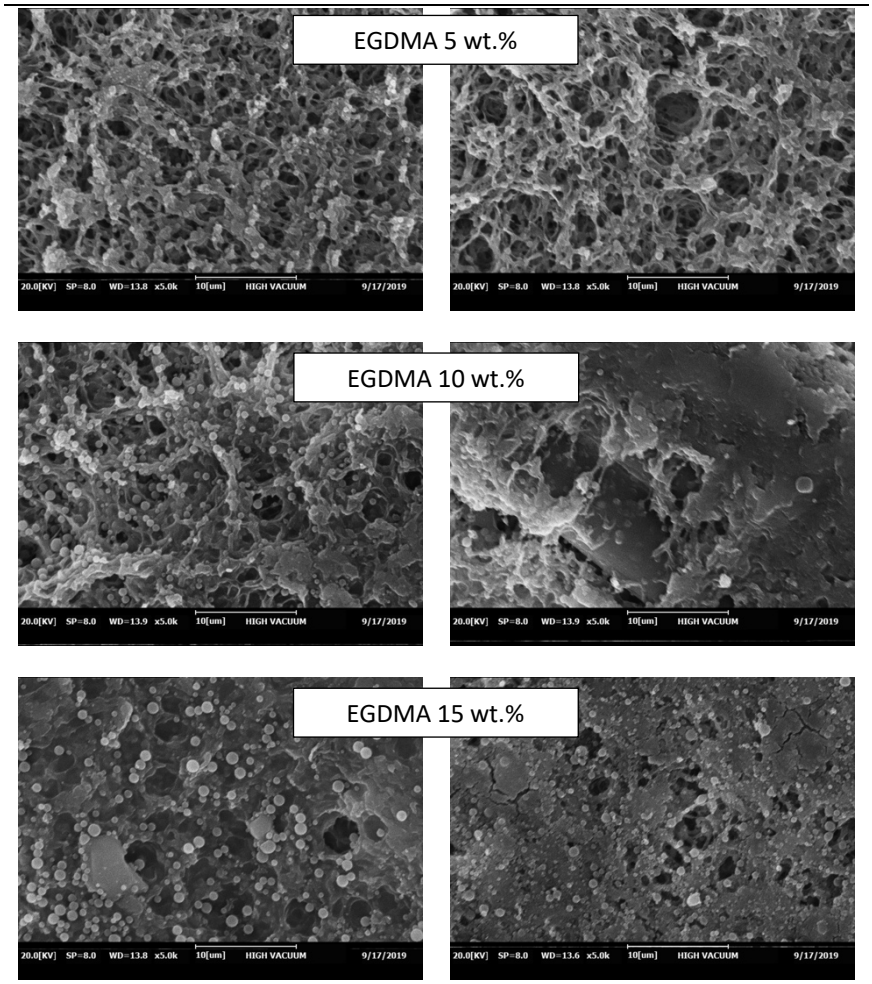

Figure 4.36. SEM micrographs of the top and bottom after modification at different EGDMA concentration and the base membrane

4.4.1.2 Functionalization with acrylic acid monomer

Based on the mechanism proposed and the experience from section 4.3.2, it was understood that acrylic acid participates more efficiently than PVP in the polymerization. This is a result of higher local concentration, higher reactivity and 'smoother copolymerization' with EGDMA. The methacrylate type monomer: EGDMA has different activity than acrylate type monomer: acrylic acid, hence the propagation rates are different. Moreover, the bifunctionality of EGDMA and higher local concentration due to the vicinity to the reaction zone promotes EGDMA dominance in the polymer network especially at high EGDMA content. The hydrogel weight grafted in Figure 4.37 at all EGDMA concentrations was higher than PVP (see Figure 4.19) verified the relevance of acrylic acid participation in two-step graft coating polymerization. Highly mobile smaller sized of polyacrylic acid molecules enter the membrane pores before the barrier formation at the membrane-bulk interface. The linear growth in the amount of

hydrogel grafted with increasing EGDMA concentration confirmed EGDMA dominance at constant acrylic acid content.

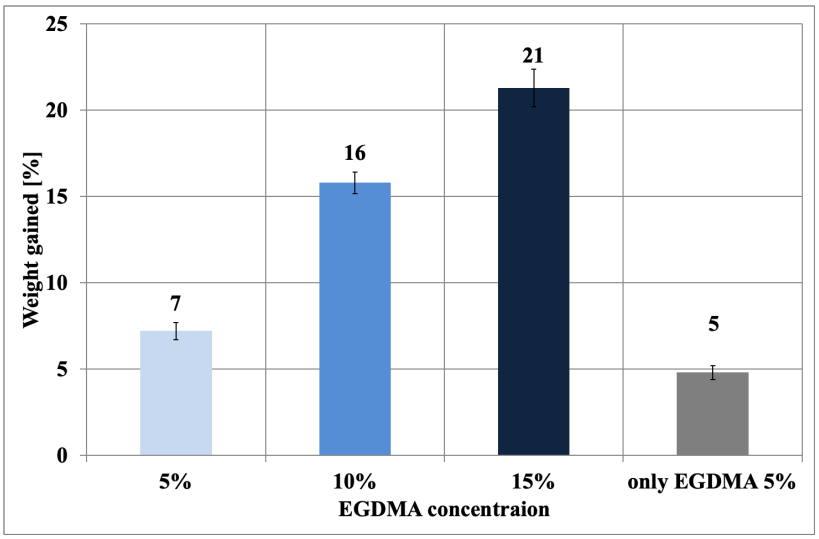

Figure 4.37. Comparison of weight gained after modification at different EGDMA concentrations with and without acrylic acid (only EGDMA)

Since polyacrylic acid and EGDMA undergo copolymerization also inside the porous structure, a cross-linked polymer network is formed inside the pores which is less hydrophilic in nature due to the EGDMA dominance. With increasing EGDMA concentration not only the cross-linking density but also the amount of grafted polymer increased inside the pores which reduced the effective pore size. Subsequently, the water uptake decreased as illustrated in Figure 4.38. The water uptake values for polyacrylic acid were higher than PVP (see Figure 4.20) confirming participation of polyacrylic acid inside the porous structure creating more water binding sites.

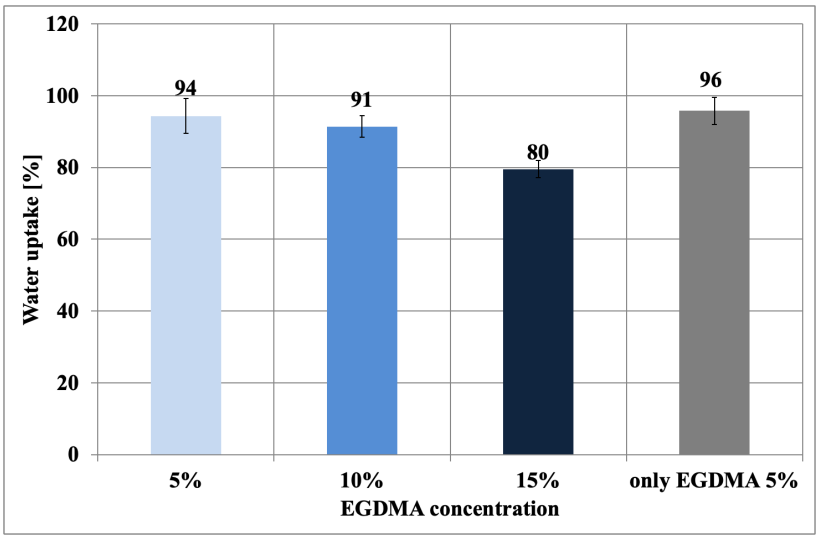

Figure 4.38. Comparison of water uptake after modification at different EGDMA concentrations with and without acrylic acid (only EGDMA)

The drop in water permeance with increasing EGDMA concentration presented in Figure 4.39 was a result of narrowing of the pore structure upon increasing polymer content with high cross-linking density inside the pores. The value of water permeance at 5 wt.% was lower for acrylic acid than PVP (see Figure 4.34) due to swelling of the polyacrylic acid chains. However, the effect of swelling was reduced with increasing EGDMA concentration as a highly cross-linked polymer network forms a rigid and dense structure. Thereby, the permeance was comparable at 10 wt.% and 15 wt.% with PVP.

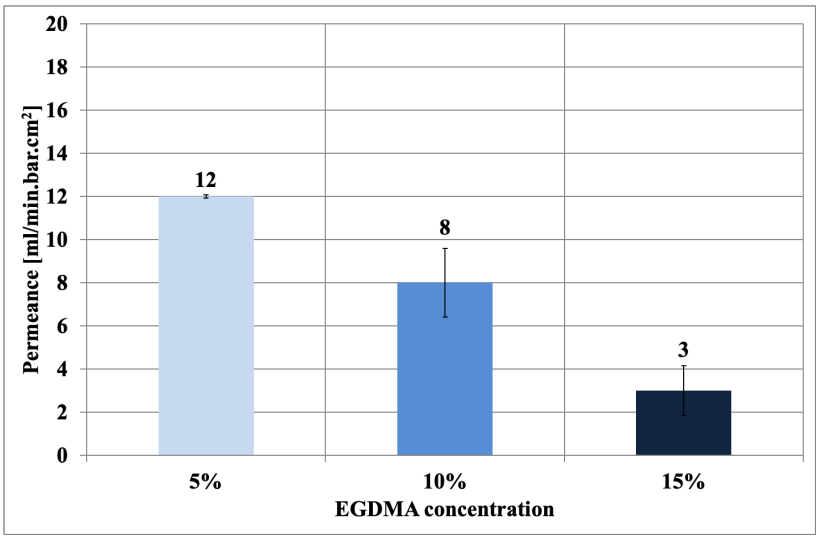

Figure 4.39. Comparison of water permeance after modification at different EGDMA concentrations with and without acrylic acid (only EGDMA)

Contact angle

The overall wetting time and starting contact angle for polyacrylic acid (see Figure 4.40) was lower than PVP (see Figure 4.35) implying higher hydrophilicity due to better incorporation of polyacrylic acid in the polymer network. However, the hydrophilicity of polyacrylic acid decreased with increasing EGDMA concentration as a consequence of the narrowing of the pore size and change in surface chemistry due to dominance of polymerized EGDMA that is less hydrophilic.

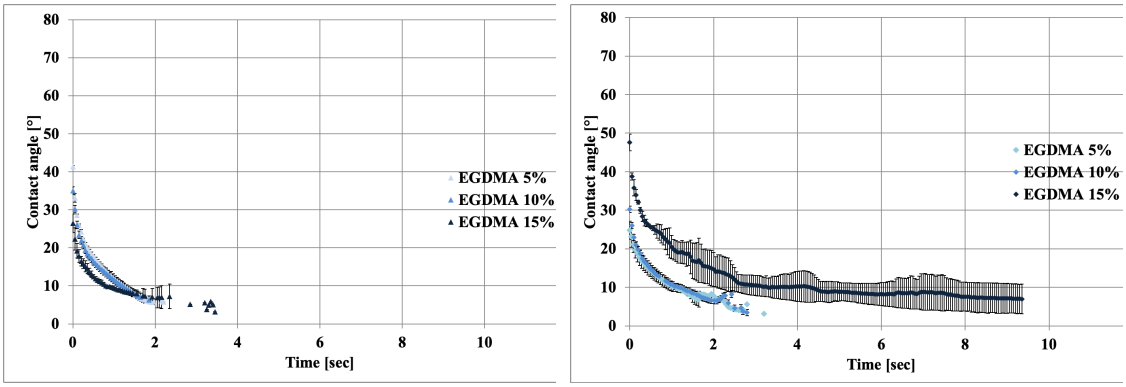

Figure 4.40. Change in contact angle with time for (a) top surface and (b) bottom surface after modification with different EGDMA concentrations

The morphology of the modified membrane was studied by analyzing SEM images in Figure 4.41. The membranes were covered with a polymerized cross-linked network of poly(EGDMA-co-AA). At higher levels of EGDMA the density of the grafting increased resulting in closely packed network. The morphology observed via SEM justified the water permeance data obtained above. The higher reactivity of acrylic acid than PVP suppressed strong homopolymerization of EGDMA and prevented dense thick layer formation and phase separation as seen in case of PVP. At concentrations above 5 wt.% high amount of grafted hydrogel was constrained in a small area which resulted in cracks.

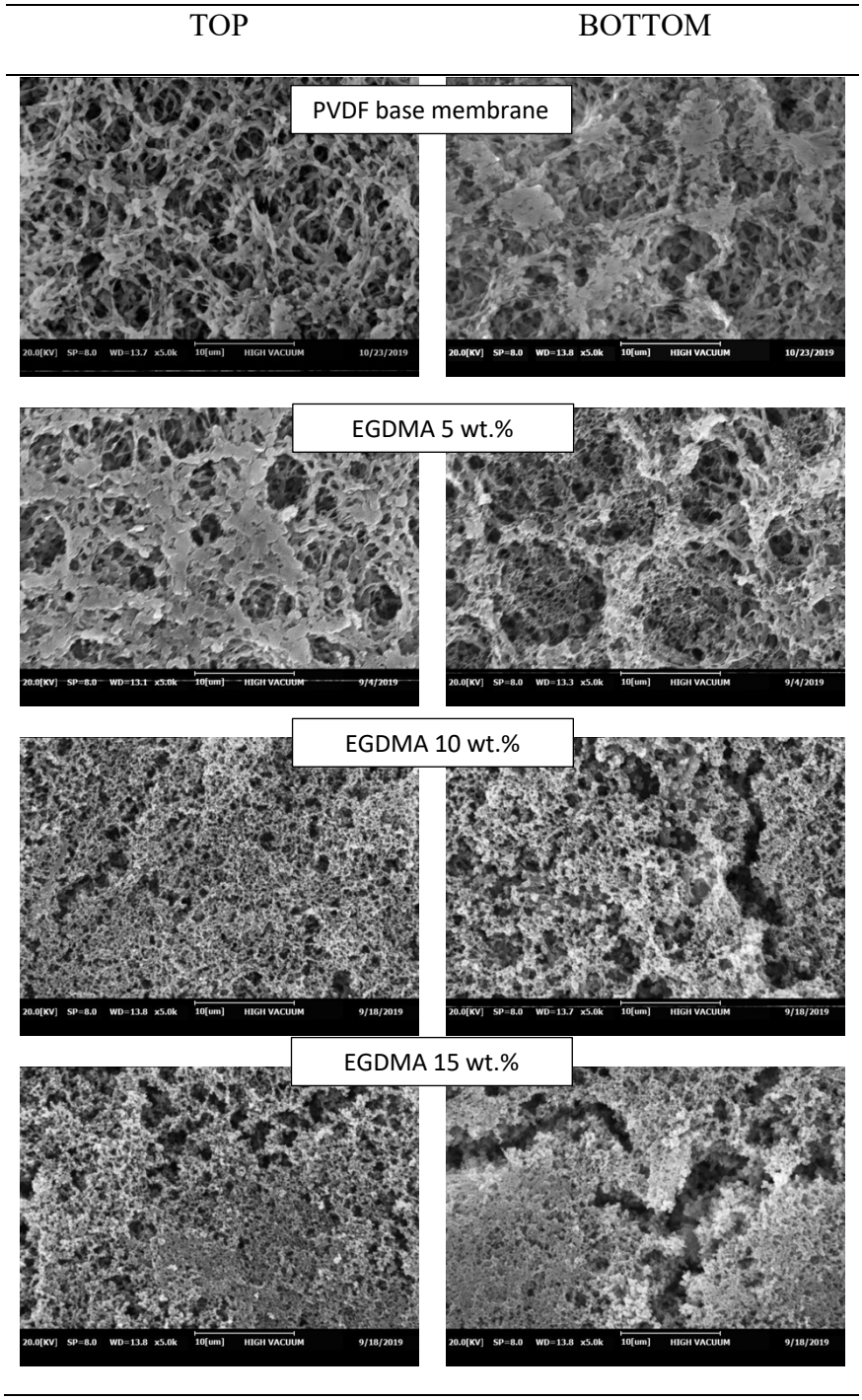

Figure 4.41. SEM micrographs of top and bottom surfaces after modification at different EGDMA concentration and the base membrane

The reactivity, structure, solubility in the aqueous medium and concentration of cross-linker are the governing factors for the dominating nature of the cross-linker. For the development of the prototypes 2.5 wt.% EGDMA is utilized along with two different vinyl monomers thermodynamically compatible with EGDMA due to their structures: acrylic acid[132,219,232] and HEMA[233,234] to obtain anti-fouling surface properties.

4.4.2 Effect of type of cross-linker: EGDMA vs TrGDMA

This section explores the option of using an alternative cross-linker: TrGDMA with less reactivity and higher solubility in the aqueous medium than EGDMA to reduce the dominating effect of the less hydrophilic cross-linked monomers in the polymer network. The behavior of two different cross-linkers was analyzed by investigating membrane characteristics and visually inspecting solution polymerization effects in the absence of the membrane.

The modifications were carried out with only cross-linkers at varying concentrations in the absence of monomer by keeping the concentration of other reagents (H_2O_2, Fe^{2+} and Vit C) constant. The hydrophilic property of dimethacrylates derives from the ethoxy groups due to the presence of oxygen which interacts with water by hydrogen bonding[235]. Therefore, TrGDMA is expected to have higher solubility in water than EGDMA before and during polymerization. Moreover, TrGDMA with more ethoxy groups tends to form relatively longer and more flexible cross-links compared to EGDMA which forms short and stiff polymer network[236].

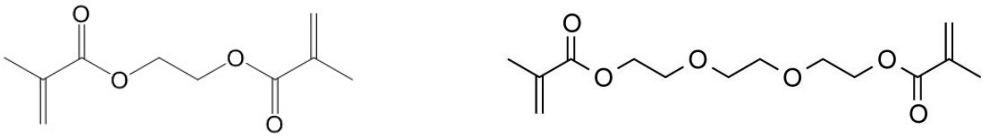

(a) EGDMA (b) TrGDMA

Figure 4.42. Chemical structures of two different cross-linkers used in this work

These properties made TrGDMA an interesting candidate to overcome the problem of polymerization induced phase separation. The molar concentration of EGDMA (mol. Wt. = 198.218 g/mol.) is higher than TrGDMA (mol. Wt. = 286.32 g/mol.) at the same mass concentration; thus, a greater number of EGDMA moles are available in the system than TrGDMA at any selected mass concentration. Also, the longer chains made TrGDMA slightly less mobile than EGDMA. Hence, EGDMA showed better mass transfer than TrGDMA in the polymerization system which was supported by the data in Figure 4.43. Very efficient autopolymerization of EGDMA in the presence of higher EGDMA moles resulted in higher grafting than TrGDMA throughout the concentration range. However, for effective polymerization in the presence of monomer low cross-linker concentrations such as 2.5 wt.% or 1.25 wt.% are a strategic pathway to restrict the influence of cross-linker in the network.

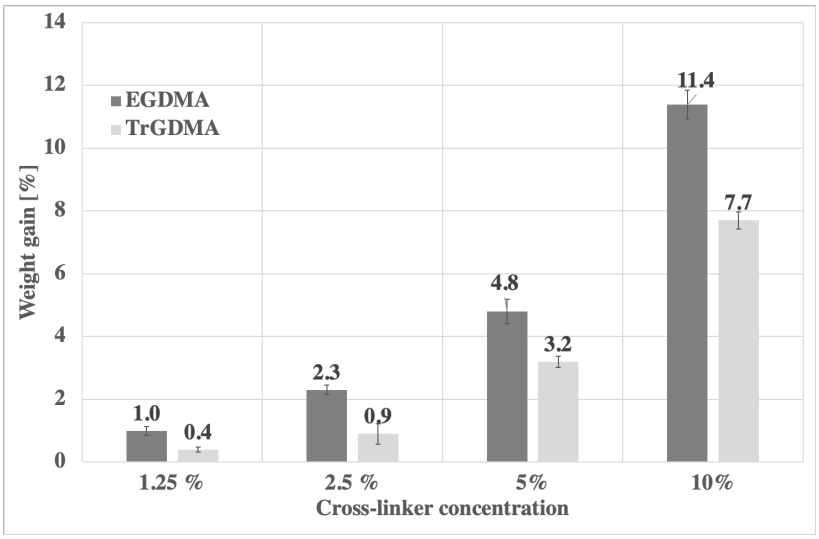

Figure 4.43. Comparison of weight gained after modification with different EGDMA and TrGDMA concentrations in the absence of any other polymers

Although the water uptake is a result of dual effect: water sorption by the hydrogel layer on the modified membranes and water held inside the porous structure, the values in the plot are dominated by the water absorbed by the pores. The change in water uptake is a result of narrowing of the pore size upon grafting. The higher cross-linking density and chain stiffness of EGDMA reduces the free volume in the polymer network. As a result, TrGDMA showed higher water uptake compared to EGDMA as shown in Figure 4.44. The drop in water uptake for TrGDMA above 2.5 wt.% could be a result of increased cross-linking density of the increased deposited content of TrGDMA at higher concentration.

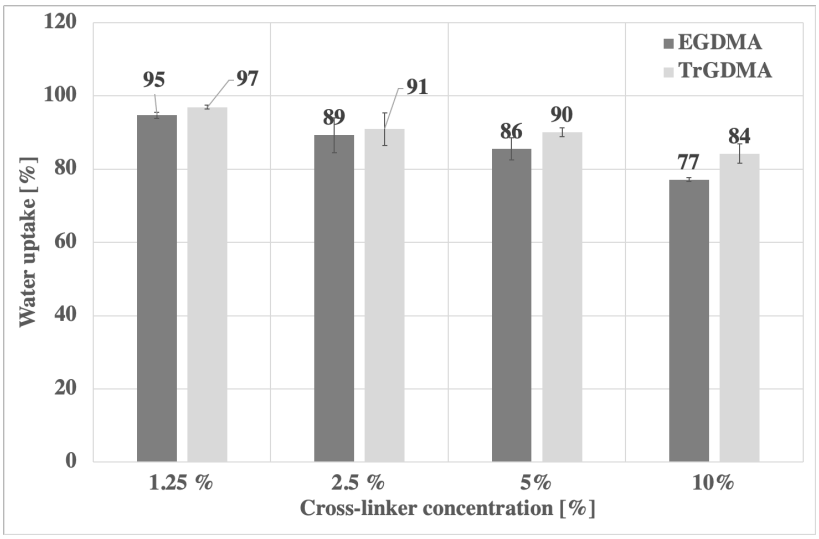

Figure 4.44. Comparison of water uptake after modification with different EGDMA and TrGDMA concentrations in the absence of any other polymers

Additional supportive data for the behavior of cross-linkers was obtained by visual inspection of the solution polymerization (see Figure 4.45). The polymerization induced phase separation in EGDMA started at 2.5 wt.% and the effect was enhanced with increasing concentration such that at 10 wt.% a gel block was formed. However, the phase separation was not detected until 10 wt.% for TrGDMA. The higher solubility, lower cross-linking density and lower molar concentration of TrGDMA provide the explanation for the observed behavior. Therefore, TrGDMA when used in appropriate fractions is a good alternative to enhance the hydrophilic functionalization by reducing cross-linker dominance and avoid phase separation during polymerization.

Effect of EGDMA	Effect of TrGDMA
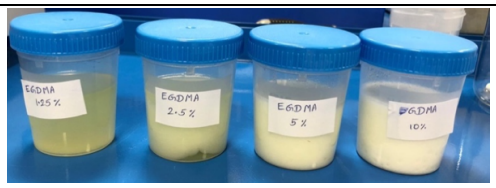	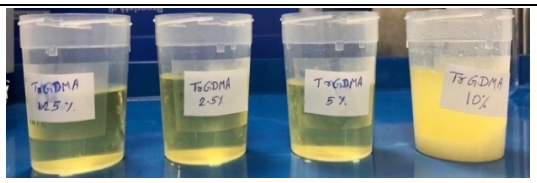
(a)	(x)

Figure 4.45. Comparison of the solubility in the aqueous medium on polymerization between EGDMA and TrGDMA at different concentrations: 1.25 wt.%, 2.5 wt.%, 5 wt.%, and 10 wt.% in the absence of any other polymers

Effect of EGDMA	Effect of TrGDMA
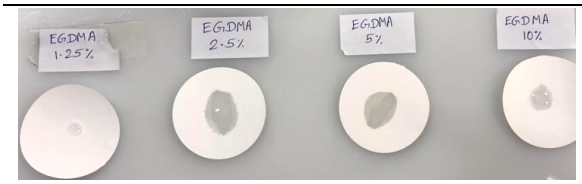	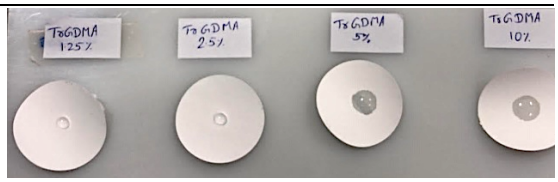
(b)	(y)

Figure 4.46. Difference in wettability after modification with EGDMA and TrGDMA at different concentrations: 1.25 wt.%, 2.5 wt.%, 5 wt.%, and 10 wt.% in the absence of any other polymer

Quick wetting tests were performed by introducing 1 mL of RO water on the surface of the dried (at 90ºC for 48 hr.) modified membranes to understand the surface hydrophilicity. At low concentrations loosely packed structure due to the low degree of cross-linking is formed. It is widely known that cross-linking increases the glass-transition temperature (T_g). At low degree of cross-linking the shift in T_g is smaller compared to high degree of cross-linking[237]. Therefore, at high temperature thermal degradation resulting in bond-breakage and loss of the properties takes place at low cross-

linking density. Hence, at 1.25 wt.% EGDMA and at 1.25 wt.% & 2.5 wt.% TrGDMA the membranes do not wet.

The visual inspection studies were conducted also with PVP and polyacrylic acid at varying concentrations. The concentration [wt.%] of each reagent are marked on the respective beakers. The results were compared for the effect of EGDMA and TrGDMA. As expected, for PVP (see a, b and c in Figure 4.47) there is no direct visible effect of PVP concentration in both the cases: EGDMA and TrGDMA. Even in the absence of a substrate long chain PVP fails to participate in the growing polymer network. With increasing EGDMA concentration the phase separation due to homopolymerization was evident, while no phase separation is noticed in TrGDMA due to higher solubility of TrGDMA in the aqueous medium.

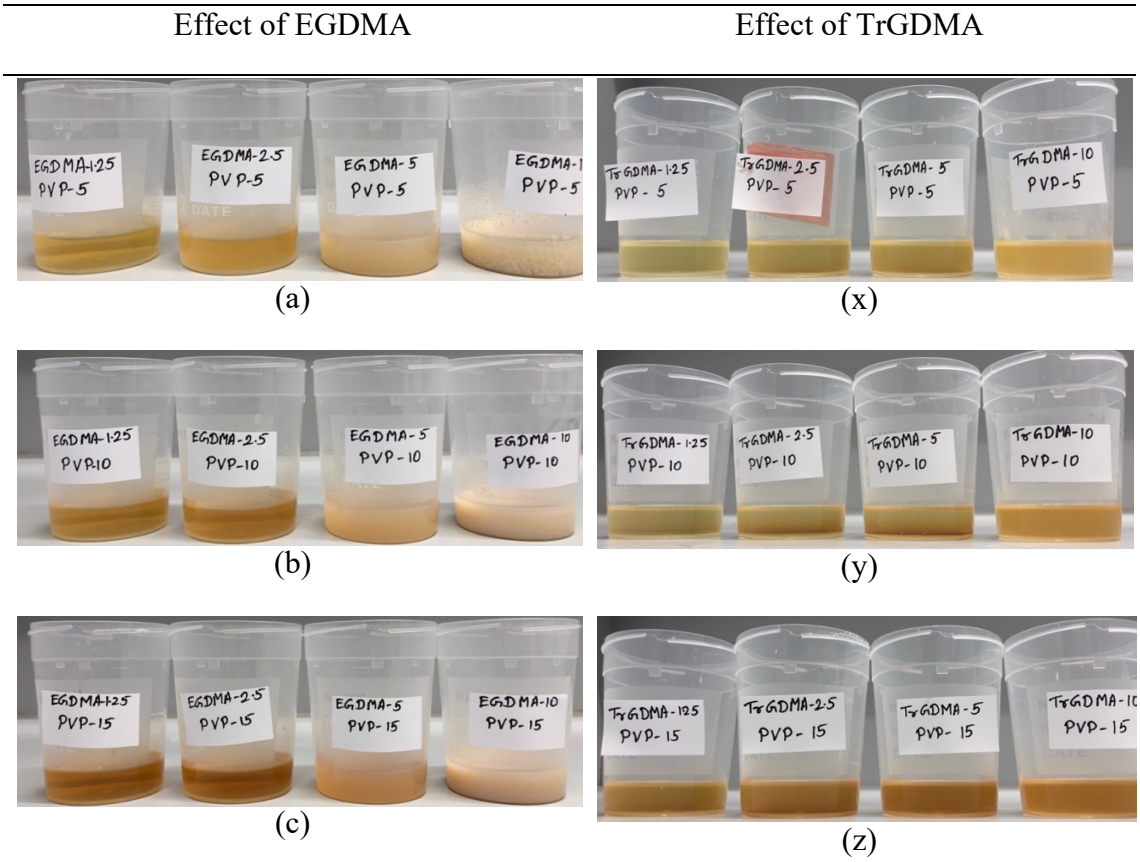

Figure 4.47. The visual inspection of solution polymerization upon adding solution 1 to solution 2. Comparison between the effect of EGDMA and TrGDMA on PVP polymerization at different concentration combinations

In case of polyacrylic acid as well no phase separation was detected for TrGDMA but at higher concentration of EGDMA gelation takes place. However, at higher concentration of polyacrylic acid the amount of gelation reduced unlike PVP. This confirmed the active

participation of acrylic acid and suppression of EGDMA homopolymerization in the presence of higher polyacrylic acid content.

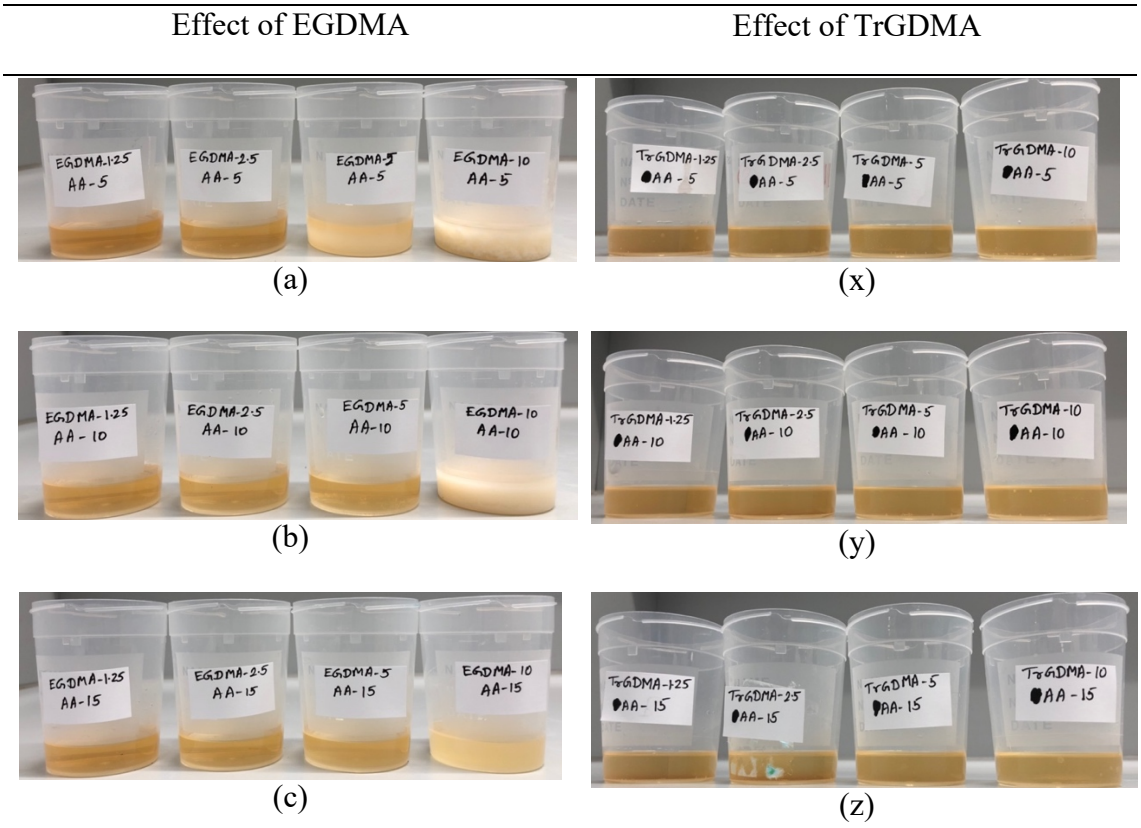

Figure 4.48. The visual inspection of the solution polymerization upon adding solution 1 to solution 2. Comparison between the effect of having EGDMA and TrGDMA polyacrylic acid polymerization at different concentration combinations

The SEM analysis for the modified membranes was performed to spot the differences in the membrane morphology due to TrGDMA and EGDMA (see Figure 4.49). At 2.5 wt.%, TrGDMA structure was relatively open while several pores were covered with polymer in case of EGDMA. At 5 wt.%, heterogenous patches of hydrogel layer can be spotted on the surface which partially covered the surface of the membrane for both. However, at 10 wt.% polymerization induced phase separation in case of EGDMA results in rough surface completely covered with thick polymer layer with having EGDMA spheres on the surface. This was supported by weight gain, drastic drop in water uptake and gelation in bulk polymerization. The SEM results showed the negative effects of polymerization on the membrane morphology such as heterogenous surface grafting, phase separation, and clogging of the pores at high cross-linker concentration.

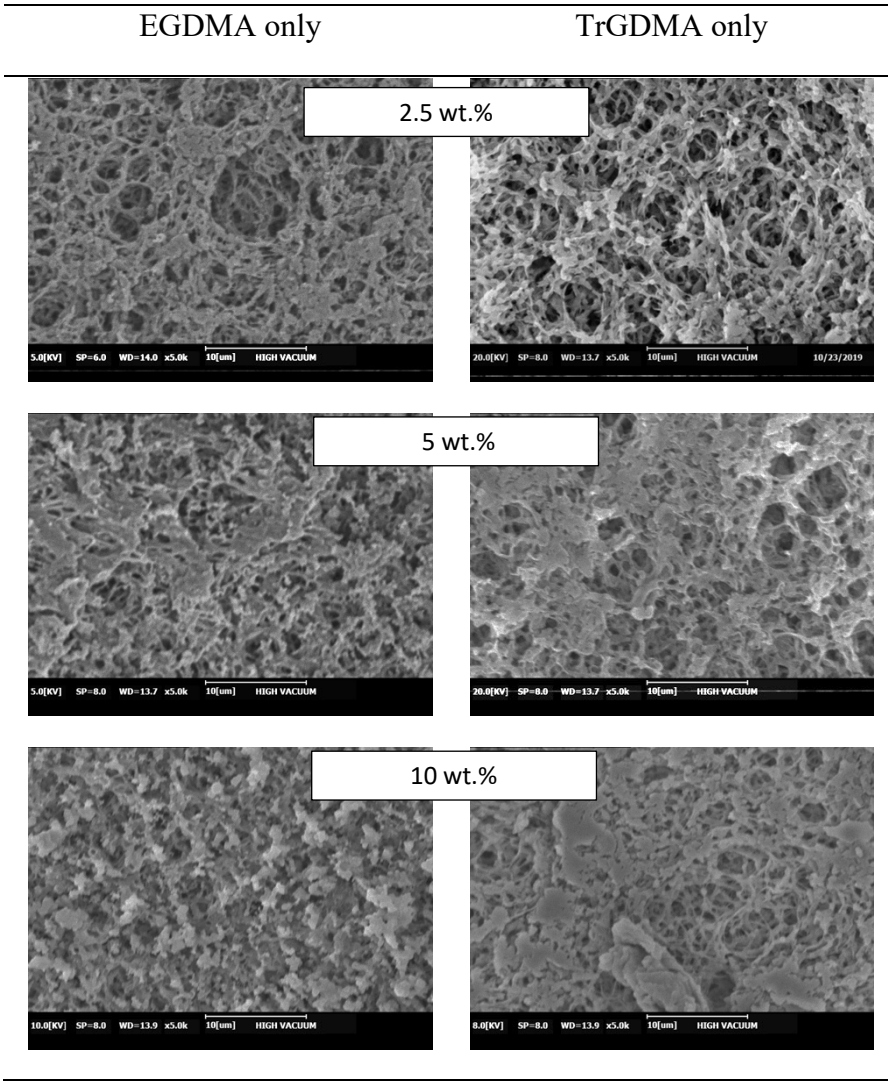

Figure 4.49. SEM micrographs of the top and bottom surface after modification with different EGDMA and TrGDMA concentrations in the absence of polymer

Appropriate fraction of TrGDMA potentially could be a better choice over EGDMA due to its solubility and lower reactivity. However, additional investigations are needed to establish the appropriate TrGDMA fraction to be implemented with polyacrylic acid and HEMA for efficient polymerization. Although TrGDMA is of vital interest for GVS for future developments it is not covered in this work due to time constrains. Therefore, only EGDMA is considered in the next work package to develop the prototypes based on polyacrylic acid and polyHEMA.

4.5 Development and characterization of prototypes

This section aims at developing two types of monomer-based prototypes with polyacrylic acid to derive pH responsive membranes and another with polyHEMA to obtain hydrophilic membranes with anti-fouling properties.

The monomers were understood to be more appropriate than polymers based on the study in above sections. The developed prototypes were analyzed by studying the membrane properties and performance characteristics to identify the best formulation for acrylic acid and HEMA each. The modified membranes were analyzed for the efficiency of grafting, flow properties, surface chemistry, and thermal stability. Additionally, the effect of pH on the flow properties as a result of conformational changes was studied. Finally, the membrane performance was evaluated by carrying out particle filtrations to understand the blocking mechanism and protein binding experiments to analyze BSA fouling.

4.5.1 Particle characterization

This sub-section discusses the properties of the model particles used in the filtration study. The use of nanoparticles in microfiltration[238–240] and ultrafiltration[241,242] processes has attracted a widespread interest in the field of separation technology. These studies have mostly utilized commercially available spherical particles made from different material (e.g., silica, polystyrene) with various functionalities (e.g., fluorescent, with functional groups – carboxyl, amines). The use of nanoparticles in filtration tests guides the development of mathematical models for solute transport through the membrane[243]. Fluorescently-labeled 200 nm polystyrene particles with carboxyl functional groups are used in this study as surrogates for cells such as extracellular vesicles[244] in bioprocessing applications. The characteristics of the particles used as the feed for filtration at pH 7 are shown in Table 4.5 and Figure 4.50 shows the particle surface charge at different pH.

Table 4.5. Characterization of the fluorescent polystyrene particles used for filtration

Particle type	Size [nm]	Particle concentration [particles/ml]	Polydispersity index (PDI)
PS (-COOH functionalized)	218 ± 3	5.91E+10	0.02

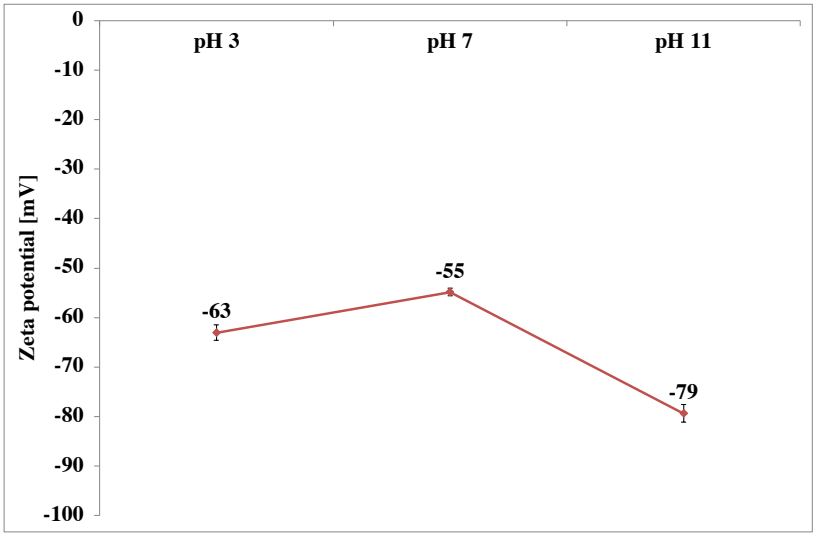

Figure 4.50. Zeta potential of fluorescent polystyrene particles (-COOH labeled) at different pH

Although polystyrene particles replicate the relevant properties of biological particles such as concentration, size and surface charge a key difference between two is the structure and deformability including softness. Moreover, the large differences between particle size and pore diameter enable studying fouling mechanism at different stages in the dead-end filtration. The biological particles are soft which can squeeze through the membrane pores at high pressure and low concentration. Helling et al.[245] examined the effect of particle deformation on retention in a pressure dependent filtration process. Furthermore, Büning et al. [246] synthesized polymeric soft particles to mimic mycoplasma and consequently study the blocking mechanism. In the recent decade, many studies have used nanoparticles as biological cell surrogates in filtration tests due to the time and cost associated with bio-assays in designated facilities[247,248]. The purpose of using hard PS particles was to establish a filtration study tool to evaluate and differentiate the modified membrane performances. The flow properties before, during, and after the filtration were calculated, and a variety of post-filtration analyses such as resistance, particle recovery, retention and SEM were done to identify the modification with the highest retention and recovery of the particles. It is well known that the filtration mechanism is an outcome of multiple factors: the properties of the membrane, particles characteristics and the solution environment. The grafted hydrogel layer architecture and the surface chemistry of the modified membranes define the particle interaction with the membrane during the filtration.

4.5.2 Stimuli responsive polyacrylic acid functionalized membranes

Polyacrylic acid membranes offer a promising and a versatile tool for the use in biomedical applications because of the properties such as customized electrostatic interactions based on pH, hydrophilic nature, and constrained protein adsorption[249,250]. The polyacrylic acid prototypes were developed in this work in an attempt to maximize the incorporation of pH responsive copolymer assemblies on the membrane which can undergo conformational changes with change in pH[251]. Moreover, the charge densities along the chains should have a beneficial effect on the separation of biological media because most protein and cellular components are negatively charged[249]. Three different formulations were used (see Table 4.6) to obtain the final membranes with reduced impact of cross-linker and enhanced influence of polyacrylic acid on the final grafted hydrogel. The concentration of the rest of the reagents was kept constant. From AE 1 to AE 2 acrylic acid concentration was increased to reduce the influence of EGDMA and in AE 3, EGDMA concentration was reduced further by keeping polyacrylic acid concentration high.

Table 4.6. Modification formulation used for developing the polyacrylic acid prototypes

Modification formulation [wt.%]	$\left[\frac{\text{Acrylic acid}}{\text{EGDMA}}\right]$	Membrane code
Acrylic acid 5 % + EGDMA 2.5 %	2	AE 1
Acrylic acid 10 % + EGDMA 2.5 %	4	AE 2
Acrylic acid 10 % + EGDMA 1.25 %	6	AE 3

4.5.2.1 Characteristics of the polyacrylic acid prototypes

From the previous experience it is understood that unlike PVP, acrylic acid actively participates in the polymerization. The goal of these modifications was to enhance the incorporation of polyacrylic acid chains in the grafted polymer network to obtain the pH responsive surface. The swelling degree and charge density depend on the grafting density and the architecture of the polymer network[252,253]. The charged interactions between biological particles and polyacrylic acid chains should prevent them from entering the porous structure due to electrostatic repulsion[232], thereby enhancing the recovery of the particles with minimal loss due to penetration and/or adsorption.

The polymerization mechanism is governed by the local concentration ratio $\left[\frac{\text{Acrylic acid}}{\text{EGDMA}}\right]$ in the reaction zone, acrylic acid homopolymerization and copolymerization efficiency of acrylic acid and EGDMA. Higher $\left[\frac{\text{Acrylic acid}}{\text{EGDMA}}\right]$ ratio means more polyacrylic acid chains in the polymer network but reduced degree of cross-linking. The local concentration ratio was doubled from AE 1 to AE 2 on doubling the acrylic acid concentration, resulting in ~ 90 % weight gain due to increased polyacrylic acid graft density in the network (see Figure 4.51). The capacity of 2.5 wt.% EGDMA to cross-link more polyacrylic acid chains was exploited at 10 wt.% forming a highly cross-linked polyacrylic acid dominated structure on the surface. Although the ratio was highest for AE 3, the degree of cross-linking was the lowest due to low EGDMA concentration (1.25 wt.%). This generated a loosely packed structure with dangling chains of polyacrylic acid. The interactions between polyacrylic acid chains result in aggregation prior to polymerization forming long polyacrylic acid chains in the presence of low EGDMA content due to the matrix effect[222]. This results in higher weight gain for AE 3 than AE 1.

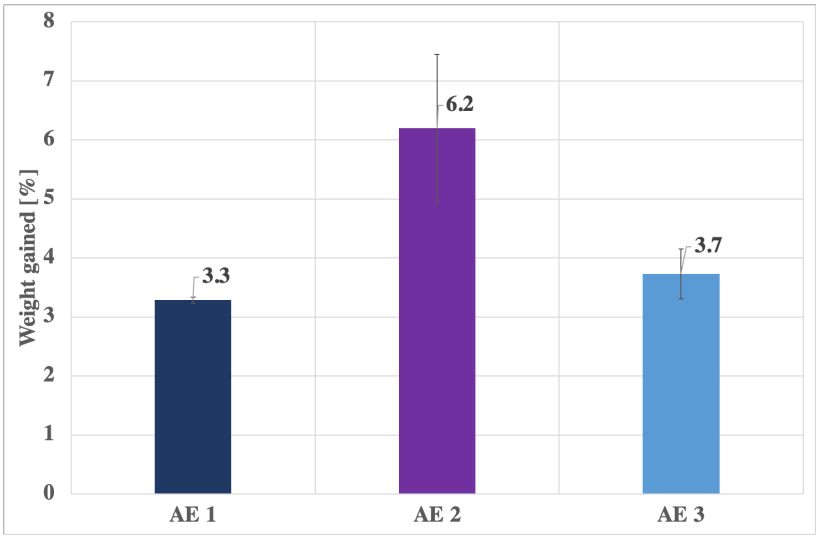

Figure 4.51. Comparison of weight gained between the different polyacrylic acid prototypes

Figure 4.52 depicts the possible hydrogel layer formation on the surface and inside the pores of the polyacrylic acid prototypes. In case of AE 1 (a), the hydrogel structure was a closely packed EGDMA layer with short polyacrylic acid chains attached to it. For AE 2 (b), higher polyacrylic acid concentration resulted in efficient copolymerization, suppressing EGDMA dominance and forming hydrogel network with long polyacrylic acid chains. Whereas for AE 3 (c), long chains of polyacrylic acid are all over the surface through loosely packed EGDMA cross-linkage.

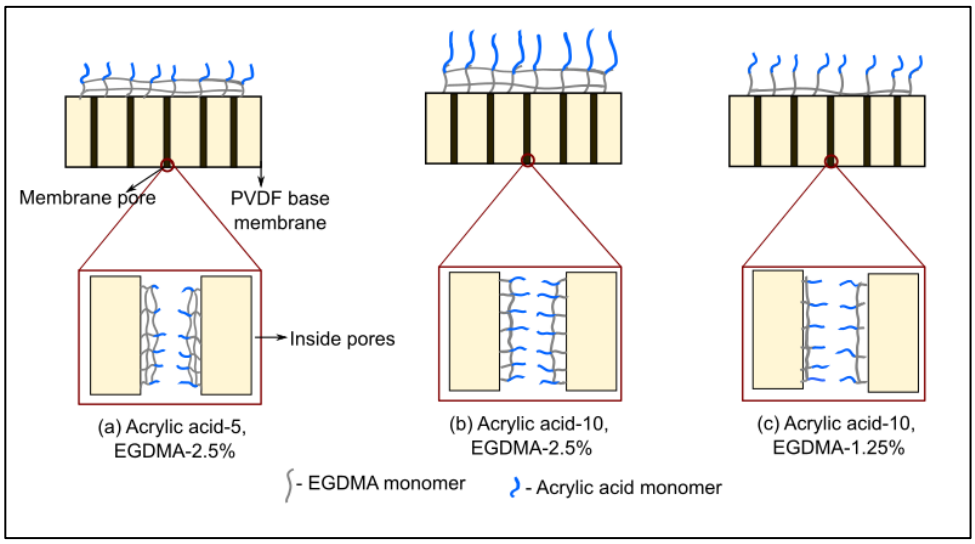

Figure 4.52. Schematic interpretation of formation of hydrogel layer for different prototypes on the surface and inside the pores

The pore size distribution plots in Figure 4.53 show decrease in pore size with increase in weight gain. Since, the weight gain is similar, no significant difference in pore size between AE 1 and AE 3 is observed. The effective pore size is a result of degree of grafting of the polymer network inside the pores. The pore size is measured by porometry, under the non-aqueous conditions, therefore precise behavior of the cross-linking degree and swelling cannot be discussed but can only be predicted. The average pore diameter was the largest for AE 3 because of the lowest grafting density. AE 2 showed the smallest pore diameter because of the highest grafting density. Narrowing of the pore diameter was less effective at lower acrylic acid concentration (AE 1) due to lower polymer content. The modified membrane was a result of combination of structural changes and surface chemistry alteration. The effect of structural changes was less with decreasing cross-linking density suggesting that EGDMA contributes to the structural changes and polyacrylic acid contributes majorly to the surface chemistry of the modified membrane.

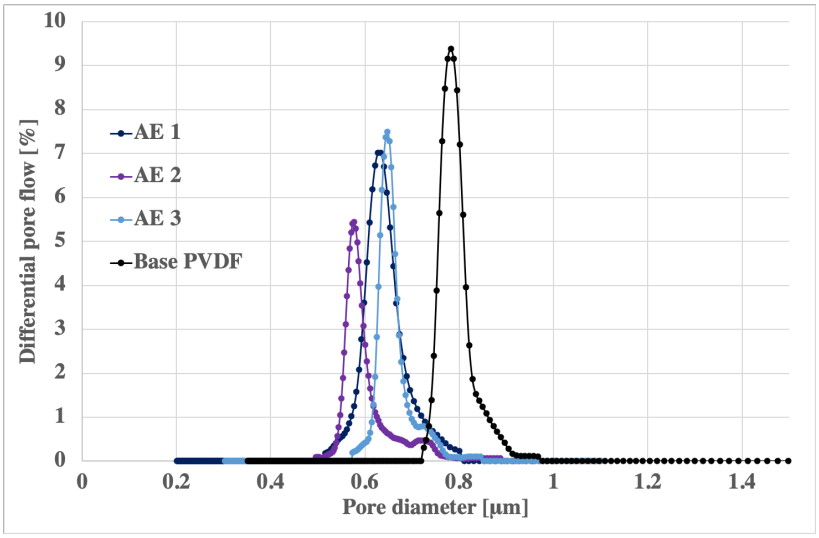

Figure 4.53. Comparison of pore size distribution between the different polyacrylic acid prototypes

Water uptake data in Figure 4.54 is a consequence of pore filling and water binding on the outer surface. The pore volume for water absorption decreases on polymer grafting with higher degree of cross-linking. And sites for water binding on the outer surface increase with increasing polyacrylic acid chains that increase the polymer network volume on the surface without changing the geometry. The highest water uptake value for AE 2 was in line with the result for weight gain and pore size distribution. Due to high amount of polymer grafting the effective pore volume was reduced but because of high polyacrylic acid content the water volume for water binding increased. The degree of cross-linking was the highest for AE 1 due to the lowest ratio of $\left[\frac{\text{Acrylic acid}}{\text{EGDMA}}\right]$. The dominant EGDMA homopolymerization along with high cross-linking degree for poly(EGDMA-co-AA) inside the pores forms a stiff network less hydrophilic in nature. The most open pores observed by porometry for AE 3 are overestimated because the measurement does not consider swelling of the chains with non-aqueous solution. The lower water uptake for AE 3 could be due to heterogeneously distributed poly(EGDMA-co-AA) chains throughout the porous structure. Due to very low content of EGDMA, loosely packed long dangling chains of polyacrylic acid are formed which further affects the interaction with water. Also, more polymer (polyacrylic acid) is grafted in case of AE 3 than AE 1 (see Figure 4.51) which affects the void volume.

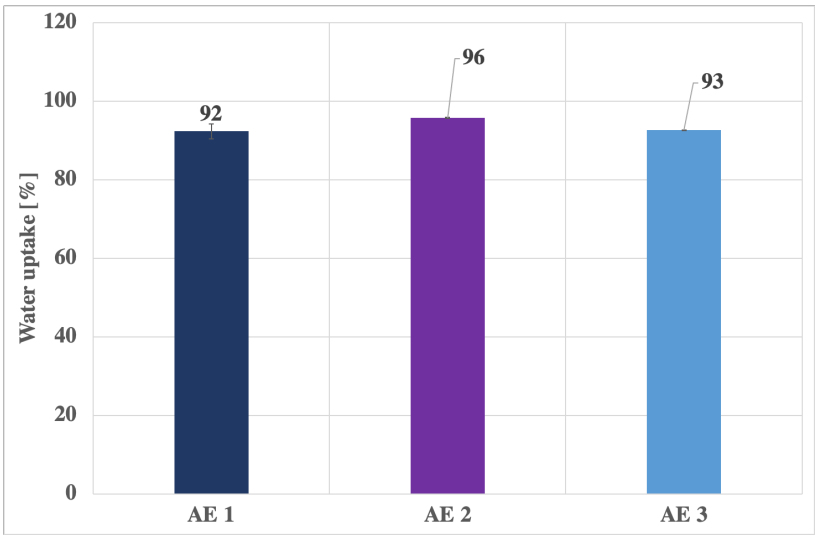

Figure 4.54. Comparison of water uptake between the different acrylic acid prototypes

The water permeance plots in Figure 4.55 further reveal more about the developed structure of the modified membranes. Depending on the amount of grafted polymer the pore volume changes: more grafting leads to less pore volume. AE 3 had the highest permeance owning the more open structure of the base membrane compared to AE 1 and AE 2 in addition to grafting with lower EGDMA content. The loosely packed AE 3 structure does not undergo structural changes such as narrowing of the pores due to low cross-linking density and low grafting. The lowest permeance displayed by AE 2 was in line with the highest weight gain, pore size distribution result and the lowest water uptake values of AE 2. The high amount of grafted polymer inside the porous structure and swelling of polyacrylic acid chains lowered the water permeance. AE 1 showed higher water permeance than AE 2 due to lower polymer grafting, higher EGDMA cross-linking density and short polyacrylic acid chains with repressed swelling effect.

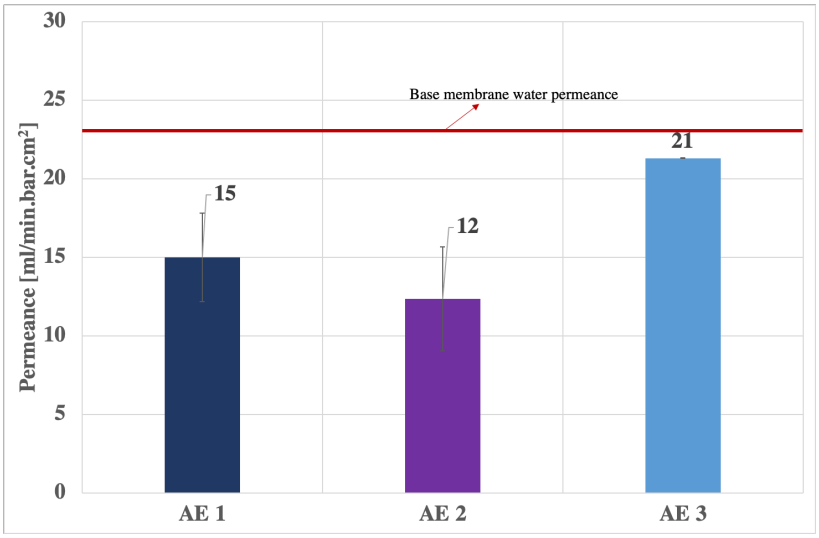

Figure 4.55. Comparison of water permeance between the different acrylic acid prototypes. The red-line shows the average water permeance for the base membrane measured for 20 samples

The grafted polyacrylic acid chains form the basis for the hydrophilic nature of the modified membranes. The polar carboxyl groups form hydrogen bonds with water allowing water to wet the membrane surface for all three modifications as shown in Figure 4.56. The starting contact angles correspond to the polyacrylic acid grafting density. However, the wetting time was the result of capillary forces acting inside the pores depending on the pore size. AE 1 showed the faster wetting possibly due to open porous structure while AE 2 and AE 3 displayed the slow wetting. The differences in the capillary action could also be introduced due to the base membrane structure and/or the spot of measurements.

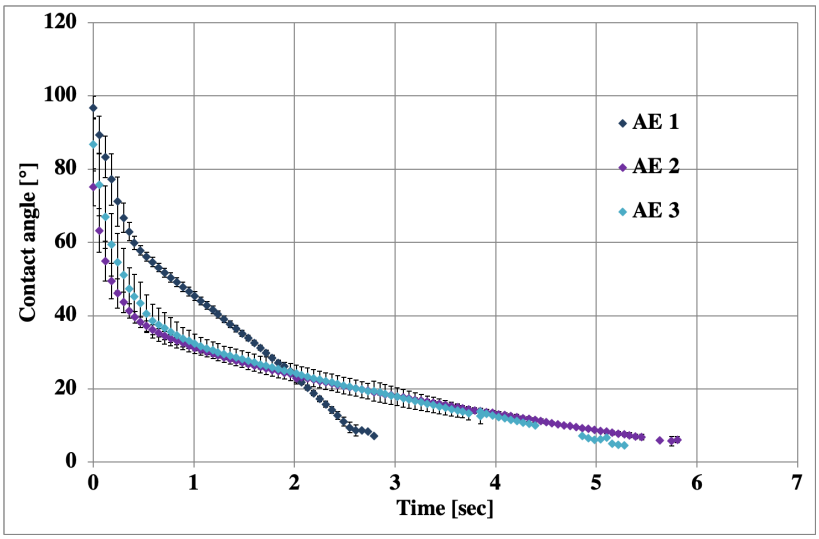

Figure 4.56. Comparison of change in contact angle with time for polyacrylic acid

Zeta potential measurements in Figure 4.57 revealed the membrane surface charge between pH 2 to 11. All the modified membrane plots exhibited negative zeta potential in the whole pH range unlike PVDF base membrane confirming successful incorporation of polyacrylic acid into the polymer network. Presence of carboxylic groups in the polyacrylic acid chain shifted the surface charge of the membrane. The dissociation of carboxylic surface groups resulted in negative surface charge. Although polyacrylic acid has pKa value around 4, no IEP was observed because possibly some chains are already deprotonated even at the pH below 4[254]. No significant differences in the trends were noted between prototypes because enough polyacrylic acid chains are incorporated on the surface to cause the change of surface charge. Furthermore, after pH 6 the surface charge stays constant possibly due to saturation of the charge density on the deprotonated carboxylic chains.

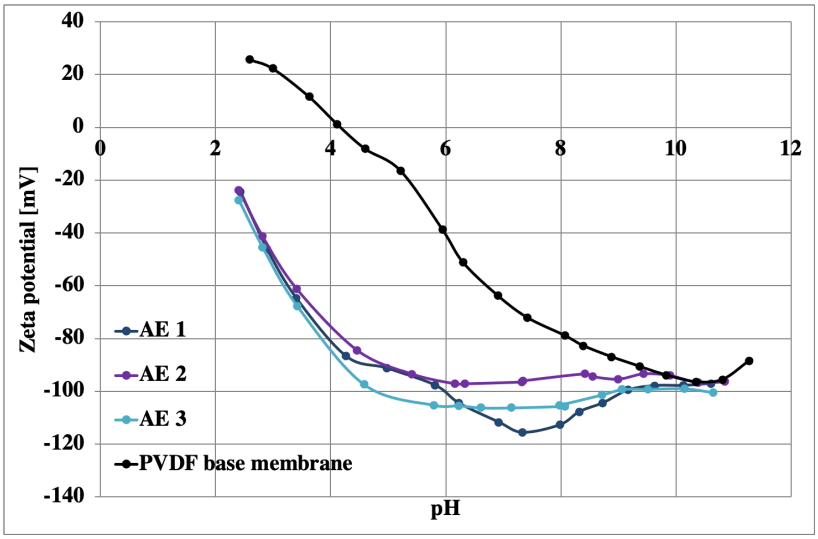

Figure 4.57. Comparison of zeta potential comparison between different polyacrylic acid prototypes with respect to the base membrane

The characterization results confirmed the predicted structure of the modified membranes mentioned in Figure 4.52. The results indicated that contributions of polyacrylic acid chains increase with decreasing cross-linker concentration however, to maximize the integration of polyacrylic acid enough (2.5 wt.%) EGDMA molecules should be present in the reaction zone. It was confirmed that EGDMA mainly influenced the structural changes upon grafting inside the pores while polyacrylic acid mainly contributed to the changes in the surface chemistry.

4.5.2.2 Performance characteristics of the polyacrylic acid prototypes

After understanding the membrane surface chemistry and structural changes brought about by modification the membrane performance was evaluated. Particle filtration was performed without stirring to study the blocking mechanism, effect of pH on the flow properties was analyzed to confirm the pH responsiveness and protein binding was investigated to determine the extent of fouling caused by BSA. Based on the membrane performance it would be possible not only to identify the effect of formulation on the membrane properties but also to establish a relationship between membrane properties and membrane performance for bioprocessing application such as cell culture concentration or purification. Hence, allowing the manufacturer (GVS) to fine-tune the membrane functionalization parameters such as cross-linker or monomer fractions to achieve the desired membrane properties for particular applications.

Particle filtration

The electrostatic repulsion between the polyacrylic acid chains grafted on the membrane surface and negatively charged particles in addition to the anti-fouling hydrophilic surface should enhance the particle retention by preventing them from entering the pores[255–257]. The blocking mechanism of the particles was studied by analyzing the fouling evolution as a function of filtration progress. The plots resulting from the filtration study are presented in Figure 4.58.

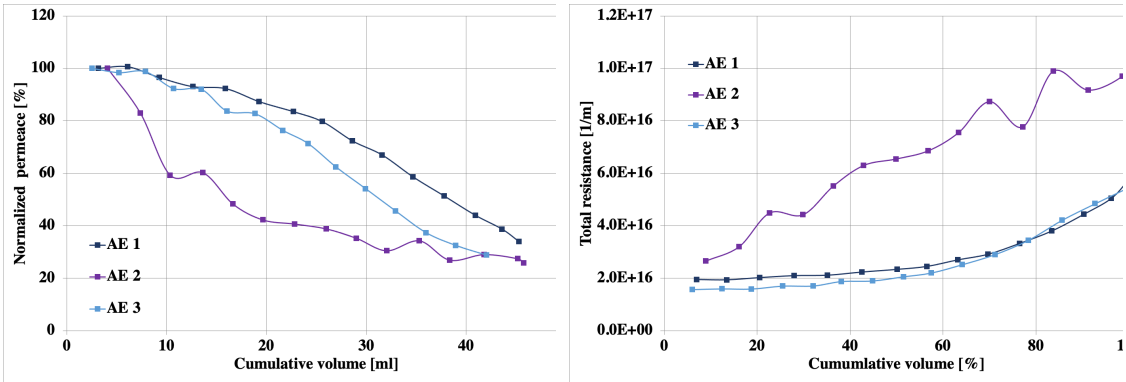

(a) (b)

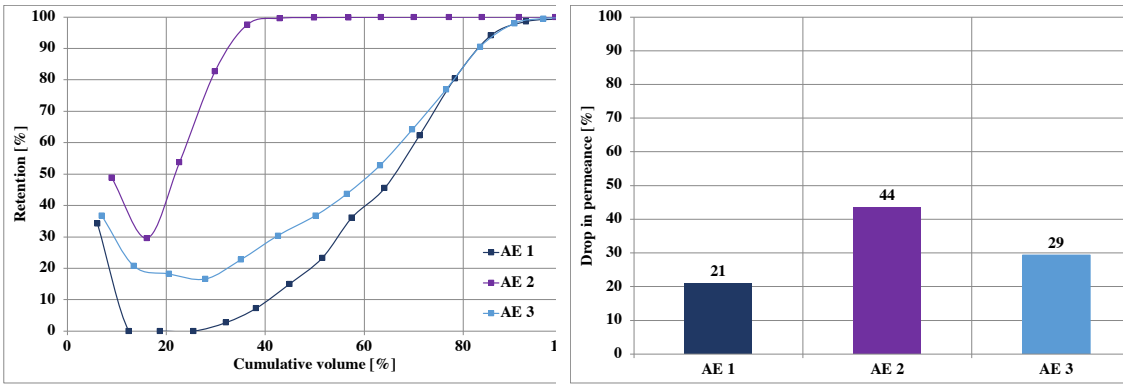

(c) (d)

Figure 4.58. Plots from the filtration study of the polyacrylic acid prototypes without stirring at 0.5 bar: (a) normalized permeance, (b) total filtration resistance, (c) particle retention, and (d) drop in water permeance

During the initial stages of filtration, sufficiently smaller particles [218 nm] (see Table 4.5) than the membrane pores [~ 450 nm], are transported through the membrane in all three cases. The concentration of the particles increases at the membrane surface as the filtration progresses. The clustering and aggregation of the particles on the membrane surface depends on the particle-membrane interaction and particle suspension stability[258]. High density of polyacrylic acid chains on the surface showed higher rejection of particles leading to faster cake layer formation by preventing particle penetration due to electrostatic repulsion. The influence of polyacrylic acid on the surface chemistry was enhanced with decreasing cross-linker concentration; polyacrylic acid chains swell more at low degree of cross-linking.

The EGDMA dominant highly cross-linked AE 1 structure had bigger pores with few polyacrylic acid short chains as seen in Figure 4.52. Due to open structure sufficiently, smaller particles are transported through the membrane. Lower density of polyacrylic acid grafting allows adsorption of particles and intermediate blocking. The particles were transported across the membrane until a cake layer was formed - after 90 % volume was filtered. Therefore, throughout the filtration, the retention was low, permeance was high and the resistance build-up for the filtration was very slow. Since, majority of the particles were transported through the membrane the drop in flux is low.

The high polyacrylic acid density along with high degree of cross-linking in AE 2 resulted in a narrowed pore size and swelling of the chains. These chains repel the particles and narrowed pore size hinder easy passage of particles through the porous structure. As a result, rate of cake layer formation was reached relatively faster which means the drop in

filtration permeance was higher and the faster rate of particle build-up was reflected in the filtration resistance plot. The low adsorption capacity of the polyacrylic acid chains allows particles to aggregate on the surface leading to faster blockage of the membrane pores. Therefore, the drop in permeance was high, and the filtration resistance increased rapidly. The irreversible adsorption of the agglomerated particles due to cake layer formation and high internal particle trapping resulted in drop of permeance after filtration.

Although the polyacrylic acid chain length was higher in AE 3 the overall grafting density was low due to low EGDMA content. AE 3 formed an open loosely packed structure with dangling chains of polyacrylic acid due to low degree of cross-linking. Thanks to the dangling chains that can interact with the particles, AE 3 retains more particles than AE 1. The membrane resistance for AE 1 and AE 3 is same, but the drop in permeance is different (AE 3 > AE 1). This could be due to the different initial permeance of the membranes. The more open AE 3 base membrane has higher surface area to absorb more particles inside the pore structure leading to higher retention, but reduced filtration permeance and lower recovery. The overall retention for AE 3 is still very low because of the open structure base membrane structure.

The goal of these prototypes was to maximize the recovery of particles by preventing losses due to adsorption and penetration. The particle recovery in Figure 4.59 was determined by calculating the concentration of particles retained and recovered from the membrane after the filtration. The results of particle recovery are in good agreement with membrane resistance. Due to high density of polyacrylic acid chains in AE 2, the recovery of the particles was the highest followed by AE 3 and AE 1 the lowest. Furthermore, the pH-responsive behavior of the acrylic acid membranes can be exploited to enhance the particle recovery by manipulating pH and/or introducing a backflushing step at high pH. Depending on the final application certain techniques can be implemented by the end user of the membrane to enhance the membrane performance.

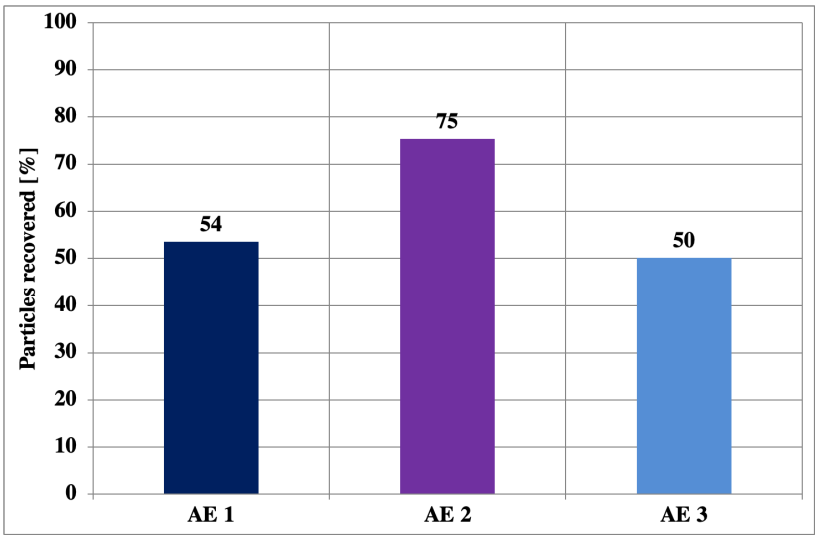

Figure 4.59. The number of particles recovered after the filtration for polyacrylic acid prototypes

The SEM micrographs of the top surface and the cross-section post filtration gave further insights into the blocking mechanism based on the location of the particles within the pore structure. Despite the surface modification strategies and washing, particles attached to the membrane surface. Majority of the particles were retained on the top surface of the membrane upon formation of the cake layer in the later part of the filtration. This can be clearly seen in the SEM micrographs for the top surface of all three prototypes in Figure 4.60. However, the cross-section SEM revealed particles entering the porous structure of the membrane. The particles were mainly concentrated in the top part of the cross-section. Relatively, less particles were observed in case of open structured AE 3 compared to AE 1 (see Figure 4.58). Particles easily enter inside the open porous structure and penetrate; but as filtration progresses particle concentration increases leading to trapping of particles inside the sponge-like membrane structure resulting in permeance drop. The particle challenge increases as filtration progresses which increases the particle load in the cake layer. The negative charge of adsorbed particles in addition to the membrane negative charge results in stronger repulsion of the incoming particles. This reduced the deposition of the particles and avoids clogging. The entering of the particles in the porous structure can be due to the breakthrough of the cake layer or could be a result of initial deposition before formation of the cake-layer. Since, no drop in retention is observed due to particle detection after cake-layer maturation it is impossible for a breakthrough to have occurred. Hence, the particles in the top-part of the membrane were possibly the result of irreversible fouling upon adsorption during the initial stages. The evolution of fouling at different stages during filtration is explained by Xiao et al.[259] The results also indicate

that the negative surface charge of the membrane is not enough to avoid the adsorption of the agglomerated particles under the given filtration conditions due to smaller size of the particles compared to the membrane pore size which get trapped inside the membrane pore structure.

Top	Cross-section

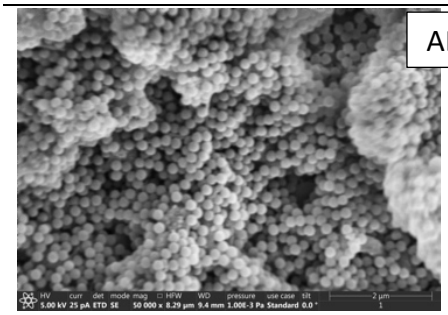

AE 1

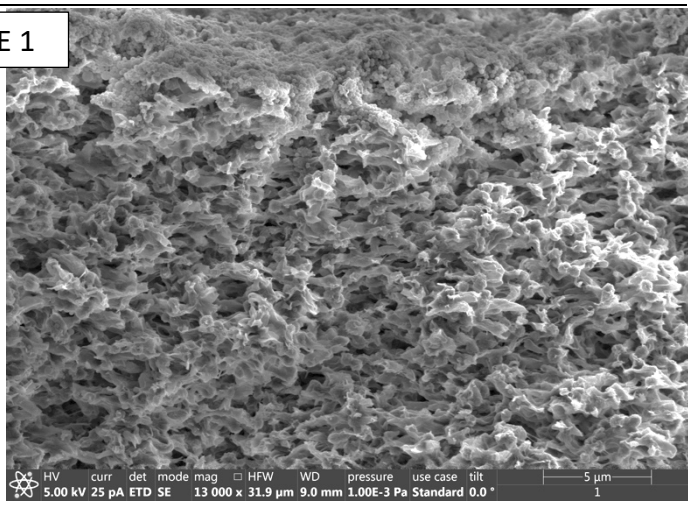

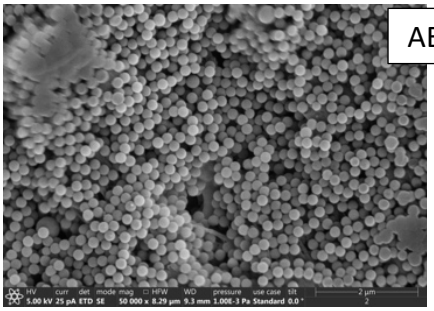

AE 2

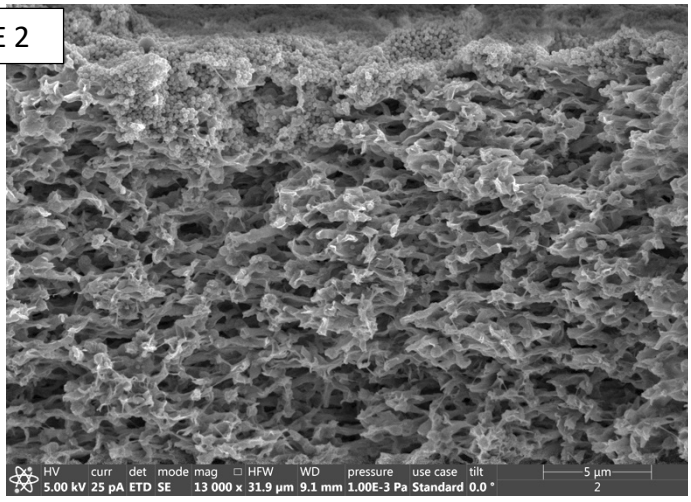

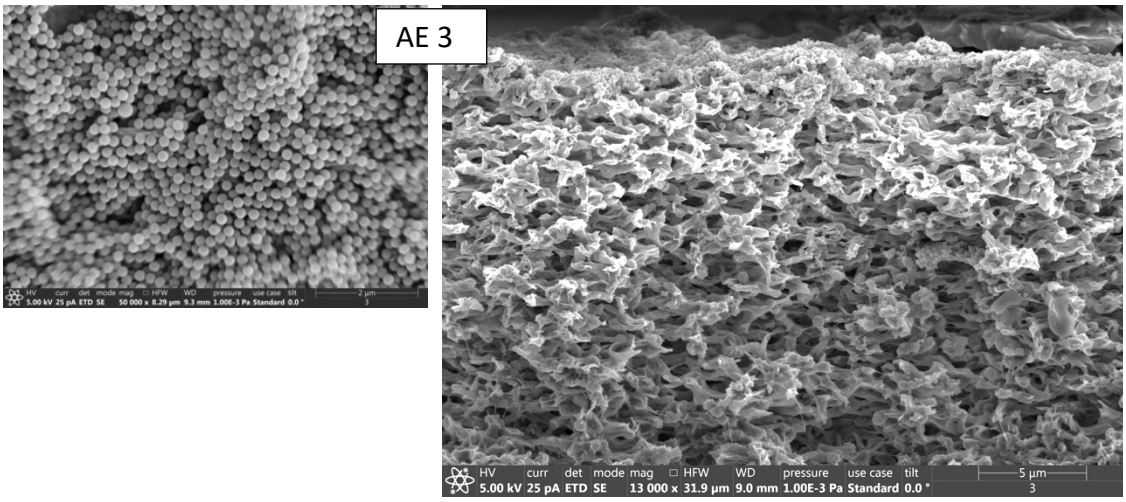

Figure 4.60. SEM micrographs of the top surface and cross-section after filtration for different prototypes of polyacrylic acid

Figure 4.61 displays the retention plots for the acrylic acid modifications carried out with a syringe filter set-up. The retention results complemented the results obtained with stirred cell filtration. The plots were more revealing about the more effective role of polyacrylic acid chains in the retention with decreasing cross-linker amount. With decreasing influence of polyacrylic acid chains on the membrane surface the retention of the particles decreased confirming that the dangling chains of acrylic acid interacted with particles enhancing the retention.

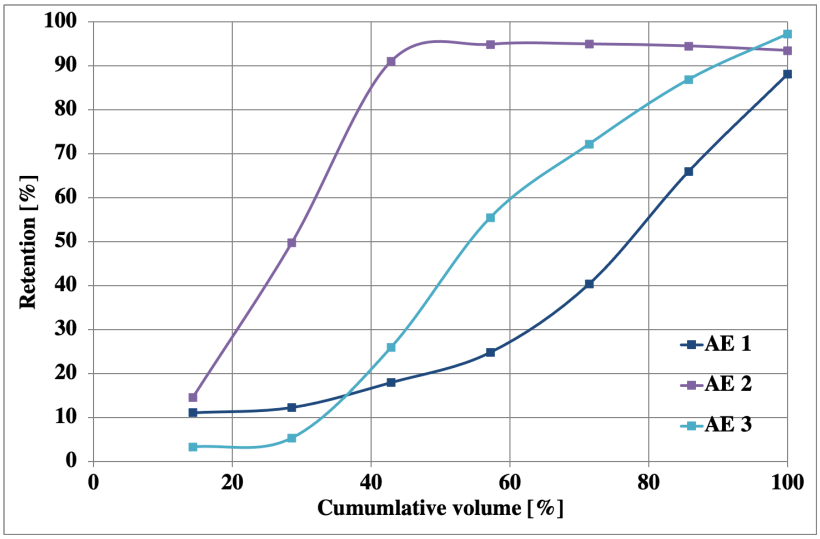

Figure 4.61. Particle retention for the syringe filtration at ~ 0.5 bar with polyacrylic acid prototypes

Figure 4.62

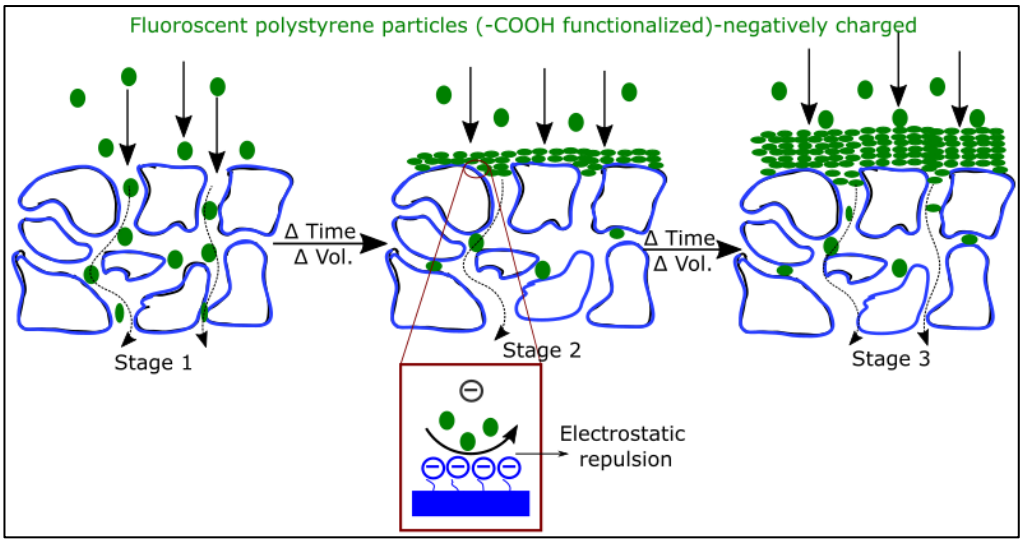

showcases the stages of fouling during the particle filtration with polyacrylic acid prototypes.

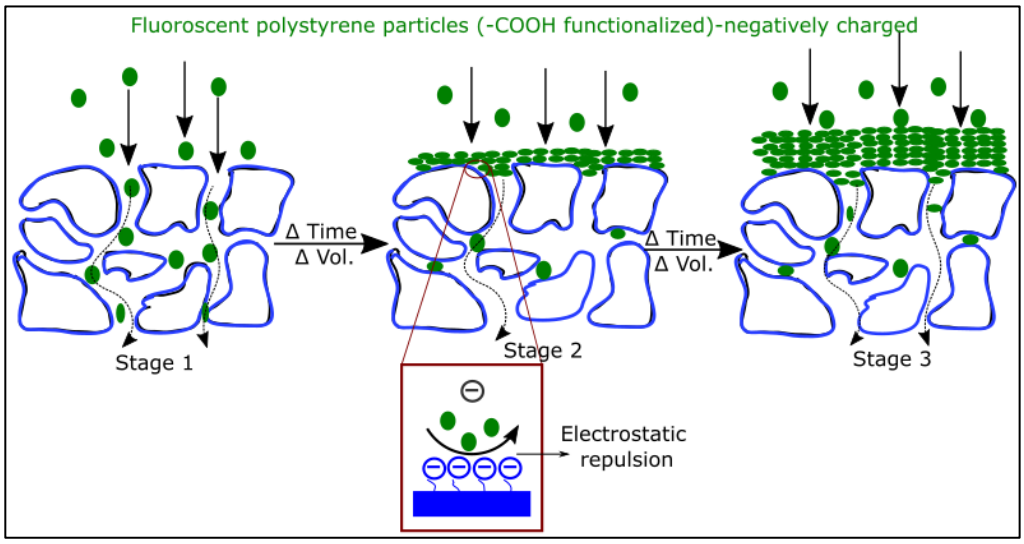

Figure 4.62. Schematic interpretation of particle blocking and cake layer formation as the filtration progresses for polyacrylic acid functionalized membranes

Effect of pH

Polyacrylic acid is utilized in this work to minimize adsorption of negatively charged biological particles on to the membrane surface based on the electrostatic interactions. Moreover, the pH responsive behavior can be further exploited to enhance the particle recovery by using an external stimulus. Conversely, positively charged particles can be captured by utilizing the polyacrylic acid functionalized membrane as an affinity filter.

Figure 4.64 shows the pH dependence of permeance for all three prototypes. The permeation rate for the membranes was slow above pH 3 due to swelling of the carboxyl chains. Dissociation of carboxyl chains takes place at pH higher than 4.3 (pKa = 4.3). As the hydroxyl ion concentration increases in the aqueous solution with pH, the dissociation of carboxyl chains is accelerated. The conformational changes attributed to pH are shown in Figure 4.63. Under high pH conditions, the dissociated chains swell as a result of electrostatic repulsion between side groups. The chains inside the pores narrow the effective pore diameter reducing the permeance. However, at low pH chains assume helical conformation reducing the steric obstruction in the pores[260]. Several studies concerning the dependence of permeance on pH have been reported[261–264].

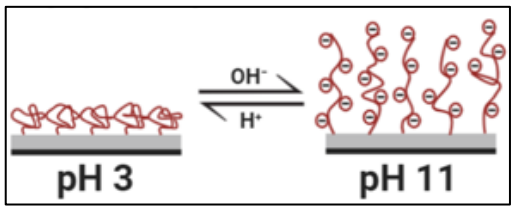

Figure 4.63. pH responsive behavior of the polyacrylic acid chains

Interestingly, the overall percentage drop in permeance with increasing pH from 3 to 11 in Figure 4.64 was different depending on the prototype. The pH dependence is regulated by the surface density of the grafted polyacrylic acid chains. AE 1 had the least drop (61 %) followed by AE 2 (73 %) and the highest drop for AE 3 (89 %). This further confirmed the hypothesis that on decreasing EGDMA concentration the influence of polyacrylic acid surface chemistry increases. Furthermore, the drop in permeance after pH 7 was not significant since the pKa value for polyacrylic acid lies between pH 3 and 7 (4.3). Therefore, the deprotonation and consequent swelling occurs between pH 3 and pH 7 leading to the drastic drop in the permeance. However, further increasing pH from 7 to 11 deprotonates remaining chains but the effect was smaller as most of the chains were already deprotonated.

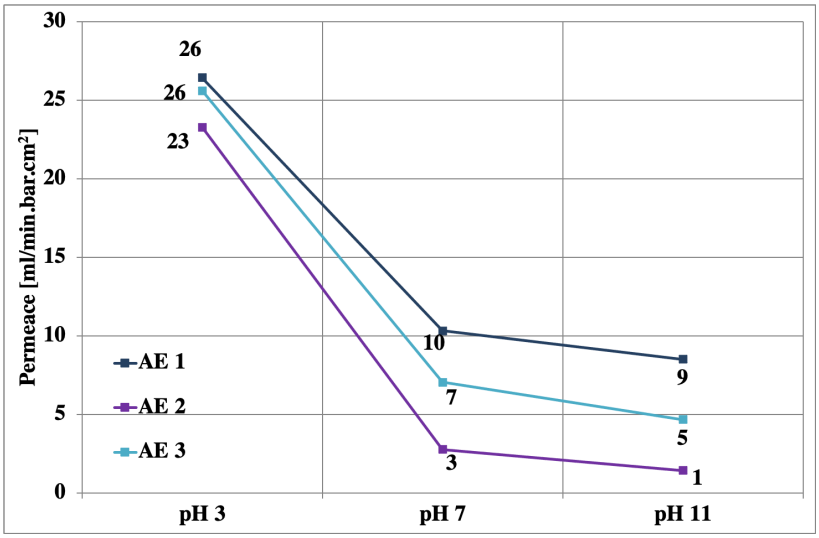

Figure 4.64. pH responsive behavior in 0.1 M PBS of the acrylic acid functionalized membrane: narrowing of the pores at basic pH due to swelling of the carboxylic chains on deprotonation resulting in lower water permeance

Protein binding

Adsorption of BSA (5 mg/ml) on polyacrylic acid prototypes in the static mode: membranes submerged in BSA solution and dynamic mode: BSA solution filtered through the membrane is reported in Figure 4.65

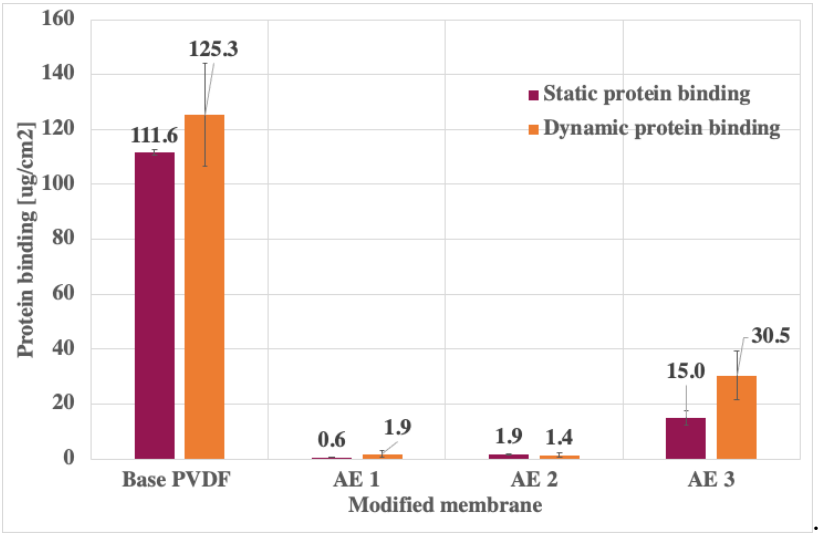

. The interaction of proteins with the membrane surface depends on the properties of the protein such as size, charge, structure and the characteristics of the membrane such as charge, hydrophilicity, morphology, and surface properties[265]. BSA is a relatively large protein (66.5 kDa) with 583 amino acid residues and isoelectric point of pH 4.7 in water at 25 °C[266,267]. In this work, BSA solution was prepared at pH 7 in 0.1 M PBS where it has negative surface charge. Immobilization of polyacrylic acid chains on the membrane surface reduces the protein binding. The carboxyl groups form hydrogen bonds with water generating a hydration layer on the surface which prevents proteins from interacting through van der Waals forces and hydrophobic interactions[268]. Moreover, the electrostatic repulsion between deprotonated carboxyl chains and BSA at pH 7 further minimizes protein adsorption.

AE 3 showed very high protein binding compared to AE 1 and AE 2 in Figure 4.65

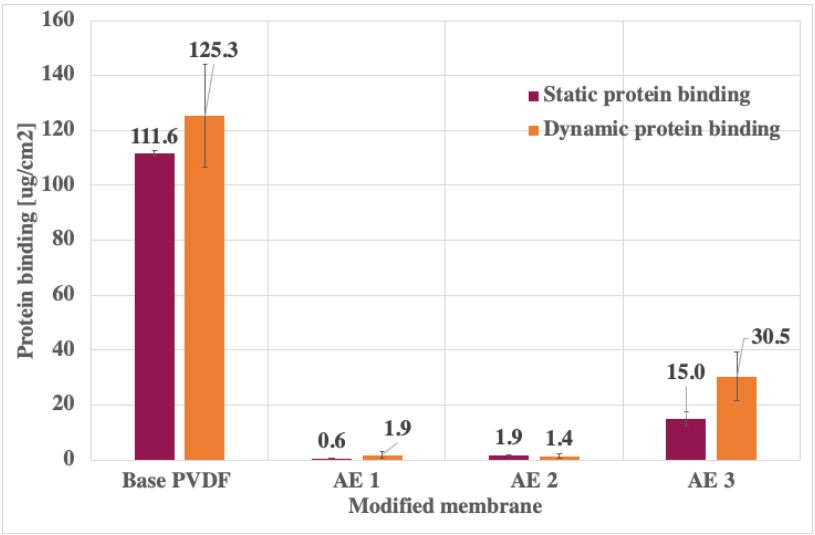

in both static and dynamic mode. The BSA adsorption depended on the degree of grafting, hydrogel

network density and the fraction of polyacrylic acid in the hydrogel coating. Although degree of grafting for AE 3 was similar to AE 1, lower hydrogel network density and lower fraction of polyacrylic acid due to less EGDMA resulted in inefficient coating. High protein binding suggested heterogenous surface grafting with inefficient functionalization inside the pores resulting in hydrogel lean spots. When exposed to BSA, it binds to the vulnerable hydrogel lean spots through van der Waals and hydrophobic interaction resulting in high protein binding. The binding in dynamic mode was higher than static because the interaction points for BSA when forced through the membrane at 0.1 bar are more allowing higher adsorption and deposition throughout the porous structure. The efficient functionalization as a result of high degree of grafting, high hydrogel network density and high fraction of polyacrylic acid throughout the porous structure leads to hydrophilic improvement preventing protein binding in AE 1 and AE 2[269]. The very low protein binding for both implied the necessity of higher content of EGDMA for efficient grafting of polyacrylic acid chains throughout the porous structure.

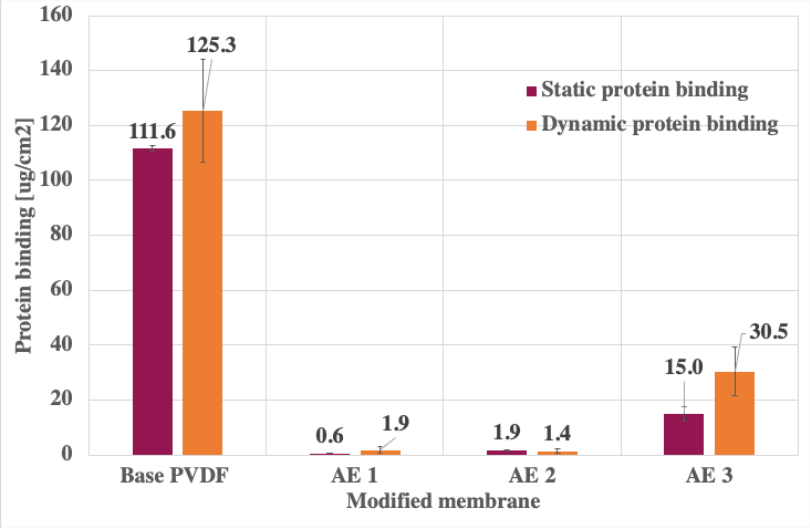

Figure 4.65. Dynamic and static protein binding with 5 mg/ml BSA for different polyacrylic acid prototypes

Figure 4.66 (a) shows the permeance values for water, PBS and BSA measured during the dynamic protein binding experiment. It is known that above pH 4.3, on dissociation of carboxyl groups the electrostatic energy overcomes the entropic contribution to the free energy resulting in chain extension[270]. This extension causes narrowing of the pores. But in the presence of salts, the high ionic strength of the solution screens the repulsive electrostatic interactions causing entropic contribution to predominate again[271]. This phenomenon explained the higher permeance for PBS and BSA than water due to presence of salts which reduced the chain swelling at a relatively high PBS concentration

of 0.1 M. The permeance for PBS and BSA was a result of membrane morphology and was independent of chain swelling. The data in Figure 4.66 (b) conveys the drop in water permeance after protein binding. The data showed the regenerating capacity of the membrane which can be improved upon further fine-tuning to maximize polyacrylic acid content. Upon rinsing with water, the permeance can be recovered to some extent but recovery to its initial value was not possible. The protein binding was a result of BSA adsorption and deposition throughout the porous structure reversibly and irreversibly[272]. The reversible fouling can be removed by washing leading to the observed recovery however, the irreversible fouling cannot be eliminated. The irreversible fouling caused the drop in permeance which was inversely proportional to the grafted polyacrylic acid chains. The extent of fouling and permeance recovery can also be further enhanced by utilizing the pH responsiveness of the chains and externally manipulating the pH of the solution[250,273].

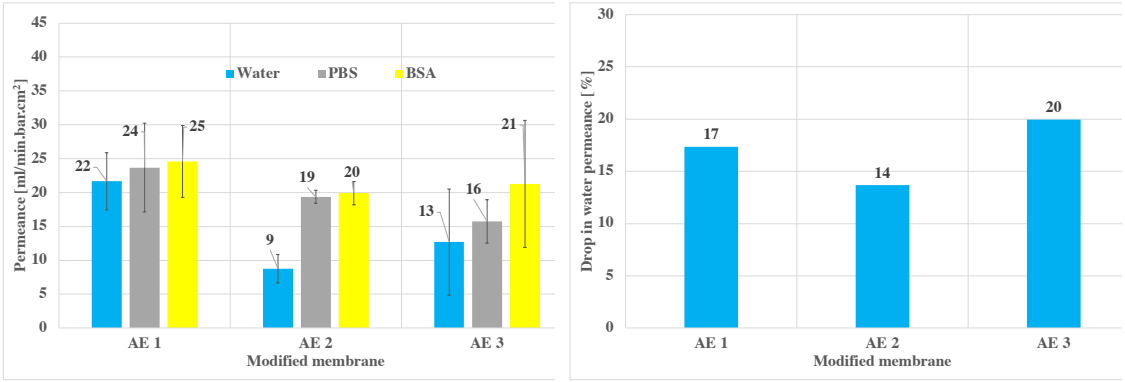

(a) (b)

Figure 4.66. Results from dynamic protein binding: (a) permeance of water, PBS and BSA and (b) drop in water permeance before and after the protein binding

4.5.3 PolyHEMA functionalized membranes

Membranes modified with polyHEMA have been used in numerous applications due to their hydrophilicity[274], biocompatibility[275,276], and anti-fouling property[130,277]. In addition to the π-bond, presence of a hydrophilic pendant hydroxy group allows its versatile modification to provide wide range of derivates for various purposes. This makes HEMA an attractive candidate for membrane grafting through polymerization[278–280] and hence was utilized to develop a new hydrophilic prototype with hydrophilic anti-fouling properties via two-step graft coating polymerization method.

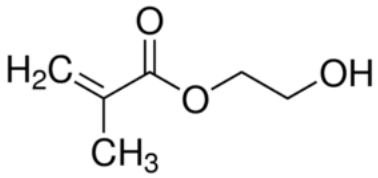

Figure 4.67. HEMA structure

HEMA, a vinyl monomer reacts in the redox initiated system by addition mechanism similar to acrylic acid due to the presence of a π-bond. Numerous studies of HEMA graft polymerization through electron transfer process have been reported in the literature[281,282]. Although, HEMA is a vinyl monomer similar to polyacrylic acid the fundamental differences between both result in different polymerization mechanism. The presence of a methacrylate group upon auto polymerization reduces the water solubility due to increase in the methyl content upon formation of a long chain. Moreover, from the thermodynamic perspective, structural similarity between HEMA and EGDMA leads to "smoother" copolymerization resulting in higher degree of grafting than acrylic acid. The goal was to create an effective hydration layer as a result of hydrogen bonding between water and hydroxy group on the surface by grafting multiple HEMA chains. This anti-fouling hydration layer should avoid proteins from interacting with the membrane surface. Similar to acrylic acid three prototypes were developed according to the formulation shown in Table 4.7 in an attempt to enhance HEMA participation and suppress EGDMA dominance in the hydrogel network.

Table 4.7. Modification formulation used for developing the HEMA prototypes with their corresponding codes

Modification formulation [wt.%]	$\left[\frac{\text{HEMA}}{\text{EGDMA}}\right]$	Membrane code
HEMA 5 % + EGDMA 2.5 %	2	HE 1
HEMA 10 % + EGDMA 2.5 %	4	HE 2
HEMA 10 % + EGDMA 1.25 %	6	HE 3

4.5.3.1 Modified membrane characterization

The effect of cross-linker and HEMA on polymerization and consequently on the final membrane properties was studied by analyzing membrane surface chemistry, morphology and flow properties. HEMA has a greater tendency to homopolymerize compared to acrylic acid because of the hydrogen bond and dipole interactions between

HEMA monomers. Hence, HEMA-HEMA interactions are thermodynamically more favorable than acrylic acid-acrylic acid interactions which are affected by interactions of highly electronegative carboxylic groups[283]. The hydrogel grafted data confirmed higher weight gain for HEMA than polyacrylic acid for same formulations.

The local concentration ratio $\left[\frac{\text{HEMA}}{\text{EGDMA}}\right]$ in the reaction zone governs the polymerization. On increasing HEMA concentration the incorporation of HEMA in the polymer network increased. The lowest local concentration ratio $\left[\frac{\text{HEMA}}{\text{EGDMA}}\right]$ for HE 1 suggests dominance of EGDMA in the polymer network due to lack of HEMA monomers near the reaction zone. However, on doubling HEMA concentration in HE 2, the weight gain increased by ~90 % in Figure 4.68. At higher HEMA concentration, the growing macroradicals have a better chance to come in contact with PolyHEMA thereby, achieve higher degree of grafting suppressing EGDMA homopolymerization. Even though the local concentration ratio was high the weight gain for HE 3 was lower than HE 1 due to lower EGDMA concentration; the lower degree of cross-linking is incapable of integrating all HEMA molecules into the polymer network. The viscosity of solution increases at higher HEMA concentration making it difficult for HEMA to diffuse towards the membrane surface with limited active macroradicals due to lower content of EGDMA.

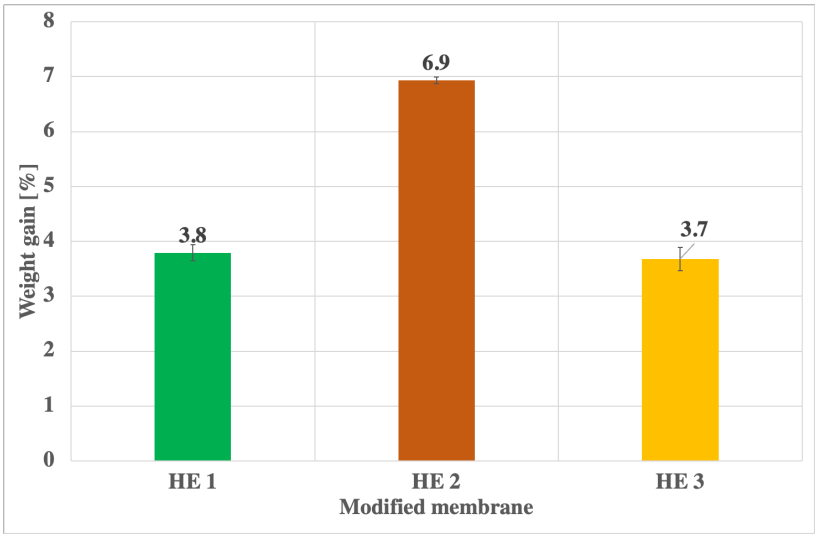

Figure 4.68. Comparison of weight gained after functionalization between the different HEMA prototypes

The shift of mean pore size towards smaller pore diameter depends on the weight gain, i.e., amount of polymer grafted in the pore well. The mean pore size in Figure 4.69 corresponds to the weight gain: higher the weight gain, lower the mean pore diameter. The cross-linking degree of the grafted polymer relies on the total polymer content and

EGDMA fraction. The shift of mean pore size towards smaller pore diameter with increasing cross-linking density in Figure 4.69 confirmed formation of highly cross-linked dense polymer network as a result of "smooth" polymerization between HEMA and EGDMA. The shift for HE 1 and HE 2 towards left was more than polyacrylic acid (Figure 4.53) and overlapping of HE 1 and HE 2 suggested that at 2.5 wt.% EGDMA a dense structure is formed narrowing the pores of the membrane. This effect was absent for polyacrylic acid because of the cascading effect of HEMA monomers during radical polymerization and more efficient copolymerization with EGDMA.

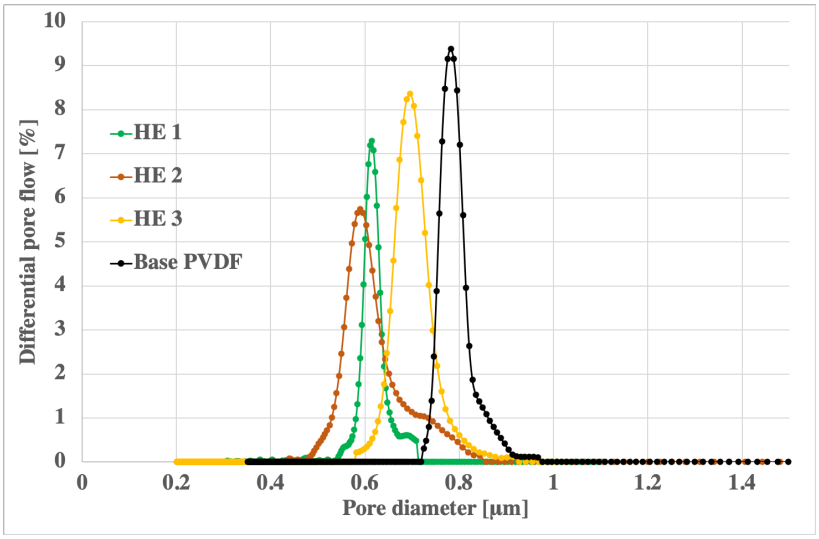

Figure 4.69. Comparison of pore size distribution between the different HEMA prototypes

The water uptake values for polyHEMA in Figure 4.70 were less than polyacrylic acid for all three formulations because the mass gained upon polymerization for polyHEMA was higher than polyacrylic acid. Higher weight gain and smaller pore size distribution than polyacrylic acid attest higher amount of polymer grafting. The weight gained by HEMA modifications corresponds to the polymer grafted in the pore wells and was inversely proportional to water uptake. PolyHEMA forms a highly cross-linked dense polymer network within the porous structure reducing the effective void volume. Moreover, ability of polyHEMA to swell was reduced as a result of rigid structure with high degree of cross-linking. Water uptake for HE 2 was the lowest whereas HE 1 and HE 3 showed similar values (see Figure 4.70). The weight gained by HE 2 was the highest compared to HE 3 and HE 1, but the total polymer concentration (HEMA + EGDMA) is almost the same. This was due to the fraction of EGDMA which not only affects the cross-linking density but also the hydrogel grafting. HE 2 had the highest polymer content resulting in highest degree of grafting thus lowest degree of swelling and free volume.

HE 3 had the highest water uptake due low degree of cross-linking forming an open structure with loosely packed chains rather than a dense polymer structure. Moreover, HE 1 should have the highest cross-linking density due to the highest fraction of EGDMA.

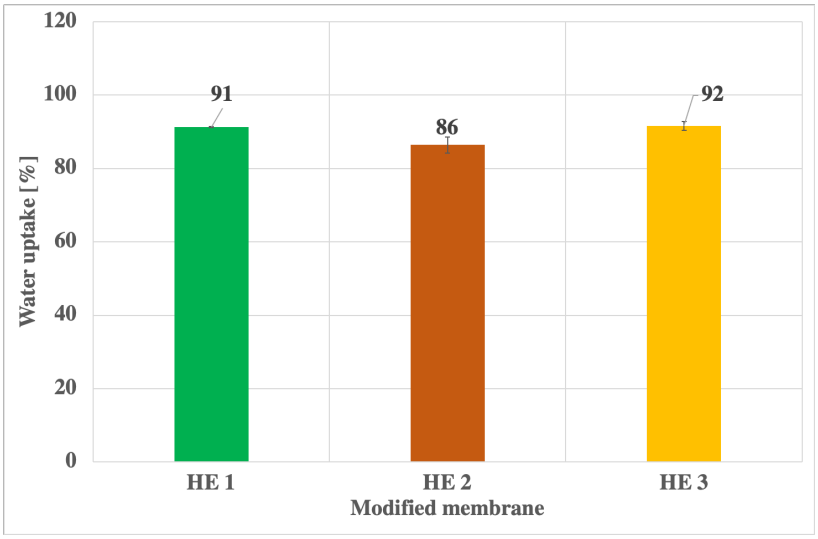

Figure 4.70. Comparison of water uptake between the different HEMA prototypes

Figure 4.71 projects the possible hydrogel network formed on the surface and inside the pores of the polyHEMA prototypes. Unlike polyacrylic acid, polyHEMA forms a dense hydrogel layer on the membrane surface. Hydrogel layer is a highly cross-linked polymer network between EGDMA and PolyHEMA which influenced the pore structure upon grafting. For HE 1, a rigid hydrogel structure is formed on the EGDMA backbone that dominated the hydrogel network. But for HE 2, HEMA rapidly converts into polyHEMA chains which were cross-linked onto the surface by EGDMA forming a dense hydrogel structure dominated by polyHEMA. And finally in case of HE 3, a loosely packed hydrogel structure mainly formed of polyHEMA chains with low degree of cross-linking was formed.

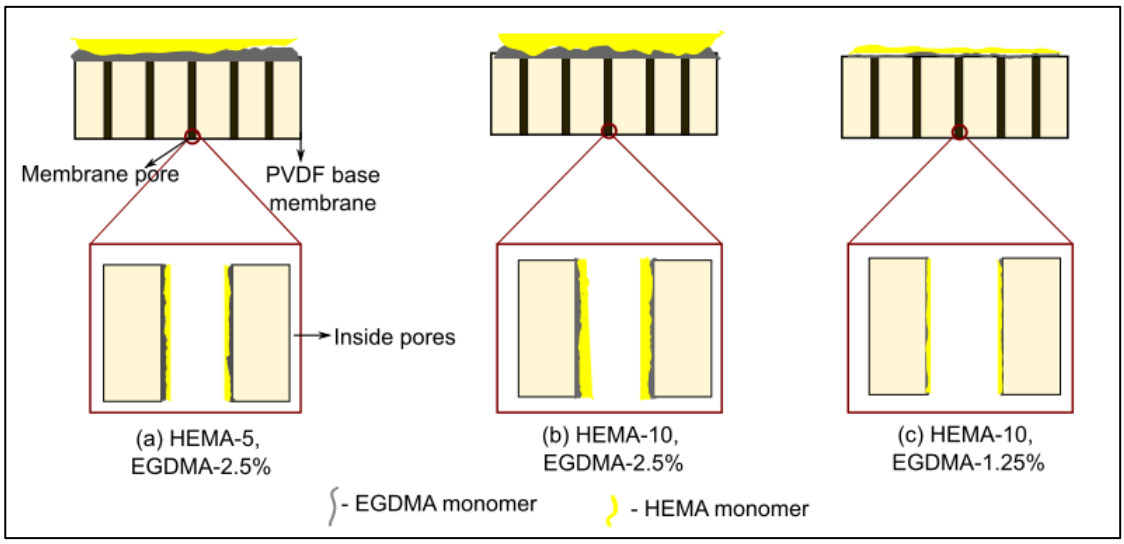

Figure 4.71. Schematic interpretation of formation of hydrogel layer for different HEMA prototypes on the surface and inside the pores

The effective pore size and hydrophilicity are the two factors that affect water permeance[123]. Grafting of polyHEMA chains on the surface of the membranes enhances hydrophilicity allowing water to permeate with ease[284]. However, for microfiltration membranes pore size plays more important role and the permeance is strongly dependent on the pore size. Therefore, selection of the base membrane with appropriate pore structure is integral to the final membrane selectivity and flux. HE 3 had the highest water permeance (see Figure 4.72) due to the relatively open base membrane structure dominated by loosely packed chains of polyHEMA. Whereas, HE 1and HE 2 had lower permeance as a result of narrowing of the pore structure upon formation of highly cross-linked dense polymer network.

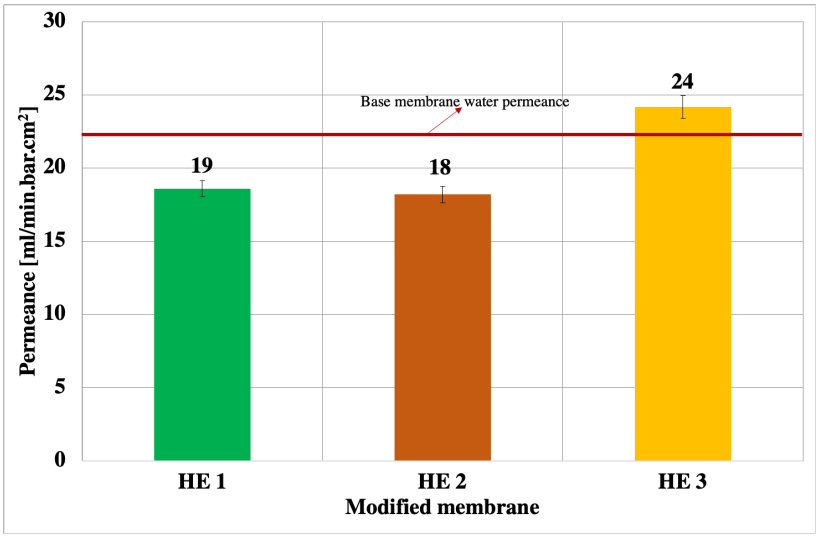

Figure 4.72. Comparison of water permeance between the different HEMA prototypes. The red-line shows the average water permeance for the base membrane measured for 20 samples

The enrichment of polyHEMA chains on the membrane surfaces promisingly improves the hydrophilicity of the prototypes due to the presence of -OH groups[285]. However, difference in the starting contact angle and the wetting time can be observed between the prototypes in Figure 4.73. HE 2 had the lowest starting contact angle ~75°, where as HE 1 and HE 3 had ~78° and ~88° respectively. HE 1 wets the fastest under 3 secs. While HE 2 and HE 3 took around 6 secs. The polyHEMA gives membranes hydrophilicity but the architecture of the grafted polymer network and surface porosity cause the distinct differences. The more open top surface accelerates the transport of water droplets through the membrane due to capillary effects[286]. Additionally, difference in surface concentration of polyHEMA chains also dictates the interaction of water droplets with the membrane. HE 2 had the highest grafting of polyHEMA but lowest pore diameter due to narrowing of the pores on grafting. Thereby, the starting contact angle was low but the wetting time was high due to the narrowed pore structure. HE 3 formed an open structure but with relatively low polyHEMA chains resulting in high starting contact angle. HE 1 due to higher fraction of EGDMA formed highly cross-linked rigid structure resulting in ~78°, however the low wetting time (< 3 secs.) could be due to an open base membrane. Moreover, the lower starting contact angle than polyacrylic acid prototypes confirmed higher polyHEMA segments in the polymer network.

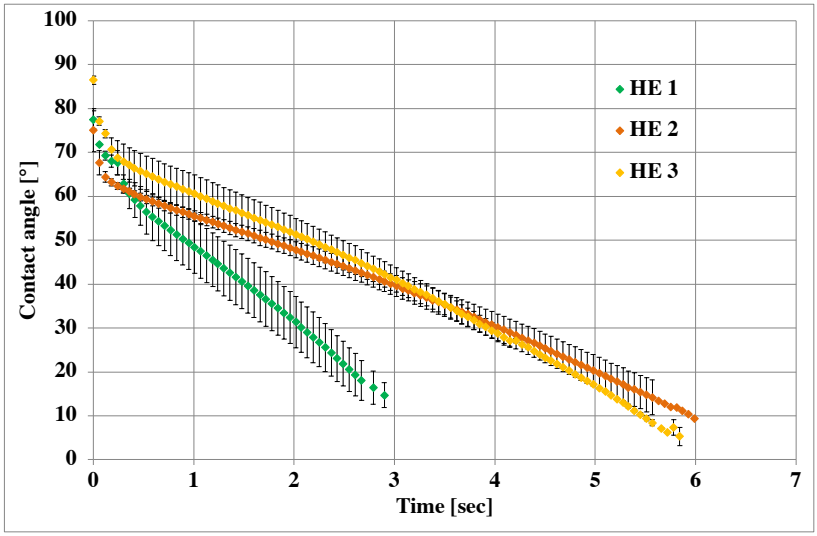

Figure 4.73. Comparison of change in contact angle with time for POLYHEMA prototypes

The polar nature of polyHEMA shifted the isoelectric point of the PVDF base membrane from pH ~4 to pH ~2.5. The surface charge decreases with increasing pH (higher hydroxyl ions in aqueous medium) and with increasing polyHEMA segments. In case of polyacrylic the charge became suddenly negative upon deprotonation (around pH 4).

Compared to the surface charge for polyacrylic acid the drop in charge is gradual. Therefore, the behavior of surface charge is fixed depending on the adsorbed ions. The influence of HEMA chains on the surface was reduced by increasing the EGDMA concentration. At 2.5 wt.% EGDMA, degree of cross-linking increased forming a dense copolymerized poly(EGDMA-co-HEMA) polymer network. Therefore, the zeta potential plots for HE 1 is above HE 2 and HE 3. The difference in surface charge as a result of the group in adsorbed ion is evident on comparing polyHEMA zeta potential data with polyacrylic acid (cf. Figure 4.57).

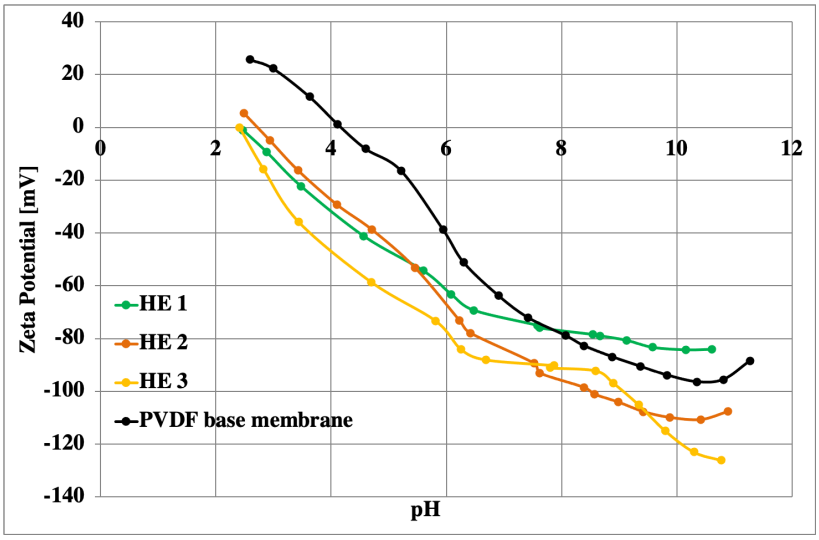

Figure 4.74. Zeta potential measurements of the different HEMA prototypes

These findings confirm that HEMA and EGDMA copolymerize smoothly to form a highly cross-linked polymer network. The degree of cross-linking is governed by the local concentration ratio in the reaction zone. On increasing the HEMA concentration, a highly cross-linked dense network dominated by polyHEMA is formed. On decreasing EGDMA concentration, a loosely packed structure with chains of HEMA is formed. EGDMA contributes the structural changes in the pores and HEMA at low concentrations largely contributes to the surface chemistry but at high concentrations is also responsible for the structural changes.

4.5.3.2 Membrane performance characterization

Similar to polyacrylic acid, the developed HEMA prototypes were characterized for their performance to establish a relationship between the membrane properties and membrane performance. The effect of HEMA modification on particle retention and protein fouling

was analyzed by carrying out the filtration study and protein binding experiments. The results were compared to identify the formulation for industrial upscaling.

Particle filtration

A comprehensive study same as polyacrylic acid was implemented to get an in-depth understanding about the blocking mechanism. The evolution of blocking mechanism was monitored by analyzing the movement of the particles with time during the filtration process. The negative surface charge on the membrane surface at pH 7 should repulse the particles additionally, the presence of hydration layer should minimize the particle interaction with the membrane. The plots resulting from the filtration study are represented in Figure 4.75.

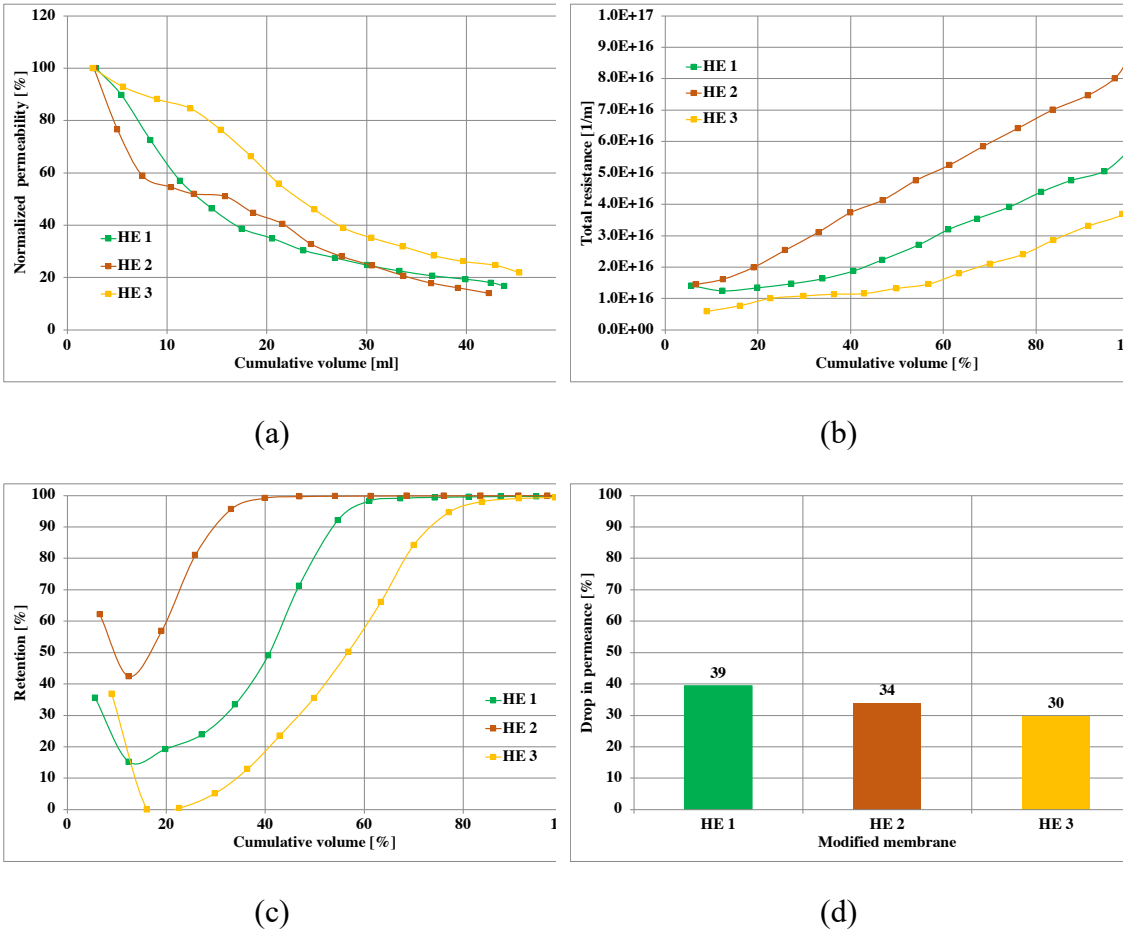

Figure 4.75. Plots from the filtration study of POLYHEMA prototypes without stirring at 0.5 bar: (a) normalized permeance, (b) total filtration resistance, (c) particle retention, and (d) drop in water permeance

Initially during the filtration, the particles penetrate the membranes due to the large difference between pore diameter and particle size. The concentration of the particles at the membrane surface increased with filtration, the deposition of the particles depends on

the interaction of the particles with membrane and particle stability[258]. The initial high retention seen for all three is the residual water present in the system after the water permeance test performed before the filtration. The high density of polyHEMA segments on the surface should increase the hydrophilicity and the swelling resulting in a strong hydration layer on the membrane surface. However, swelling of the grafted polyHEMA chains depends on the degree of cross-linking. With increasing cross-linking degree, the swelling ability of polyHEMA chains is compromised and a rigid polymer network is formed. The cross-linking degree increases with EGDMA content. The retention was the result of the pore structural changes upon hydrogel grafting.

The low ratio of $\frac{\text{HEMA}}{\text{EGDMA}}$ in HE 1 resulted in a rigid highly cross-linked polymer structure dominated by EGDMA which gives rise to a relatively weaker hydration layer due to lower fraction of polyHEMA and lack of swelling. This allows particles to adsorb leading to intermediate blocking. However, formation of rigid hydrogel structure inside the pores reduces the effective pore diameter. Thereby, hindering the passage of particles as the concentration at the surface increases and eventually resulting in a cake layer formation after 60 % filtration progress. The reduction of filtration permeance corresponds to the particle build-up on the membrane surface, this increased the filtration resistance as seen in Figure 4.75. The highest drop of water permeance after filtration was because of the irreversible fouling possibly caused not just by weak hydration layer but due to the mechanical interactions between the particles inside the porous structure and the membrane walls. Since the particle size is smaller than the pore size certain particles enter the porous structure.

The higher polyHEMA density in case of HE 2 creates a strong hydration layer on the surface additionally, and mass gain upon grafted polymer reduces the effective pore diameter. The strong hydration layer does not allow particles to interact with the membrane reducing the adsorption and intermediate blocking. Moreover, upon increasing particle concentration at the surface a cake layer is formed relatively quickly after 40 % filtration progress. The corresponding increase in filtration resistance due to particle build-up also results in reduction in permeance. The lower drop in water permeance for HE 2 than HE 1 confirms low adsorption capacity upon higher grafting of polyHEMA.

The reduction in EGDMA content in HE 3 results in lower grafting of polymer although polyHEMA fraction is higher. This results in an open structure with low density of

polyHEMA chains on the surface. The loosely packed open structure with polyHEMA chains interact with the particles preventing them from entering the pores but higher permeance due to open structure lead to higher particle penetration. PolyHEMA chains became effective only at high particle concentration. Therefore, during majority of the filtration (80 %) particles transported through the membrane resulting in fouling via adsorption and intermediate blocking. As a result, the permeance was relatively higher and the filtration resistance was low due to inefficient particle build-up at the surface. Also, the water permeance drop was the lowest for HE 3 as majority of the particles pass through the membrane due to the large difference in pore diameter and particle size.

The prototypes aim at maximizing the recovery of the particles after filtration by retaining maximum particles and preventing loss of particles by fouling. However, particles significantly smaller in size than membrane pores were chosen to study filtration mechanism. Figure 4.76 illustrates the particle recovery from the retentate and the membrane surface after filtration. It further supports the hypothesis that formation of a strong hydration layer reduces particle interaction with the membrane. The strong hydration layer and the reduced pore diameter for HE 2 prevented particles from entering the pores and can be recovered to some extent by washing. The lower recovery for HE 1 could be a result of weak hydration layer due to EGDMA dominance in the polymer network and lower degree of swelling. Whereas, HE 3 forms a loosely packed open structure which allows majority of the particles to penetrate as seen from the retention data. Thereby, resulting in less particles entrapped in the membrane.

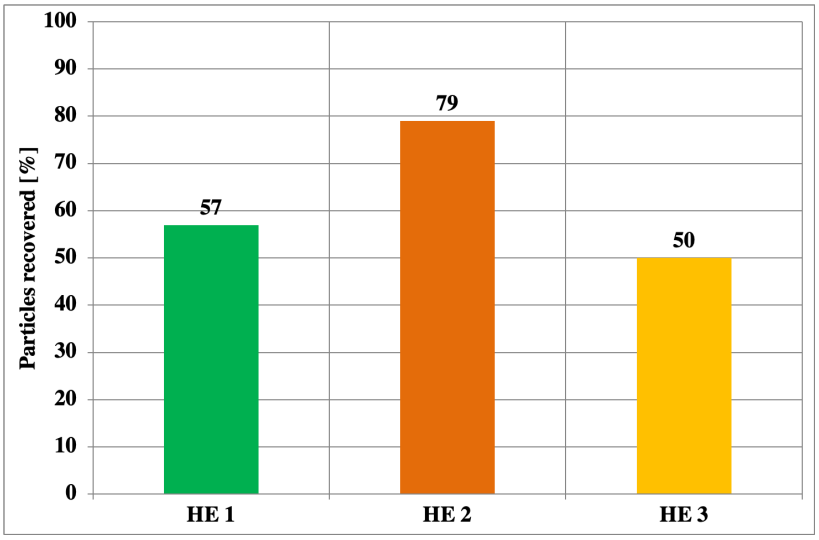

Figure 4.76. The number of particles recovered after the filtration for POLYHEMA prototypes

SEM micrographs were obtained for the top surface and the cross-section of the POLYHEMA prototypes after filtration to get further insights into the blocking mechanism. Homogenous deposition of particles on the top-surface of the membrane can be observed after filtration indicating adsorption and aggregation of the particles despite of the hydration layer and particle stability. The particle concentration at the membrane surface increases as the filtration progresses. Since, no additional stabilizers are added in the suspension such as surfactants it is possible that decreased energy barrier facilitates aggregation resulting in irreversible fouling at the open membrane surface. The addition of stabilizers (surfactants) was avoided to prevent alteration of the membrane surface properties which affects the filtration performance as reported by Pazouki et al.[287] It should be noted that the filtrations were carried out without stirring to allow the natural particle build-up based on the particle-membrane interaction. Cross-section of HE 1 revealed the high density grafting possibly of EGDMA dominant polymer inside the porous structure. The fibers from the dense polymer network can be spotted in Figure 4.77. However, similar dense polymer network was not seen for HE 2 and HE 3. High HEMA concentration competes for the radicals and suppresses EGDMA autopolymerization in the porous structure. While, reduced EGDMA concentration at high polyHEMA content results in loosely packed polyHEMA chains on the surface of the membrane. The particles were observed in the top part of the membrane in the cross-section micrographs for all the prototypes. During the initial stages of the filtration, sufficiently smaller sized particles can easily penetrate the membrane. This leads to fouling of the open structure via adsorption and intermediate blocking as explained in the fouling evolution model by Xiao and coworkers[288]. The weak hydration layer due to dominant EGDMA in HE 1 allowed particles to adsorb on the surface. Furthermore, irreversible fouling inside the porous structure of HE 1 by particle adsorption is evident from the SEM micrographs. The EGDMA dominance in the polymer network inversely affects the filtration efficiency. In case of HE 2, although particles were deposited irreversibly on the top part of the membrane, no particles are observed inside the porous structure. The effective polymerization inside the porous structure avoids adsorption and clogging. In addition to the functionalized surface that reduces particles from entering. HE 3 forms an open structure which allows particle passage through the membrane, however lower mass gain upon grafting due to low EGDMA content results in heterogenous polyHEMA chains on the membrane surface. The heterogeneity allowed particles to irreversibly deposit on the membrane surface and inside the porous structure.

Top	Cross-section
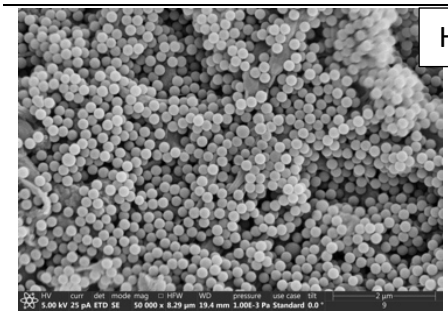	HE 1 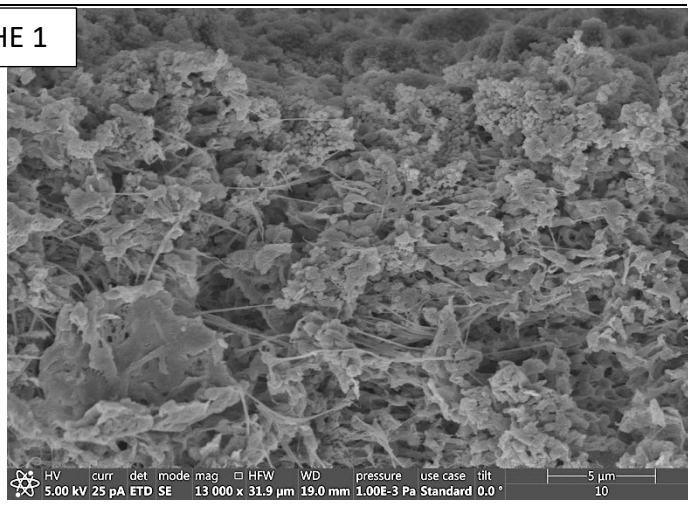
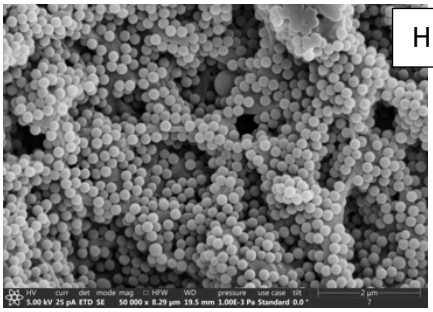	HE 2 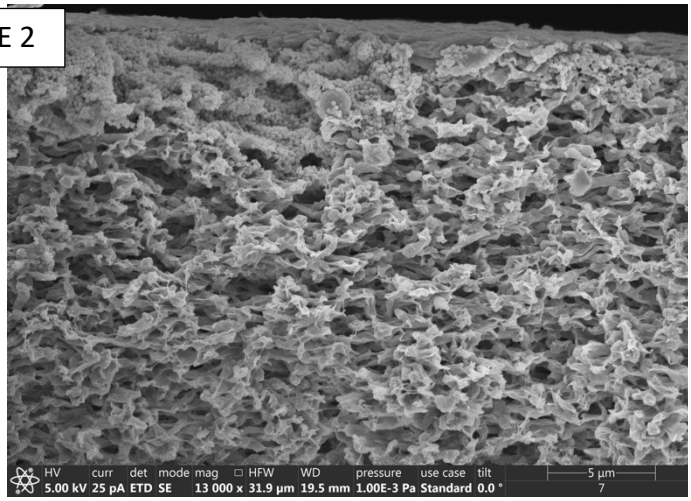

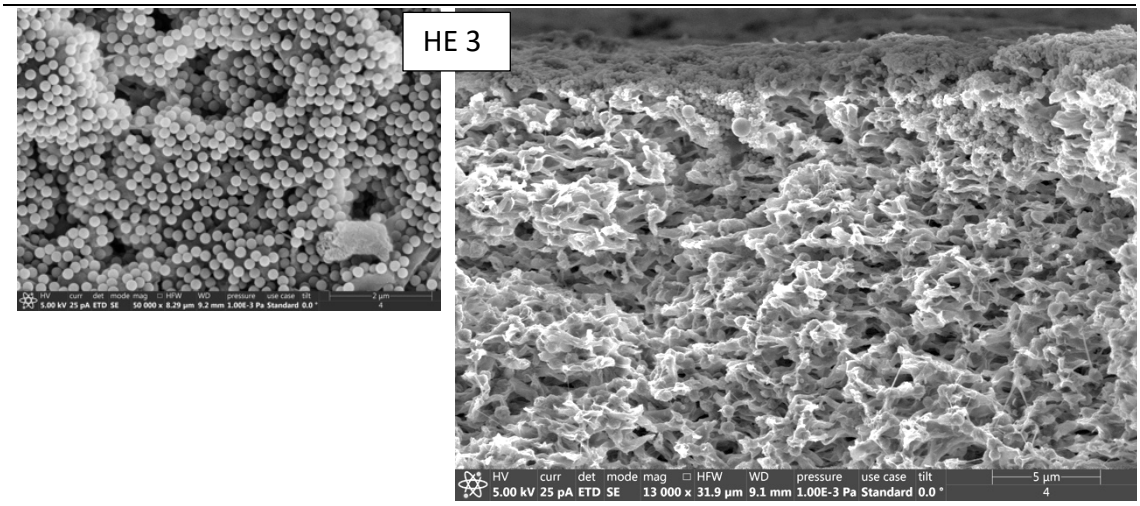

Figure 4.77. SEM micrographs of the top surface and cross-section after filtration for different prototypes of POLYHEMA

Figure 4.78 demonstrates the particle retention for HEMA prototypes carried out in the syringe filter system in a dead-end-filtration process. The results further supported the claim that strong hydration layer and HEMA chains enhance particle retention. HE 2 displayed the highest retention due to structural changes and strong hydration layer. However, drop in retention was observed in the last permeate is due to the breakthrough of the cake layer as a result of either high particle load or over pressure. HE 3 lead to the cake-layer formation through eventual build-up of the particles thanks to the interaction of HEMA chains with the particles. Interestingly, HE 1 fails to form a cake layer upon complete blocking of the pores until end of the filtration. The restricted swelling of grafted polyHEMA due to higher EGDMA fraction and weak hydration layer allowed continues penetration of the particles supporting the claim that high EGDMA content

inversely affects filtration efficiency. The results obtained by syringe filtration further bolster the theories explained for the Amicon cell filtration.

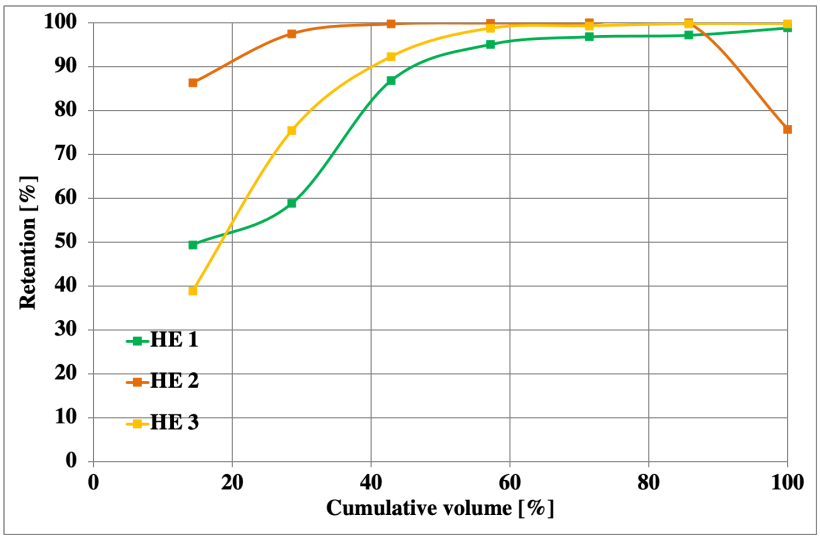

Figure 4.78. Particle retention for syringe filtration of POLYHEMA at ~ 0.5 bar with POLYHEMA prototypes

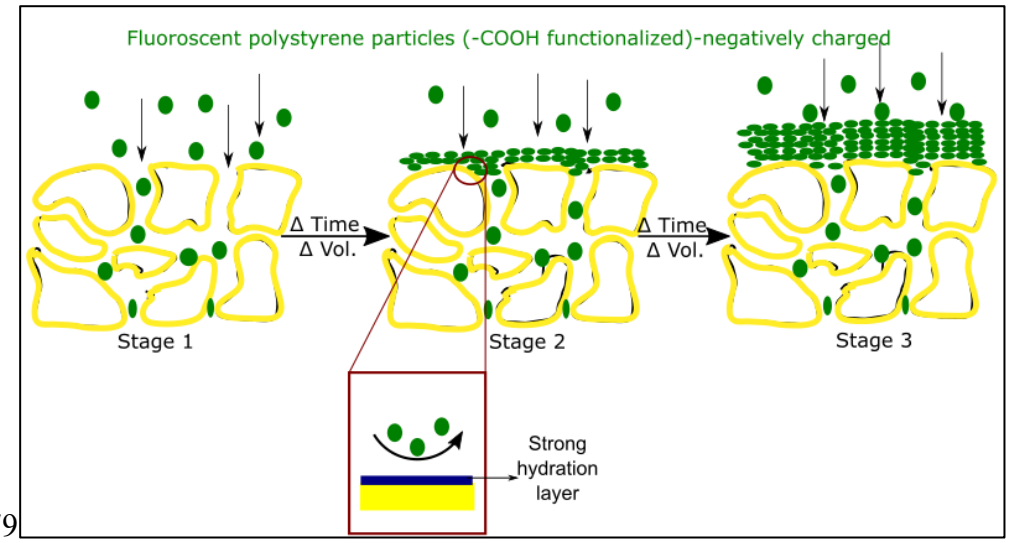

Figure 4.79 represents the blocking mechanism involved in the filtration with polyHEMA prototypes. At stage 1, particles penetrate due to smaller size than the pore diameter. As the particle challenge increases in stage 2, the hydration layer becomes effective in preventing particles from interacting with the membrane. This results in particle aggregation at the membrane surface. In stage 3, a strong cake layer is formed retaining all the particles on the surface.

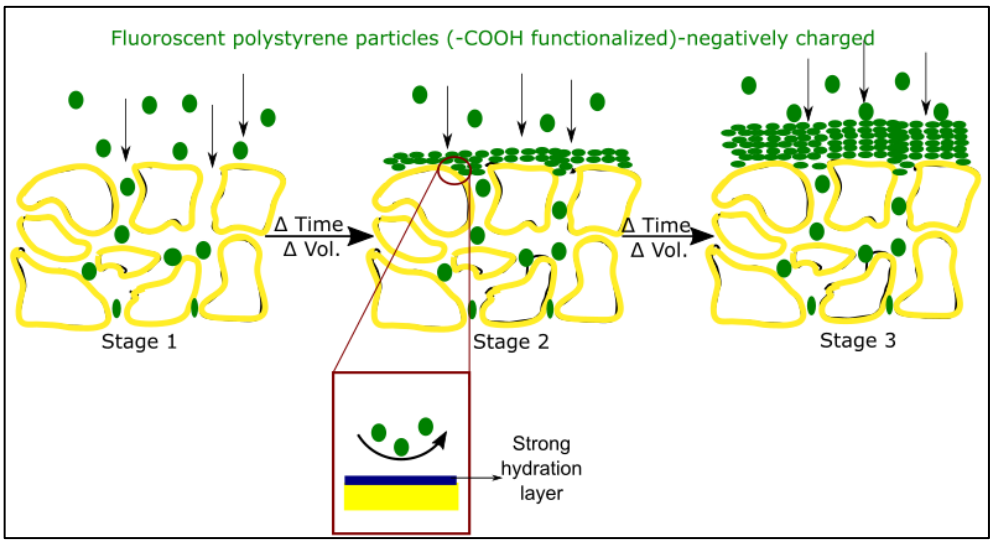

Figure 4.79. Schematic interpretation of particle blocking and cake layer formation as the filtration progresses for HEMA prototypes

The filtration results confirmed that the retention of the particles is governed by the structural changes upon hydrogel formation and surface chemistry changes upon HEMA domination. Ideally, for effective HEMA filtration the dual effect of hydration layer and HEMA chains for particle retention should actively play a role to minimize the particle interaction with the membrane. Additionally, narrowing of the pores helped avoid particles from entering. Nevertheless, the base membrane porous structure holds a key for creating effective functionalized membrane and consequently a membrane with high selectivity.

Protein binding

To investigate the protein binding ability of polyHEMA prototypes, experiments in static and dynamic mode were conducted with stable BSA (66.5 kDa) solution at pH 7 in 0.1 M PBS. Figure 4.80 demonstrates the protein binding for polyHEMA prototypes in static and dynamic mode carried out with BSA (5 mg/ml). The effect of protein fouling on water permeation recovery was also analyzed. Numerous studies have suggested operating: away from the protein isoelectric point (IEP, for BSA = ~4.7)[289,290], at low ionic strength of the solution[291] and with hydrophilic membrane surface chemistry[292]. PolyHEMA chains in its fully hydrated state are highly hydrophilic due to the presence of hydroxyl group. Membranes grafted with polyHEMA chains interact with water by creating hydrogen bonds and forming a hydration layer highly resistant to protein adsorption in aqueous medium[293]. Moreover, the uptake of the proteins is reduced based

on the zeta potential data due to the electrostatic repulsions between negatively membrane surface and negatively charged BSA at pH 7[294].

Therefore, higher polyHEMA density on the surface reduces the protein adsorption of the membrane. HE 3 binds the most amount of protein compared to HE 1 and HE 2. Low EGDMA content results in low degree of grafting forming loosely packed polyHEMA chains heterogeneously distributed on the surface. This creates hydrogel lean patches in the porous structure where BSA can bind. Similar phenomenon was observed for polyacrylic acid at low EGDMA content however, the lower protein binding for HE 3 than AE 3 confirmed "smoother" copolymerization of methacrylates (EGDMA-HEMA) resulting in higher grafting. Dynamic protein binding values were higher than static mode due to different mass transfer conditions. Also, dynamic mode enables higher number of interaction points for BSA within the porous structure in contrast to static mode.

HE 1 and HE 2 showed very low protein binding (< 5 µg/cm^2) when exposed to 6.5 mg/cm^2 of BSA because of higher degree of grafting of polyHEMA chains in the presence of 2.5 wt.% EGDMA. The preliminary results obtained are proof of the concept for development of the polyHEMA membranes with very low protein binding. Further in-depth study can be performed to understand the influence of concentration, protein type, ionic strength and pH. But due to time constraints it was not considered in this work. The detailed molecular study about the interactions of proteins with surfaces are reported in literature[275,276].

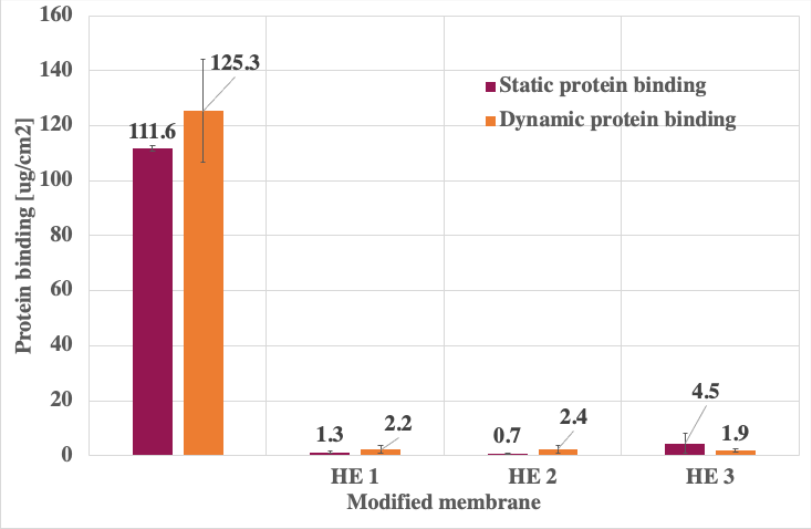

Figure 4.80. Dynamic and static protein binding with 5 mg/ml BSA for different POLYHEMA prototypes

The fouling of the membranes due to adsorption of BSA was analyzed by determining the drop in water permeance before and after protein binding along with monitoring of the permeance of PBS and BSA during dynamic protein binding experiments. Since, polyHEMA chains do not undergo conformational changes like polyacrylic acid, no difference between water, PBS & BSA permeance was observed. The permeance in Figure 4.80 plot (a) was expected as a result of mass gained leading to pore structure changes upon hydrogel grafting. HE 1 showed the lowest permeance because of EGDMA dominance in the porous structure of the base membrane with smaller pore size. HE 3 due to the open structure had the higher permeance than HE 2 which was expected to have the lowest permeance due to the highest mass gain upon grafting. Plot (b) in Figure 4.81 represents the drop in water permeance reflecting the extent of irreversible protein fouling due to adsorption and deposition of BSA. HE 3 showed the highest fouling because of formation of heterogenous polyHEMA chains, the modification homogeneity is not maintained in HE 3. Fouling in HE 1 is due to the weaker hydration layer formed because of EGDMA dominance and the drop is the least for HE 2, thanks to the strong hydration layer.

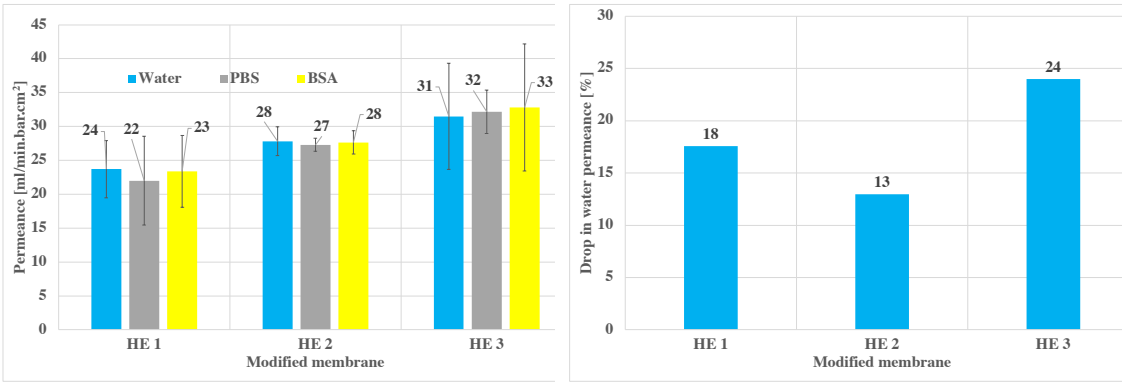

(a) (b)

Figure 4.81. Results from dynamic protein binding: (a) permeance of water, PBS and BSA and (b) drop in water permeance before and after the protein binding

4.5.4 Prototype formulation for the industrial trial

Polyacrylic acid and polyHEMA can be successfully grafted on to the PVDF membrane via two-step graft coating polymerization and show promising potential to be utilized as new membrane products for bioprocessing applications. Final membrane properties were influenced based on the chosen EGDMA-monomer ratio; the lower the ratio higher the influence on the surface chemistry. Insufficient EGDMA leads to inhomogeneous polymerization creating hydrogel lean spots vulnerable for protein binding. AE 2 showed

the best responsive behavior and highest particle recovery along with very low protein binding, therefore was selected for the industrial upscaling.

The ideal hydrogel structure with HEMA should form a strong hydration layer on the surface with polyHEMA chains that can additionally interact with the particles. Formation of a highly cross-linked dense hydrogel layer due to high amount of polymer content leads to an ineffective rigid coating instead of chains. Therefore, a formulation with lower net polymer content (EGDMA + HEMA) should be considered. Hence, after assessing the availability of chemicals formulation: 1.5 wt.% EGDMA and 6.5 wt.% HEMA was selected to perform industrial upscaling of the HEMA prototype.

4.6 Industrial upscaling

A relationship between modification formulation and membrane properties was established in section 4.5. And the effect of membrane properties on the performance was revealed by understanding the filtration mechanism and protein fouling. Based on the obtained results one formulation for each: polyacrylic acid and polyHEMA was chosen for the industrial upscaling. The chosen polyacrylic acid and polyHEMA formulation is mentioned in Table 4.8 and Table 4.9 respectively. For convenience the industrially modified polyacrylic acid and polyHEMA membranes were referred as prototype A and H respectively.

Table 4.8. Polyacrylic acid formulation selected for the industrial trial

Solution 1 [wt. %]			Solution 2 [wt. %]			
H_2O_2	EGDMA	IPA	AA	$FeCl_2.4H_2O$	Vit C	RO water
6	2.5	91.5	10	0.28	1	88.72

Table 4.9. PolyHEMA formulation selected for the industrial trial

Solution 1 [wt. %]			Solution 2 [wt. %]			
H_2O_2	EGDMA	IPA	HEMA	$FeCl_2.4H_2O$	Vit C	RO water
6	1.5	92.5	6.5	0.28	1	92.22

The industrial upscaling was carried out in the production facility of GVS on the industrial membrane post-treatment line. The analysis of the industrial prototypes is divided into

two parts. In the first part, prototype H is characterized for its flow properties, pore size, wettability, thermal stability and chemical compatibility not only to confirm the successful upscaling but also to make sure that it satisfies the industrial standards as a "new" hydrophilic product. This characterization data also formed a basis for defining the membrane specifications of the potential new hydrophilic product in the later stages. The second part of the study concerns comparison of prototype A and prototype H with a competitor membrane (reference) for their performance. Relevant membrane characteristics, particle retention, protein binding and cell culture filtration for all three membranes was carried out. The PVDF based competitor membrane is widely used for bioprocessing applications due to its very low protein binding.

4.6.1 Membrane characterization – industrial standards

Flow and pore size properties – defining the specifications

The earlier results showed that base membrane plays an integral role in defining the modified membrane properties and consequently membrane performance. Therefore, base membrane properties need to be predefined to obtain modified membrane with consistent desired properties and performance. Nevertheless, the results clearly suggested that industrial trial is successful in hydrophilizing the membrane. Furthermore, in the industry the design of experiments (DOE) trials is performed to understand the variation of properties under the set conditions. The trials are aimed at predicting the final membrane properties as a result of base membrane characteristics (input variables). These experiments were aimed to establish validity, reliability and reproducibility[295]. Once this is achieved the base membrane characteristics for obtaining the desired final membrane properties can be defined and the specifications for the obtained hydrophilic membrane can be set according to the customer requirements.

Thermal stability and sterilization

GVS proposes five years of shelf life for its hydrophilic membrane products. Although real time aging provides the best data, due to market conditions where products become obsolete in a short time new products need to get to the market soon. Real time aging does not meet this criterion therefore, accelerated aging test provides an alternative means. Accelerated aging test is performed at 90°C for 16 days in the absence of moisture to determine the effects, if any, on the integrity of the functionalized membranes due to

passage of time. The tests are performed at elevated temperatures to simulate real time aging in a reduced amount of time.

Meanwhile, the developed membranes shall be used in the filter devices such as syringe filter, amicon cell, and centrifugal filters for various bioprocessing applications. The devices used for such applications are sterilized in various ways such as autoclave, gamma rays, and ethylene oxide (Eto) to avoid contamination of the valuable product[296]. It is crucial for the membranes to maintain their integrity after sterilization. The industrially modified HEMA membrane was sterilized using autoclave to pose the toughest challenge to the modified layer compared to other sterilization methods. The membrane was exposed to high temperature (121ºC) steam under pressure (bar) inside an autoclave, which potentially can degrade weak coatings.

The effect of thermal stress without moisture in case of accelerated aging and with moisture (steam) in case of autoclave on the membrane was analyzed by monitoring the flow properties and the hydrophilicity of prototype H before and after thermal exposure. Figure 4.82 demonstrates the effect of thermal stress on the flow properties and membrane pore after accelerated aging (a) and autoclave (b). The results indicated that the modified surface layer in both the cases was not compromised and membranes maintain their integrity. The interpenetrating cross-linked network in the modified layer was a result of efficient copolymerization of EGDMA-HEMA. The highly cross-linked polymer network is covalently bonded to the PVDF membrane generating a strongly bound layer which is unaffected by high temperatures. It was assumed that the degradation of materials as a result of temperature involves chemical reactions which follow the Arrhenius reaction rate function. The function states that in a homogenous process a 10°C change in temperature results in two time or half time change in a chemical reaction rate (Q_{10})[297,298]. However, PVDF is known for having excellent thermal stability due to the presence of highly electronegative fluorine atoms and high bond dissociation energy of the C-F bonds. Additionally, the superior thermal stability is attributed to its crystalline phase and high flexibility due to the amorphous region[299]. PVDF can withstand a wide temperature range between – 40°C (T_g) to 160°C (T_m) and has demonstrated thermal decomposition above 316°C[300,301]. These eminent properties of the base membrane further enhance the thermal stability of the membrane. The differences observed before and after in both are possibly derived from the distinct measurement spots on the PVDF flat sheet membrane.

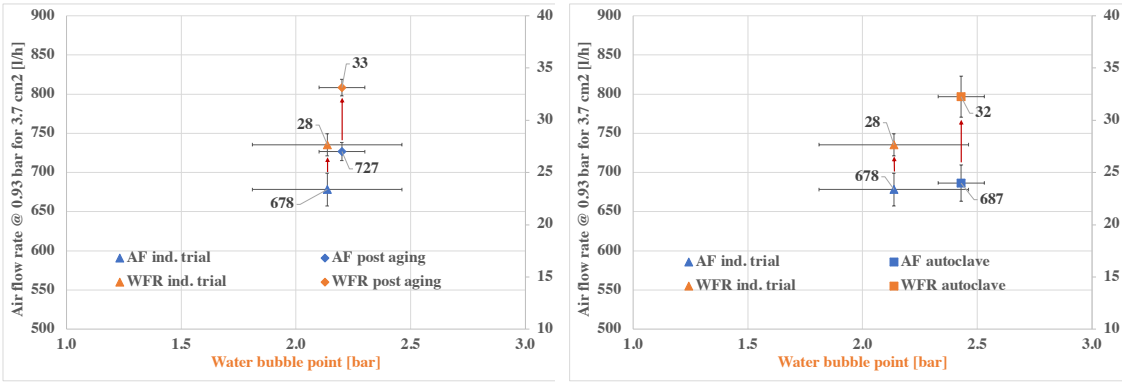

(a) (b)

Figure 4.82 Effect on the flow properties and pore size of prototype H after exposing to (a) thermal stress (90°C for 16 days), and (b) autoclave (120°C steam for 20 min.)

Figure 4.83 shows the effect on hydrophilicity of the membrane in terms of the contact angle and wetting time before and after the thermal stress. Interestingly, the wetting time and the initial contact angle increases after accelerated aging test whereas for the membrane after autoclave it does not change even though the temperature used is 121°C (higher than 90°C). Kinetics of the material deterioration is a complex phenomenon which depends on the temperature, humidity and the material properties[302]. The increased contact angle and wetting time was a due to deterioration of the modified layer upon extended exposure to high temperature. Although, covalent bonds need very high energy to break (>90°C) the extended exposure (16 days) generates vibrations between the bonds of the polymer network. Chemical reactions take place according to Arrhenius reaction rate function at elevated temperatures which can disrupt the modified layer resulting in shrinking. However, the hydrogel layer absorbs water in the presence of moisture in the environment which prevents shrinking of the network even at higher temperature (121°C).

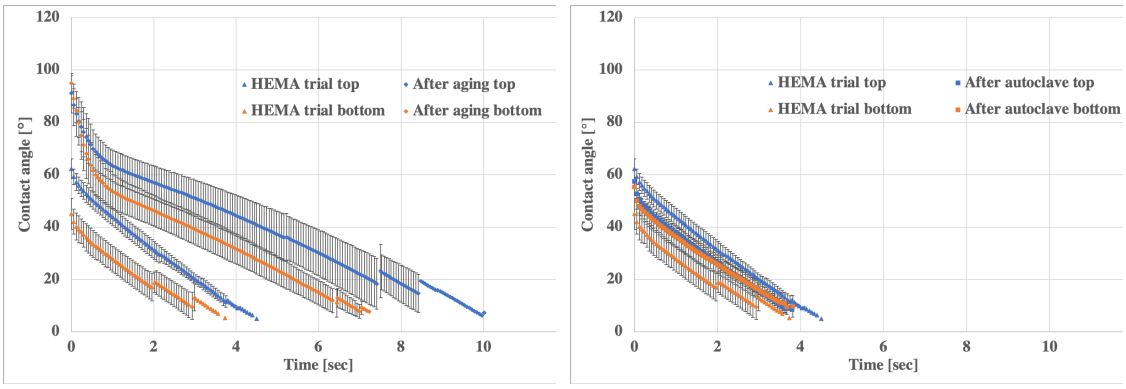

(a) (b)

Figure 4.83 Effect on the wettability (dynamic contact angle) of prototype H after exposing to (a) thermal stress (90°C for 16 days), and (b) autoclave (120°C steam for 20 min.),

Chemical compatibility

Assuring that the chemical solutions are compatible with the membrane helps in achieving consistent results and lengthen the life of the product. Assessing the chemical compatibility can be difficult as varying concentrations of the same solution can affect the membrane differently. Reaction between membrane and chemicals used leads to degradation of the membrane surface making membrane unusable. Therefore, developed membranes need to have good chemical resistance to be compatible for various processes used by the potential customers. The chemical compatibility tests were performed with 40 chemicals including acids, bases and organic solvents for prototype H to generate a chemical compatibility chart shown in Table 4.10. The chemical was qualified as recommended if the membrane properties: wettability, water bubble point, flow rate, and thickness did not change by more than 10 % before and after exposure to the chemical for 48h at room temperature. The objective of the chemical compatibility chart was to help identify end users about the resistance of the filter materials to the certain chemicals. Additionally, once the membrane is installed in the filtration device such as syringe filter the chemical compatibility with the material device needs to be verified again.

Table 4.10. Chemical compatibility chart for the industrial prototype H

Number	Chemicals	Recommended yes/no
Acids		
1	Acetic acid 5%	yes
2	Acetic acid 10%	yes
3	Galcial acetic acid	yes
4	Hydrocholric acid 6N	yes
5	Hydrocholric acid 1N	yes
6	Hydrocholric acid 0.1N	yes
7	Nitric Acid 6N	yes
8	Sulfuric acid 6N	yes
Alcohols		
9	Butanol	yes
10	Ethanol <=50%	yes
11	Ethanol pure	yes
12	Methanol	yes
13	IPA	yes
Bases		
14	NaOH 0.1N	yes
15	NaOH 1N	yes
16	NaOH 6N	Not recommended
17	KOH 3N	yes
18	Urea	yes
19	Ammonium hydroxide 3N	yes
20	Ammonium hydroxide 6N	yes
21	Triethylamine	yes
Esters		
22	Butyl acetate	yes
23	Ethyl acetate	yes
Solvents		
24	Acetone	yes
25	Cyclohexanone	yes
26	DMAC	Not recommended
27	DMSO	Not recommended
28	DMF	Not recommended
29	Hexane	yes
30	Tetrahydrofuran	yes
31	Ethylene glycol	yes
32	Toluene	yes
33	Chloroform	yes
34	Glycerol	yes
35	Gasoline	yes
36	Pentane	yes
Others		
37	Hydrogen peroxide 30%	yes
38	Hydrogen peroxide 3%	yes
39	SDS 5%	yes
40	Polyethylene glycol	yes

The membrane showed good compatibility with majority of the chemicals except for the PVDF solvents: DMAC, DMSO, and DMF which are known to dissolve PVDF[303]. The high chemical resistance of the grafted layer assured formation of a stable coating with strong covalent bonds between EGDMA-HEMA and PVDF substrate. Additionally, the highly chemical resistant base PVDF membrane enhances the chemical stability of the membrane against most of the chemicals[301]. However, the membrane changed its color to brown, reduced in thickness becoming brittle, and lost its properties upon 48 h contact with strong alkali solution (6 N NaOH). Although membrane properties were retained in case of 3 N KOH the membrane discoloration still occurred. Studies have reported degradation of PVDF on exposure to strong alkaline solution[304]. Early investigations observed the discoloration of white PVDF membrane to brown and ultimately back when immersed in alkaline solutions for hours[305]. Shinohara[306] explained the change in color as a result of formation of C=C bonds upon dehydrofluorination in PVDF chain. Hoa and Ouellette[307] further demonstrated that NaOH solution attacked PVDF in $\propto$ conformation. Later several studies confirmed the elimination of HF and formation of the carbon-carbon double bonds resulting in change in color and brittleness[308]. This explains the effect of

6N NaOH on the membrane observed during the compatibility tests. Moreover, many factors that can affect the chemical resistance such as temperature, exposure time, chemical concentration, pressure should also be considered.

4.6.2 Comparison study

In this section the membrane properties and the performance of the industrial prototypes A and H is compared with the competitor membrane (reference).

4.6.2.1 Membrane properties

Although the base material of the GVS prototypes and the reference membrane was PVDF the morphology, surface chemistry and physio-chemical properties were different. The difference in the membrane characteristics were demonstrated by performing porometry, zeta potential measurements and analyzing the morphology by SEM. Subsequently, the filtration performance and protein binding ability were evaluated and compared. These preliminary results compared the properties and performance of the developed prototypes to a widely accepted product for bioprocessing applications.

Porometry

The pores of the membranes were characterized using capillary flow porometry. Figure 4.84 exhibits the pore size distribution for the prototypes and the reference membrane and Table 4.11 shows the additional information derived from the porometry measurement. The nominal pore size of the reference membrane was 0.22 µm, while the GVS prototypes were developed from the base membrane with nominal pore size 0.45 µm. The bigger pore size enabled efficient grafting and swelling of the hydrogel throughout the porous structure. Moreover, the deposition of polymer inside the pores would eventually reduce the effect pore size. The large ratio between membrane pores and particles (200 nm) used for filtration allow electrostatic and steric repulsions to be effective for particle retention[309] and potentially can retain even smaller particles. Tarzaskus et al.[256] reported retention of silica nanoparticles based on the electrostatic repulsions. The pore size distribution data showed that the porous structure of the reference membrane was narrower than the GVS prototypes as suggested by the nominal pore size values. Although it should be noted that the polyacrylic acid and polyHEMA chains have the ability to swell which is underestimated in the porometry measurement.

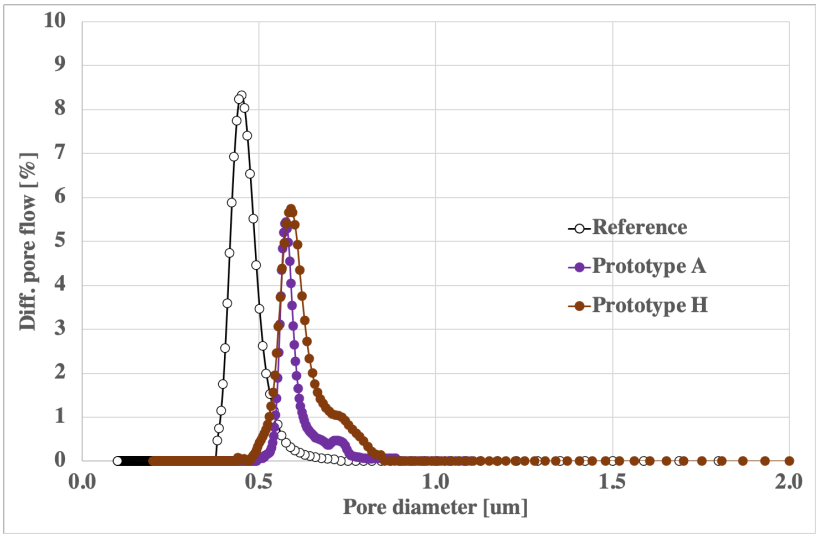

Figure 4.84. Pore size distribution comparison between the reference membrane and GVS porotypes

The variation and the mean of the pore size from Table 4.11 confirmed that the reference membrane had smaller pores compared to GVS prototypes; no significant difference between GVS prototypes was observed. The porosity values were comparable, whereas the thickness of the prototypes was 72 µm higher than the reference membrane because of the polyester support used for PVDF membrane synthesis. Therefore, the difference in the pore size distribution and thickness could be the determining factors for the particle retention performance of the membranes.

Table 4.11. Membrane characteristics comparison between the reference and GVS prototypes

Characteristic	Reference	Prototype A	Prototype H
Max. pore size [µm]	0.73	0.89	0.86
Mean pore size [µm]	0.45	0.58	0.60
Min. pore size [µm]	0.38	0.50	0.44
Porosity [%]	53.45	51.65	50.46
Thickness [µm]	113	185	185

SEM

The top and bottom surface morphologies of the three membranes were characterized using SEM and the micrographs are shown in Figure 4.85. The images revealed that all three membranes had a highly asymmetrical structure. The reference membrane had a

homogenous pore size distribution on the surface with small openings. The prototypes had far from cylindrically shaped pores with broadly distributed diameter impossible to define. As a consequence, particles can easily enter the pores. The heterogenous distribution of the grafted polymer can be spotted on the prototype surface.

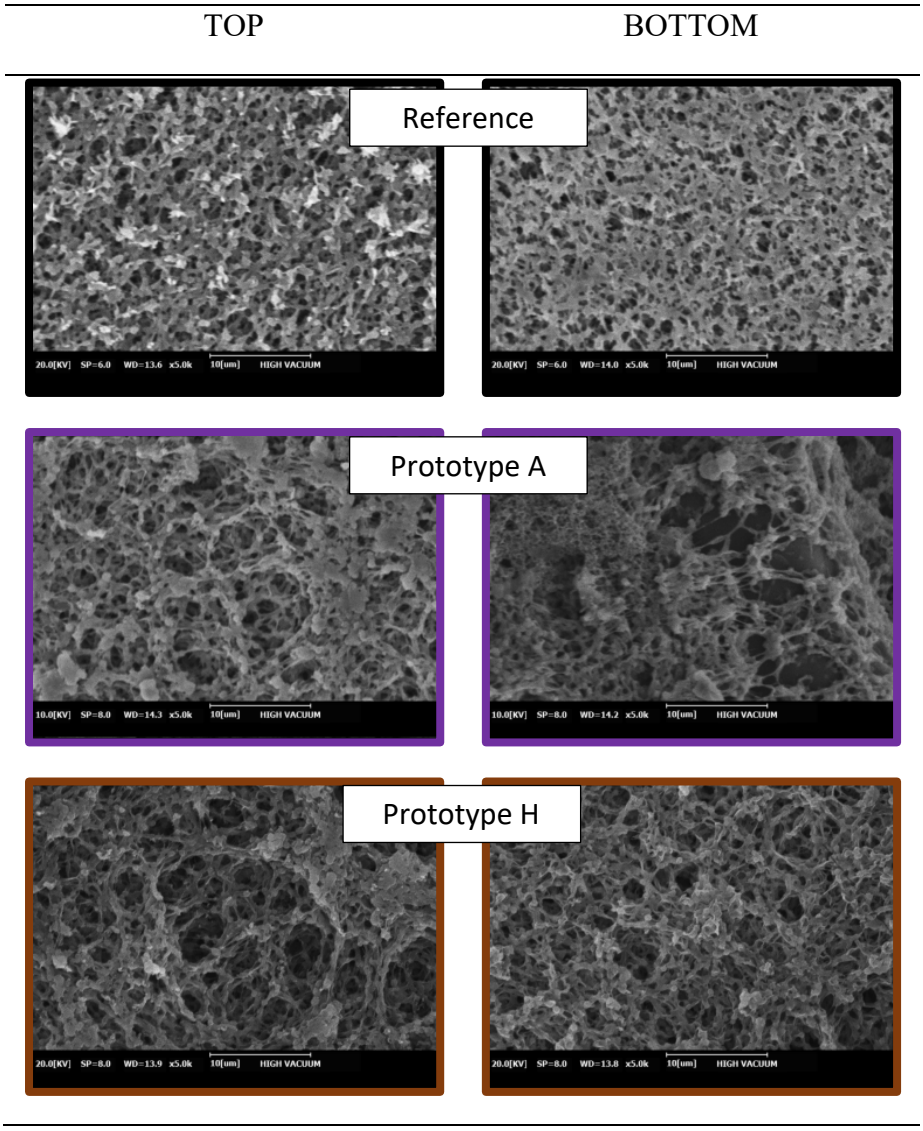

Figure 4.85. SEM micrographs of the top and bottom surface of the reference membrane and GVS prototypes

Zeta potential

The surface charge of the membranes as a function of pH evaluated by zeta potential measurements is shown in Figure 4.86. It is well known that the membranes used for bioprocessing applications usually have a negative surface charge to avoid the adsorption of negatively charged biological particles on the surface[110]. Prototype A and the reference membrane do not have an isoelectric point and share a similar trend of zeta potential hinting similar surface chemistry. However, polyHEMA had an IEP around pH 3 and the

zeta potential sharply decreased with increase in pH. All three membranes had a negative zeta potential in the most of the pH range. This should result in electrostatic repulsion of the negatively charged particles avoiding them from entering the membrane.

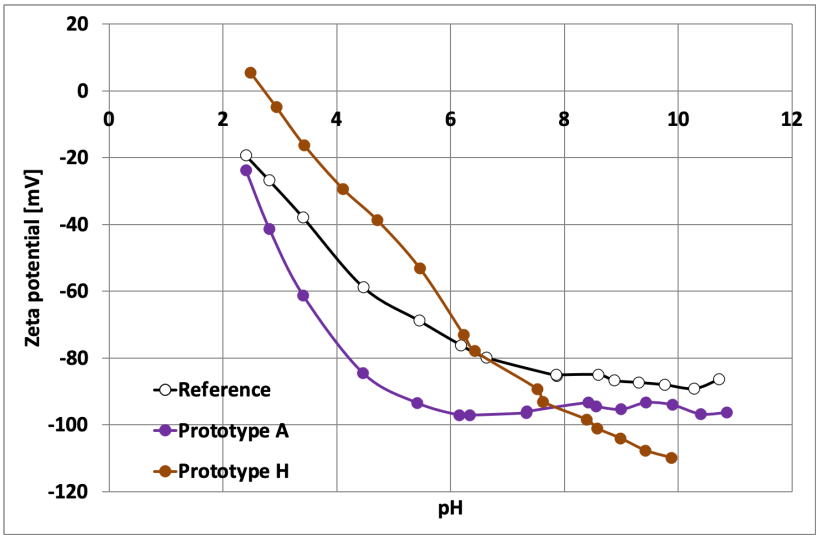

Figure 4.86. Zeta potential measurement comparison between the competitor membrane and industrially modified acrylic acid and HEMA membrane

The prototype membranes had a different morphology and pore size distribution compared to the reference membranes. The reference membrane had a closed sponge like structure with negative surface charge while the prototype membranes had an open sponge like structure with negative surface charge. The base PVDF material used for modification is open and supported which results in thick and open final membrane. The base material governs the porous structure which undergoes changes depending on the degree of cross-linker, while the surface chemistry is dictated by the functional groups. The hydrogel layer and chains grafted on the surface of the prototypes are activated in the aqueous medium which play a crucial role in membrane filtration as understood in section 4.5.

4.6.2.2 Membrane performance

In this section the filtration performance and protein binding ability of the reference membrane is evaluated and compared with the industrially developed prototypes. Often times in the bioprocessing applications the feed solution contains multiple components which foul the membrane and compromise the surface chemistry reducing the capacity and the life of the filter. Therefore, throughput volume capacity of the membranes was examined by filtering cell culture media through the membrane to estimate the membrane behavior in the actual application with biofluids.

Filtration study

The water permeance for the membranes in Figure 4.87 (a) shows that even though the prototypes had bigger pores the difference in permeance compared to the reference membrane is not significant due to swelling of the grafted hydrogel. Moreover, prototype A has less permeance than the reference membrane due to the narrowing of the pores with decarboxylation of -COOH which results in swelling of the polyacrylic acid chains at pH 7. Interestingly, prototype membranes with bigger pore size displayed higher particle retention than the reference membrane with smaller pores in Figure 4.87 (c). The functional groups on the surface of the prototypes are activated in the aqueous medium. The carboxyl group and pendant hydroxyl group in prototype A and H respectively, interact with water by forming hydrogen bonds. This resulted in formation of a strong hydration layer at the surface. Moreover, reduced EGDMA concentration (from 2.5 wt.% to 1.5 wt.%) in case of prototype H decreased the degree of cross-linking and increased the swelling of the polyHEMA segments on the surface forming a strong hydration layer. The polyacrylic acid forms long chains which further extend at pH 7 due to decarboxylation. As a result, the steric and electrostatic repulsions[255] reduce the particle interaction with the membrane surface[256]. However, due to the open pore structure during the initial stages of filtration particles were adsorbed and deposited in the membrane displaying low retention. But as filtration progressed particles aggregated at the interface increasing filtration resistance (d) and eventually forming a cake-layer that prevented particle penetration into the membrane. Since, particle fouling does not lead to complete blocking of the pores but rather eventual build-up of the particles the permeance during filtration decreased linearly and until the cake layer was formed.

On the contrary, the reference membrane showed very low retention and low filtration resistance. The apparent initial high retention for the first permeate is due to the residual water in the system. The results suggested that there was no particle-membrane interaction which allowed particle aggregation or clustering at the surface. Also, membrane showed low adsorption capacity towards the particles. Therefore, majority of the particles passed through the membrane without strong resistance. But in the last stages of filtration particle build-up can be observed due to pore blocking rather than membrane-particle interaction. The higher filtration permeance is the result of continuous passage of particles through the membrane.

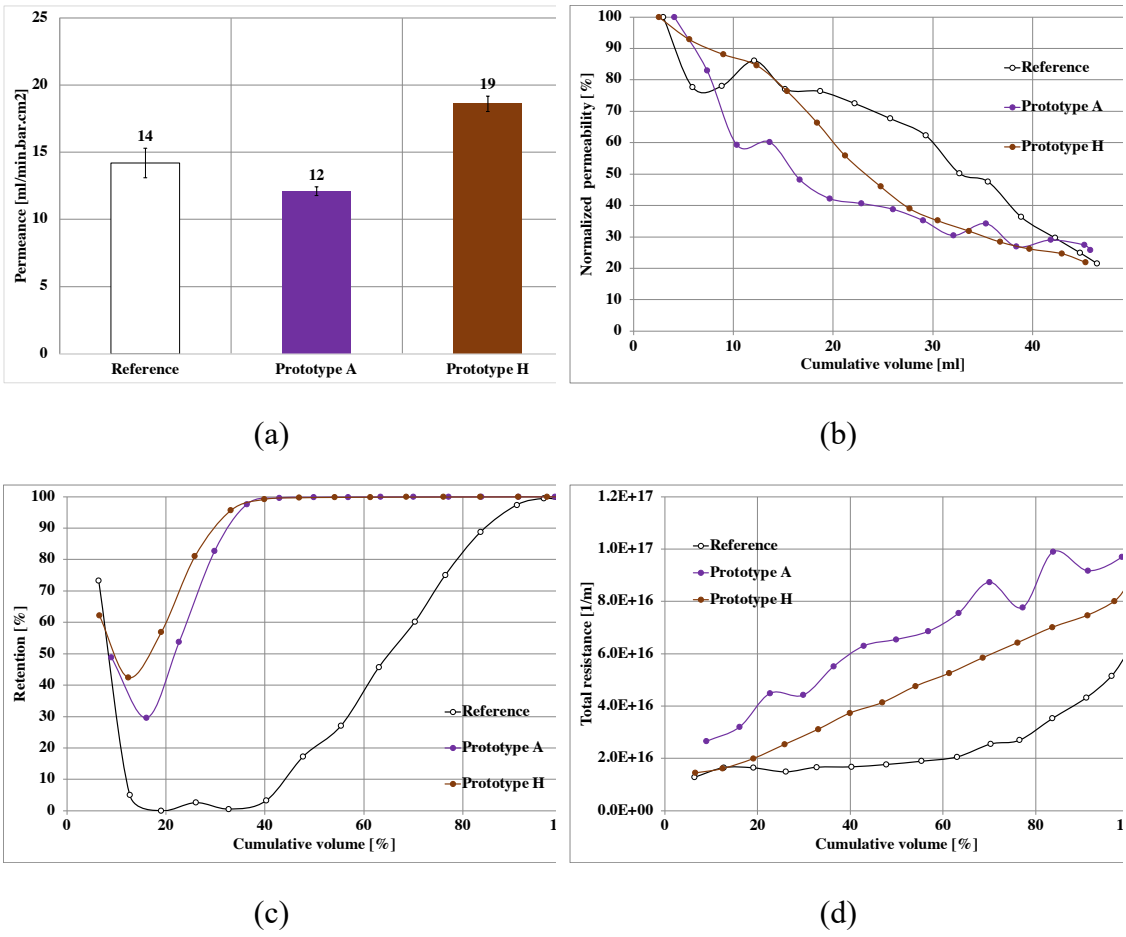

Figure 4.87. Plots from the filtration study of prototype A, prototype H and the competitor' membrane (reference) at 0.5 bar: (a) water permeance, (b) normalized filtration resistance, (c) particle retention, and (d) total filtration resistance

For bioprocessing application, it is crucial to avoid loss of valuable particles either by adhesion or by penetration which is the major problem with the current membranes specially for the concentration and purification resulting in low recovery[56,60,310]. Figure 4.88 shows (a) the drop in water permeance due to particle fouling and (b) particle recovery from the retentate and membrane surface after filtration. The flux drop was the lowest for the reference membrane as majority of the particles passed through the membrane. The higher values for prototypes were due to the irreversible fouling caused by deposition and adsorption of particles during the initial stages of the filtration. The particle recovery was the result of interaction between membrane and particles. Highest recovery for prototype A is due to the strong electrostatic repulsions while for prototype H steric repulsions played a role. The particles recovery from the retentate side was the lowest for the reference membrane however less particles were potentially trapped in the membrane as most of the particles penetrated in the permeate side due to lack of membrane-particle interactions.

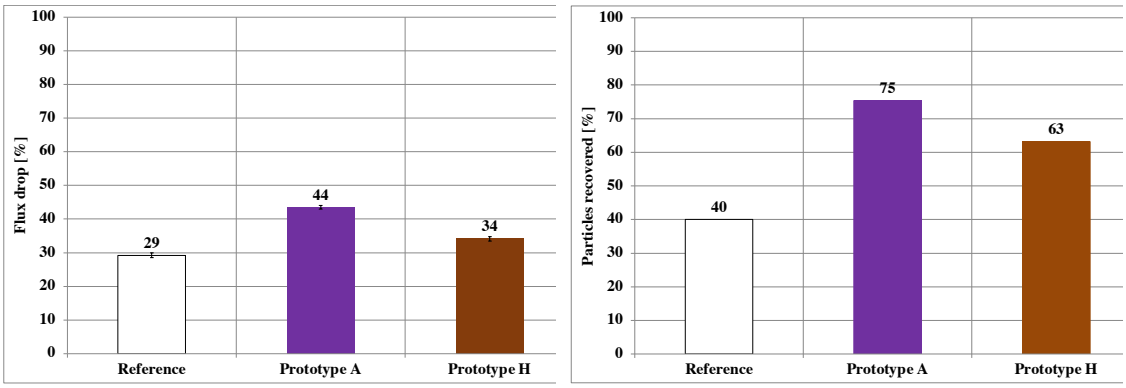

(a) (b)

Figure 4.88. (a) Drop in water permeance as a result of fouling and (b) Recovered particles from the retentate and washing step from the membrane surface

SEM post filtration

The SEM micrographs in Figure 4.89 of the membrane's top surface and cross-section after filtration were analyzed to monitor the particle blocking. The particle concentration on the top surface of the reference membrane was relatively less than the prototypes. The slow build-up of the particles on the surface due to particle penetration explains the low concentration. The cross-section images confirmed the asymmetric structure of the membranes with high tortuosity. A layer of particles on the top of the membrane surface and irreversible fouling in the top part of the cross-section for prototypes was observed. Adsorption and deposition of the particles in the initial stages of filtration leads to irreversible fouling of the open surface structure. As the filtration progresses the aggregated particles were compacted at the membrane interface, resulting is destabilization and adsorption on the surface. However, due to penetration of the majority of the particles, not enough were left to form a cake-layer at the top surface of the membrane.

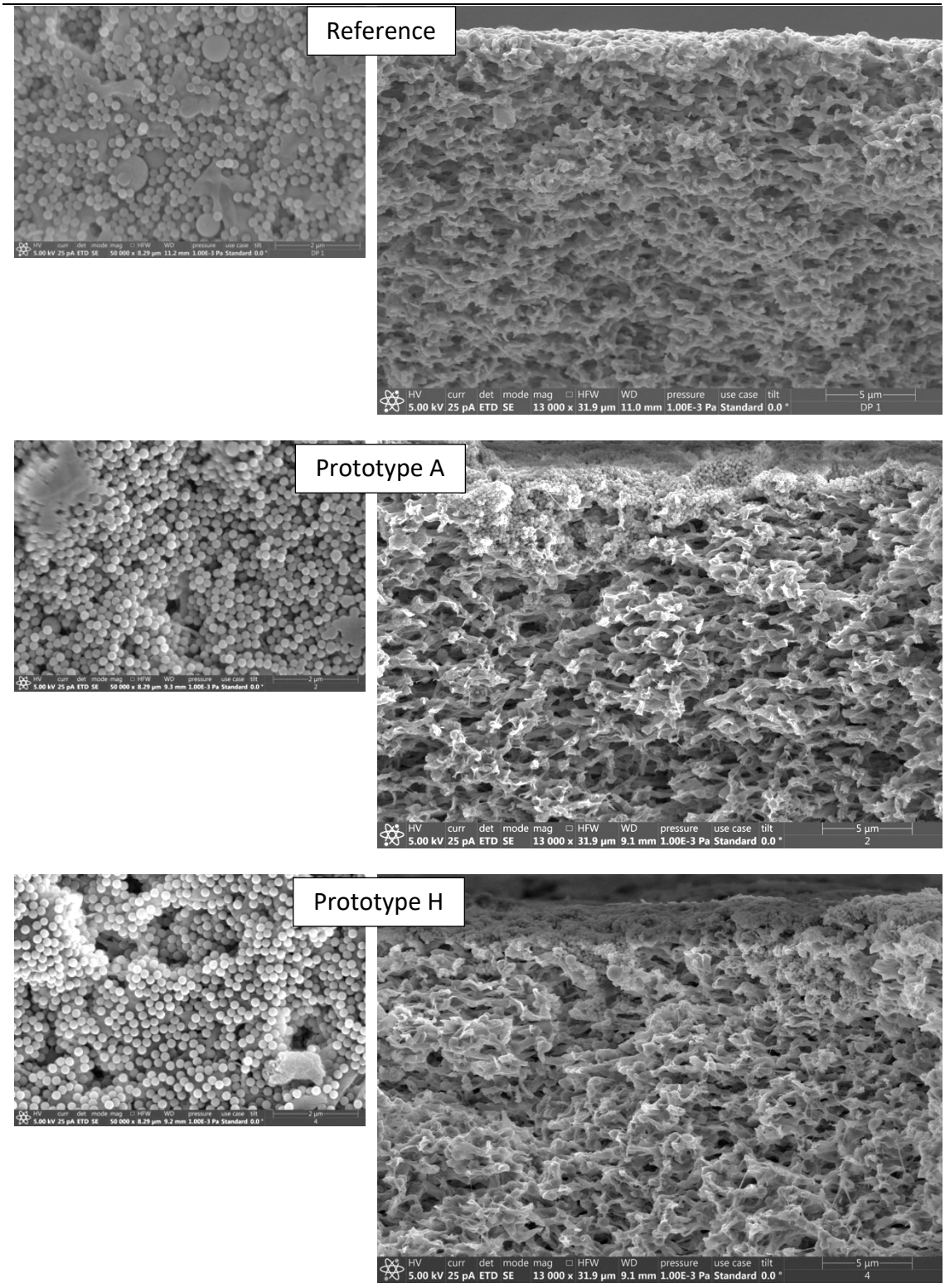

Figure 4.89. SEM micrographs of the top surface and cross-section after filtration for prototype H, prototype A and the competitor's membrane (reference)

Based on the results it was possible to predict the anti-fouling mechanism for each of the membranes. Figure 4.90 shows the proposed retention mechanism (a) reference membrane, (b) prototype A and (c) prototype H.

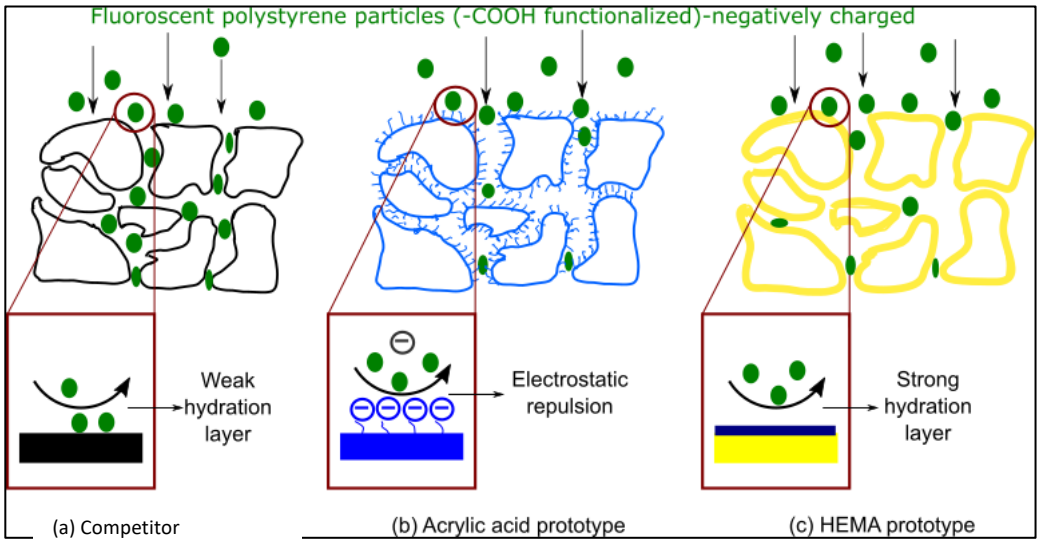

Figure 4.90. Schematic interpretation of blocking mechanism during particle filtration for (a) competitor membrane, (b) prototype A & (c) prototype H

Protein binding

Protein binding ability of the prototypes was compared to the reference membrane and the base PVDF membrane. The study was carried out in static and dynamic mode and the results are displayed in Figure 4.91. It is well known that hydrophobic surfaces destabilize proteins resulting in higher protein binding[311]. The entropic gain due to dehydration at the hydrophobic interface drives protein adhesion. Hydrophobic dehydration is a result of the interactions between the protein's internal hydrophobic regions and the hydrophobic surface[312]. This explains very high BSA binding for PVDF base membrane. The obvious higher binding in dynamic mode is due to the adsorption and deposition of BSA inside the porous structure upon pushing BSA solution through the membrane maximizing the interaction points. The drastic drop in protein binding from the upon modification validates the successful grafting of the hydrogel layer on the membrane surface. The dual effect of steric and electrostatic repulsions for the prototypes as a result of efficient grafting of polyacrylic acid chains and polyHEMA segments reduced the protein adsorption. Prototypes showed a very low protein binding similar to the reference membrane claimed as the benchmark for its low protein binding ability by the manufacturer. These preliminary promising results showed the potential of the prototypes to be further fine-tuned and used for bioprocessing applications.

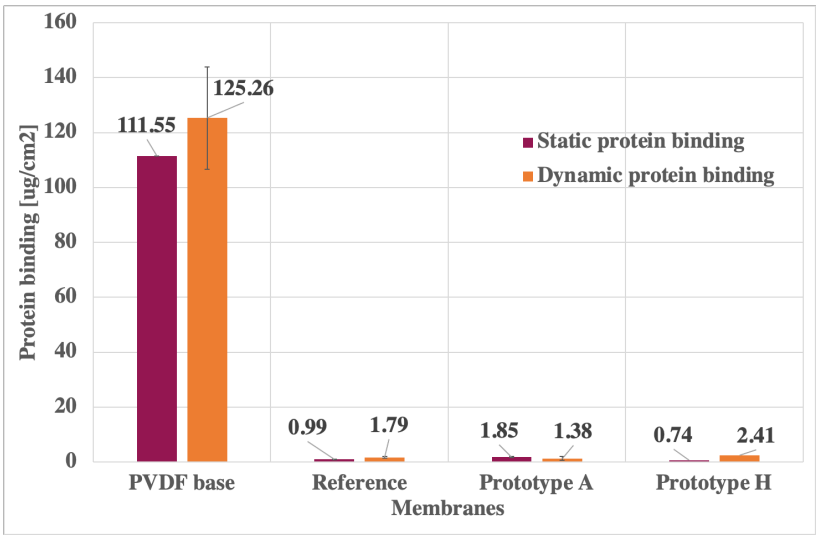

Figure 4.91. Dynamic and static protein binding with 5 mg/ml BSA for the competitor membrane and developed prototypes with reference to the base membrane (unmodified)

Figure 4.92 (a) shows water, PBS and BSA permeances which reflect the pore structure of the each membrane. The lowest water permeance for prototype A was due to narrowing of the pores as a result of polyacrylic acid chain extension due to decarboxylation. However, due to the shielding of the salts at effect at high ionic strength in PBS and BSA solution the swelling of the chains was diminished. Figure 4.92 (b) demonstrated the drop in water permeance due to irreversible protein binding. The low values (< 15%) suggested that membranes have a good regeneration capability upon washing the reversibly bound protein from the surface.

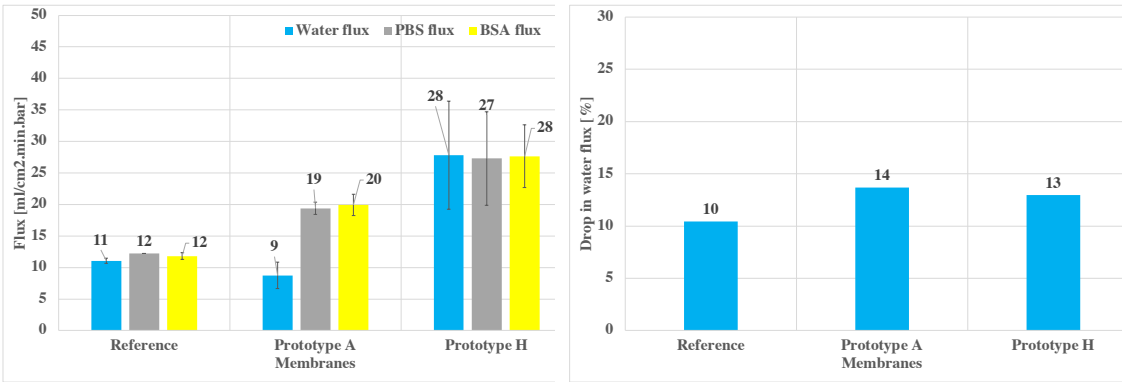

(a) (b)

Figure 4.92. Results from dynamic protein binding: (a) permeance of water, PBS and BSA and (b) drop in water permeance before and after the protein binding

Two-step graft coating polymerization method was successfully scaled-up to obtain polyacrylic acid and polyHEMA prototypes. The prototype H showed promising results for the industrial characterization of the membrane to be implemented in the devices.

Besides showing superior retention than the reference membrane due to the active surface layer formed upon functionalization, prototypes presented very low protein binding. Therefore, prototypes can be considered as serious candidates for the bioprocessing applications upon further fine-tuning to obtain the desired results.

4.7 Effect of pore size on functionalization

From the experience in section 4.6, it was obvious that the base membrane played an integral role in defining the properties of the modified membrane and consequently affecting the performance. For the bioprocessing applications the size requirements for the microfiltration membranes vary from 0.2 µm to 1.2 µm. In this section, the functionalization is extrapolated from 0.45 µm to other available pore sizes of the PVDF base membrane to study the effect of pore size on the polymerization mechanism.

The base membranes were characterized for their thickness, pore structure and morphology. Since proteins bind to non-polar regions of the membranes as a result of hydrophobic interactions, protein binding was determined for the functionalized membranes to evaluate the efficiency of polymerization. Furthermore, efficiency of polyacrylic acid grafting inside the porous structure for each pore size was analyzed by mapping copper bound to carboxyl groups using sophisticated SEM-EDX technique. The base PVDF membrane and HEMA membranes were used as a reference.

4.7.1 Base membrane characterization

PVDF base membranes produced by GVS with pore sizes: 0.1 µm, 0.2 µm, 0.45 µm, 0.8 µm, and 1.2 µm were considered for the study. Thickness and the porous structure directly affect the polymerization mechanism during membrane functionalization. To manifest efficient polymerization the diffusion of reagents across the interface and throughout the porous structure should be effective. The diffusion path length depends on the thickness and the influence of polymerization induced diffusion barrier depends on the membrane morphology. With increasing pore size and surface porosity the impact of the barrier is reduced as pore size directly affects the mass transfer conditions. The membrane thickness increased with increasing pore size as seen from Figure 4.93 (a) with an exception for 0.2 µm. The mean pore size significantly varies between the membranes as revealed by the pore size distribution measurement in Figure 4.93 (b). The ease of diffusion of small molecules (much smaller than the pore sizes) does not solely depend

on the pore size but is also affected by the tortuosity, thickness, porosity, and pore geometry.

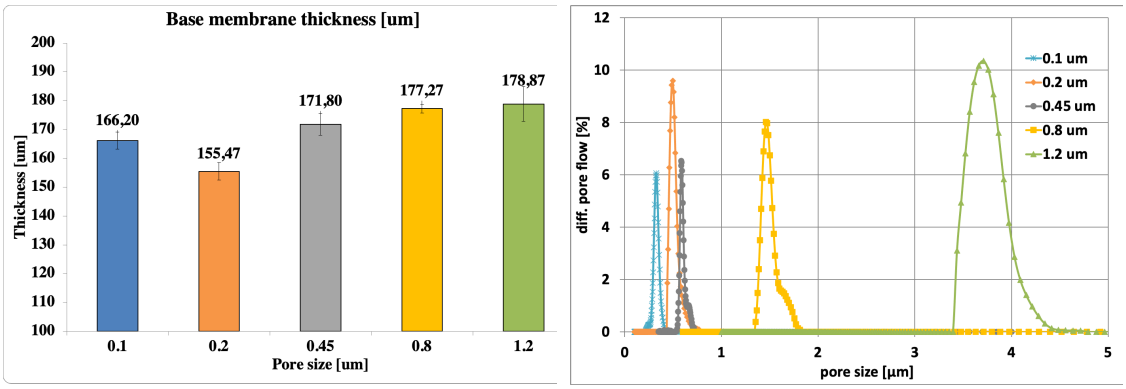

(a) (b)

Figure 4.93. Base membrane characteristics of different pore sizes: (a) Membrane thickness and (b) pore size distribution

The surface porosity was inspected by obtaining the SEM micrographs of the top surface of the membranes and the SEM images are displayed in Figure 4.94. 0.1 µm showed a thin polymer layer on the top surface with small pores and low surface porosity. As the pore size increased, the membrane structure became open and the surface porosity increased.

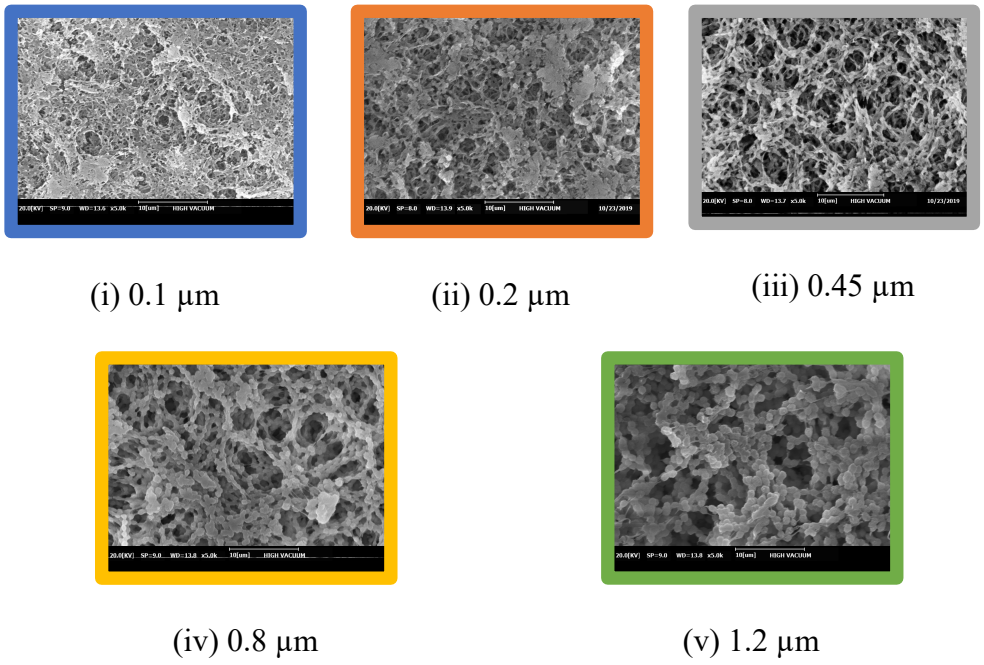

(i) 0.1 µm (ii) 0.2 µm (iii) 0.45 µm

(iv) 0.8 µm (v) 1.2 µm

Figure 4.94. SEM micrographs of the top surface of the base membranes of different pore sizes

4.7.2 Static protein binding: all the pore sizes

The plots (a) and (b) in Figure 4.95 show the static protein binding results for polyacrylic acid and polyHEMA respectively for different pore sizes. The protein binding decreased with increasing pore size for both polyHEMA and polyacrylic acid modifications. The protein binding is directly proportional to the hydrophobic nature and inversely proportional to the specific surface area. Hydrogel lean regions are hydrophobic in nature which were generated due to inefficient polymerization inside the porous structure where BSA can bind through hydrophobic interactions. Therefore, the results suggested that efficiency of polymerization decreases with decreasing pore size. Furthermore, the specific surface area decreases with increasing pore size, lowering the interaction points for BSA hence decreasing protein binding.

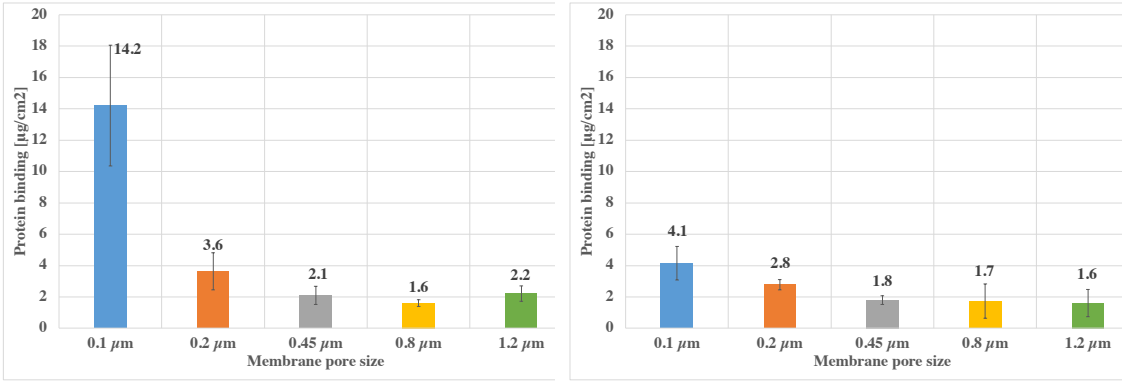

(a) (b)

Figure 4.95. Effect of pore size on protein binding. Static protein binding results for the functionalized membranes of different pore sizes: (a) Acrylic acid functionalized & (b) HEMA functionalized

The efficiency of grafting inside the porous structure depends on the influence of barrier formed in the reaction zone. The polymerization induced barrier hinders the diffusion of reagents across the membrane-bulk interface. However, the rate of formation of the barrier and subsequently its impact on diffusion depends on the surface porosity (pore size). As the surface porosity increases with pore size, the barrier formation is delayed and reagents can easily diffuse into the pore structure resulting in efficient polymerization throughout the porous structure. The predicted hydrogel layer formation for various pore sizes as a consequence of barrier formation is represented in Figure 4.96.

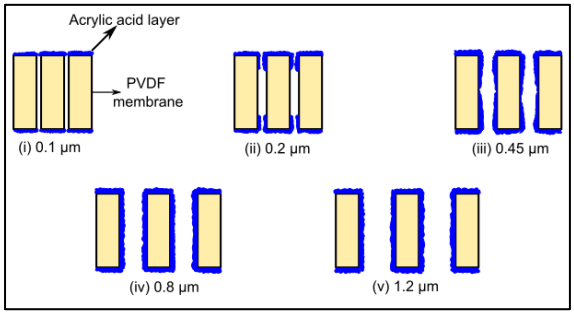

Figure 4.96. Schematic interpretation of effect of pore size on polymerization and consequently on the formation of the hydrogel layer assuming ideal cylindrical pores

4.7.3 SEM-EDX results

The analysis of the cross-section of polyacrylic acid modified membranes of various pore sizes was performed using SEM-EDX technique to monitor the polymerization inside the porous structure. The copper bound to the polyacrylic acid groups was mapped to determine the polyacrylic acid graft density inside the pores. PolyHEMA modified and base PVDF membranes of 0.45 µm were also analyzed as a reference due to their inability to bind copper. SEM-EDX has been used in numerous studies to investigate membrane fouling and surface characterization. Soffer et al. utilized SEM-EDX to identify iron concentration on the fouled membrane[313]. Hamid and coworkers evaluated copper (II) adsorption on polysulfone/zeolite blend sheet membranes[314]. SEM-EDX results: cross-section micrographs and copper mapping are presented in Figure 4.96; the yellow color corresponds to the concentration of copper. The copper ions are directly proportional to the polyacrylic acid concentration. It was evident that with increasing pore size the polyacrylic acid concentration increased inside the cross-section. A gradient of polymerization is formed along the cross-section. For 0.1 µm the gradient is high as a result of inefficient polyacrylic acid grafting inside the small pores. Whereas, 0.8 µm shows no gradient due to high grafting density inside the big pores. The polyHEMA and base PVDF membranes show low concentration of bound copper ions due to absence of the carboxylic groups. The adsorption of Cu is also dependent on the mass of polyacrylic acid coating. The specific surface area decreases at very high pore size, which negatively affects the amount of hydrogel grafted. Therefore, the gradient intensity of Cu was less for 1.2 µm because of low specific area which led to slightly higher protein binding.

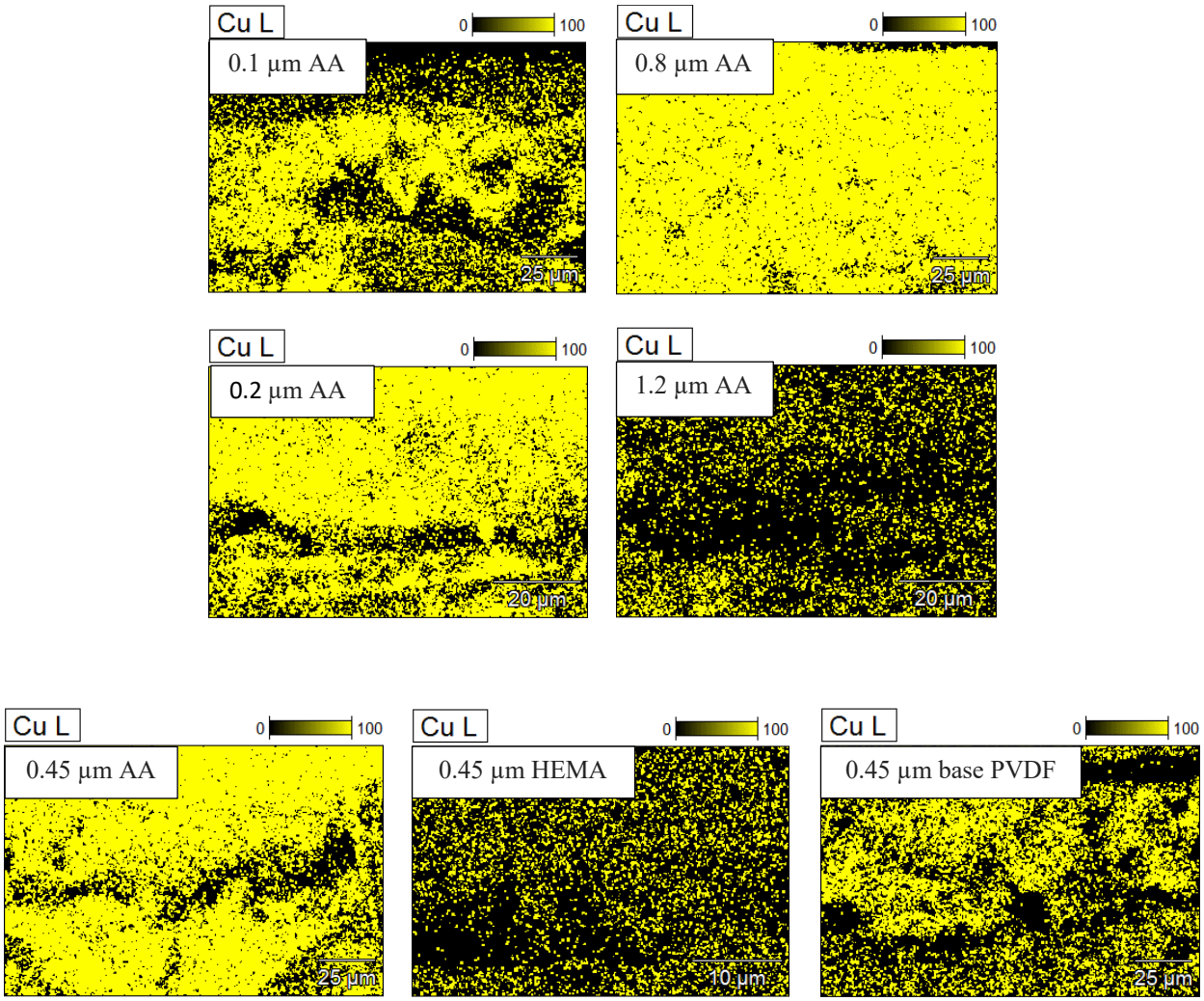

Figure 4.97. SEM micrograph of the cross-section of the acrylic acid functionalized membrane along with the mapping of bound copper (yellow) onto the membrane using SEM-EDX. HEMA functionalized and base PVDF membranes are used as a reference

Based on the findings for the effect of pore size on polymerization the relationship between polymerization efficiency and pore structure was established and is shown in Figure 4.98.

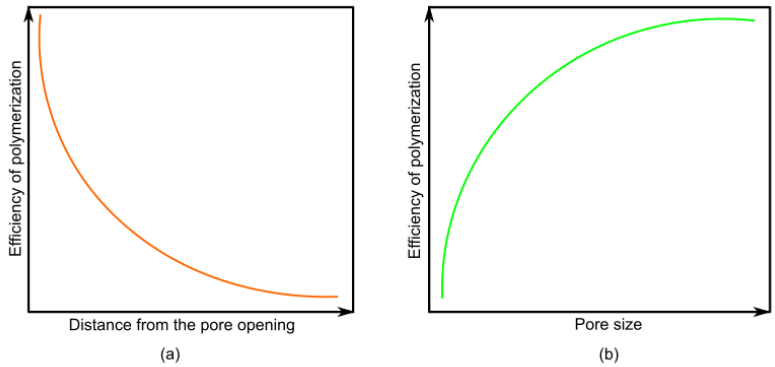

Figure 4.98. (a) Efficiency of polymerization decreases as the distance from the pore opening increases into the pore, and (b) Efficiency of polymerization increases with increasing pore size

The efficiency of polymerization depends on monomer concentration, pore geometry (especially the curvature of the pore) and the active membrane surface area for grafting. These results indicate that extrapolation of the modification methodology can be successfully carried out specially for the bigger pore sizes. It also suggests that the methodology is better suited for open membranes which delay the barrier formation allowing efficient diffusion thereby efficient polymerization.

5 CONCLUSION

The development of two types of hydrophilic membranes with varying surface properties exhibiting superior particle retention and improved anti-fouling performance was fruitfully accomplished in this work. The commercial MF flat sheet PVDF membranes were functionalized at the industrial scale via novel two-step graft coating polymerization. This work is a successful attempt to produce hydrophilic MF membranes employing tailor-made surface properties at an industrial scale in a roll-to-roll process to obtain membranes for bioprocessing applications. Numerous findings revealed during the progression of the work are presented in this section.

The surface functionalization methodology developed in this work is not only versatile but also robust, fast, requires no external energy (cheap), and is scalable. The two-step surface graft coating involves redox initiated (Fenton's reagent) radical polymerization. In the first step, the initiator along with a cross-linker are absorbed into the base membrane and the activator along with a polymer are introduced in the second step. Variety of chemical substances with abstractable hydrogen and desired cross-linker/polymer pair could be utilized for obtaining custom-adapted surface properties by varying their concentration ratio. As the proof of the concept, two functionalized membranes were obtained with a monomer (acrylic acid) and a polymer (PVP) using EGDMA as a cross-linker. The modified membranes were characterized for surface properties (ATR-FTIR, zeta potential, contact angle, etc.) demonstrating the success of this approach.

It was also revealed that base membrane characteristics directly affect the final membrane properties. Therefore, it is recommended to establish a standard protocol for selecting appropriate base membranes for the desired pore size of the final hydrophilic membrane.

In another scheme, multiple modifications were carried out with acrylic acid and PVP using EGDMA as the cross-linker at varying concentrations to understand the polymerization mechanism. The mechanism study demonstrated that efficiency of polymerization depends on the reactivity, local concentration ratio, and copolymerization efficiency in the reaction zone. Vinyl monomers (such as acrylic acid) were found to be more effective to attain hydrophilic membrane with efficient surface grafting on the surface and into the pores than long chain polymers (such as PVP) due to better mass

transfer because of smaller size and better copolymerization efficiency because of the presence of a π-bonds.

Moreover, EGDMA was confirmed to dominate the polymer network during polymerization due to its higher local concentration and higher reactivity. In the presence of less reactive PVP, homopolymerization of EGDMA led to phase separation resulting in polymer spheres. TrGDMA was analyzed as an alternative cross-linker to EGDMA to minimize the dominance of the cross-linker in the polymer network. TrGDMA was verified to be a better choice than EGDMA due to its higher water solubility, longer flexible chain and lower reactivity. However, due to time constraints emphasis was given on EGDMA in this work as the primary interest for GVS. The future work is planned to implement TrGDMA in the functionalization at industrial scale.

With EGDMA as the cross-linker acrylic acid and HEMA – vinyl monomers – were chosen to develop two prototypes with hydrophilic anti-fouling surface properties in addition to pH responsive behavior for polyacrylic acid. The prototypes were narrowed down from the multiple modifications prepared for each monomer with varying EGDMA/monomer concentration ratios; which were further characterized for their surface properties, particle retention and protein fouling performance. Cross-linker influenced the structural changes and monomer affected the surface chemistry of the modified membrane. Polyacrylic acid formed pH responsive dangling chains at higher acrylic acid concentration that repelled the particles via electrostatic repulsion hence minimized the fouling. The effect of cross-linker was reduced at higher acrylic acid concentration. Due to the structural similarity HEMA and EGDMA resulted in a smooth copolymerization forming a highly cross-linked polymer network. A hydration layer dominated with polyHEMA at the membrane surface and reduces the particle adhesion on to the membrane. The effectiveness of the hydration layer can be increased by reducing the degree of cross-linking.

The successful upscaling of the functionalization was carried out for both the prototypes at the industrial scale in a roll-to-roll process. Prototypes qualified the internal industrial preliminary requirements for permeability, chemical compatibility, thermal stability, and hydrophilicity to be accepted as the new hydrophilic products. The prototypes performed better at particle retention than the competitor membrane with smaller pores due to the grafted chains and the hydration layer on the surface. They also showed very low protein

binding ability comparable to the competitor with lower surface area. The results demonstrate great potential for the prototypes to be developed for bioprocessing applications upon further investigations.

The modification was extended to other membrane pore sizes to establish the relationship between pore size and efficiency of polymerization. Gradient of polymerization was observed in the cross-section of the membrane. The gradient of polymerization was inversely proportional to the membrane pore size. The efficiency of polymerization increased with increasing base membrane pore size. This could help GVS to fine-tune modification parameters based on the base membrane pore size.

Membrane characterization establishes a relationship between the effect of cross-linker/monomer ratio and final membrane properties; which further allows to understand the role of cross-linker and monomer in imparting membrane properties. Membrane performance characterization further establishes a relationship between membrane properties and membrane performance. The filtration protocol and protein binding act as bridge to help predict the membrane performance for a certain desired application. With this information the manufacturer could directly obtain the desired product based on two-step graft coating polymerization by fine-tuning the process parameters/formulation.

6 OUTLOOK

Commercial MF membranes have been successfully functionalized via developed methodology at an industrial scale to obtain desired surface properties to minimize fouling and enhance the separation performance. The preliminary performance and characterization results for the developed prototypes show considerable potential to implement developed membranes for bioprocessing applications. Nevertheless, additional investigation and refinement studies are still required to qualify the prototypes as finished filter products for the bioprocessing market.

The functionalization degree and homogeneity can be improved for the industrial modification by establishing a strong relationship between the base membrane specifications and the final modified membrane properties at an industrial level. This could eliminate the deviations in the properties of the modified membranes caused by the base membrane. Furthermore, “Design Of Experiments” (DOE) industrial trials should be carried out to identify the optimum time for recharging the solution bath 1, and time for renewing the solution bath 2. This is relevant since, these parameters are consumption dependent and will change based on the membrane pore size and reagent concentration.

There are still gaps to fill before the membranes can actually be used for a specific application. Since, one of the major applications is cell culture filtration a step closer towards the actual application would be evaluate the capacity of the membrane to filter cell culture media and the effect of media on the surface properties.

The developed membrane is a flat sheet, the membranes used for actual applications are in various forms of products such as syringe filter, centrifugal filters, amicon cells, and other types of membrane modules. Membrane properties should not be compromised upon processing into the various membrane products. The developed membranes should be integrated into various membranes modules and the validation of membrane properties after processing should be performed.

The developed membranes can also be utilized in cross-flow filtration and sequential filtration to enhance the recovery. Therefore, the filtration mechanism study should be carried out in cross-flow filtration mode and in a sequential filtration protocol. Furthermore, the “real” biological particles are soft and deformable unlike hard

polystyrene particles. Therefore, filtration efficiency with the actual bioprocess fluids such as extracellular vesicles (EV) containing cell culture media should be evaluated for concentration and purification experiments using these filters. This should also be a step forward in understanding filtration for EV research.

Further investigations are also needed to exploit the pH-responsive nature for the polyacrylic acid chains grafted on the surface of the membrane to increase the particle recovery. Additionally, the efficiency of polymerization can be enhanced by examining the modified membrane properties with alternate cross-linker: TrGDMA.

The results presented in this work in addition to the proposed future work could enable GVS to introduce a new line of hydrophilic products into the market for bioprocessing applications.

REFERENCES

1. Michaels, A. S. & Matson, S. L. Membranes in biotechnology: State of the art. *Desalination* **53**, 231–258 (1985).

2. van Reis, R. & Zydney, A. Bioprocess membrane technology. *J. Memb. Sci.* **297**, 16–50 (2007).

3. GlobeNewswire. Global pharmaceutical membrane filtration market size to register 12% CAGR through 2027. (2021).

4. Zydney, A. L. New developments in membranes for bioprocessing – A review. *J. Memb. Sci.* **620**, 118804 (2021).

5. Yvan, L. Treatment of fluorinated polymers and products obtained thereby. *ACM SIGGRAPH Computer Graphics* vol. 28 131–134 (1994).

6. Kenneth, M., Robert, J. & William, B. Process for Graft Copolymerization of a Pre-formed Substrate. (1982).

7. Sternberg, S. Process for grafting amino acid molecules onto preformed polymer surfaces and products prepared thereby. (1980).

8. Steuck, M. J. Porous membrane having hydrophilic surface and process. (1986).

9. Hatti-Kaul, R. & Mattiasson, B. *Isolation and purification of proteins*. (CRC Press, 2003).

10. Heath, C. A. & Belfort, G. Synthetic membranes in biotechnology: Realities and possibilities. *Bioseparation* **47**, 45–88 (2006).

11. Fröhlich, H., Villian, L., Melzner, D. & Strube, J. Membrane technology in bioprocess science. *Chemie Ing. Tech.* **84**, 905–917 (2012).

12. Selatile, M. K., Ray, S. S., Ojijo, V. & Sadiku, R. Recent developments in polymeric electrospun nanofibrous membranes for seawater desalination. *RSC Adv.* **8**, 37915–37938 (2018).

13. Aydogan, N., Gurkan, T. & Yilmaz, L. Treatment by nanofiltration of the bleed stream of a continuous alcohol fermentor. *Sep. Sci. Technol.* **39**, 1059–1072 (2005).

14. Tessier, L., Bouchard, P. & Rahni, M. Separation and purification of benzylpenicillin produced by fermentation using coupled ultrafiltration and nanofiltration technologies. *J. Biotechnol.* **116**, 79–89 (2005).

15. Ortega, L. M., Lebrun, R., Noël, I. M. & Hausler, R. Application of nanofiltration in the recovery of chromium (III) from tannery effluents. *Sep. Purif. Technol.* **44**, 45–52 (2005).

16. Madaeni, S. S., Tahmasebi, K. & Kerendi, S. H. Sugar syrup concentration using reverse osmosis membranes. *Eng. Life Sci.* **4**, 187–190 (2004).

17. Laufenberg, G., Hausmanns, S. & Kunz, B. The influence of intermolecular interactions on the selectivity of several organic acids in aqueous multicomponent systems during reverse osmosis. *J. Memb. Sci.* **110**, 59–68 (1996).

18. Grote, F., Ditz, R. & Strube, J. Downstream of downstream processing: development of recycling strategies for biopharmaceutical processes. *J. Chem. Technol. Biotechnol.* **87**, 481–497 (2012).

19. El-Safty, S. & Nguyen, D. H. Organic–Inorganic Mesoporous Silica Nanotube Hybrid Anodic Alumina Membranes for Ultrafine Filtration of Noble Metal Nanoparticles. *Noble Met.* (2012).

20. Singhvi, R., Schorr, C., O'Hara, C., Xie, L. & Wang, D. I. C. Clarification of animal cell culture process fluids using depth microfiltration. *Biopharm* **9**, 35–41 (1996).

21. Yigzaw, Y., Piper, R., Tran, M. & Shukla, A. A. Exploitation of the adsorptive properties of depth filters for host cell protein removal during monoclonal antibody purification. *Biotechnol. Prog.* **22**, 288–296 (2006).

22. Waterson, R. Novel depth filtration technologies: Strategies for process development. *Pharm. Eng.* (1990).

23. Charlton, H. R., Relton, J. M. & Slater, N. K. H. Characterisation of a generic monoclonal antibody harvesting system for adsorption of DNA by depth filters and various membranes. *Bioseparation* **8**, 281–291 (1999).

24. Melin, T. & Rautenbach, R. *Membranverfahren: Grundlagen der Modul-und Anlagenauslegung*. (Springer-Verlag, 2007).

25. Ho, C. C. Membranes for Bioseparations. *Bioprocess. Value-Added Prod. from Renew. Resour.* 163–183 (2007) doi:10.1016/B978-044452114-9/50008-6.

26. Baker, R. W. *Membrane Technology and Applications*. (2004).

27. Bird, R. B., Stewart, W. E., Lightfoot, E. N. & Meredith, R. E. Transport phenomena. *J. Electrochem. Soc.* **108**, 78C (1961).

28. Geankoplis, C. J. *Transport processes and Separation Process Principles*. (Pearson, 2003).

29. Islam, M. A. & Ulbricht, M. Microfiltration membrane characterization by gas-liquid displacement porometry: Matching experimental pore number distribution with liquid permeability and bulk porosity. *J. Memb. Sci.* **569**, 104–116 (2019).

30. Nagy, E. *Basic equations of mass transport through a membrane layer*. (Elsevier, 2018).

31. Ferry, J. D. Ultrafilter Membranes and Ultrafiltration. *Chem. Rev.* **18**, 373–455 (1936).

32. Kuriyel, R. & Zydney, A. L. Sterile filtration and virus filtration. in *Downstream*

Processing of Proteins 185–194 (Springer, 2000).

33. Sundaram, S., Auriemma, M., Howard, G., Brandwein, H. & Leo, F. Application of membrane filtration for removal of diminutive bioburden organisms in pharmaceutical products and processes. *PDA J. Pharm. Sci. Technol.* **53**, 186–201 (1999).

34. Charcosset, C. Membrane processes in biotechnology: an overview. *Biotechnol. Adv.* **24**, 482–492 (2006).

35. Aranha-Creado, H., Peterson, J. & Huang, P. Y. Clearance of murine leukaemia virus from monoclonal antibody solution by a hydrophilic PVDF microporous membrane filter. *Biologicals* **26**, 167–172 (1998).

36. Liu, S. *et al.* Development and qualification of a novel virus removal filter for cell culture applications. *Biotechnol. Prog.* **16**, 425–434 (2000).

37. Nabais, A. M. A. & Cardoso, J. P. Purification of benzylpenicillin filtered broths by ultrafiltration and effect on solvent extraction. *Bioprocess Eng.* **21**, 157–163 (1999).

38. Adikane, H., Singh, R. K. & Nene, S. N. Recovery of penicillin G from fermentation broth by microfiltration. *J. Memb. Sci.* **162**, 119–123 (1999).

39. Alves, A. M. B., Morao, A. & Cardoso, J. P. Isolation of antibiotics from industrial fermentation broths using membrane technology. *Desalination* **148**, 181–186 (2002).

40. Van Reis, R. *et al.* High performance tangential flow filtration. *Biotechnol. Bioeng.* **56**, 71–82 (1997).

41. Nyström, M., Aimar, P., Luque, S., Kulovaara, M. & Metsämuuronen, S. Fractionation of model proteins using their physiochemical properties. *Colloids Surfaces A Physicochem. Eng. Asp.* **138**, 185–205 (1998).

42. Baruah, G. L. & Belfort, G. Optimized recovery of monoclonal antibodies from transgenic goat milk by microfiltration. *Biotechnol. Bioeng.* **87**, 274–285 (2004).

43. Mulder, M. *Basic Principles of Membrane Technology*. (Springer, Dordrecht, 1996). doi:https://doi.org/10.1007/978-94-009-1766-8.

44. György, B. *et al.* Detection and isolation of cell-derived microparticles are compromised by protein complexes resulting from shared biophysical parameters. *Blood, J. Am. Soc. Hematol.* **117**, e39–e48 (2011).

45. Mathivanan, S., Ji, H. & Simpson, R. J. Exosomes: extracellular organelles important in intercellular communication. *J. Proteomics* **73**, 1907–1920 (2010).

46. Raposo, G. & Stoorvogel, W. Extracellular vesicles: exosomes, microvesicles, and friends. *J. Cell Biol.* **200**, 373–383 (2013).

47. Szatanek, R. *et al.* The methods of choice for extracellular vesicles (EVs)

characterization. *Int. J. Mol. Sci.* **18**, (2017).

48. Théry, C., Zitvogel, L. & Amigorena, S. Exosomes: Composition, biogenesis and function. *Nat. Rev. Immunol.* **2**, 569–579 (2002).

49. Paolini, L., Zendrini, A. & Radeghieri, A. Biophysical properties of extracellular vesicles in diagnostics. *Biomark. Med.* **12**, 383–391 (2018).

50. Gilligan, K. E. & Dwyer, R. M. Engineering Exosomes for Cancer Therapy. *Int. J. Mol. Sci.* **18**, (2017).

51. Borrelli, D. A. *et al.* Extracellular vesicle therapeutics for liver disease. *J. Control. Release* **273**, 86–98 (2018).

52. Lamparski, H. G. *et al.* Production and characterization of clinical grade exosomes derived from dendritic cells. *J. Immunol. Methods* **270**, 211–226 (2002).

53. Chen, C. *et al.* Microfluidic isolation and transcriptome analysis of serum microvesicles. *Lab Chip* **10**, 505–511 (2010).

54. Escudier, B. *et al.* Vaccination of metastatic melanoma patients with autologous dendritic cell (DC) derived-exosomes: results of thefirst phase I clinical trial. *J. Transl. Med.* **3**, 10 (2005).

55. Morse, M. A. *et al.* A phase I study of dexosome immunotherapy in patients with advanced non-small cell lung cancer. *J. Transl. Med.* **3**, 9 (2005).

56. Vergauwen, G. *et al.* Confounding factors of ultrafiltration and protein analysis in extracellular vesicle research. *Sci. Rep.* **7**, 2704 (2017).

57. Li, J., He, X., Deng, Y. & Yang, C. An Update on Isolation Methods for Proteomic Studies of Extracellular Vesicles in Biofluids. *Molecules* **24**, (2019).

58. Grote, F., Fröhlich, H. & Strube, J. Integration of Ultrafiltration Unit Operations in Biotechnology Process Design. *Chem. Eng. Technol.* **34**, 673–687 (2011).

59. Schäfer, A. I., Pihlajamäki, A., Fane, A. G., Waite, T. D. & Nyström, M. Natural organic matter removal by nanofiltration: effects of solution chemistry on retention of low molar mass acids versus bulk organic matter. *J. Memb. Sci.* **242**, 73–85 (2004).

60. Guo, W., Ngo, H. H. & Li, J. A mini-review on membrane fouling. *Bioresour. Technol.* **122**, 27–34 (2012).

61. Maa, Y. F. & Hsu, C. C. Investigation on fouling mechanisms for recombinant human growth hormone sterile filtration. *J. Pharm. Sci.* **87**, 808–812 (1998).

62. Bellucci, F. *et al.* Temperature gradient affecting mass transport in synthetic membranes. *J. Memb. Sci.* **7**, 169–183 (1980).

63. Hermia, J. Constant Pressure Blocking Filtration Laws - Application To Power-law Non-newtonian Fluids. *Inst. Chem. Eng. Trans.* **60**, 183–187 (1982).

64. Iritani, E. & Katagiri, N. Developments of blocking filtration model in membrane filtration. *KONA Powder Part. J.* **2016**, 179–202 (2016).

65. Ho, C.-C. & Zydney, A. L. A Combined Pore Blockage and Cake Filtration Model for Protein Fouling during Microfiltration. *J. Colloid Interface Sci.* **232**, 389–399 (2000).

66. Zydney, A. L. & Ho, C.-C. Effect of membrane morphology on system capacity during normal flow microfiltration. *Biotechnol. Bioeng.* **83**, 537–543 (2003).

67. Ho, C.-C. & Zydney, A. L. Effect of membrane morphology on the initial rate of protein fouling during microfiltration. *J. Memb. Sci.* **155**, 261–275 (1999).

68. Nilsson, J. L. Protein fouling of uf membranes: Causes and consequences. *J. Memb. Sci.* **52**, 121–142 (1990).

69. Marshall, A. D., Munro, P. A. & Trägårdh, G. The effect of protein fouling in microfiltration and ultrafiltration on permeate flux, protein retention and selectivity: A literature review. *Desalination* **91**, 65–108 (1993).

70. Belfort, G., Davis, R. H. & Zydney, A. L. The behavior of suspensions and macromolecular solutions in crossflow microfiltration. *J. Memb. Sci.* **96**, 1–58 (1994).

71. Sun, S., Yue, Y., Huang, X. & Meng, D. Protein adsorption on blood-contact membranes. *J. Memb. Sci.* **222**, 3–18 (2003).

72. Velasco, C., Ouammou, M., Calvo, J. I. & Hernández, A. Protein fouling in microfiltration: deposition mechanism as a function of pressure for different pH. *J. Colloid Interface Sci.* **266**, 148–152 (2003).

73. Nakamura, K. & Matsumoto, K. Adsorption behavior of BSA in microfiltration with porous glass membrane. *J. Memb. Sci.* **145**, 119–128 (1998).

74. Nakamura, K. & Matsumoto, K. Properties of protein adsorption onto pore surface during microfiltration: Effects of solution environment and membrane hydrophobicity. *J. Memb. Sci.* **280**, 363–374 (2006).

75. Martínez, F. *et al.* Protein Adsorption and Deposition onto Microfiltration Membranes: The Role of Solute–Solid Interactions. *J. Colloid Interface Sci.* **221**, 254–261 (2000).

76. Su, T. J., Lu, J. R., Cui, Z. F. & Thomas, R. K. Fouling of ceramic membranes by albumins under dynamic filtration conditions. *J. Memb. Sci.* **173**, 167–178 (2000).

77. Kim, K., Fane, A., Nystrom, M. & Pihlajamaki, A. Chemical and Electrical Characterization of Virgin and Protein-Fouled Polycarbonate Track-Etched Membranes by FTIR and Streaming-Potential Measurements. *J. Memb. Sci.* **134**, 199–208 (1997).

78. Causserand, C., Nyström, M. & Aimar, P. Study of streaming potentials of clean and fouled ultrafiltration membranes. *J. Memb. Sci.* **88**, 211–222 (1994).

79. Clark, W. M., Bansal, A., Sontakke, M. & Ma, Y. H. Protein adsorption and fouling in ceramic ultrafiltration membranes. *J. Memb. Sci.* **55**, 21–38 (1991).

80. Bowen, W. R. & Gan, Q. Properties of microfiltration membranes: Adsorption of bovine serum albumin at polyvinylidene fluoride membranes. *J. Colloid Interface Sci.* **144**, 254–262 (1991).

81. Zhao, Z.-P., Wang, Z. & Wang, S.-C. Formation, charged characteristic and BSA adsorption behavior of carboxymethyl chitosan/PES composite MF membrane. *J. Memb. Sci.* **217**, 151–158 (2003).

82. Wavhal, D. S. & Fisher, E. R. Modification of polysulfone ultrafiltration membranes by CO2 plasma treatment. *Desalination* **172**, 189–205 (2005).

83. Chen, V. Performance of partially permeable microfiltration membranes under low fouling conditions. *J. Memb. Sci.* **147**, 265–278 (1998).

84. He, M. *et al.* Zwitterionic materials for antifouling membrane surface construction. *Acta Biomater.* **40**, 142–152 (2016).

85. Norde, W. Protein adsorption at solid surfaces: A thermodynamic approach. *Pure Appl. Chem.* **66**, 491–496 (1994).

86. Wei, Q. *et al.* Protein interactions with polymer coatings and biomaterials. *Angew. Chemie - Int. Ed.* **53**, 8004–8031 (2014).

87. Ognier, S., Wisniewski, C. & Grasmick, A. Influence of macromolecule adsorption during filtration of a membrane bioreactor mixed liquor suspension. *J. Memb. Sci.* **209**, 27–37 (2002).

88. Carić, M. Đ., Milanović, S. D., Krstić, D. M. & Tekić, M. N. Fouling of inorganic membranes by adsorption of whey proteins. *J. Memb. Sci.* **165**, 83–88 (2000).

89. Le, M. S. & Gollan, K. L. Fouling of microporous membranes in biological applications. *J. Memb. Sci.* **40**, 231–242 (1989).

90. Zhang, R. *et al.* Antifouling membranes for sustainable water purification: strategies and mechanisms. *Chem. Soc. Rev.* **45**, 5888–5924 (2016).

91. Simone, S. *et al.* Preparation of hollow fibre membranes from PVDF/PVP blends and their application in VMD. *J. Memb. Sci.* **364**, 219–232 (2010).

92. Bi, Q., Li, Q., Tian, Y., Lin, Y. & Wang, X. Hydrophilic modification of poly (vinylidene fluoride) membrane with poly (vinyl pyrrolidone) via a cross-linking reaction. *J. Appl. Polym. Sci.* **127**, 394–401 (2013).

93. Pieracci, J., Crivello, J. V & Belfort, G. Photochemical modification of 10kDa polyethersulfone ultrafiltration membranes for reduction of biofouling. *J. Memb. Sci.* **156**, 223–240 (1999).

94. Ostuni, E., Chapman, R. G., Holmlin, R. E., Takayama, S. & Whitesides, G. M. A Survey of Structure-Property Relationships of Surfaces that Resist the Adsorption

of Proteins. *Langmuir* **17**, 5605–5620 (2001).

95. Dai, J. *et al.* High-capacity binding of proteins by poly(acrylic acid) brushes and their derivatives. *Langmuir* **22**, 4274–4281 (2006).

96. Yu, K. & Han, Y. Effect of block sequence and block length on the stimuli-responsive behavior of polyampholyte brushes: hydrogen bonding and electrostatic interaction as the driving force for surface rearrangement. *Soft Matter* **5**, 759–768 (2009).

97. Deng, B. *et al.* Antifouling microfiltration membranes prepared from acrylic acid or methacrylic acid grafted poly(vinylidene fluoride) powder synthesized via pre-irradiation induced graft polymerization. *J. Memb. Sci.* **350**, 252–258 (2010).

98. Jeon, S. I., Lee, J. H., Andrade, J. D. & De Gennes, P. G. Protein—surface interactions in the presence of polyethylene oxide: I. Simplified theory. *J. Colloid Interface Sci.* **142**, 149–158 (1991).

99. Krishnan, S., Weinman, C. J. & Ober, C. K. Advances in polymers for anti-biofouling surfaces. *J. Mater. Chem.* **18**, 3405–3413 (2008).

100. Liu, X., Neoh, K. G. & Kang, E. T. Redox-Sensitive Microporous Membranes Prepared from Poly(vinylidene fluoride) Grafted with Viologen-Containing Polymer Side Chains. *Macromolecules* **36**, 8361–8367 (2003).

101. Zhai, G. *et al.* Poly(vinylidene fluoride) with Grafted Zwitterionic Polymer Side Chains for Electrolyte-Responsive Microfiltration Membranes. *Langmuir* **19**, 7030–7037 (2003).

102. Wang, W. C. *et al.* Synthesis and characterization of fluorinated polyimide with grafted poly(N-isopropylacrylamide) side chains and the temperature-sensitive microfiltration membranes. *Ind. Eng. Chem. Res.* **42**, 3740–3749 (2003).

103. Huang, X.-J., Xu, Z.-K., Wan, L.-S., Wang, Z.-G. & Wang, J.-L. Novel Acrylonitrile-Based Copolymers Containing Phospholipid Moieties: Synthesis and Characterization. *Macromol. Biosci.* **5**, 322–330 (2005).

104. Hamza, A., Pham, V. A., Matsuura, T. & Santerre, J. P. Development of membranes with low surface energy to reduce the fouling in ultrafiltration applications. *J. Memb. Sci.* **131**, 217–227 (1997).

105. Khayet, M., Feng, C. Y. & Matsuura, T. Morphological study of fluorinated asymmetric polyetherimide ultrafiltration membranes by surface modifying macromolecules. *J. Memb. Sci.* **213**, 159–180 (2003).

106. Rana, D., Matsuura, T., Narbaitz, R. M. & Feng, C. Development and characterization of novel hydrophilic surface modifying macromolecule for polymeric membranes. *J. Memb. Sci.* **249**, 103–112 (2005).

107. Miyata, T., Yamada, H. & Uragami, T. Surface Modification of Microphase-Separated Membranes by Fluorine-Containing Polymer Additive and Removal of Dilute Benzene in Water through These Membranes. *Macromolecules* **34**, 8026–

8033 (2001).

108. Sivakumar, M. *et al.* Preparation and performance of cellulose acetate–polyurethane blend membranes and their applications – II. *J. Memb. Sci.* **169**, 215–228 (2000).

109. Malaisamy, R., Mahendran, R., Mohan, D., Rajendran, M. & Mohan, V. Cellulose acetate and sulfonated polysulfone blend ultrafiltration membranes. I. Preparation and characterization. *J. Appl. Polym. Sci.* **86**, 1749–1761 (2002).

110. Ulbricht, M. Advanced functional polymer membranes. *Polymer (Guildf).* **47**, 2217–2262 (2006).

111. Du, J. R., Peldszus, S., Huck, P. M. & Feng, X. Modification of poly(vinylidene fluoride) ultrafiltration membranes with poly(vinyl alcohol) for fouling control in drinking water treatment. *Water Res.* **43**, 4559–4568 (2009).

112. Xu, Z., Li, L., Wu, F., Tan, S. & Zhang, Z. The application of the modified PVDF ultrafiltration membranes in further purification of Ginkgo biloba extraction. *J. Memb. Sci.* **255**, 125–131 (2005).

113. Boributh, S., Chanachai, A. & Jiraratananon, R. Modification of PVDF membrane by chitosan solution for reducing protein fouling. *J. Memb. Sci.* **342**, 97–104 (2009).

114. Katoa, K., Emiko, U., En-Tang, K., Yoshikimi, U. & Yoshito, I. Polymer surface with graft chains. *Prog. Polym. Sci.* **28**, 209–259 (2003).

115. Bhattacharya, A. & Misra, B. N. Grafting: a versatile means to modify polymers: Techniques, factors and applications. *Prog. Polym. Sci.* **29**, 767–814 (2004).

116. Yamamoto, S., Ejaz, M., Tsujii, Y. & Fukuda, T. Surface Interaction Forces of Well-Defined, High-Density Polymer Brushes Studied by Atomic Force Microscopy. 2. Effect of Graft Density. *Macromolecules* **33**, 5608–5612 (2000).

117. Ejaz, M., Yamamoto, S., Tsujii, Y. & Fukuda, T. Fabrication of Patterned High-Density Polymer Graft Surfaces. 1. Amplification of Phase-Separated Morphology of Organosilane Blend Monolayer by Surface-Initiated Atom Transfer Radical Polymerization. *Macromolecules* **35**, 1412–1418 (2002).

118. Pyun, J. & Matyjaszewski, K. Synthesis of Nanocomposite Organic/Inorganic Hybrid Materials Using Controlled/"Living" Radical Polymerization. *Chem. Mater.* **13**, 3436–3448 (2001).

119. Goldstein, J. I. *et al. Scanning electron microscopy and x-ray microanalysis*. *Scanning Electron Microscopy and X-ray Microanalysis* (2017). doi:10.1007/978-1-4939-6676-9.

120. Castilho, L. R., Deckwer, W.-D. & Anspach, F. B. Influence of matrix activation and polymer coating on the purification of human IgG with protein A affinity membranes. *J. Memb. Sci.* **172**, 269–277 (2000).

121. Thom, V., Jankova, K., Ulbricht, M., Kops, J. & Jonsson, G. Synthesis of photoreactive α-4-azidobenzoyl-ω-methoxy-poly(ethylene glycol)s and their end-on photo-grafting onto polysulfone ultrafiltration membranes. *Macromol. Chem. Phys.* **199**, 2723–2729 (1998).

122. Thom, V. H. *et al.* Optimizing Cell−Surface Interactions by Photografting of Poly(ethylene glycol). *Langmuir* **16**, 2756–2765 (2000).

123. Yang, Q., Xu, Z.-K., Dai, Z.-W., Wang, J.-L. & Ulbricht, M. Surface modification of polypropylene microporous membranes with a novel glycopolymer. *Chem. Mater.* **17**, 3050–3058 (2005).

124. Zhao, B. & Brittain, W. J. Polymer brushes: surface-immobilized macromolecules. *Prog. Polym. Sci.* **25**, 677–710 (2000).

125. Liu, Z.-M., Xu, Z.-K., Wan, L.-S., Wu, J. & Ulbricht, M. Surface modification of polypropylene microfiltration membranes by the immobilization of poly(N-vinyl-2-pyrrolidone): a facile plasma approach. *J. Memb. Sci.* **249**, 21–31 (2005).

126. Ulbricht, M. & Belfort, G. Surface modification of ultrafiltration membranes by low temperature plasma II. Graft polymerization onto polyacrylonitrile and polysulfone. *J. Memb. Sci.* **111**, 193–215 (1996).

127. Kou, R.-Q. *et al.* Surface Modification of Microporous Polypropylene Membranes by Plasma-Induced Graft Polymerization of α-Allyl Glucoside. *Langmuir* **19**, 6869–6875 (2003).

128. Taniguchi, M., Pieracci, J., Samsonoff, W. A. & Belfort, G. UV-Assisted Graft Polymerization of Synthetic Membranes: Mechanistic Studies. *Chem. Mater.* **15**, 3805–3812 (2003).

129. Pieracci, J., Crivello, J. V & Belfort, G. UV-Assisted Graft Polymerization of N-Vinyl-2-pyrrolidinone onto Poly(ether sulfone) Ultrafiltration Membranes Using Selective UV Wavelengths. *Chem. Mater.* **14**, 256–265 (2002).

130. Taniguchi, M. & Belfort, G. Low protein fouling synthetic membranes by UV-assisted surface grafting modification: varying monomer type. *J. Memb. Sci.* **231**, 147–157 (2004).

131. Belfer, S., Purinson, Y., Fainshtein, R., Radchenko, Y. & Kedem, O. Surface modification of commercial composite polyamide reverse osmosis membranes. *J. Memb. Sci.* **139**, 175–181 (1998).

132. Freger, V., Gilron, J. & Belfer, S. TFC polyamide membranes modified by grafting of hydrophilic polymers: an FT-IR/AFM/TEM study. *J. Memb. Sci.* **209**, 283–292 (2002).

133. Faibish, R. S. & Cohen, Y. Fouling-resistant ceramic-supported polymer membranes for ultrafiltration of oil-in-water microemulsions. *J. Memb. Sci.* **185**, 129–143 (2001).

134. Choi, W. C., Kim, J. D. & Woo, S. I. Modification of proton conducting membrane

for reducing methanol crossover in a direct-methanol fuel cell. *J. Power Sources* **96**, 411–414 (2001).

135. Feichtinger, J., Schulz, A., Walker, M., Schumacher, U. & Kerrews, J. Plasma modifications of membranes for PEM fuel cells. *J. New Mater. Electrochem. Syst.* **5**, 155–162 (2002).

136. Nunes, S. P., Sforça, M. L. & Peinemann, K.-V. Dense hydrophilic composite membranes for ultrafiltration. *J. Memb. Sci.* **106**, 49–56 (1995).

137. Dickson, J. M., Childs, R. F., McCarry, B. E. & Gagnon, D. R. Development of a coating technique for the internal structure of polypropylene microfiltration membranes. *J. Memb. Sci.* **148**, 25–36 (1998).

138. Hvid, K. B., Nielsen, P. S. & Stengaard, F. F. Preparation and characterization of a new ultrafiltration membrane. *J. Memb. Sci.* **53**, 189–202 (1990).

139. Wei, J., Helm, G. S., Corner-Walker, N. & Hou, X. Characterization of a non-fouling ultrafiltration membrane. *Desalination* **192**, 252–261 (2006).

140. Gero, D. Fuzzy Nanoassemblies: Toward Layered Polymeric Multicomposites. *Science (80-.).* **277**, 1232–1237 (1997).

141. Misra, G. S. & Bajpai, U. D. N. Redox polymerization. *Prog. Polym. Sci.* **8**, 61–131 (1982).

142. Sarac, A. S. Redox polymerization. *Prog. Polym. Sci.* **24**, 1149–1204 (1999).

143. Jellinek, H. Photodegradation and high temperature degradation of polymers. *Pure Appl. Chem.* **4**, 419–458 (1962).

144. Bokare, A. D. & Choi, W. Review of iron-free Fenton-like systems for activating H2O2 in advanced oxidation processes. *J. Hazard. Mater.* **275**, 121–135 (2014).

145. Fenton, H. J. H. LXXIII.—Oxidation of tartaric acid in presence of iron. *J. Chem. Soc.* **65**, 899–910 (1894).

146. Baxendale, J. H., Evans, M. G. & Kilham, J. K. The kinetics of polymerisation reactions in aqueous solution. *Trans. Faraday Soc.* **42**, 668–675 (1946).

147. Barb, W. G., Baxendale, J. H., George, P. & Hargrave, K. R. Reactions of ferrous and ferric ions with hydrogen peroxide. Part II.—The ferric ion reaction. *Trans. Faraday Soc.* **47**, 591–616 (1951).

148. Dainton, F. S. On the Existence of Free Atoms and Radicals in Water and Aqueous Solutions Subjected to Ionizing Radiation. *J. Phys. Colloid Chem.* **52**, 490–517 (1948).

149. Davies, M. J. & Slater, T. F. Studies on the metal-ion and lipoxygenase-catalysed breakdown of hydroperoxides using electron-spin-resonance spectroscopy. *Biochem. J.* **245**, 167–173 (1987).

150. Arthur, J. C., Hinojosa, O. & Bains, M. S. ESR study of reactions of cellulose with ·OH generated by Fe+2/H2O2. *J. Appl. Polym. Sci.* **12**, 1411–1421 (1968).

151. Haber, F., Weiss, J. & A, P. R. S. L. The catalytic decomposition of hydrogen peroxide by iron salts. *Proc. R. Soc. London. Ser. A - Math. Phys. Sci.* **147**, 332–351 (1934).

152. Neyens, E. & Baeyens, J. A review of classic Fenton's peroxidation as an advanced oxidation technique. *J. Hazard. Mater.* **98**, 33–50 (2003).

153. Johnson, L. M., Fairbanks, B. D., Anseth, K. S. & Bowman, C. N. Enzyme-mediated redox initiation for hydrogel generation and cellular encapsulation. *Biomacromolecules* **10**, 3114–3121 (2009).

154. Bautista, P., Mohedano, A. F., Casas, J. A., Zazo, J. A. & Rodriguez, J. J. An overview of the application of Fenton oxidation to industrial wastewaters treatment. *J. Chem. Technol. Biotechnol. Int. Res. Process. Environ. Clean Technol.* **83**, 1323–1338 (2008).

155. Hebeish, A. & Guthrie, T. J. *The Chemistry and Technology of Cellulosic Copolymers*. (1981).

156. Khan, M. M. T. & Martell, A. E. Metal ion and metal chelate catalyzed oxidation of ascorbic acid by molecular oxygen. II. Cupric and ferric chelate catalyzed oxidation. *J. Am. Chem. Soc.* **89**, 7104–7111 (1967).

157. Butruk, B., Trzaskowski, M. & Ciach, T. Fabrication of biocompatible hydrogel coatings for implantable medical devices using Fenton-type reaction. *Mater. Sci. Eng. C* **32**, 1601–1609 (2012).

158. Sychev, A. Y. & Isak, V. G. Iron compounds and the mechanisms of the homogeneous catalysis of the activation of O2 and H2O2 and of the oxidation of organic substrates. *Russ. Chem. Rev.* **64**, 1105 (1995).

159. Hilal, N., Ismail, A. F. & Wright, C. J. PVDF Membranes for Membrane Distillation Controlling Pore Structure, Porosity, Hydrophobicity, and Mechanical Strength. *Membr. Fabr.* 249–284 (2015).

160. Steuck, M. Porous membrane having hydrophilic surface and process. (1986).

161. Matson, S. L. Chapter 8 Membrane bioseparations. *Membr. Sci. Technol.* **2**, 353–413 (1995).

162. Butruk, B., Trzaskowski, M. I. & Ciach, T. Fabrication of biocompatible hydrogel coatings for implantable medical devices using Fenton-type reaction. *Mater. Sci. Eng. C* **32**, 1601–1609 (2012).

163. Jena, A. & Gupta, K. Advances in pore structure evaluation by porometry. *Chem. Eng. Technol.* **33**, 1241–1250 (2010).

164. Halisch, M. & Cano-Odena, A. 2013: Capillary Flow Porometry - Assessment of an Alternative Method for the Determination of Flow Relevant Parameters of

Porous Rocks. *Capill. Flow Porometry - Assess. an Altern. Method Determ. Flow Relev. Parameters Porous Rocks* 1–12 (2013).

165. Johnson, D. J., Oatley-Radcliffe, D. L. & Hilal, N. State of the art review on membrane surface characterisation: Visualisation, verification and quantification of membrane properties. *Desalination* **434**, 12–36 (2018).

166. Abd Mutalib, M., Rahman, M. A., Othman, M. H. D., Ismail, A. F. & Jaafar, J. *Scanning Electron Microscopy (SEM) and Energy-Dispersive X-Ray (EDX) Spectroscopy*. *Membrane Characterization* (Elsevier B.V., 2017).

167. Smith, B. C. *Fundamentals of Fourier Transform Infrared Spectroscopy*. (Taylor & Francis, 2011). doi:https://doi.org/10.1201/b10777.

168. PerkinElmer. FT-IR Spectroscopy Attenuated Total Reflectance (ATR). *PerkinElmer Life Anal. Sci.* 1–5 (2005).

169. Stuart, B. H. *Infrared Spectroscopy: Fundamentals and Applications*. *John Wiley & Sons, Ltd* vol. 8 (2005).

170. Hunter, R. *Zeta Potential in Colloid Science Principles and Applications*. (Academic Press London, 1988).

171. Oatley-Radcliffe, D. L., Aljohani, N., Williams, P. M. & Hilal, N. *Electrokinetic Phenomena for Membrane Charge*. *Membrane Characterization* (Elsevier B.V., 2017).

172. Möckel, D., Staude, E., Dal-Cin, M., Darcovich, K. & Guiver, M. Tangential flow streaming potential measurements: Hydrodynamic cell characterization and zeta potentials of carboxylated polysulfone membranes. *J. Memb. Sci.* **145**, 211–222 (1998).

173. Elimelech, M., Chen, W. H. & Waypa, J. J. Measuring the zeta (electrokinetic) potential of reverse osmosis membranes by a streaming potential analyzer. *Desalination* **95**, 269–286 (1994).

174. Hunter, R. *Zeta potential in Colloidal Science Principles and Applications*. *Academic Press* vol. 2 (Academic Press London, 1981).

175. Lyklema, J. *Fundamentals of interface and colloid science: Particulate colloids*. (Elsevier, 2005).

176. Yuan, Y. & Lee, T. R. Contact Angle and Wetting Properties BT - Surface Science Techniques. in (eds. Bracco, G. & Holst, B.) 3–34 (Springer Berlin Heidelberg, 2013). doi:10.1007/978-3-642-34243-1_1.

177. Energy dispersive X-ray spectroscopy. https://en.wikipedia.org/wiki/Energy-dispersive_X-ray_spectroscopy (2021).

178. Zhao, C., Nie, S., Tang, M. & Sun, S. Polymeric pH-sensitive membranes - A review. *Prog. Polym. Sci.* **36**, 1499–1520 (2011).

179. Winter, W. T. Measurement of suspended particles by quasi-elastic light scattering, Barton E. Dahneke, Ed., Wiley, New York, 1983, 570 pp. Price:$39.95. *J. Polym. Sci. Polym. Lett. Ed.* **21**, 1020 (1983).

180. Pecora, R. *Dynamic Light Scattering: Applications of Photon Correlation Spectroscopy*. *Physics and Astronomy* (2008).

181. FORD, J. L. Particle Size Analysis in Pharmaceutics and Other Industries. Theory and Practice. *J. Pharm. Pharmacol.* **45**, 1015–1015 (1993).

182. Charles S. Johnson, D. A. G. Laser Light Scattering. in *Spectroscopy in Biochemistry* 72 (Taylor & Francis, 1981).

183. Derjaguin, B. & Landau, L. Theory of the stability of strongly charged lyophobic sols and of the adhesion of strongly charged particles in solutions of electrolytes. *Prog. Surf. Sci.* **43**, 30–59 (1993).

184. Verwey, E. J. W. Theory of the stability of lyophobic colloids. *J. Phys. Chem.* **51**, 631–636 (1947).

185. Adair, J. H., Suvaci, E. & Sindel, J. Surface and Colloid Chemistry. in (eds. Buschow, K. H. J. et al.) 1–10 (Elsevier, 2001).

186. Cano-Sarmiento, C. *et al.* Zeta Potential of Food Matrices. *Food Eng. Rev.* **10**, 113–138 (2018).

187. Ross, S. & Morrison, E. D. *Colloidal systems and interfaces*. (John Wiley and Sons, New York, NY (US), 1988).

188. Shaw, D. J. & Costello, B. *Introduction to colloid and surface chemistry*. (Elsevier, Oxford, 1993).

189. Everett, D. H. *Basic principles of colloid science The Royal Society of chemistry*. *Cambridge, UK* (1988).

190. Jablonski, A. Efficiency of anti-Stokes fluorescence in dyes. *Nature* **131**, 839–840 (1933).

191. Albrecht, C. & Lakowicz, J. *Principles of fluorescence spectroscopy*. (Springer, 2008).

192. Sharma, A. & Schulman, S. G. *Introduction to fluorescence spectroscopy*. vol. 13 (Wiley-interscience, 1999).

193. Al-Amoudi, M. S. *et al.* Spectral studies to increase the efficiency and stability of laser dyes by charge-transfer reactions for using in solar cells: Charge-transfer complexes of Ponceau S with p-chloranil, chloranilic and picric acids. *Res. Chem. Intermed.* **41**, 3089–3108 (2015).

194. Aebersold, R. H., Leavitt, J., Saavedra, R. A., Hood, L. E. & Kent, S. B. Internal amino acid sequence analysis of proteins separated by one- or two-dimensional gel electrophoresis after in situ protease digestion on nitrocellulose. *Proc. Natl. Acad.*

Sci. **84**, 6970 LP – 6974 (1987).

195. Ulbricht, M., Matuschewski, H., Oechel, A. & Hicke, H. G. Photo-induced graft polymerization surface modifications for the preparation of hydrophilic and low-protein-adsorbing ultrafiltration membranes. *J. Memb. Sci.* **115**, 31–47 (1996).

196. Skoog, D. A., Holler, F. J. & Crouch, S. R. *Principles of instrumental analysis*. (Cengage learning, 2017).

197. Mohapatra, S. Sterilization and Disinfection. *Essentials of Neuroanesthesia* 929–944 (2017) doi:10.1016/B978-0-12-805299-0.00059-2.

198. Bottino, A., Camera-Roda, G., Capannelli, G. & Munari, S. The formation of microporous polyvinylidene difluoride membranes by phase separation. *J. Memb. Sci.* **57**, 1–20 (1991).

199. Cui, Z., Drioli, E. & Lee, Y. M. Recent progress in fluoropolymers for membranes. *Prog. Polym. Sci.* **39**, 164–198 (2014).

200. Kolthoff, I. M. & Medalia, A. I. The reaction between ferrous iron and peroxides. II. Reaction with hydrogen peroxide, in the presence of oxygen. *J. Am. Chem. Soc.* **71**, 3784–3788 (1949).

201. Karakhanov, E. A., Narin, S. Y. & Dedov, A. G. On the mechanism of catalytic hydroxylation of aromatic hydrocarbons by hydrogen peroxide. *Appl. Organomet. Chem.* **5**, 445–461 (1991).

202. Brockway, C. E. & Moser, K. B. Grafting of poly (methyl methacrylate) to granular corn starch. *J. Polym. Sci. Part A Gen. Pap.* **1**, 1025–1039 (1963).

203. Zhu, S. & Hamielec, A. E. Kinetics of network formation via free-radical mechanisms—Polymerization and polymer modification. in *Makromolekulare Chemie. Macromolecular Symposia* vol. 69 247–256 (Wiley Online Library, 1993).

204. Zhu, X., Lu, P., Chen, W. & Dong, J. Studies of UV crosslinked poly(N-vinylpyrrolidone) hydrogels by FTIR, Raman and solid-state NMR spectroscopies. *Polymer (Guildf).* **51**, 3054–3063 (2010).

205. Asenjo-Sanz, I. *et al.* Preparation and Preliminary Evaluation of Povidone Single-Chain Nanoparticles as Potential Drug Delivery Nanocarriers. *Med One* **4**, e190013 (2019).

206. Griffiths, M. C., Strauch, J., Monteiro, M. J. & Gilbert, R. G. Measurement of Diffusion Coefficients of Oligomeric Penetrants in Rubbery Polymer Matrixes. *Macromolecules* **31**, 7835–7844 (1998).

207. Braun, D. Origins and development of initiation of free radical polymerization processes. *Int. J. Polym. Sci.* **2009**, (2009).

208. Dubinsky, S., Grader, G. S., Shter, G. E. & Silverstein, M. S. Thermal degradation of poly (acrylic acid) containing copper nitrate. *Polym. Degrad. Stab.* **86**, 171–178

(2004).

209. Özer, E. T. *et al.* Removal of diethyl phthalate from aqueous phase using magnetic poly (EGDMA–VP) beads. *J. Hazard. Mater.* **229**, 20–28 (2012).

210. Koczkur, K. M., Mourdikoudis, S., Polavarapu, L. & Skrabalak, S. E. Polyvinylpyrrolidone (PVP) in nanoparticle synthesis. *Dalt. Trans.* **44**, 17883–17905 (2015).

211. Betz, N. *et al.* A FTIR study of PVDF irradiated by means of swift heavy ions. *J. Polym. Sci. Part B Polym. Phys.* **32**, 1493–1502 (1994).

212. Kaczmarek, H. & Szalla, A. Photochemical transformation in poly (acrylic acid)/poly (ethylene oxide) complexes. *J. Photochem. Photobiol. A Chem.* **180**, 46–53 (2006).

213. Gonzaga, V. de A. M., Chrisostomo, B. A., Poli, A. L. & Schmitt, C. C. Preparation, characterization and photostability of nanocomposite films based on poly (acrylic acid) and montmorillonite. *Mater. Res.* **21**, (2018).

214. Zangi, R. & Engberts, J. B. F. N. Physisorption of Hydroxide Ions from Aqueous Solution to a Hydrophobic Surface. *J. Am. Chem. Soc.* **127**, 2272–2276 (2005).

215. Zimmermann, R., Freudenberg, U., Schweiß, R., Küttner, D. & Werner, C. Hydroxide and hydronium ion adsorption — A survey. *Curr. Opin. Colloid Interface Sci.* **15**, 196–202 (2010).

216. Yang, Q., Chung, T.-S. & Weber, M. Microscopic behavior of polyvinylpyrrolidone hydrophilizing agents on phase inversion polyethersulfone hollow fiber membranes for hemofiltration. *J. Memb. Sci.* **326**, 322–331 (2009).

217. Huang, F. L. *et al.* Dynamic wettability and contact angles of poly (vinylidene fluoride) nanofiber membranes grafted with acrylic acid. *Express Polym. Lett.* **4**, (2010).

218. Huang, X. *et al.* Treatment of oily waste water by PVP grafted PVDF ultrafiltration membranes. *Chem. Eng. J.* **273**, 421–429 (2015).

219. Deng, B. *et al.* Antifouling microfiltration membranes prepared from acrylic acid or methacrylic acid grafted poly(vinylidene fluoride) powder synthesized via pre-irradiation induced graft polymerization. *J. Memb. Sci.* **350**, 252–258 (2010).

220. Ouellette, R. & Rawn, D. Introduction to Organic Reaction Mechanisms. in *Organic Chemistry (second edition) Structure,Mechisms,Synthesis* 51–86 (Academic Press, 2018).

221. Achilias, D. S. A review of modeling of diffusion controlled polymerization reactions. *Macromol. theory simulations* **16**, 319–347 (2007).

222. Laborie, F. Influence of the solvents on the γ-ray polymerization of acrylic acid. I. *J. Polym. Sci. Polym. Chem. Ed.* **15**, 1255–1274 (1977).

223. Chapiro, A. & Dulieu, J. Influence of solvents on the molecular associations and on the radiation initiated polymerization of acrylic acid. *Eur. Polym. J.* **13**, 563–577 (1977).

224. Cutié, S. S., Smith, P. B., Henton, D. E., Staples, T. L. & Powell, C. Acrylic acid polymerization kinetics. *J. Polym. Sci. Part B Polym. Phys.* **35**, 2029–2047 (1997).

225. Hendri, J., Hiroki, A., Maekawa, Y., Yoshida, M. & Katakai, R. Permeability control of metal ions using temperature-and pH-sensitive gel membranes. *Radiat. Phys. Chem.* **60**, 617–624 (2001).

226. Park, H. W., Jin, H.-S., Yang, S. Y. & Kim, J.-D. Tunable phase transition behaviors of pH-sensitive polyaspartamides having various cationic pendant groups. *Colloid Polym. Sci.* **287**, 919–926 (2009).

227. H. F. Mark, N. M. B. *Encyclopedia of Polymer Science and Technology--Plastics, Resins, Rubbers, Fibers: Supplement*. (Interscience Publishers, 1976).

228. Aso, C. Polymerization of ethylene glycol dimethacrylate. *J. Polym. Sci.* **39**, 475–486 (1959).

229. Kim, J. Y., Cho, C. H., Palffy-Muhoray, P. & Kyu, T. Polymerization-induced phase separation in a liquid-crystal-polymer mixture. *Phys. Rev. Lett.* **71**, 2232 (1993).

230. Serbutoviez, C., Kloosterboer, J. G., Boots, H. M. J. & Touwslager, F. J. Polymerization-Induced Phase Separation. 2. Morphology of Polymer-Dispersed Liquid Crystal Thin Films. *Macromolecules* **29**, 7690–7698 (1996).

231. Miller-Chou, B. A. & Koenig, J. L. A review of polymer dissolution. *Prog. Polym. Sci.* **28**, 1223–1270 (2003).

232. Borzęcka, N. H., Kozłowska, I., Gac, J. M. & Bojarska, M. Anti-fouling properties of poly(acrylic acid) grafted ultrafiltration membranes – experimental and theoretical study. *Appl. Surf. Sci.* **506**, 144658 (2020).

233. Zhao, Y.-H., Wee, K.-H. & Bai, R. Highly hydrophilic and low-protein-fouling polypropylene membrane prepared by surface modification with sulfobetaine-based zwitterionic polymer through a combined surface polymerization method. *J. Memb. Sci.* **362**, 326–333 (2010).

234. Sui, Y., Wang, Z., Gao, X. & Gao, C. Antifouling PVDF ultrafiltration membranes incorporating PVDF-g-PHEMA additive via atom transfer radical graft polymerizations. *J. Memb. Sci.* **413**–**414**, 38–47 (2012).

235. Garcia-Fierro, J. L. & Aleman, J. V. Sorption of water by epoxide prepolymers. *Macromolecules* **15**, 1145–1149 (1982).

236. Price, C. A. The effect of cross-linking agents on the impact resistance of a linear poly (methyl methacrylate) denture-base polymer. *J. Dent. Res.* **65**, 987–992 (1986).

237. Nielsen, L. E. Cross-linking–effect on physical properties of polymers. *J. Macromol. Sci. Part C* **3**, 69–103 (1969).

238. Trzaskus, K., Elshof, M., Kemperman, A. & Nijmeijer, K. Understanding the role of nanoparticle size and polydispersity in fouling development during dead-end microfiltration. *J. Memb. Sci.* **516**, 152–161 (2016).

239. Pontius, F. W., Amy, G. L. & Hernandez, M. T. Fluorescent microspheres as virion surrogates in low-pressure membrane studies. *J. Memb. Sci.* **335**, 43–50 (2009).

240. Lee, J.-K., Liu, B. Y. H. & Rubow, K. L. Latex sphere retention by microporous membranes in liquid filtration, pt. 2. *Environ. Eng.* **5**, 22–23 (1992).

241. Springer, F., Laborie, S. & Guigui, C. Removal of SiO2 nanoparticles from industry wastewaters and subsurface waters by ultrafiltration: Investigation of process efficiency, deposit properties and fouling mechanism. *Sep. Purif. Technol.* **108**, 6–14 (2013).

242. Tsurumi, T. *et al.* Mechanism of removing monodisperse gold particles from a suspension using cuprammonium regenerated cellulose hollow fiber (BMM hollow fiber). *Polym. J.* **22**, 304–311 (1990).

243. Agasanapura, B., Baltus, R. E., Tanneru, C. T. & Chellam, S. Effect of electrostatic interactions on rejection of capsular and spherical particles from porous membranes: Theory and experiment. *J. Colloid Interface Sci.* **448**, 492–500 (2015).

244. Heinemann, M. L. *et al.* Benchtop isolation and characterization of functional exosomes by sequential filtration. *J. Chromatogr. A* **1371**, 125–135 (2014).

245. Helling, A. *et al.* Passage of soft pathogens through microfiltration membranes scales with transmembrane pressure. *J. Memb. Sci.* **522**, 292–302 (2017).

246. Büning, D. *et al.* Soft synthetic microgels as mimics of mycoplasma. *Soft Matter* **17**, 6445–6460 (2021).

247. Kosiol, P. *et al.* Determination of pore size gradients of virus filtration membranes using gold nanoparticles and their relation to fouling with protein containing feed streams. *J. Memb. Sci.* **548**, 598–608 (2018).

248. Kosiol, P., Hansmann, B., Ulbricht, M. & Thom, V. Determination of pore size distributions of virus filtration membranes using gold nanoparticles and their correlation with virus retention. *J. Memb. Sci.* **533**, 289–301 (2017).

249. Kelley, E. G., Albert, J. N. L., Sullivan, M. O. & Epps Thomas H., I. I. I. Stimuli-responsive copolymer solution and surface assemblies for biomedical applications. *Chem. Soc. Rev.* **42**, 7057–7071 (2013).

250. Uhlmann, P. *et al.* In-situ investigation of the adsorption of globular model proteins on stimuli-responsive binary polyelectrolyte brushes. *Langmuir* **23**, 57–64 (2007).

251. Currie, E. P. K., Sieval, A. B., Fleer, G. J. & Stuart, M. A. C. Polyacrylic Acid

Brushes: Surface Pressure and Salt-Induced Swelling. *Langmuir* **16**, 8324–8333 (2000).

252. Wu, T. *et al.* Behavior of Surface-Anchored Poly(acrylic acid) Brushes with Grafting Density Gradients on Solid Substrates: 1. Experiment. *Macromolecules* **40**, 8756–8764 (2007).

253. Akkahat, P., Mekboonsonglarp, W., Kiatkamjornwong, S. & Hoven, V. P. Surface-Grafted Poly(acrylic acid) Brushes as a Precursor Layer for Biosensing Applications: Effect of Graft Density and Swellability on the Detection Efficiency. *Langmuir* **28**, 5302–5311 (2012).

254. Houbenov, N., Minko, S. & Stamm, M. Mixed polyelectrolyte brush from oppositely charged polymers for switching of surface charge and composition in aqueous environment. *Macromolecules* **36**, 5897–5901 (2003).

255. Breite, D., Went, M., Prager, A. & Schulze, A. The critical zeta potential of polymer membranes: How electrolytes impact membrane fouling. *RSC Adv.* **6**, 98180–98189 (2016).

256. Trzaskus, K. W., de Vos, W. M., Kemperman, A. & Nijmeijer, K. Towards controlled fouling and rejection in dead-end microfiltration of nanoparticles - Role of electrostatic interactions. *J. Memb. Sci.* **496**, 174–184 (2015).

257. Bijlard, A. *et al.* Functional colloidal stabilization. *Adv. Mater. Interfaces* **4**, 1600443 (2017).

258. Aimar, P. & Bacchin, P. Slow colloidal aggregation and membrane fouling. *J. Memb. Sci.* **360**, 70–76 (2010).

259. Xiao, K. *et al.* A systematic analysis of fouling evolution and irreversibility behaviors of MBR supernatant hydrophilic/hydrophobic fractions during microfiltration. *J. Memb. Sci.* **467**, 206–216 (2014).

260. Ito, Y., Ochiai, Y., Park, Y. S. & Imanishi, Y. pH-sensitive gating by conformational change of a polypeptide brush grafted onto a porous polymer membrane. *J. Am. Chem. Soc.* **119**, 1619–1623 (1997).

261. Maeda, M., Kimura, M., Hareyama, Y. & Inoue, S. pH-dependent ion transport across polymer membrane. pH-induced reversible conformational change of transmembrane poly (L-aspartic acid) domain in polymer membrane. *J. Am. Chem. Soc.* **106**, 250–251 (1984).

262. Aoyama, M., Youda, A., Watanabe, J. & Inoue, S. Synthesis and circular dichroic and photoresponsive properties of a graft copolymer containing an azoaromatic polypeptide branch and its membrane. *Macromolecules* **23**, 1458–1463 (1990).

263. Kinoshita, T., Iwata, T., Takizawa, A. & Tsujita, Y. Ionic salt permeabilities and membrane potentials of asymmetric polypeptide membrane. *Colloid Polym. Sci.* **261**, 933–937 (1983).

264. Kinoshita, T. *et al.* Solute permeability enhancement at a specific pH by an

amphiphilic copolypeptide membrane. *Macromolecules* **27**, 1389–1394 (1994).

265. Dee, K. C., Puleo, D. A. & Bizios, R. An introduction to tissue-biomaterial interactions. *Choice Rev. Online* **40**, 40-3433-40–3433 (2003).

266. Majorek, K. A. *et al.* Structural and immunologic characterization of bovine, horse, and rabbit serum albumins. *Mol. Immunol.* **52**, 174–182 (2012).

267. Ge, S., Kojio, K., Takahara, A. & Kajiyama, T. Bovine serum albumin adsorption onto immobilized organotrichlorosilane surface: influence of the phase separation on protein adsorption patterns. *J. Biomater. Sci. Polym. Ed.* **9**, 131–150 (1998).

268. Yan, L., Li, Y. S., Xiang, C. B. & Xianda, S. Effect of nano-sized Al2O3-particle addition on PVDF ultrafiltration membrane performance. *J. Memb. Sci.* **276**, 162–167 (2006).

269. Rana, D. & Matsuura, T. Surface modifications for antifouling membranes. *Chem. Rev.* **110**, 2448–2471 (2010).

270. Yamakawa, H. *Modern theory of polymer solutions*. (Harper & Row, 1971).

271. Kontturi, K., Mafe, S., Manzanares, J. A., Svarfvar, B. L. & Viinikka, P. Modeling of the salt and pH effects on the permeability of grafted porous membranes. *Macromolecules* **29**, 5740–5746 (1996).

272. Hashino, M. *et al.* Effect of kinds of membrane materials on membrane fouling with BSA. *J. Memb. Sci.* **384**, 157–165 (2011).

273. He, Y. *et al.* Structure and pH-sensitive properties of poly (vinylidene fluoride) membrane changed by blending poly (acrylic acid) microgels. *Polym. Adv. Technol.* **24**, 934–944 (2013).

274. Shim, J. K., Na, H. S., Lee, Y. M., Huh, H. & Nho, Y. C. Surface modification of polypropylene membranes by γ-ray induced graft copolymerization and their solute permeation characteristics. *J. Memb. Sci.* **190**, 215–226 (2001).

275. Koehler, J. A., Ulbricht, M. & Belfort, G. Intermolecular forces between proteins and polymer films with relevance to filtration. *Langmuir* **13**, 4162–4171 (1997).

276. Koehler, J. A., Ulbricht, M. & Belfort, G. Intermolecular forces between a protein and a hydrophilic modified polysulfone film with relevance to filtration. *Langmuir* **16**, 10419–10427 (2000).

277. Taniguchi, M., Kilduff, J. E. & Belfort, G. Low fouling synthetic membranes by UV-assisted graft polymerization: monomer selection to mitigate fouling by natural organic matter. *J. Memb. Sci.* **222**, 59–70 (2003).

278. Li, Y., Liu, L. & Fang, Y. Plasma-induced grafting of hydroxyethyl methacrylate (HEMA) onto chitosan membranes by a swelling method. *Polym. Int.* **52**, 285–290 (2003).

279. Belfer, S. *et al.* Modification of NF membrane properties by in situ redox initiated

graft polymerization with hydrophilic monomers. *J. Memb. Sci.* **239**, 55–64 (2004).

280. Belfer, S., Bottino, A. & Capannelli, G. Preparation and characterization of layered membranes constructed by sequential redox-initiated grafting onto polyacrylonitrile ultrafiltration membranes. *J. Appl. Polym. Sci.* **98**, 509–520 (2005).

281. Oster, G. & Yang, N.-L. Photopolymerization of vinyl monomers. *Chem. Rev.* **68**, 125–151 (1968).

282. Tripathy, S. S., Jena, S., Misra, S. B., Padhi, N. P. & Singh, B. C. A study on graft copolymerization of methyl methacrylate onto jute fiber. *J. Appl. Polym. Sci.* **30**, 1399–1406 (1985).

283. Martín-Gomis, L., Cuervo-Rodriguez, R., Fernández-Monreal, M. C., Madruga, E. L. & Fernández-García, M. Monomer reactivity ratios and glass-transition temperatures of copolymers based on dimethyl amino ethyl methacrylate and two structural hydroxy-functional acrylate isomers. *J. Polym. Sci. Part A Polym. Chem.* **41**, 2659–2666 (2003).

284. Hu, M.-X., Yang, Q. & Xu, Z.-K. Enhancing the hydrophilicity of polypropylene microporous membranes by the grafting of 2-hydroxyethyl methacrylate via a synergistic effect of photoinitiators. *J. Memb. Sci.* **285**, 196–205 (2006).

285. Tao, M., Liu, F. & Xue, L. Hydrophilic poly(vinylidene fluoride) (PVDF) membrane by in situ polymerisation of 2-hydroxyethyl methacrylate (HEMA) and micro-phase separation. *J. Mater. Chem.* **22**, 9131–9137 (2012).

286. Li, J.-H., Xu, Y.-Y., Zhu, L.-P., Wang, J.-H. & Du, C.-H. Fabrication and characterization of a novel TiO2 nanoparticle self-assembly membrane with improved fouling resistance. *J. Memb. Sci.* **326**, 659–666 (2009).

287. Pazouki, M., Wilton, A. N. & Latulippe, D. R. An experimental study on sterile filtration of fluorescently labeled nanoparticles–the importance of surfactant concentration. *Sep. Purif. Technol.* **218**, 217–226 (2019).

288. Xiao, K., Shen, Y. & Huang, X. An analytical model for membrane fouling evolution associated with gel layer growth during constant pressure stirred dead-end filtration. *J. Memb. Sci.* **427**, 139–149 (2013).

289. Ghosh, R. & Cui, Z. F. Fractionation of BSA and lysozyme using ultrafiltration: effect of pH and membrane pretreatment. *J. Memb. Sci.* **139**, 17–28 (1998).

290. Kim, K.-J. & Fane, A. G. Performance evaluation of surface hydrophilized novel ultrafiltration membranes using aqueous proteins. *J. Memb. Sci.* **99**, 149–162 (1995).

291. Fane, A. G., Fell, C. J. D. & Waters, A. G. Ultrafiltration of protein solutions through partially permeable membranes—the effect of adsorption and solution environment. *J. Memb. Sci.* **16**, 211–224 (1983).

292. Nabe, A., Staude, E. & Belfort, G. Surface modification of polysulfone ultrafiltration membranes and fouling by BSA solutions. *J. Memb. Sci.* **133**, 57–72 (1997).

293. Wang, Y., Kim, J.-H., Choo, K.-H., Lee, Y.-S. & Lee, C.-H. Hydrophilic modification of polypropylene microfiltration membranes by ozone-induced graft polymerization. *J. Memb. Sci.* **169**, 269–276 (2000).

294. Sack, R. A., Jones, B., Antignani, A., Libow, R. & Harvey, H. Specificity and biological activity of the protein deposited on the hydrogel surface. Relationship of polymer structure to biofilm formation. *Invest. Ophthalmol. Vis. Sci.* **28**, 842–849 (1987).

295. Cox, D. R. & Reid, N. *The theory of the design of experiments*. (CRC Press, 2000).

296. Dempsey, D. J. & Thirucote, R. R. Sterilization of medical devices: a review. *J. Biomater. Appl.* **3**, 454–523 (1988).

297. Hukins, D. W. L., Mahomed, A. & Kukureka, S. N. Accelerated aging for testing polymeric biomaterials and medical devices. *Med. Eng. Phys.* **30**, 1270–1274 (2008).

298. Janting, J., Theander, J. G. & Egesborg, H. On Thermal Acceleration of Medical Device Polymer Aging. *IEEE Trans. Device Mater. Reliab.* **19**, 313–321 (2019).

299. Lovinger, A. & Reed, D. Inhomogeneous Thermal Degradation of Poly(vinylidene fluoride) Crystallized from the Melt. *Macromolecules* **13**, 989–994 (1980).

300. Saxena, P. & Shukla, P. A comprehensive review on fundamental properties and applications of poly(vinylidene fluoride) (PVDF). *Adv. Compos. Hybrid Mater.* **4**, 8–26 (2021).

301. Liu, F., Hashim, N. A., Liu, Y., Abed, M. R. M. & Li, K. Progress in the production and modification of PVDF membranes. *J. Memb. Sci.* **375**, 1–27 (2011).

302. Nelson, W. *Simulation Methods for Accelerated Testing - Statistical Models , Test plans, and data analysis*. vol. 21 (Wiley Online Library, 2005).

303. Bottino, A., Capannelli, G., Munari, S. & Turturro, A. Solubility parameters of poly(vinylidene fluoride). *J. Polym. Sci. Part B Polym. Phys.* **26**, 785–794 (1988).

304. Nguyen, T. Degradation of Poly[vinyl Fluoride] and Poly[vinylidene Fluoride]. *J. Macromol. Sci. Part C* **25**, 227–275 (1985).

305. Komaki, Y. Growth of fine holes by the chemical etching of fission tracks in polyvinylidene fluoride. *Nucl. Tracks* **3**, 33–44 (1979).

306. Shinohara, H. Fluorination of polyhydrofluoroethylenes. II. Formation of perfluoroalkyl carboxylic acids on the surface region of poly (vinylidene fluoride) film by oxyfluorination, fluorination, and hydrolysis. *J. Polym. Sci. Polym. Chem. Ed.* **17**, 1543–1556 (1979).

307. Hoa, S. V & Ouellette, P. Stress corrosion cracking of poly (vinylidene fluoride) in sodium hydroxide. *Polym. Eng. Sci.* **23**, 202–205 (1983).

308. Benzinger, W. D., Parekh, B. S. & Eichelberger, J. L. High temperature ultrafiltration with Kynar® poly (vinylidene fluoride) membranes. *Sep. Sci. Technol.* **15**, 1193–1204 (1980).

309. Polyakov, Y. S. & Zydney, A. L. Ultrafiltration membrane performance: Effects of pore blockage/constriction. *J. Memb. Sci.* **434**, 106–120 (2013).

310. Howell, J. A., Sanchez, V. & Field, R. W. *Membranes in bioprocessing: theory and applications*. (Springer Science & Business Media, 2012).

311. Maa, Y. & Hsu, C. C. Membrane fouling in sterile filtration of recombinant human growth hormone. *Biotechnol. Bioeng.* **50**, 319–328 (1996).

312. Garrett, Q., Griesser, H. J., Milthorpe, B. K. & Garrett, R. W. Irreversible adsorption of human serum albumin to hydrogel contact lenses: a study using electron spin resonance spectroscopy. *Biomaterials* **20**, 1345–1356 (1999).

313. Soffer, Y., Gilron, J. & Adin, A. Streaming potential and SEM-EDX study of UF membranes fouled by colloidal iron. *Desalination* **146**, 115–121 (2002).

314. Hamid, S. A., Azha, S. F., Sellaoui, L., Bonilla-Petriciolet, A. & Ismail, S. Adsorption of copper (II) cation on polysulfone/zeolite blend sheet membrane: Synthesis, characterization, experiments and adsorption modelling. *Colloids Surfaces A Physicochem. Eng. Asp.* **601**, 124980 (2020).

Appendix I: LIST OF TABLES

Appendix II: LIST OF FIGURES